

Modelling and Investigating the Circadian Pattern in Components of Human Pain Circuitry

Xinyu Li

Wolfson College

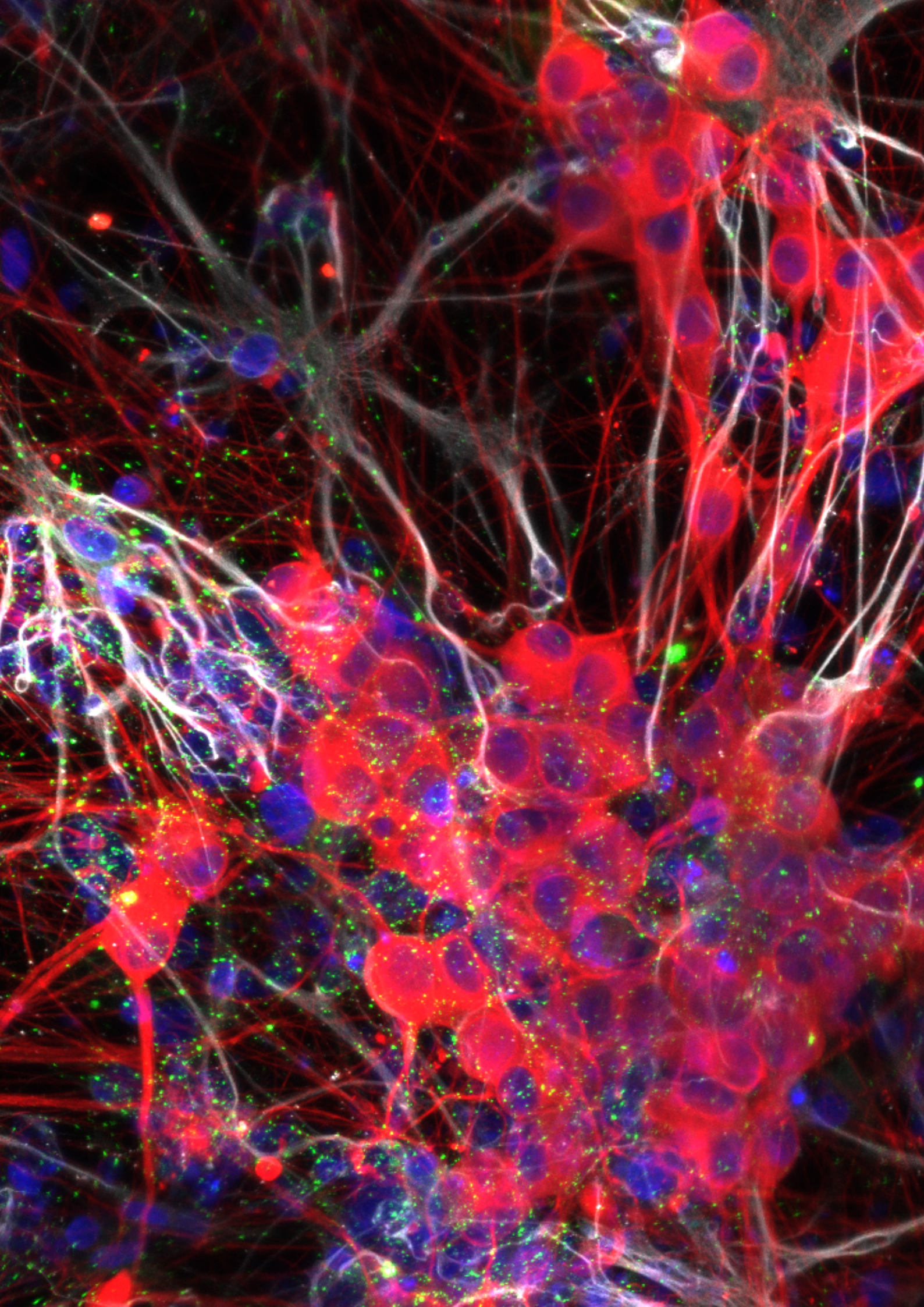
NDCN, University of Oxford

A Cruel Angel's Thesis submitted in partial fulfilment for the degree of

Doctor of Philosophy in Clinical Neurosciences

Word count: 32903

October 2025



Abstract

Human induced pluripotent stem cell (hiPSC)-derived models are useful tools for the study of pain that bridge the gap of fundamental interspecies differences in traditional animal models. However, currently available protocols for hiPSC-derived sensory neurons only generate certain clinically relevant subtypes of pain-detecting nociceptors *in vitro*, with notably a lack of neuropeptide secretion.

The present project has developed a novel hiPSC-based protocol for nociceptors that exhibit both baseline and chemically evoked secretion of calcitonin gene-related peptide (CGRP). Compared to benchmark protocols described in the literature, our method produced nociceptors with distinct pain-related phenotypes, including differential expression of subtype-specific markers (*cMET* and *TRKA*), co-expression of CGRP with somatostatin, and altered electrophysiological responsiveness to noxious heat.

The current project also confirmed the presence of an autonomous, oscillating molecular clock in sensory neurons differentiated *in vitro*, as an intrinsic feature of neuronal maturation. The molecular clock in nociceptors was associated with temporally dynamic gene transcription, protein abundance, translocation & phosphorylation, sodium channel dynamics, and firing activities.

Together, these findings established an integrated framework for generating functionally diverse nociceptors *in vitro*, with innate circadian molecular oscillations. The present study enables modelling of both physiological and pathological pain in human sensory ganglia, with close resemblance to *ex vivo* human nociceptors of electrophysiological, biochemical, and circadian properties.

Abbreviations

The following table does not contain abbreviations in Table S1.

4PL	Four-parameter logistic
AMPK	Adenosine monophosphate-activated protein kinase
ANOVA	Analysis of variation
AraC	Cytosine-beta-arabinofuranoside
ARI	Adjusted rand index
ATXN2L	Ataxin-2 like protein
BDNF	Brain-derived neurotrophic factor
bFGF	Basic FGF
BL	Baseline
BMAL1	Basic Helix-Loop-Helix Brain and muscle ANTR-Like 1
BMP	Bone morphogenetic protein
BP	BrainPhyz
CCG	Clock controlled gene
CDE	Cliff's delta effect size
CI	Calcium imaging
CIP	Congenital insensitivity to pain
CGRP	Calcitonin gene-related peptide
CLOCK	Circadian locomotor output cycles kaput
CNQX	Cyanquixaline
CNS	Central nervous system
CP	Cranial placode
CRY	Cryptochrome
C_T	Quantification cycle
DE	Differential expression

Dex	Dexamethasone
DkTx	Knotted toxin
DRG	Dorsal root ganglia
dSMADi	Dual SMAD inhibition
EDF	Extended depth of field
ELISA	Enzyme-linked immunosorbant assay
EM	Electron microscopy
FACS	Fluorescence-activated cell sorting
FC	Flow cytometry
FGF	Fibroblast growth factor
FK	Forskolin
FMO	Fluorescence minus one
GABA	Gamma-glutamic acid
GDNF	Glial-derived neurotrophix factor
GO	Gene ontology
GPCR	G-protein coupled receptors
GSK3	Glycogen synthase kinase 3
GTN	Nitroglycerin
GWAS	Genome-wide association study
HCA	Hierarchical clustering analysis
hEPI-NCSCs	Human epidermal neural crease stem cells
hESCs	Human embryonic stem cells
hiPSCs	Human induced pluoripotent stem cells
IF	Immunofluorescence
iNocieptors	HiPSC-derived nociceptors
iNPC	Induced neuronal progenitor cells
iPSC	Induced pluripotent stem cells
IR	Immunoreactivity

IS	Inflammatory soup
ISH	*In situ* hybridisation
ISL1	Islet-1
KI	Knock-in
KD	Knockdown
KO	Knockout
LDCV	Large deep core vesicle
LTMR	Low-threshold mechanoreceptor
MEA	Multi-electrode array
N1C	No primary control
N2A	Neurobasal-A
N2C	No secondary control
NC	Neural crest
NGF	Nerve growth factor
NGN	Neurogenin
NHDF	Normal human dermal fibroblast
NLS	Nuclear localisation signal
NMDAR	N-methyl-D-aspartate receptor
NSAID	Nonsteroidal anti-inflammatory drug
NSC	No-staining control
NT-3/4	Neurotrophin-3/4
OD	Optical density
P2X3R	P2X purinergic ion channel type 3 receptor
PACAP	Pituitary adenylate cyclase-activating peptide
PAG	periaqueductal gray
PBMC	Peripheral blood mononuclear cell
PER	Period
PHOX2A	Paired homeobox 2A

PML	Promyelocytic leukemia protein
PNS	Peripheral nervous system
PPI	Protein-peotein interaction
PPP4	protein phosphatase 4
PPTA	Preprotachykinin A
PRDM	PR-Domain containing methyltransferase
PTM	Post-translational modification
RIPA	Radioimmunoprecipitation assay
RET	Rearranged during Transformation tyrosine receptor kinase
RRE	REVERB/ROR-response element
RT-qPCR	Reverse transcription/real-time quantitative polymerase chain reaction
RUNX	Runt-related genes
SBDS	Similarity bright detail score
SC	Schwann cell
SCN	Suprachiasmatic nucleus
SDS	Sodium dodecyl sulfate
SGC	Satellite glial cell
SgII	Secretogranin II
SHOX2	Short stature homeobox 2
SNP	Single-nucleotide polymorphism
snRNAseq	Single-nucleus RNA sequencing
SP	Substance P
sSMADi	Single SMAD inhibition
SST	Somatostatin
SSTR	Somatostatin receptor
TAD	Transactivation domain
TF	Transcription factor
TG	Trigeminal ganglia

TP	Trigeminal placode
TRK	Tropomyosine receptor kinase
TRP	Transient receptor potential
TRPA1	Transient receptor potential channel subfamily A member 1
TRPM8	Transient receptor potential channel subfamily M member 8
TRPV1	Transient receptor potential channel subfamily V member 1
TTFL	Transcription-translation feedback loop
TTX	Tetrodotoxin
UMAP	Unifrom manifold approximation and projection
VEGF-A	Vascular endothelial growth factor
VGSC	Voltage-gated sodium channel
VIP	Vasoactive intestinal peptide
VNTR	Variable number tandem repeat
WDR	Wide dynamic range
WNT	Wingless & Int-1
WT	Wild type
Zcchc12	Zinc-finger CCHC domain-containing 12

Table of Contents

Abstract **1**

Abbreviations **2**

Table of Contents **7**

List of Figures **11**

List of Tables **17**

Publications & Repurposed Sections with Statement of Authorship **19**

Journal publications 19

Conference attendance 19

Statement of authorship on repurposed data and writing 20

Acknowledgement **21**

1 Introduction **22**

1.1 Background 22

1.1.1 Neuroanatomy of the human nociception system 22

1.1.2 The molecular basis of mammalian circadian rhythm 35

1.1.3 Circadian patterns in mammalian pain 43

1.2 Rationale, aims & proposed methodology 53

2 Development & Optimisation of Components Modelling Human Sensory Ganglia **55**

2.1 Overview 55

2.2 Generation of DRG (neural crest) non-peptidergic iNociceptors *in vitro* . . . 61

2.3 Generation of TG CGRP+ peptidergic iNociceptors *in vitro* 71

2.3.1 Optimisation of the induction efficiency of sensory neurons of placodal identity . . . 71
2.3.2 Optimisation of maturation conditions for peptidergic cell fate specification in TG iNociceptors . . . 75
2.3.3 Functional characterisation of TG CGRP+ peptidergic iNociceptors 78
2.3.4 Applying TG CGRP+ peptidergic iNociceptor models to the study of migraine pathobiology . . . 90
2.4 Generation of a hiPSC-based neurovascular TG assembloid model . . . 95
2.5 Discussion . . . 103
2.5.1 Generation of neuropeptide secreting TG iNociceptors . . . 103
2.5.2 Glia-facilitated survival and cell fate specification of iNociceptors . 105
2.5.3 TRPV1 & Peripheral thermo-sensors . . . 107

3 Investigation of the Molecular Oscillations and Pain-Related Functional Relevance in iNociceptors 111

3.1 Overview . . . 111
3.2 Transcriptional analysis of clock gene oscillations in Chambers' DRG iNociceptors . . . 113
3.2.1 Quantifying chemically induced oscillations of clock gene transcription 113
3.2.2 Temporal dynamics of the transcription of pain-related genes in iNociceptors . . . 120
3.3 Global changes of protein abundance in FK synchronised Chamber's iNociceptors . . . 121
3.4 Functional relevance of circadian properties in peripheral sensory neurons . 138
3.4.1 Diurnal firing patterns in iNociceptors . . . 138
3.4.2 Diurnal regulations of Na_V 1.7 localisation . . . 141
3.4.3 Diurnal regulations of Na_V 1.7 phosphorylation . . . 145
3.4.4 Diurnal distribution of neuropeptides . . . 148
3.5 Discussion . . . 150
3.5.1 Reflections on the methodology of circadian research in iNociceptors 150

3.5.2 Circadian rhythmicity in iNociceptors 154

4 Conclusion & Discussion **156**

4.1 Conclusion 156

4.2 Reflection on using iNociceptors as a pain model system as major methodologies in the current study 158

4.3 Discussion on the major biological findings of the current project and future directions 161

4.3.1 Development & cell fate specification of sensory neurons 161

4.3.2 Profiling & stratification of sensory neurons 161

4.3.3 Sexual dimorphism 162

4.3.4 Circadian properties of sensory neurons 163

4.3.5 Reflection on understanding migraine pathology with stem cell technologies 163

Supplementary Information **165**

S1 Material & Methods 165

S2 Supplementary tables 183

S2.1 HiPSC lines 183

S2.2 Primers 184

S2.3 Antibodies 187

S3 Supplementary information & figures 190

S3.1 HiPSC Quality check 190

S3.2 Supplementary information on the optimisation of Trk-typing in DRG and TG iNociceptor progenitors 193

S3.3 Supplementary information on the optimisation of iNociceptor MEA 196

S3.4 Supplementary information on the TG peptidergic iNociceptor protocol 202

S3.5 Supplementary information on the impact of DAPT in the Chambers' cocktail on the induction efficiency of neuronal progenitors in the Chambers' protocol 219
S3.6 Supplementary information on determining the appropriate methodology for transcriptional circadian studies *in vitro* 224
S3.7 Optimisation of quantifying circadian protein via ImageStream in NHDFs as a pilot test and positive control 229
S3.8 Supplementary information on subcellular proteomics of FK synchronised Chambers' iNociceptors. 236

Bibliography **239**

List of Figures

1 Neuroanatomy of the peripheral and spinal components of the human nociception system. 22

2 Neurotrophins as the major regulators of sensory neuron development. Deriving from common neurogenic progenitors, the action of neurotrophins drives sensory neuron diversification via the action of specialised high affinity TRK channels. While proprioceptors and mechanoreceptors are embryologically dependent on the expression of one core TRK channel, nociceptors rely on combined action of TRKA and TRKB for specification and maturation, respectively. Illustrated by Li. 26

3 Proportion of cells co-expressing *TRKB* with conventional peptidergic and non-peptidergic markers in human and mouse TGs. 28

4 The spinal gate and supraspinal processing centres. 33

5 The mammalian TTFL network 35

6 Confirmation of DRG iNociceptor identities by Chambers' method. 62

7 Selective expression of sensory neuron markers in SBAD03 DRG iNociceptor cultures. 63

8 Representative distribution of TRP channels and conventional peptidergic/non-peptidergic markers in post-mortem human DRGs. 64

9 Phenotypic modulations of DRG iNociceptors in astrocyte co-cultures. . . . 65

10 Responses to noxious heat in SBAD03 DRG iNociceptors. 67

11 Further experiments and analysis based on batch-differential heat responsiveness in SBAD03 Chambers' iNociceptors. 69

12 Differentiation of hiPSCs towards TP lineage. 72

13 Temporal profiling of ectodermal transcription factor topology in developing SBAD03 TP organoids. 74

14 No effect of DAPT shock on neuronal commitment in 3D TPs. 76
15 Maturation outcomes of SBAD03 TG iNociceptors modulated by the presence of glia. 77
16 Directed differentiation of peptidergic TG iNociceptors. 79
17 TRP channel expression in SBAD03 TG iNociceptors compared to primary human and mouse TGs. 80
18 Confirming neuropeptide immunoreactivities in mature SBAD02 TG iNociceptors generated from 2D placodes. 83
19 CGRP secretion in response to stimuli in mature WT TG iNociceptors. . . . 85
20 Expression and distribution of neuropeptide receptors in human TG *in vitro* and *ex vivo*. 86
21 Comparison between TRPV1-dependent noxious heat responsiveness in SBAD03 TG and DRG iNociceptors by MEA. 89
22 Generation of TPs from migraine patient-specific iPSC lines. 92
23 Confirmation of successful differentiation and maturation of d70 TG iNociceptors in WT and patient-derived lines by RT-qPCR. 92
24 Baseline and stimulated CGRP secretion in mature TG iNociceptors in WT and patient-derived lines. 94
25 Confirmation of peptidergic cell fate in TG iNociceptor cultured as organoids without ArC treatment. 96
26 Optimisation of a 3D iPSC-derived vessel model 98
27 Extensive CD31+ endothelial network visualised in whole mount BL6 female DRGs. 99
28 Visualisation of major cell types and spatial distribution in primary mouse TGs. 100
29 CD31 geometry in hiPSC-derived vessel organoids. 101
30 Representative confocal image of endothelial association in proximity to neuronal soma in the neurovascular assembloid. 102

31 Evaluation of stable reference genes for mRNA relative quantification by RT-qPCR in SBAD03 DRG iNociceptors. 114
32 Challenges of using unsynchronised undifferentiated hiPSCs as the universal control sample for relative quantification. 115
33 Relative expression of *PER2* (top) & *BMAL1* (bottom) in SBAD03 DRG iNociceptors normalised with different single or double reference genes. . . 116
34 Transcriptional analysis of clock gene expression in chemically synchronised SBAD03 DRG non-peptidergic iNociceptors. 118
35 Demonstration of species- and location-dependent variations of core clock gene transcript abundance. 119
36 Circadian-driven variations of pain-related transcript abundances in SBAD03 DRG iNociceptors. 120
37 Lack of core TTFL protein immunoreactivities in chemically synchronised undifferentiated hiPSCs. 122
38 Confirmation of BMAL1 protein expression in chemically synchronised Chambers' iNociceptors by western blotting. 122
39 Sample preparation and quality check prior to proteomics analysis. 125
40 Efficacy of membrane/cytosol fractionation. 126
41 Top hits with diurnally differential expressions in cytoplasmic and membrane fractions of chemically synchronised Chambers' iNociceptors. 127
42 Representative proteins identified with diurnally differential expressions in chemically synchronised Chambers' iNociceptors with known functions related to pain. 129
43 Activation matrix of GO pathways enriched at +16 compared to +4 in cytoplasmic protein fractions of chemically synchronised Chambers' iNociceptors. 136
44 Activation matrix of GO pathways enriched at +16 compared to +4 in membrane protein fractions of chemically synchronised Chambers' iNociceptors. 137

45 Diurnal responsiveness to selective TRPV1 antagonist AMG9810 in SBAD03 TG iNociceptors. 138
46 Diurnal responsiveness to selective $Na_V1.7$ antagonist PF-05089771 in SBAD03 DRG iNociceptors. 140
47 Axonal distribution of Na_V 1.7 in chemically synchronised primary murine DRG cultures. 142
48 Axonal distribution of Na_V 1.7 in chemically synchronised primary murine TG cultures. 143
49 Axonal distribution of Na_V 1.7 in chemically synchronised Chambers' DRG iNociceptors. 144
50 Diurnally differential phosphorylation status of Na_V 1.7 in chemically synchronised Chambers' iNociceptors based on subcellular localisation. . . 145
51 CGRP distribution in primary TGs from diurnally harvested female WT mice. 149

52 Schematics of experimental timelines during iNociceptor maturation. 159
S1 Representative brightfield morphology of iPSCs from patient-dervied lines. 190
S2 FC analysis of the expression level of pluripotency markers TRA-1-60 and NANOG in patient-derived iPSCs, extracted from Oxford StemTech reports. 191
S3 Quality control of $Na_V1.7$-HALO iPSC line. 192
S4 Trk-typing of DRG/TG iNociceptor by FC. 194
S5 Gating strategy of Trk-typing of DRG and TG iNociceptor progenitors. . . . 195
S6 Demonstration of sample selection prior to MEA analysis. 196
S7 Timeline of MEA experiments in mature iNociceptors. 198
S8 Optimisation of medium composition for SBAD03 DRG iNociceptor firing activities. 199
S9 Optimisation of media composition and synchronisation method for diurnal spontaneous activities in SBAD03 DRG iNociceptors by MEA. 201
S10 Available methods of deriving placodes from the literature. 202
S11 Morphological consistencies of growing sSMADi TPs on 2D platforms. . . 203

S12 Investigating on placodal contents dervied from the sSMADi TP protocol on 2D platforms. 205
S13 Titration of DMSO pre-treatment for TP induction. 206
S14 Temporal profiling of ectodermal transcription factor topology in developing SBAD03 TP organoids by IF. 207
S15 Workflow of the quantification of expression and distribution of immunolabelled transcription factors in 3D TPs. 209
S16 Maturation outcomes of TG iNociceptors derived from 2D platforms modulated by the presence of glia. 213
S17 Expression of cMET and RET in mature peptidergic TG iNociceptors. . . . 214
S18 Rat astrocytes alone as negative control for ELISA and MEA assays 215
S19 Optimisation of imaging conditions when applying neuropeptide ImageStream in mature TG iNociceptor-astrocyte co-cultures. 218
S20 Representative brightfield images of DRG iNociceptors differentiated with and without DAPT, at d8, d12, and d16 (post-AraC treatment). 220
S21 Trk-typing of SBAD02 DRG grown with/without DAPT and TG iNociceptor progenitors at the time of detachment prior to maturation on 2D platforms. . 221
S22 Temporal expression profiles of key markers in early SBAD02 DRG and TG iNociceptors from 2D culturing conditions. 223
S23 Evaluation of stable reference genes for mRNA relative quantification by RT-qPCR in NHDFs. 224
S24 Relative expression of *PER2* (top) and BMAL1 (bottom) in NHDFs normalised with different single or double reference genes. 226
S25 Transcriptional abundance of canonical TTFL gene expression in chemically synchronised NHDFs. 227
S26 Variation in C_T levels of reference gene candidates in NHDF and Chambers' DRG iNociceptors. 228

S27 Typical quality control and data clean-up process for ImageStream on quantifying TTFL protein expression and translocation in NHDFs as a positive control. 229
S28 Complete ImageStream results of PER2 expression in chemically synchronised NHDFs. 231
S29 Complete ImageStream results of BMAL1 expression in chemically synchronised NHDFs. 232
S30 Complete ImageStream results of CRY1 expression in chemically synchronised NHDFs. 233
S31 Representative images of BMAL1, PER2, and CRY1 in NHDFs from ImageStream analysis. 235
S32 Sample clustering based on non-biased HCA for subcellular fraction proteomics in chemically synchronised Chmaber's iNociceptors. 236
S33 Confirmation of BMAL1 protein expression in chemically synchronised Chambers' iNociceptors by western blotting. 238

List of Tables

1 Empirical evidence of the co-expression and/or co-localisation of CGRP, SP, and SST in the literature. . . . 30

2 Empirical evidence of daily fluctuations in mammalian pain sensitivities from behavioural results, aligned to light and dark phases. . . . 47

3 Empirical evidence of channel-specific electrophysiological properties of Chambers' variations. . . . 56

4 Currently available protocols for the differentiation of peptidergic nociceptors *in vitro*. . . . 59

5 Summary of mouse primary DRG vasculature based on CD31 geometry analysis. . . . 97

6 Comparison of phenotypical outcomes between peptidergic iNociceptor protocols from the current project and available literature. . . . 104

7 Commonly used or preferred reference genes for RT-qPCR in mammalian circadian models (*rodent example italicised*). . . . 113

8 List of top hits with diurnally differential expressions in cytoplasmic protein fractions of FK synchronised Chambers' iNociceptors. . . . 130

9 List of top hits with diurnally differential expressions in membrane protein fractions of FK synchronised Chambers' iNociceptors. . . . 135

10 Comparisons between common methods for quantifying the circadian oscillations of clock genes. . . . 152

S1 List of supplier and catalog information of materials used in the current study 166

S2 Demographic and clinical information (if relevant) of WT HiPSC lines used in this project. . . . 183

S3 Primer sequences used in the current project. . . . 186

S4 List of primary antibodies (with conjugation and differential epitopes if applicable) used in this project. 188
S5 List of secondary antibodies used in this project. 189
S6 Normality testing of diurnal firing rates of chemically synchronised SBAD03 DRG iNociceptors by MEA. 201
S7 Choice of references for normalising secretive CGRP. 216

Publications & Repurposed Figures with Statement of Authorship

Journal publications

Liting Wei, ..., Xinyu Li, ..., M. Zameel Cader. "The molecular drivers of pain rhythmicity as novel therapeutic opportunities". In: *Nat. Commun.* (2026). *In press.*[1]

Galbha Duggal, Xinyu Li, ..., M. Zameel Cader. "A highly efficient method to differentiate CGRP-expressing peptidergic nociceptors from human induced pluripotent stem cells". In: *Stem Cell Rep* (2026). *In press.*[2]

Xinyu Li, ..., M. Zameel Cader. "Methodology & Molecular basis of the circadian rhythmicity of pain in preclinical research: A narrative review". (2026). *In prep.*[3]

Conference attendance

Xinyu Li *et al.* "A trigeminal peptidergic nociceptor model to study migraine". In: *International Society for Stem Cell Research Annual Meeting* (2024). [Poster]. *Travel Grant & Merit Award Recipient.*

Xinyu Li, and M. Zameel Cader. "Modelling the bidirectional communication between trigeminal nociceptors and vessel endothelia in a hiPSC-derived migraine neurovascular assembloid". In: *Cell symposia: Engineering development and disease in organoids* (2024). [Poster].

Statement of authorship on repurposed data and writing

Section 1.1.3 contains a condensed passage from a literature review paper I am leading since 2024. The original narrative review includes a detailed evaluation of experimental designs and methodology in preclinical research and known molecular mechanisms for circadian pain. For the benefit of the world limit, only a summary is presented here. More information about the review can be provided upon request.

Tissue culture, protein extraction, liquid chromatography mass spectrometry proteomics, and raw data generation for Section 3.3 were conducted by Dr. Liting "Tina" Wei of the Cader lab and collaborators from Department of Biochemistry and Molecular Biology at the University of Southern Denmark. I performed further bioinformatics analysis.

Four transcriptomics datasets[4–7] and sequences derived from protein data bank files were obtained from publicly available sources.

Figure S2 was extracted from the quality control report from Oxford StemTech, as part of their stem cell reprogramming services. Other information can be shared upon request, including global screening array karyotyping in comparison to parent lines obtained from patients.

Otherwise, I certify that all figures (including data generation, analysis, graphing, and schematics) included in the current progress were original and independent work. No other person has contributed to the practical execution of the current project.

Acknowledgement

Although everything presented in this thesis was independent work, I have used the plural first-person pronoun *we* in my writing as a tribute for my appreciation to the following people that have supported the completion of my DPhil in various ways:

Gratitude to I, me, and myself. Thanks for hanging on.

Gratitude to the support from mom and dad.
Gratitude to Dr. Matthew James Sutcliffe, for insisting on me writing with LaTeX. Life has been so much easier.

Gratitude to the Cader Lab. Apologies to Zam for dragging on the writing till literally the deadline. Thanks to Tina for training and project collaborations.
Gratitude to people who have provided technical assistance to the fulfilment of my experiments: Dr. Robert "Bobby" Hedley and Vasiliki Tsioligka from the Dunn School of Pathology Flow Cytometry Facility; Dr. Alan Wainman from the Dunn School Bioimaging Facility; Dr. Deirdre Kavanagh, Dr. Niloufer Irani, and Dr. Lior Pytowski from Micron.
Gratitude to all research animals.

Gratitude to all my friends. All colour combinations in this thesis are made friendly to red-green colour blindness. The effort is a dedication for my life-long best friend, who have beta-ed my figure aesthetics and genuinely hopes I can get Nobel Prize so the signed copy of my thesis he will get would be more valuable than it already is.
Gratitude to Neo Culture Technology.

Finally, gratitude to the Oxford cats, with special dedication to Rhiannon and Bouncy. Sleep well, and I will sing the *Lullaby for a Cat*.

1 Introduction

1.1 Background

1.1.1 Neuroanatomy of the human nociception system

Pain is the physiological process that entails the sensory detection and emotional experiences of actual and potential tissue damages[8]. The neural circuitry of pain includes an ascending detection pathway and a descending modulation pathway. In particular, the term nociception refers to the somatosensory component of pain that registers and encodes noxious stimuli[9].

Stratification of nociceptors

The soma of sensory neurons resides in dorsal root ganglia (DRG) and trigeminal ganglia (TG)[10]. Within each anatomical structure, sensory neurons can be categorised based on the type of stimuli encoded (termed as modalities), physical properties of axons, and the molecular profiles.

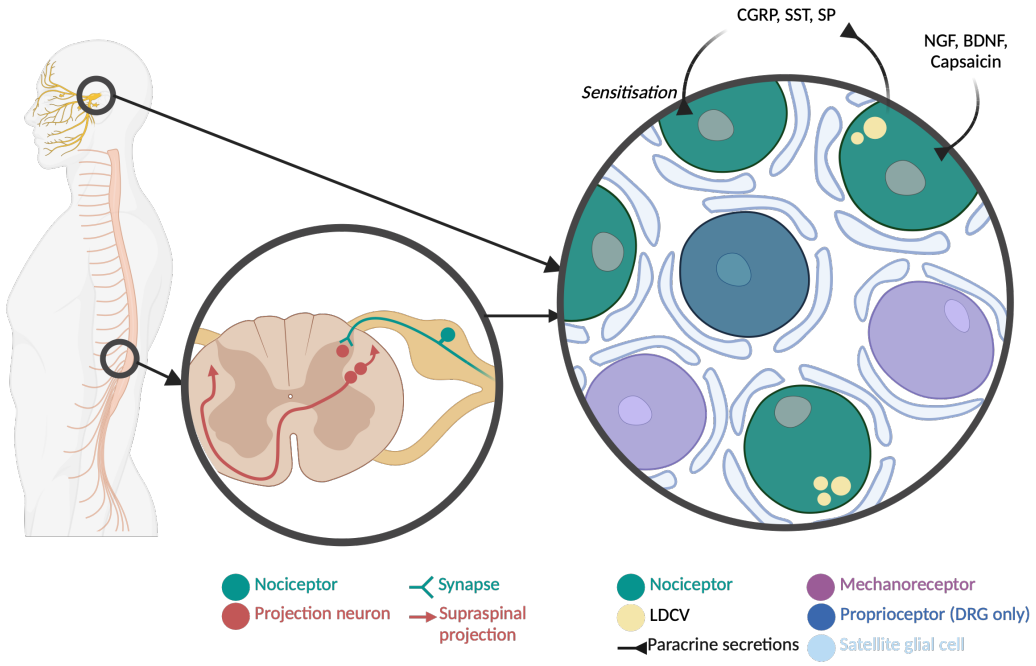


Figure 1: Neuroanatomy of the peripheral and spinal components of the human nociception system. Illustrated with BioRender.

It has been hypothesised that pain of different modalities is population-coded, as selective neural assemblies dedicated to separate types of information[11]: nociceptors for pain, mechanoreceptors for touch and pressure, and proprioceptors for the position and movement of individual body parts[10]. Some studies also recognise innocuous thermoceptors and itch-sensing pruriceptors as separate categories[11]. Nociceptors constitute 80% of total neurons in both DRGs and TGs as the most prominent neuronal subtype[10].

The selective detection of noxious thermal, mechanical, or chemical inputs is achieved by the activation of specialised ion channels, such as members from the transient receptor potential (TRP) family[9]. For example, non-selective cation channel TRP subfamily V member 1 (TRPV1) is an integrated chemical and thermal detector[12], reactive to noxious heat[13], capsaicin[14–16], inflammatory signals[17], lipids[17], and protons[18] (also see Section 2.5.3). TRP channel subfamily A member 1 (TRPA1) is responsive to extreme cold and chemical irritants such as mustard oil[19]. In human, TRPA1+ nociceptors are essentially all TRPV1+[20]. TRP channel subfamily M member 8 (TRPM8) defines another distinct cohort of nociceptors sensitive to coldness and menthol[21].

Besides types of responding stimuli, sensory neurons can be stratified based on biophysical properties such as the size and myelination of nerve fibres, which results in differences of conduction velocities[22]. Nociceptors mostly consist of fast conducting thinly myelinated A_δ and slow conducting unmyelinated small diameter C fibres[9,23,24]. Thickly myelinated A_β fibres are considered to partake in pain processing either as low-threshold mechanoreceptors (LTMRs) for gating acute pain[25] or as high threshold polymodal mechanonociceptors for ultrafast pain conduction[26]. Conventionally, C fibres are further categorised based on neurochemical signatures, as peptidergic [positive for TRPV1 & calcitonin gene-related peptide (CGRP)] and non-peptidergic [positive for P2X purinergic ion channel type 3 receptor (P2X3R)] nociceptors based on rodent studies, albeit concerns of interspecies differences and limited translational efficiencies[27].

The development of transcriptomic profiling techniques has enabled the detailed examination of gene expression profiles in human DRGs and TGs at the single-cell level. Sensory neurons and support cell types can therefore be clustered based on similarities in gene

expression, while also permitting interspecies comparisons. Transcriptomic analysis confirms the broad categorisation of nerve fibre classes and refines the definition of subpopulations by the expression of crucial marker genes. Major clusters of nociceptors are evolutionarily conserved in human and murine TGs, such as TRPV1+ peptidergic and TRPM8+ cold nociceptors[5]. Recent research has also identified a population of human nociceptors with convergent expressions of TRPV1/CGRP with P2X3R but not in murine counterparts[4–6,20,27–31]. It is thereby estimated that most human nociceptors display some aspects of the conventional peptidergic phenotype[23,27].

To avoid confusion, we use the term "peptidergic" and "non-peptidergic" adhering to conventional definition when discussing published literature in the following sections. Traditional categorical terminologies will be refined with representative markers or functional descriptions (e.g. "CGRP-secreting peptidergic" or "capsaicin-irresponsive non-peptidergic") whenever applicable, especially for newer bodies of work.

Overall, the classification of nociceptors is evolving toward high-throughput molecular profiling atlases, which can be integrated with spatial and functional information. Clustering based on transcriptomic profiles is inherently modular, which is frequently interpreted as populations with independent or even mutually exclusive functions. While the molecular and functional segregation is robust between non-noxious mechanoreceptors and nociceptors, more recent research has challenged the concept of strict selective tuning in subpopulations of nociceptors[32]. *In vivo* calcium imaging has identified a significant fraction of nociceptors as functionally polymodal, as noxious mechano- and thermo-sensing populations overlap in both DRGs and TGs[32,33]. It is suggested that the functional relevance of nociceptor subpopulations lies along a spectrum of sensitivities over a range of noxious stimuli.

Sodium channels of nociceptors

Electric signalling through nociceptors is transduced by altered membrane potentials through a range of sodium and potassium membrane channels[9,22].

Voltage-gated sodium channels (VGSCs) are the major contributors to membrane depolarisation in nociceptors, of which pore-forming alpha subunits function either

independently or with auxiliary beta subunits[34].

Isoforms of VGSC alpha subunits are encoded by different genes and classified by their susceptibility to the neurotoxin tetrodotoxin (TTX)[34,35]. Na_V 1.7 (*SCN9A*) is the most abundant VGSC in nociceptors *in vivo* and the major contributor to TTX-sensitive currents[36–38]. Channel dynamics suggests that Na_V 1.7 is likely an amplifier of sub-threshold currents for action potential initiation, axonal signal propagation, and the release of neuropeptides and neurotransmitters[39–42]. Na_V 1.7 loss-of-function results in structural alterations of axons and a drastic loss of membrane conductance, which leads to congenital insensitivity to pain (CIP)[41,43].

In C-fibres, TTX-resistant currents are mediated by Na_V 1.8 (*SCN10A*) and partially contributed to by Na_V 1.9 (*SCN11A*)[44,45]. Na_V 1.8 directly contributes to the sodium current during the rising phase of action potentials. The involvement of Na_V 1.8 in repetitive firing and neuronal excitability[46,47] has attracted research interest in its potential role in chronic pain conditions such as inflammatory pain (e.g.[48–51]), neuropathy (e.g.[49,50,52,53]), and osteoarthritis (e.g.[54]) in animal models. In comparison, Na_V 1.9 is activated at more hyperpolarised voltages than other VGSCs in nociceptors, followed by a characteristic ultra-slow inactivation[45]. Gain-of-function of Na_V 1.7[55–57], Na_V 1.8[58], and Na_V 1.9[59–62] has all been associated with abnormal pains in human.

Major VGSCs such as Na_V 1.7 and 1.8 form superclusters along the axons[63,64]. Small GTPase-containing vesicles traffic Na_V 1.7 and other membrane proteins to axons for polarised ion channel distribution[63,65]. Therefore, small-diameter nociceptors are particularly vulnerable to changes in the activities and distributions of VGSCs, leading to axon injuries[45] and neuropathic pain[52].

Neurotrophins & Cell fate specification during the development of nociceptors

Neurotrophins, such as nerve growth factor (NGF), brain-derived neurotrophic factor (BDNF), and neurotrophin-3/4 (NT-3/4), are critical regulators of the survival and differentiation of sensory neurons during development[66]. Members of the high affinity

tropomyosin receptor kinase (TRK) family selectively recognise individual neurotrophin members: TRKA to NGF, TRKB to BDNF and NT-4, and TRKC to NT-3. The tempo-spatially selective expression of TRK receptors confers the differentiation of specific sensory fibre subtypes[10,67] (Figure 2).

During embryogenesis, the mammalian ectoderm gives rises to four lineages: PAX6+ neuroectoderm for central nervous system (CNS) neurons, SOX10+ neural crest and SIX1+ cranial placodes for peripheral nervous system (PNS) progenitors, and non-neuronal ectoderm[10]. Both neural crest and cranial placodes (CPs) are neural border structures adjacent to the neural tube that later specifies into the spinal cord and the brain[68].

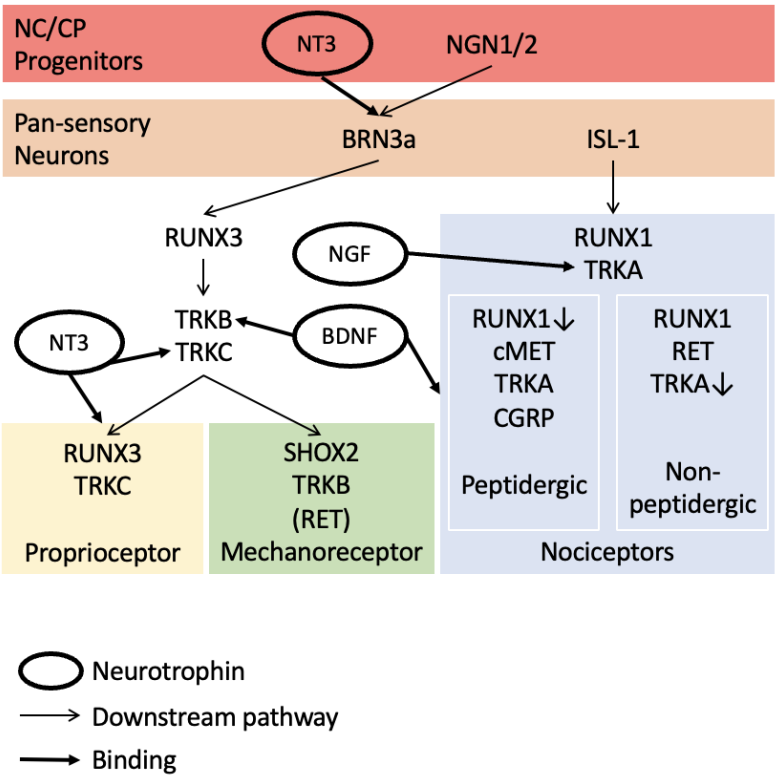


Figure 2: Neurotrophins as the major regulators of sensory neuron development.
Deriving from common neurogenic progenitors, the action of neurotrophins drives sensory neuron diversification via the action of specialised high affinity TRK channels. While proprioceptors and mechanoreceptors are embryologically dependent on the expression of one core TRK channel, nociceptors rely on combined action of TRKA and TRKB for specification and maturation, respectively. Illustrated by Li.

Most sensory neurons are derived from neural crest and migrate into spinal and orofacial ganglia. The low affinity neurotrophin receptor p75 is a hallmark gene of neural crest derivatives, which can be activated by all types of neurotrophin[69]. In parallel, the cranial

ectoderm develops into individual neurogenic and non-neurogenic placodes[68]. Neurogenic trigeminal placodes (TPs) receive migrating neural crest cells, thus containing sensory neurons of both neural crest and cranial placode origins[10].

In both TG and DRG, neurogenesis begins with the expression of neurogenins NGN1 and NGN2 in two consecutive neurogenic waves[70–73], followed by the expression of pan-sensory neuronal markers BRN3a (encoded by *POU4f1*)[74,75] and ISLET-1 (ISL-1)[67,75].

Members of the Runt-related genes (RUNX) further distinguish the outcome of each wave of neurogenesis[76]. BRN3a directly activates RUNX3 which defines TRKC+ proprioceptor progenitors in the first wave of neurogenesis[74,77,78]. In contrast, transcription factor Short stature homeobox 2 (SHOX2) competes against RUNX3 from the communal pool of TRKB+/TRKC+ precursors[76,79], from which sustained TRKB expression defines future LTMRs[80,81]. TG intrinsically lacks proprioceptors as orofacial proprioception is driven by sensory neurons in the mesencephalic trigeminal nucleus of the brainstem[5,10,82]. Therefore, the outcome following the first wave of neurogenesis in TG is essentially all TRKB+ large diameter sensory neurons[83].

During the second wave of sensory neurogenesis, PR-Domain containing methyltransferase 12 (PRDM12) initiates and, together with BRN3a, maintains TRKA expression in nociceptors[74,84,85]. PRDM12 and ISL-1 further act as upstream regulators of RUNX1 that specifies nociceptive cell fates[67]. Unlike proprioceptors of which cell fate specification depends almost exclusively on NT-3 and TRKC signalling, the specification and survival of nociceptors require sequential actions of several factors, the impact of which extends beyond the period of embryogenesis[86].

In mice, the level of Runx1 expression further diversifies immature nociceptors[76,87,88]. Early TrkA+/Runx1- progenitors directly form thinly myelinated A_δ peptidergic fibres[11]. By contrast, TrkA+/Runx1+ progenitors suppress TrkA and CGRP during maturation, which leads to a non-peptidergic cell fate in small diameter C-fibres[87,89]. Murine non-peptidergic nociceptors rely on glia-derived neurotrophic factor (GDNF) by the postnatal expression of Rearranged during Transformation tyrosine receptors kinase (Ret)[79]. In contrast, hepatocyte growth factor cMET extinguishes Runx1 expression to retain TrkA for

a prospective peptidergic cell fate in the rest of C-fibres[90].

Although TRKB defines mechanoreceptors in mammalian embryos, both peptidergic and non-peptidergic C-fibres gradually acquire TRKB expression to grow responsiveness and dependence to BDNF during maturation[86]. Co-expression of TRKA/TRKB has been identified in both rodent and human DRGs[30]. According to a recent publication of single cell atlases of mammalian TGs[5], up to one half of peptidergic nociceptors express *TRKB* while one third of non-peptidergic nociceptor express TRKB in human TGs. In comparison, about two thirds of both peptidergic and non-peptidergic nociceitors are also *TRKB+* in mice (Figure 3)[5].

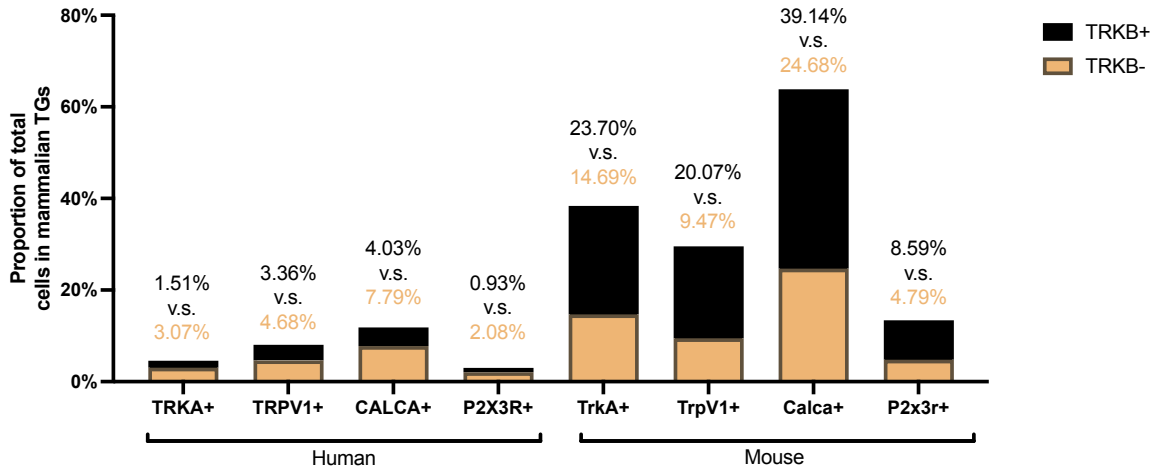


Figure 3: Proportion of cells co-expressing TRKB with conventional peptidergic and non-peptidergic markers in human and mouse TGs.
Percentages representing the fraction of total cells in either human or mouse TGs, including non-neruonal cells. Data extracted from[5].

Consequently, autocrine and paracrine actions of NGF and BDNF can modulate pain threshold in mature nociceptors. NGF is particularly involved in inflammatory pain. Blockade of NGF signalling reduces pain in rodent models[91] and randomised clinical trials[92–94], granting it a promising therapeutic option for osteoarthritis[95]. BDNF modulates the sensitivity of inflammatory and thermal pain in the periphery[96,97], through the reversible enhancement of T-type calcium channels[98].

Despite the progress in understanding the pathway leading to peptidergic cell fates in rodents, less is known in human embryological development. Given that the peptidergic and non-peptidergic division is less distinct in human, the current knowledge in murine and chick

embryo (for detailed reviews see[10]) might not be completely translatable[27,99]. For example, half of the nociceptors in adult murine DRGs are small diameter C fibres that retains TrkA and CGRP expression[66], while in human essentially all C-fibres display peptidergic features based on conventional definitions[20,27,29,30]. Broad expression of Na_V 1.8, Na_V 1.9, TRPV1, substance P (SP), and CGRP is a unique feature in human nociceptors compared to rodents[4–6,20,27–30,73]. There are also significantly more nociceptors in human with co-expression of TRKA/RET[30], TRKA/TRPV1[30], TRKA/Na_V1.8[4,30], TRKA/Na_V1.9[30], TRPV1/P2X3R[20], CGRP/P2X3R[20,29] compared to rodent counterparts.

Neuropeptides

Unlike prototypical neurons, the pseudo-unipolar morphology of nociceptors exhibit biochemical equivalence by bidirectional trafficking of biochemical signals to both the peripheral and central termini[9]. The unique structure of nociceptors leads to autocrine and paracrine communications at both the periphery and with the spinal cord, via growth factors such as neurotrophins, neuropeptides, and neurotransmitters[100].

Neuropeptides are a diverse class of regulatory peptides secreted by neurons[101]. The abundance and variety of neuropeptides result from alternative splicing and post-translational modifications (PTMs).

Neuropeptides are produced in the soma and stored in large, dense core vesicles (LDCVs) throughout the somata (Figure 1a Ganglion panel) and axonal termini of nociceptors[102]. The content and trafficking of LDCVs are subject to complex regulations throughout the nervous system[103,104]. LDCVs may contain the precursors of multiple kinds of neuropeptides, sometimes functionally diverse and opposing, which undergo maturation during translocation along the axons[102,105,106]. LDCVs can also carry excessive ion channels and membrane receptors, thus a potential reservoir for excitability modulators[102,107,108]. The release of LDCV contents at axonal termini requires calcium signalling[109,110].

TG and DRG are both major sites of neuropeptide synthesis[111]. Co-expression and co-localisation of neuropeptides such as CGRP, SP, and somatostatin (SST) have been identified

in human and rodent nociceptors (Table 1).

NEUROPEPTIDES	CO-EXPRESSION	CO-LOCALISATION
CGRP & SP/PPTA	Human DRG (snRNAseq[28]), *Rat DRG (ISH[112])*	*Guinea pig DRG (IR[113]), Rat TG (IR[105,106,114,115])*
CGRP & SST	Human DRG (spatial transcriptomics[4]), Human TG (snRNAseq[5]), *Rat DRG (ISH[112])*	
SP/PPTA & SST	Rat DRG (ISH[112])	Human TG (IR[116])

Table 1: Empirical evidence of the co-expression and/or co-localisation of CGRP, SP, and SST in the literature, (rodent model italicised).
IR, immunoreactivity; ISH, in situ hybridisation; snRNA, single-nucleus RNA sequencing.

CGRP & SP

CGRP exists in two structurally similar isoforms, αCGRP and βCGRP, individually transcribed by *CALCA* and *CALCB* in a tissue-specific fashion[111]. *CALCA* expression is widely distributed in the nervous system, producing calcitonin (exon 4) or αCGRP (exon 5 and 6) via alternative splicing. Although βCGRP is conventionally understood as an enteric peptide, expression of *CALCB* has been confirmed in mouse and human TG more recently[5,117]. The two isoforms display distinct subcellular localisation patterns in trigeminal sensory neurons, with βCGRP exhibiting primarily cytosol distributions[117]. In comparison, only αCGRP is transported to the axons[117]. As a hallmark of peptidergic nociceptors, CGRP-immunoreactive LDCVs can also contain SP[105], SST[105], TRPV1[107], or δ-opioid receptors[102]. NGF, BDNF and TRPV1 agonists, such as capsaicin and rutaecarpine, are known to stimulate the secretion and deplete intracellular stock of CGRP from peripheral nerve endings[111].

Another major pro-inflammatory neuropeptide SP is a splice variant of the gene preprotachykinin A (*PPTA*, alternatively named *TAC1*)[118,119]. Peripheral release of SP by sensory nerve endings recruit immune cells and modulates inflammation[120,121]. Whereas central secretion of SP modulates excitability of the spinal dorsal horn by acutely amplifying synaptic glutamate actions and increasing receptive fields of deep dorsal wide dynamic range (WDR) neruons[122].

Both CGRP and SP are implicated as crucial factors during the development and

maintenance of neuropathic and inflammatory pain for long. Neurogenic inflammation involves antidromic electric signalling travelling from the spinal cord to the periphery, which triggers the secretion of CGRP and SP to peripheral tissues[123]. Both CGRP and SP are potent vasodilators that plausibly further contribute to the chronicity of pathological pain via endocyte actions[122,124]. Ablation of either, via genetic silencing, local immunoneutralisation, or abolishing relevant signalling pathways, has demonstrated promising efficacy in attenuating pathological pain in several types of preclinical models[124–126]. In particular, targeting the CGRP pathway is clinically relevant for migraine treatment[127–129]. However, clinical understandings of the analgesic effect of targetting CGRP for other chronic pain are currently limited.

In contrast, trials targetting the SP receptor NK1R did not yield clinical benefit[130,131]. Additionally, a recent study has identified no significant changes in the transmission of acute or chronic pain in mice with global double knockout (KO) of *CALCA* and *TAC1*, challenging the classic view that both neuropeptides are essential in the physiological and pathological development of pain[132].

Importantly, neuropeptides are modulators rather than switch-like transmitters, as the kinetics, direct downstream targets, and major functions largely differ between neuropeptides and neurotransmitters. Due to long-range target sites and the lack of specific reuptake mechanism, the action of neuropeptides is generally considered to be slower and longer lasting than neurotransmitters[133]. The responsiveness to SP depend on cell type-specific receptors and yield distinct and sometimes opposite site-specific effects. For example, SP-dependent peripheral inflammation is achieved by the activation of Mrgprb2 in murine mast cells instead of NK1R, which triggers downstream inflammatory cascades[125]. Admission of SP paradoxically elicits pain in the spinal cord and abolishes pain in the brain[122,134,135]. Consequently, global KO of SP will plausibly abolish multiple regulatory pathways involved in nociception besides the signal transmission.

Combined, newer body of work indicates that the functions of CGPR and SP should be subject to more refined re-examination, including site-, cell type-, and pathway-specific actions in individual patholgoical conditions to improve therapeutic benefits.

SST

SST is an anti-inflammatory and antinociceptive peptide that exists in two isoforms (full-length SST28 and shorter, neuron-predominant SST14) from the alternative cleavage of preprosomatostatin[133]. Pro-inflammatory signals can trigger both local and remote release of SST in nociceptors[136–138]. Among the five types of somatostatin G-protein coupled receptors (GPCR), subtype 2A is co-expressed with CGRP+ nociceptors in DRG[139]. Postsynaptic somatostatin receptor (SSTR) subtype 4 is counter-regulatory to inflammation and protective against hyperalgesia[136,140]. Agonists for SSTR4 generate potent anti-hyperalgesic efficacy in preclinical studies, granting the channel a potential target for novel analgesics[141,142].

The spinal gate & projection neurons

From DRG and TG, the central processes of nociceptors relay to the superficial layers of dorsal spinal cord and the *subnucleus caudalis* of the brain stem, respectively[24].

The spinal gray matter is conventionally stratified into ten laminae based on the distribution and organisation of neuron subtypes, of which the superficial dorsal region (lamina I and II) receives the majority of nociceptive inputs[24]. Additionally, multimodal WDR neurons in the deep dorsal horn lamina V receive converging signals from all three types of sensory fibres and partake in the spatial summation of nociception[143].

Most neurons residing in the superficial dorsal horn are interneurons that synapse within the spinal cord, of which the majority is glutaminergic for fast synaptic transmission[24]. In the superficial dorsal horn lies a fine network of mechano- and pain-sensing afferent endings, excitatory and inhibitory interneurons, glia, which also receives top-down modulation via the endogenous pathway[144–146] (Figure 4).

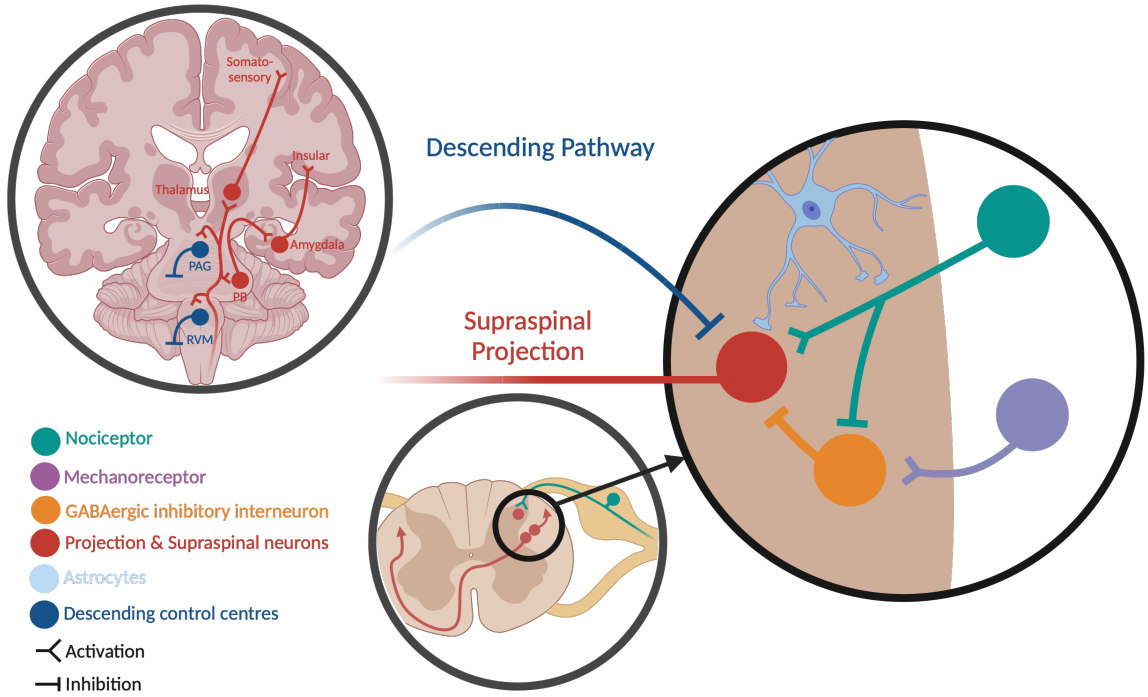


Figure 4: The spinal gate and supraspinal processing centres. Illustrated by BioRender.

The gate control theory of pain proposes a spinal brake mechanism that regulates nociceptor inputs via γ-glutamic acid (GABA)[144–146]. GABAergic inhibitory interneurons in the lamina II *substantia gelatinosa* impose an activation threshold on spinal outputs via projection neurons. Nociceptive signals are further relayed only when the peripheral signal surpasses the threshold. Similar regulatory network is also present in the brain stem, to which trigeminal afferents relay[24]. Altered spinal glial[147–151] and neuronal[150,152–161] architecture, especially the loss of GABAergic gate control, are frequently observed in chronic pathological pain conditions.

Once the spinal threshold is surpassed, nociceptive signals are sent to supraspinal processing centres by projection neurons[162]. One major subset of nociceptive projection neurons is embryologically defined by the transcription factor paired homeobox 2A (PHOX2A) via the anterolateral system ascending along the spinal cord[163–165]. Similar to the periphery, spinal sensory circuitry consists of diverse populations encoding for different stimuli[33]. The circuits for pain and itch are biochemically heterogenous and functionally distinct in the spinal cord[166].

Major supraspinal targets of the ascending pathway include brainstem, thalamus, amygdala,

and multiple cortices integrating sensory, emotional, and cognitive information[9,162,167,168].

Glia in the PNS

Glia are the major non-neuronal components of the nervous system that support neurons in various physiological processes such as development, cytoarchitecture, inflammation and pain modulation, and pathogen recognition[169]. In the PNS, satellite glial cells (SGCs) and Schwann cells (SCs) attend to the intercellular architecture of ganglia and nerve fibres, respectively. Peripheral neuroglial communications in sensory ganglia occur via chemical signalling and direct physical contacts[170].

Neuronal ganglia consist of a unique structure in which SGCs tightly surround and electrically isolate neuronal soma[170,171] (Figure 1a Ganglion panel). Biochemical heterogeneity has been observed in SGCs of TGs, DRGs, and sympathetic ganglia[172,173]. SGCs could be further stratified into subclusters based on functional diversity and molecular signatures[174]. Abnormal coupling between neurons and SGCs, or between multiple SGCs, has been observed in acute and chronic pain in preclinical models[175].

Along the extending axons outside ganglia, SCs commit to myelinating cell fates via dose-dependent paracrine actions from neighbouring neurons during embryogenesis[172]. Meanwhile, small-diameter axons remain associated with non-myelinating SCs in Remak bundles[176]. Both subtypes support axonal structures and metabolic homeostasis independent to the status of myelination, although the major molecular players remain unknown[177]. The involvement of SCs in neuropathic pain has been widely recognised (review see[178]). As SCs canonically orchestra nerve regeneration after tissue injury in the periphery[179], dysfunctions of SC-initiated signalling can lead to peripheral sensitisation via the action of tumour necrosis factor-α[178].

1.1.2 The molecular basis of mammalian circadian rhythm

Most readily observable as the near 24-hour cycle of behaviours and physiological homeostasis, the mammalian circadian rhythm is a self-sustaining physiological property fundamentally governed by an evolutionary conserved motif of circadian genes, namely the transcription-translation feedback loop (TTFL)[180].

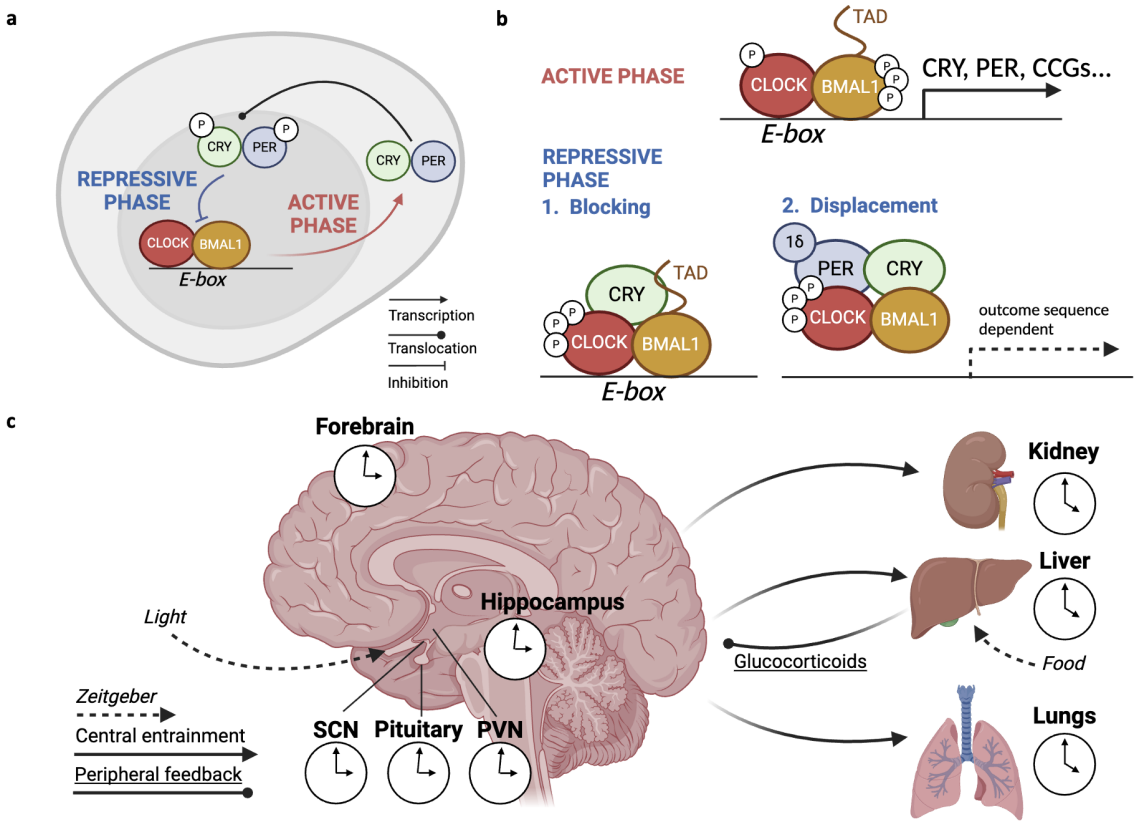


Figure 5: The mammalian TTFL network.
(a) A simplified schematics of the self-sustaining cycle of the core loop. (b) Schematics of diurnally differential phosphorylation of CLOCK/BMAL1 dimer and different modes of transcriptional deactivation by CRYs and PERs. (c) Schematics of the cross-talks between peripheral and central clocks.
CCGs, clock controlled genes. Illustrated in BioRender.

Conserved across multiple phyla, the core TTFL consists of a positive arm driving the upregulation of transcription factors on the negative arm, which in turn down-regulates genes on the positive arm. The outcome is a self-imposed oscillation of transcription activities (Figure 5a).

The core loop is further embedded in a larger regulatory network for fine-tuned, tissue-specific expression modulations. The complex transcriptional regulation of cellular

circadian rhythmicity is achieved mainly through the combined action of three clock-controlled elements: the DNA cis-element E-/E'-box, the DBP response element D-box, and REVERB/ROR-response elements (RREs)[181]. Selective recruitment of clock gene transcripts to compartmentalised translation machinery enhances temporally sensitive translation activation[182].

Beyond expression, PTMs further modulate the subcellular localisation, stability, and kinetics of transcription factor actions[183,184]. Overall, the abundance and activities of the circadian machinery is autonomously regulated at multiple levels including the transcription, translation, PTMs, and degradation of clock genes.

CLOCK & NPAS2

Circadian locomotor output cycles kaput (CLOCK) is a basic helix-loop-helix-PAS transcription factor. Despite being a critical part of the positive arm, transcription of CLOCK is frequently independent on time of day[182]. Paralog protein NPAS2 is the functional substitute of CLOCK in the mammalian clock system. CLOCK canonically carries a more prominent role than NPAS2, as Npas2 KO mice had altered amplitudes for *Per2* and *Bmal1* expression while Npas/Clock double KO completely abolished transcription oscillations[185]. Besides canonical roles in circadian rhythmicity, CLOCK is also recognised as a human-specific hub gene for the frontal pole module in brain development compared to other primates[186], involved in neuron migration[187].

BMAL1

BMAL1 (Basic Helix-Loop-Helix/Brain and muscle ANTR Like 1, alternatively ARNTL or MOP3) is the other major component of the positive arm. The promoter region of *BMAL1* contains both the E-box and two RREs, which ties the regulation of *BMAL1* to both the core feedback loop and the REVERB/ROR adjacent loop[188,189].

In human but not mice, *BMAL1* transcripts undergo alternative splicing that produces two

isoforms: the canonical isoform BMAL1b that shuttles CLOCK to the nucleus[190], and the negative regulator BMAL1a which lacks nuclear localisation signal (NLS) and retains cytoplasmic CLOCK by competitive binding[191].

The lack of functional redundancy in the core clock machinery grants BMAL1 a unique importance[192,193]. Consequently, BMAL1 is commonly regarded as the only indispensable element of the mammalian TTFL to maintain molecular rhythmicity. Ablation of Bmal1 can directly result in the loss of circadian rhythm at molecular and behavioural levels in mice[192–195].

The function of BMAL1 extends beyond clock regulation in a tissue-specific manner[193,196,197], as regional knockdown (KD)[198] and KO[199,200] of Bmal1 can induce abnormalities without abolishing the behavioural clock. BMAL1 has been reported to engage in development[194], immune and inflammation[201–205], insulin-related metabolic homeostasis[206–209] and ageing[194,210,211]. In the nervous system, BMAL1 regulates axonal myelination[212], regeneration[199,213] and synaptic plasticity[214]. S6K1-mediated phosphorylation engages BMAL1 with circadian driven-protein translation in the cytosol[215] and diurnally rhythmic synaptic localisation[214]. Impairment of Bmal1 can underlie psychiatric[216–219], motor[212,220], neurodegenerative[199,200,220–222], endocrine[216,223–225], and metabolic[206–208] disorders.

CRY & PER

The negative arm of core TTFL consists of two families of co-suppressors PERIOD (PER, with mammalian orthologs 1-3[226–228]) and CRYPTOCHROME (CRY, with ortholog 1 & 2[229,230]).

Circadian repressors maintain and tighten periodicity of the mammalian circadian system[231] via individual and interactive actions. Complex interaction between members of the PER and CRY family is revealed by the plethoric phenotypes in combined KO mice models[230]. Cry1[232,233], Per1[234,235] and Per2[236] single KO mice all have accelerated molecular and locomotor rhythms in mouse models, while Cry2 KO triggers a delay[233]. Arrhythmicity has also been observed in Per2 KO mice[235], which can be rescued by Per2/Cry2 double KO[237].

Combined Per1/Cry2, double Cry or double Per KOs completely abolished behavioural rhythmicity in mice[233,234,238]. No single PER or CRY protein alone is sufficient to restore circadian rhythmicity in triple KOs[239].

In the classic TTFL model, CRY and PER proteins suppress CLOCK/BMAL1 activity by two distinct modes of binding (Figure 5b). CRY proteins block CLOCK/BMAL1/E-box activities by simultaneously binding to the PAS domain of CLOCK and the transactivation domain (TAD) of BMAL1 in the CLOCK-BMAL1 heterodimer[240]. The competitive binding of CRY orthologs sequesters the CLOCK/BMAL1 against co-activators, leading to suppression of transcriptional activation. CRY2 binds to CLOCK with less affinity than CRY1, which can be compensated by additional PER2 binding[240].

In comparison, direct binding of PERs to CLOCK/BMAL1 is considered less stable or functionally relevant in mammals compared to *Drosophila* counterparts[241]. Nuclear entry and engagement with CLOCK/BMAL1 of PER mostly rely on CRY[242]. The nuclear entry of Cry1 is circadian driven[243]. As a consequence, active PER2 exhibits regular and rhythmic nuclear localisation facilitated by either CRY ortholog[232,244]. Although PER3 is often considered non-essential, the CRY-dependent nuclear PER complex can contain all three PER and both CRY orthologs, together with other transcriptional repressors[245]. Alternatively, PER2 can interact with CLOCK/BMAL1 heterodimer indirectly via promyelocytic leukemia protein (PML)-facilitated nuclear localisation and binding[190]. Overall, about a quarter of total Per2 remains cytoplasmic regardless of circadian time[243]. Once entering the nucleus, PER recruits casein kinases to remove the CLOCK/BMAL1/CRY complex from DNA[246]. However, the exact transcriptional impact of PER-initiated displacement depends on the promoter or enhancer sequence.

Although the negative arm is conventionally considered to have similar temporal patterns of expression and distribution, a more recent study revealed that the acrophase of Cry1 expression is more closely aligned with that of Bmal1, both temporally from the oscillation of Per2[243]. Consequently, the presence Cry1/Per2 complex rather than Cry1 protein alone is more antiphase to that of Bmal1.

Besides directly serving as the repressive arm of TTFL, most PER and CRY repressors

are directly associated with metabolic functions. For example, PER1 exerts liver-specific functions on oxidative substrate selection[247]. PER2 co-regulates transcription factors including REVERBα of the adjacent loop to modulate metabolism[248]. The cryptochromes are tied to cell metabolism via adenosine monophosphate-activated protein kinase (AMPK)-dependent[249] and -independent[250] pathways, depending on the state of pluripotency. CRY1, therefore, can act as a positive regulator of pluripotency maintenance[250].

Furthermore, both PER1 and PER2 engage in DNA damage responses and tumour suppression, as the loss and alteration of either PER1 (e.g.[251–253]) or PER2 (e.g.[254–256]) have been associated with multiple types of cancer. Despite sequence similarity and assumed functional redundancy, either PER ortholog is subject to distinct and diverse PTMs[257] and functional regulations[233]. Although PER1 and PER2 exert independent and non-redundant roles over the transcription regulation of some genes[234], it appears that PER2 is more important than PER1 in mammals[246]. Loss of Per2 has been associated with deficits in stress responses[258] and greater vulnerability to substance addiction[259].

Kinase action in the core loop

The activity and stability of circadian proteins are actively regulated by PTMs, among which phosphorylation plays a multimodal and indispensable role.

The major class of enzyme responsible for clock gene phosphorylation is the casein kinase family. Casein kinase 1 consists of six isoforms, among which 1δ and 1ϵ are well-known circadian regulators[260]. Casein kinase 1δ stably binds to PER proteins, of which two competing phosphorylation sites act as switches of PER stability[261]. The extent of PER phosphorylation is correlated with PER polymerisation[262]. Nuclear entry of casein kinase 1δ in complex with PER and CRY during the repressive phase hyperphosphorylates CLOCK, which is otherwise hypophosphorylated in the active phase[246,263].

Besides casein kinase, glycogen synthase kinase 3 (GSK3) is another prominent contributor of circadian-modulating phosphorylation, with known engagement with PER2[264], CRY2[264], CLOCK[265], and BMAL1[266] in the core loop, as well as REV-ERBα[267] in the adjacent

loop. Both isoforms of GSK3 demonstrate diurnal variations in phosphorylation-driven inactivation with distinct peaks of activities[268].

BMAL1 is hyperphosphorylated in the repressive phase in opposite trend to that of CLOCK. The phosphorylation and degradation of BMAL1 appear to be maintained independently from transcriptional activation, with partial contribution from S6K1[215] and GSK3[268]. Although purified BMAL1 protein can be a substrate to major casein kinases *in vitro*, dual inhibition of casein kinase $1\delta/\epsilon$ inhibition produced conflicting results on nuclear BMAL1 phosphorylation[246,269]. Mitogen-activated protein kinase (MAPK) is reported to inhibit BMAL1 by phosphorylation on multiple cites[270]. Bmal1 remains hyperphosphorylated in the liver of double Cry KO mice[246]. Dephosphorylation of BMAL1 is associated with protein phosphatase 4 (PPP4) action[261].

In mice, neither constitutive transcription nor abolishing RREs in the transcriptional activation of Bmal1 directly impairs the rhythmicity of Bmal1 phosphorylation, and consequently, Bmal1 degradation[189,271]. Even in absence of canonical Bmal1 promoter control, the amount net Bmal1 protein remain oscillating due to tonic protein degradation, thus maintaining circadian regulations on *Per2*-luciferase activities[189,271].

Molecular mechanism of cellular period definition

Cooperative and progressive hyperphosphorylation of PER proteins is considered the master rhythm and molecular time-definer of the circadian clock, with active integration of environmental cues[262,263,272,273]. The dual actions between short-period associating PER1 and long-period associating PER2 confine the specific period[236].

PER phosphorylation likely drives circadian timing by mediating rapid nuclear entry and repressing action after a critical delay period during which PER proteins accumulate around the nucleus[262], as casein kinase $1\delta\&\epsilon$ double KO leads to perpetual hypophosphorylation and perinuclear disposition of Per[274].

As PER phosphorylation can alternatively lead to degradation, PER stability is positively associated with cellular circadian period[272]. Stabilisation of CRY proteins lengths

circadian period[275,276], as CRY proteins directly regulate PER2 transcription[233] and protect phosphorylated PER species from degradation[257]. By contrast, genetic variations of casein kinases[277,278] or phosphorylation sites on PER2[279] can induce large alterations in the circadian period.

Besides PER regulations, other phase definition machineries have also been identified through reverse genetics methods. Variations in the Bmal1 TAD sequence alters circadian periods in murine fibroblasts via Cry1 actions[280]. The level of CLOCK/BMAL1 transactivation and consequently, the length of transcriptional feedback, can be altered by PPP4-induced BMAL1 dephosphorylation[261].

Peripheral & Central clocks

The exact proportion of circadian regulation of all protein coding genes is species- and tissue-specific, ranging from 43% in mice[281] to 82% in non-human primates in at least one organ[282]. It is estimated that most human cell types possess molecular oscillators[283]. Multiple universal cellular processes are known to be directly tied to circadian control, such as RNA post-transcriptional modification[284], translation quality control[285], cellular metabolism[286,287], cell cycle[288–290], and oxidative stress responses[291].

Major players from TTFL also differ in a species- and tissue-specific manner[281,282]. Yet, the mechanism of selective and rhythmic gene expression driven by a cell type-specific subset of oscillating TTFL genes is still unknown.

The innate clock in individual cells is loosely synchronised by local paracrine signalling[292] and ultimately governed by the principal pacemakers in the hypothalamic suprachiasmatic nucleus (SCN)[293,294]. The SCN orchestrates the biological clock under the influence of environmental factors, among which light is the most powerful cue[295]. Light detection by retinal photoreceptors modulates GABAergic neurons in the SCN, which informs downstream hormonal and neuronal activities[283,296–299]. Within the SCN, the core neurons integrate external inputs while the shell neurons generate robust circadian oscillations in gene expression[300]. Neurons in the SCN display intrinsic daily cycles of electric activities,

coupled to nuclear regulations of the TTFL and cytosolic messengers[300]. Consequently, isolated SCN can maintain indefinite, independently phased oscillations of clock gene expression[301,302].

The acrophase of clock gene expression can vary among individual peripheral tissues[303], different parts of the brain[304] and the SCN. Distinct patterns of core oscillators have been identified in *ex vivo* peripheral tissues, such as the eye[305], secretary glands[303,305], liver[303,306–309], heart[307,309], spleen[309], lungs[303,309], and fibroblasts[310]. Despite the presence of molecular clock machineries in individual cells, it is believed that most types of peripheral cells gradually lose intercellular phase coherence *ex vivo* without synchronisation cues.

Independent to light, entrainment via food anticipatory activities can synchronise the SCN via Bmal1 action[311]. It is also possible to locally synchronise certain peripheral tissues such as the liver without the SCN. Hepatocyte oscillators can synchronise to feeding cycles independent of central entrainment in mice with SCN lesion[312,313], or when Bmal1 was selectively abolished in the SCN and forebrain[309].

Overall, the circadian organisation of cellular functions can be understood as a three-step model (Figure 5c): the cell-autonomous circadian clock throughout the body, internal and external entrainment cues as synchronisation inputs, and circadian-regulated tissue-specific functional outputs[229].

1.1.3 Circadian patterns in mammalian pain

The wide distribution of circadian machineries in mammalian systems indicates the importance of temporal regulations of core cellular and physiological processes, which include the regulation of pain perception. Emerging evidence from preclinical studies suggests that the timing of pain perception, modulation, and response to analgesic treatments are subject to circadian rhythmicity, which could have profound implications for both the understanding and management of pain[314].

Models to study the behavioural patterns of human circadian pain

Most behavioural evaluation of the daily fluctuations of human pain thresholds is derived from uncontrolled clinical observations and randomised controlled trials[314]. Clinical reports can include both healthy volunteers and patients of defined pathological conditions, which might face the issue of lacking standardised measures of outcomes and difficulties of recruiting sufficient sample sizes for each time point[315]. Randomised controlled trials tend to include more socio-economically and physiologically homogenous samples, which leads to challenges of external validity[316]. However, it is still possible to systematically review the association between circadian phases and certain types of pain or mathematically model the pattern of fluctuation (e.g.[314,317]).

Although lab-based experiments of human subjects with controlled light, metabolism, activities, and sleep are common in the more general field of chronobiology, it was introduced relatively recent to the studies of circadian pain (e.g.[318,319]). Common considerations of experimental designs include substance use (e.g. common analgesics, nicotine, alcohol, and cannabis), sleep disturbances, menstrual cycles, and age[320].

Models to study the behavioural patterns and molecular basis of mammalian circadian pain in preclinical rodent models

Preclinical animal studies provide an essential complement to human physiological research by preserving systemic interactions, allowing easier and controlled genetic and/or pathological modifications, and permitting combined behavioural and molecular research.

Both pain and circadian rhythmicity have been modelled in rodent[321,322]. Unless modified otherwise, lab animals display innate, intact, and indefinite oscillations of multiple physiological processes, to which a diverse range of models can be applied to approximate human pain conditions.

The ease of genetic modification in animals further allows direct labelling and/or interference of clock components or pain-related genes, which facilitates the investigation of functional interactions. Reporters such as luciferase and fluorescent protein tagging support live and continuous monitoring *in vivo* (e.g.[323]) and *ex vivo* (e.g.[324]), which hugely improve the temporal resolution of sampling for molecular assays. Empirical evidence of the association between clock disruption and pathological pain usually begins by genetically or transcriptionally altering a core clock gene (see sections below).

However, studies with lab rodents must consider potential drawbacks of indirect behavioural measures, pool translational efficiency, and fundamental interspecies differences[325–327]. For example, melatonin, a critical circadian hormone in human, is lacking in most strains of lab mice except for CBA and C3H, despite overall similar circadian physiology[327–329]. The nocturnal nature of rodents imposes further challenges to compare with human physiology, which demands precautions and consistency over experimental designs.

Limitations in current research methodologies of mammalian circadian pain

One challenge of the emerging intersection of circadian and pain studies is the lack of standardised methodology, presented as poor and inconsistent experimental designs between published protocols, insufficient method reporting, sampling disparity, and significant female under-representation[3].

The choice for specific pain models can be a factor of discrepancies between findings, especially when interspecies comparisons are discussed. Thermal and mechanical hypersensitivities commonly measured in rodent pain assays are not prevalent in human with chronic pain conditions, despite being accurate reflections of the development of pain pathology. Home-cage behaviours are common measures for circadian studies[330] and sometimes proxies for "quality of life" when spontaneous pain behaviours are identified

(e.g.[331–333]).

In addition, conflicting results can be introduced due to technical variability of assay equipments. For example heat pain induced by thermoelectric Peltier-type thermodes demonstrated circadian variations in human[318] while laser-induced heat pain via contact thermodes did not[334,335]. When testing multiple kinds of pain together, some studies reported rhythmicity in some modalities but not others (e.g.[336,337]).

The nocturnal nature of rodents imposes further challenges to align *in vivo* results. Although chemical synchronisation unifies cellular oscillators in similar ways in nocturnal and diurnal species *ex vivo*, *in vivo* experiments require precautions of inconsistencies in light exposure and operation time, which are frequently under-reported.

Conserved behavioural patterns of mammalian circadian pain

In this section, we use the term "sensitivity" loosely to include all behavioural aspects of pain perception that are common quantitative measures in pain assays. An increased sensitivity can refer to, objectively or subjectively, a lowered threshold of activation and signal transduction, a lowered tolerance, or a higher intensity of pain when the same stimulus is applied.

There is no direct evidence that the daily variations in pain thresholds mechanistically depends on the phase of locomotor activities[338]. However, light exposure, food intake, sleep, mobility, and individual differences can be co-factors of pain perception, especially under pathological conditions[339]. Therefore, we aligned current pre-clinical and clinical findings by light and dark phases (Table 2).

In healthy human, daily rhythmicity of pain threshold has been discovered in multiple modalities, including pressure/mechanical[319,337,340], noxious hot[318,336] and cold[336]from a combination of clinical observations, randomised trials, and controlled lab experiments.

A recent controlled lab experiment modelled sinusoidally rhythmic threshold of thermal pain matching with daily fluctuations of melatonin, heart rate, and parasympathetic activities in healthy men[318]. Another experiment identified a similar wave pattern of mechanical pain

in 23 healthy volunteers, including both men and women[319]. The two studies estimated that 80% to 93% of variation in daily changes of human physiological pain thresholds can be attributed to circadian mechanisms[318,319]. Mathematical modelling of human data further implies that the sleep cycle does not surpass circadian-driven variation of pain perception under physiological conditions in human, estimated to account for 20% impact[318,341].Combined, the majority of data indicates a higher sensitivity to mechanical and thermal pain at night[318,319,342].

In comparison, many types of chronic pain have been observed to shift, disrupt, or possibly abolish the innate temporal patterning of pain perception (review see[314,343–345]). For instance, fibromyalgia[346], migraine[347], osteoarthritis[348], and rheumatoid arthritis[349] are associated with higher pain scores in the morning. Whereas pain intensity peaks at night in patients with diabetic neuropathy and/or postherpetic neuralgia[350,351]. Common analgesic treatment, such as morphine, gabapentin, and nortriptyline, could reduce pain scores but did not reset or alter the circadian rhythmicity of neuropathic pain[350,352].

In preclinical models, innate circadian variations of pain threshold via behavioural assays have been reported in wild type naïve animals (formalin[353,354]; thermal[355,356]; postoperative[357]), in animals with induced chronic pain without investigating naïve behaviours (neuropathic[358–360]), in animals with induced chronic pain but not naïve counterparts (migraine[361]; neuropathic[331,362–364]), or in both naïve and pathological (migraine[1]; neuropathic[365]).

Opposite acrophase of inflammatory and thermal/mechanical pain oscillations, acute or chronic, has been noticed in some pre-clinical research (Table 2review see[366]). Research on acute inflammatory pain in human is limited, currently leading to no conclusive pattern[345].

In conclusion, the circadian rhythmicity of pain is a conversed and integrated feature of mammalian pain, which can be altered under pathological conditions. However, there is currently no known factor that dictates the acrophase time of pain intensity based on the type of pain pathology.

PAIN TYPE	MORE SENSITIVE AT LIGHT PHASE	MORE SENSITIVE AT DARK PHASE	NO DIFFERENCE
Naïve cold		Human[336]	Human[337]
Naïve hot	Mice[355,366]	Human[318,336], Mice[356,365]	Human[335]
Naïve inflammation	Mice (Formalin[354])	Mice (Formalin[329,353,366])	
Naïve mechanical		Human[337,340], Mice[367]	Human[336], Mice[336,361–363,368]
Fibromyalgia	Human[346]		
Migraine	Human[347], Mice (Nitroglycerin-induced[1,361])		
Neuropathy	Mice (Chemotherapy-induced[331], Constriction-induced[358], Nerve ligation-induced[359,363–365,368]), Rats (Constriction-induced[358])	Human (Diabetic[350,351]), Mice (Diabetic[362])	
Osteoarthritis	Human[348]		
Rheumatoid arthritis	Human[349]		

Table 2: Empirical evidence of daily fluctuations in mammalian pain sensitivities from behavioural results, aligned to light and dark phases.

Current understandings of the molecular basis of mammalian circadian pain

Two major streams of hypotheses have been proposed to account for the mechanism that gives rise to circadian pattern of pain[338]: The *Circadian Gatekeeper* hypothesis claims that such pattern is mainly established by a tonic central control via the descending pathway of pain; whereas the *Distributed Rhythm* hypothesis suggests that circadian properties are present in multiple neuronal and supportive cell types of the pain pathway, which generates an integrated clock pattern of pain.

Therefore in this section, we review published evidence of the presence of clock throughout the ascending pathway and the potential functional relevance to pain processing.

Genomic associations

The impact of TTFL on pain can be manifested when genetic alterations of core clock genes exert influences over the pain system. In human, PER3 variable number tandem repeat (VNTR) polymorphism is reported to affect the innate opioid pathway[369]. One recent genome-wide association study (GWAS) associates PER3 with susceptibility to chronic pain in females only[370]. Another study reports that mutations in casein kinase 1δ which phosphorylates PER2 can drive familial migraine and an advanced sleep phase[371].

One report found that global Per2 loss-of-function abolished the development of mechanical hypersensitivity without impacting acute physiological pain sensitivity in male mice with neuropathic pain[364]. In comparisons, neither conventional double KO of Per1/2[361] nor Cry1/2[1] attenuated the development of chronic pain in nitroglycerin (GTN)-induced chronic migraine models. However, the lack of circadian repressors abolished the circadian variations in pain thresholds once mechanical allodynia was established[1,361]. Furthermore, Per2 loss-of function by partial deletion was found to shift the phase of formalin-induced pain behaviours in $Per2^{Brdm1}$ mice compared to wild-type[354].

Clock mechanism in mammalian sensory ganglia

In the periphery, direct investigation of core clock gene dynamics in murine TG[1,353,361,372] and DRG[331] supported the presence of an innate oscillating peripheral clock present at the

level of transcriptional regulations. Although single-cell transcriptomics has confirmed the expression of clock genes in post-mortem human TG[373] and DRG[374], the ability to further map out cell-type specific clock patterns is so far limited due to the lack of reports in time of death. It is at least reported in one recent study that sensory neurons and SGCs individually possess autonomous molecular oscillations with close phase coherence in mice[1]. It is likely that different neuronal subtypes exhibit further diversified patterns of molecular oscillations, as electric inputs of peripheral tactile and nociceptive afferents to the spinal dorsal horn are both circadian, in temporally inverse relations[317].

Although the molecular mechanism of circadian-regulated peripheral outputs of nociception is still largely unknown, current evidence has identified the multifaceted involvement of BMAL1 in sensory neurons. BMAL1 can directly regulate the expression of pain-related genes such as SP[354] via transcriptional activations of E-box in promoters. Bmal1 also directs peripheral axon regeneration by mediating tidal expressions of epigenetic factors Tet3[213]. Functionally, Bmal1 KO in pan-sensory neurons abolished circadian variations of pain thresholds in a mouse migraine model[1]. Selective Bmal1 KO in Na_V 1.8+ nociceptors reduced chronic pain development in a murine osteoarthritis model[375]. These results imply the possibility of a sensory neuron-specific function of Bmal1 contributing to both physiological and pathological pain, partially by regulating pain-related gene expression.

Nociceptor-specific ion channels are potential targets of circadian regulations, which can lead to oscillations in electric and biochemical outputs. Speculations of the circadian relevance of TRP channels in mammals rooted from evidence in *Drosophila*[376]. Central circadian pacemaker neurons in *Drosophila* rely on inputs from peripheral thermo-sensing neurons to entrain to environmental temperatures, likely through the activation of TrpA1[377,378]. Although the extent of conserved functional regulation of TRP channels is still unknown, biphasic transcription has been observed for TrpA1 in naïve mouse TGs[353], TrpV3 in neuropathic mouse DRGs[331], and for TRPV1 in human oesophagus[379]. TrpV1 level also varied within daytime in male mice[331].

Circadian regulations in the spinal dorsal horn

As a critical relay centre of pain, the spinal cord is likely an ensemble of multiple cell type-specific clocks acting in tandem, along with external modulations from both the peripheral afferents and the descending central control.

Clock genes expressions are detected in bulk in the spinal cord[373,374,380,381] and known to oscillate in spinal astrocytes[382,383] and microglia[384]. Although less is known about the cellular clocks in interneuron subtypes, neuronal genes such as N-methyl-D-aspartate receptor (NMDAR)[358], Na+/K+ ATPase[385], cyclooxygenases[386], glutamine synthase[386], cFOS[353], and TRPA1[353] all display circadian rhythmicity in bulk expression in the spinal cord. Although the endogenous opioid pathway is circadian regulated and melatonin-dependent[387,388], no daily fluctuation in opioid receptor expression was detected in the spinal cord[365]. The local expression pattern of clock genes can be altered after central sensitisation or spinal cord injury[358,382,386,389].

The spinal gate clock is likely co-regulated both biochemically and electrically. Tonic release of biochemical signals in the spinal cord has been identified, such as SP[354] from peripheral afferents and dopamine[367] from the hypothalamic A11 nucleus.

It is technically challenging to fully model the complex electric circuitry of the spinal gate due to the complexity of interneuron types and networks. However, with simplifying assumptions of circadian-patterned peripheral sensory inputs without influences from top-down modulation, a mathematical model describes how the spinal gate contributes to a higher spinal threshold of pain during the day due to stronger A_β activities[317].

Presence of clock in supraspinal centres of pain

Limited experiments have been conducted to directly link the circadian rhythmicity to pain functions in supraspinal pain centres[338]. Although most observations were not exclusively related to pain, certain somatosensory and mood-regulating centres–and the brain overall–have been shown to possess clock gene oscillations and functional fluctuations.

Besides the master clock SCN, multiple regions within the hypothalamus exhibit oscillating clock gene expressions[390,391]. Signalling molecules such as pituitary adenylate cyclase-activating peptide (PACAP) and BDNF have been found to be strong oscillators that mediates

metabolism-dependent circadian activities in several nuclei of the hypothalamus[390], both of which also can serve as pain mediators. Neuropathic pain induced by partial sciatic nerve ligation shifted the phase of circadian oscillations in melatonin receptor 1A/1B transcripts in murine hypothalamus[392].

The periaqueductal gray (PAG) receives direct neuronal inputs from the SCN[393] and displays a clock gene rhythm *ex vivo* when chemically synchronised[394]. A population of GABAergic neurons in ventrolateral PAG is responsible for regulating sleep[395]. Opioid receptor expression was found to be regulated by time-of-day in the murine PAG, disrupted under neuropathic pain[365]. Similarly, molecular clock rhythmicity has also been found in the amygdala[394,396]. Disruptions of clock in either region has been associated with depression[394,396], which is known as a frequent co-morbidity with chronic pain[397].

The somatosensory cortex expresses Per1 but no oscillation could be detected *ex vivo*[398]. Recent studies have identified circadian changes of the expression synaptic markers and dendritic morphology associated with locomotor activities and light conditions, suggesting temporal regulation of synaptic plasticity[399–401].

Overall, innate molecular oscillations in both clock-related and known pain-modulating gens have been identified in supraspinal pain centres. However, the direct functional relevance to pain processing is yet to be established.

Impact of other systems

Besides the neuronal and glial clocks of the pain pathway, it is generally agreed that the daily variations in pain sensation are influenced, if not directly co-modulated, by systemic circadian factors such as locomotor activities, body temperature, hormones, and immune/inflammatory activities[345,402,403]. Both pain pathology and disrupted circadian rhythms can directly alter the immune and endocrine systems, which possess distinct rhythms[345] and can further feedback to pain perception which modifies pain thresholds in a vicious cycle[338,339]. In musculoskeletal pain disorders such as osteo- and rheumatic arthritis, pain exacerbations can be a direct consequence of movement and activity, thereby co-relating to the active phase.

In summary, the current evidence supports the *Distributed Rhythm* hypothesis of a coordinated network of region- and cell type-specific clocks. Complex interactions with other systems such as the immune and endocrine functions further contribute to the modulation of a tightly controlled temporal output of pain.

1.2 Rationale, aims & proposed methodology of the current study

Following the *Distributed Rhythm* hypothesis, previous work in our lab has identified that cell type-specific molecular oscillations exhibit in primary sensory neurons and SGCs, and that the peripheral nociceptive clock is the major driver of behaviour oscillations of pain thresholds[1]. Based on these results, the current project hypothesises that an autonomous molecular clock relevant to pain function is a conversed feature in the human nociceptive pathway, especially of the nociceptors as the critical starting point of pain detection.

Molecular studies, such as transcriptomic analysis, on post-mortem human tissue can provide some insights on the level of expression and distribution by cell types of clock genes. However, currently available studies provided no temporal continuity as most human post-mortem tissues were sampled in a range of time after death, exact timing usually unspecified in experimental designs[396]. There are additional concerns addressing the potential light pollution for post-mortem tissue collection at night[3].

Therefore, the current project aims to seek alternative methods that resembles the developmental process and molecular signature of human nociceptors, meanwhile allowing the induction of clock oscillations in controlled environment. More specifically, we will undertake further investigation in the circadian rhythmicity of human nociception using human induced pluripotent stem cell (hiPSC)-based models.

HiPSC-derived *in vitro* models are powerful tools that mimic developmental processes and produce transcriptionally comparable components of the human physiology, which compensate for fundamental interspecies differences of rodent models and ethical challenges for tissue collections from human *ex vivo* (review see[404]).

Notably, HiPSC-based experiments provide valuable cell type-specific models usually in sacrifice of tissue complexity, systemic interactions, and integrated behavioural responses. Consequently, one limitation of iPSC-derived nociceptor (iNociceptor) cultures is the variation in differentiation efficacies and transcriptomic outcomes, owing to genetic background of cell lines, initial density, and culture conditions[405]. Therefore, the current project will characterise hiPSC-derived cultures in depth, including the roles of supportive

cells co-developed or co-cultured with iNociceptors. We will also supplement primary cells and tissues as positive controls for functional comparisons.

Although hiPSC-derived neuronal models of pain (e.g.[41]) and circadian rhythmicity (e.g.[406]) individually exist, few reports integrate both aspects (e.g.[1]). By optimising the *in vitro* conditions to combine both aspects of stem cell technology, the current project aims to answer whether the circadian rhythmicity in the expression of TTFL components is present in hiPSC-derived *in vitro* cultures, and if so, whether such pattern has significant correlations to nociceptive functions on a cellular basis. We hope that the current project can shed light on the molecular mechanism of human pain rhythmicity by fulfilling the following aims:

1. Develop and optimise iNociceptor models that resemble multiple types of neuronal components of the human nociceptive circuitry (Chapter 2 and relevant supplementary sections). Cell identities will be verified via a combination of transcriptional, immunolabelling, and electrophysiological methods.

2. Establish culture conditions that robustly induce and monitor molecular oscillations of core clock genes, via verified oscillator cell types as positive controls (Section S3.3, S3.6-S3.7).

3. Investigate the circadian rhythmicity of core TTFL components in iNociceptors, via transcriptional and proteomics methods (Chapter 3).

4. Evaluate the correlation between cellular circadian patterns and nociceptive functionality, including expression profiles of neuropeptides & ion channels and electrophysiological properties (Chapter 3).

2 Development & Optimisation of Components Modelling Human Sensory Ganglia

2.1 Overview

Pioneer work from Chambers and colleagues[407,408] identified dual SMAD inhibitions (dSMADi) as the critical step to induce early ectoderm that is the progenitor to all CNS and PNS neurons. Mature sensory neurons derived by Chambers variations exhibit transcriptomic profiles comparable to human DRGs, with markers of all three sensory neuron subtypes expressed[409–412]. The original Chambers protocol yields 60% TRKA+ nociceptor progenitors by flow cytometry (FC) at d10[408]. However, the exact proportion of each sensory neuron subtype derived from Chambers' variations can be protocol- and batch-dependent. Progenitors of nociceptors, mechanoreceptors, and proprioceptors can be separately purified by fluorescence-activated cell sorting (FACS)[408] and the less invasive immunopanning[413] based on TRK channel expression.

A combined approach of sensory neuron categorisation is increasingly more common for *ex vivo* tissue by matching transcriptomic landscapes and sensitivities to a diverse ranges of sensory modalities in individual cells (see Stratification of nociceptors in Section 1.1.1). In comparison, studies of sensory neurons derived *in vitro* reference back to names and key markers from clusters defined by *ex vivo* sequencing assays to confirm authenticity. A widely recognised hallmark for successful differentiation is the prominent expression of Na_V 1.7 which is the major VGSC of all sensory neurons[41,414]. Soma size and baseline electrophysiological properties might vary depending on the method and stage of differentiation[415].

Although global single-cell transcriptomic assays are frequently recruited for nociceptors derived *in vitro*, functional characterisation is often limited to responses to selected stimuli for key markers of interest. For example, Chambers' iNociceptors express an

array of functional ion channels, which can be pharmacologically modulated (Table 3). In particular, Chambers' nociceptors broadly express TRPV1[416]. However, most cells derived from variations of the Chambers' protocol lack electrophysiological responsiveness to capsaicin with no proposed explanation[411,417]. Consequently, Chambers' iNociceptors are conventionally regarded as non-peptidergic.

CHANNEL	METHODS	PROPERTIES
TRPV1	Calcium imaging	Minor response to capsaicin[411,417], especially when pre-treated with NGF[418]
	Patch clamp	Response to capsaicin, concentration-dependent[416,419], in 10% cells in healthy control line[420]
	Genetically encoded voltage indicators	Thermal allodynia at 40 degrees in erythromelalgia patient lines[421]
TRPA1	Calcium imaging	Response to allyl isothiocyanate (AITC) in about 10% cells in healthy control line[420]
TRPM8	Calcium imaging	Response to menthol in <10% cells in healthy control line[420]
$GABA_AR$	Calcium imaging	Moderate response to GABA, concentration-dependent[417]
	Patch clamp	Response to GABA, concentration-dependent[411,416]
Purinergic	Calcium imaging	Response to ATP derivatives, especially when pre-treated with NGF[418]
	Patch clamp	Response to ATP and derivatives[408,416,419]
	MEA	Response to ATP, concentration-dependent[419]
HCN1	Patch clamp	Fast hyperpolarisation-activated currents & voltage relaxations[411]
KCNQ	Patch clamp	Response to pan- and selective channel opener retigabine & ICA-096673[411]
ASICs	Calcium imaging	Response to pH drop in majority of cells[420]
	Patch clamp	Response to pH drop[411]

Table 3: Empirical evidence of channel-specific electrophysiological properties of Chambers' variations.

Published attempts for deriving human "peptidergic" nociceptors *in vitro*, therefore, mainly focus on the production of TRPV1-expressing, capsaicin-responsive, neural crest neurons, either via chemical induction[99,414,422], ectopic expression of key transcription factors[423–425], or a combination of both[426–428] (Table 4). Alternatively, recent research of *in vitro* nociceptor development has also adapted 3D organoid research, aiming to model ganglion tissue complexity to facilitate cell fate specification with dynamic innate spatial organisation (e.g. DRG[73] & TG[429]). TG, in contrast to DRG, consists of neurons from both CPs and

neural crest, the latter of which migrates into TPs during development[83]. Neural progenitors from CPs and neural crest share the same set of transcription factors, such as TFAP2A and PAX3, which mark the neural border intermediates before further development[68,83,430]. The transition to either specific lineage is fine-tuned by the crosstalk between bone morphogenetic protein (BMP), fibroblasts growth factor (FGF) and Wingless & Int-1 (WNT) pathways in a tempo-spatially sensitive manner[68,431].

Mature TG and DRG neurons are usually assumed to be similar, despite different cellular compositions, differential transcriptomic profiles, and distinct innervation destinations[432]. Although small molecule cocktails that generate CP progenitors have been defined and verified in the literature, fewer studies specifically address TG models (e.g.[433–436]) than DRG protocols. Preliminary attempt demonstrated retained trigeminal identity following neuronal enrichment and maturation[436]. There is also a general lack of in-depth molecular profiling of cultured TG nociceptors compared to the DRG counterparts, *in vitro* or *ex vivo*. The most striking gap across iNociceptor models of either DRG or TG origin is the lack of neuropeptide production. Few studies have specifically tested for the secretion of neuropeptides (Table 4), in particular CGRP. Given the clinical significance of CGRP and its receptors, the gap remains in literature for a reproducible method of generating CGRP-secreting iNociceptors.

AUTHOR	STARTING CELL TYPE	METHOD OF DIFFERENTIATION	CONVENTIONAL PEPTIDERGIC MARKERS				COMMENTS
			CGRP	SST	SP	TRPV1	
Wainger et al. (2015)[424]	Fibroblasts (mouse & human)	2D, TF transduction	IF (mice only)				Low neuronal conversion rate; Inadequate characterisation in human samples.
Blanchard et al. (2015)[423]	Fibroblasts (mouse & human)	2D, TF transduction	IF (mice only)			RT-qPCR, Capsaicin CI	Low neuronal conversion rate; Acclaimed pseudounipolar morphology.
Lee et al. (2015)[427]	Blood iNPCs	2D, TF transduction + Chemical induction	RT-qPCR		RT-qPCR, IF	RT-qPCR, Capsaicin CI	
Wilson et al. (2018)[99]	hEPI-NCSCs	2D, Chemical induction	RT-qPCR, IF		RT-qPCR, IF	RT-qPCR, Capsaicin CI	Unconventional morphology.
Muller et al. (2018)[434]	hiPSCs	2D & 3D, Chemical induction	ELISA		IF, ELISA	IF	Characterisation at d22; 2D and 3D Schwann cell co-cultures.
Guimaraes et al. (2018)[422]	hiPSCs	2D, Chemical induction			ELISA	IF, anandamine induced SP release	
Vojnits et al. (2019)[428]	Blood iNPCs	2D, TF transduction + Chemical induction				Capsaicin CI	Same chemical induction as Chambers[408]
Hulme et al. (2020)[426]	hESCs	2D, TF transduction + Chemical induction		IF		IF	

Table continues next page.

AUTHOR	STARTING CELL TYPE	METHOD OF DIFFERENTIATION	CONVENTIONAL PEPTIDERGIC MARKERS				COMMENTS
			CGRP	SST	SP	TRPV1	
Schrenk-Siemens et al. (2022)[425]	hESCs	2D, TF transduction + Chemical induction				ISH, Capsaicin CI	Modified from[424]; Focusing on TRPV1-responsive and PIEZO2+ mechanosensitive variations.
Deng et al. (2023)[414]	hiPSCs	2D, Chemical induction	RT-qPCR, IF		RT-qPCR, IF, EM, ELISA	RT-qPCR, IF, Capsaicin CI	
Kalia et al. (2024)[437]	hiPSCs	2D, Commercially available kit (RealDRG^{TM})			IF	IF, thermal MEA, Capsaicin CI	Acclaimed faster induction than Chambers[408]; Mature measurement at d35.
Kim et al. (2024)[429]	hiPSCs	3D, Chemical induction				Capsaicin CI	
Lu et al. (2024)[73]	hESCs	3D, Chemical induction	snRNAseq			Capsaicin CI	Major aim to match with human sensory neurogenesis, no mature data.

Table 4: Currently available protocols for the differentiation of peptidergic nociceptors in vitro.
CI, calcium imaging; ELISA, enzyme-linked immunosorbent assay; EM, electron microscopy; hEPI-NCSCs, human epidermal neural crest stem cells; hESCs, human embryonic stem cells; IF, immunofluorescence; ISH, in situ hybridisation; iNPCs, induced neural progenitor cells; MEA, multi-electrode array; RT-qPCR, reverse transcription/real-time quantitative polymerase chain reaction; snRNAseq, single nucleus RNA sequencing; TF, transcription factor.

Overall, the current project has identified the need to generate a reproducible hiPSC-derived nociceptor protocol that can produce neuropeptides and be readily adapted to different biophysical platforms. Therefore, the following chapter aims to:

1. Reproduce a variation of the Chambers' protocol and explore culture conditions that generate eletrophysiologically active TRPV1 (Section 2.2).

2. Reproduce a TP protocol and improve the efficiency of neruonal differentiation (Section 2.3.1 & S3.4).

3. Optimise culturing conditions for and characterise neuropeptide-secreting TG iNociceptors (Section 2.3.2-2.3.3 & S3.4). Available multi-omics datasets of post-mortem human sensory ganglia will be used to compare molecular profiles.

4. Identify potential factors that diversify nociceptor cell fates *in vitro* (Section 2.3.2-2.3.3 & S3.4).

5. Incorporate iNociceptors with vascular components for increased tissue complexity that better approximate the cytoarchitecture of primary sensory ganglia (Section 2.3.4).

2.2 Generation of DRG (neural crest) non-peptidergic iNociceptors *in vitro*

The current project began by reproducing a Chambers variation of DRG iNociceptors[438] using the healthy wild type (WT) hiPSC line SBAD03.

At d12, most cells derived were sensory neuron progenitors positive for TRKA and/or TRKB by immunolabelling. Proportion of total TRKA+ cells at d12 (about 55%, Figure S21) was similar to reported values[408].

To facilitate long-term culturing, we treated replated cultures with cytosine-β-arabinofuranoside (AraC) to remove pre-mitotic non-neuronal cells[416]. TRKA expression was lost by d65, while TRKB expression was significantly upregulated in mature cultures (Figure 6 & 16a), both patterns matching with mammalian non-peptidergic nociceptor development *in vivo*.

Despite relatively high expression at d12, the expression of peptidegic marker cMET was extinguished and superseded by non-peptidergic marker RUNX1 and RET by d60 (Figure 6 & 16a). Most mature cells were TRPV1-immunoreactive (Figure 6 & 7), similar to reports from published literature[416]. The hallmark of non-peptidergic cell fate P2X3R was prominently present and co-expressed with TRPV1 in Chambers' iNociceptors (Figure 7a-b).

In constrast, high transcript abundance of *TRPM8* could also be confirmed in mature Chambers' iNociceptors, whereas *TRPA1* transcripts could not be amplified (Figure 7c). Similarly *in vivo*, TRPV1 expression is widely present in multiple subtypes of nociceptors in adult human DRGs, while TRPM8 and TRPA1 displayed minimal co-expression (Figure 8).

Despite upregulated transcription of *SP* (splice variance specific), *SST*, and CGRP propeptide, there was a lack of CGRP immunoreactivity (Figure 6).

The presence of mechanoreceptors in mature Chambers' culture was expected to be minimal despite no purification, as TRKA-/TRKB+ progenitors were scarce in progenitors (Figure S21). The expression of *PIEZO1* was low compared to that of *PIEZO2* in mature iNociceptors, which is ubiquitously present in DRG neurons *in vivo*[439,440] and *in vitro*[425] for painful and non-painful mechanosensation.

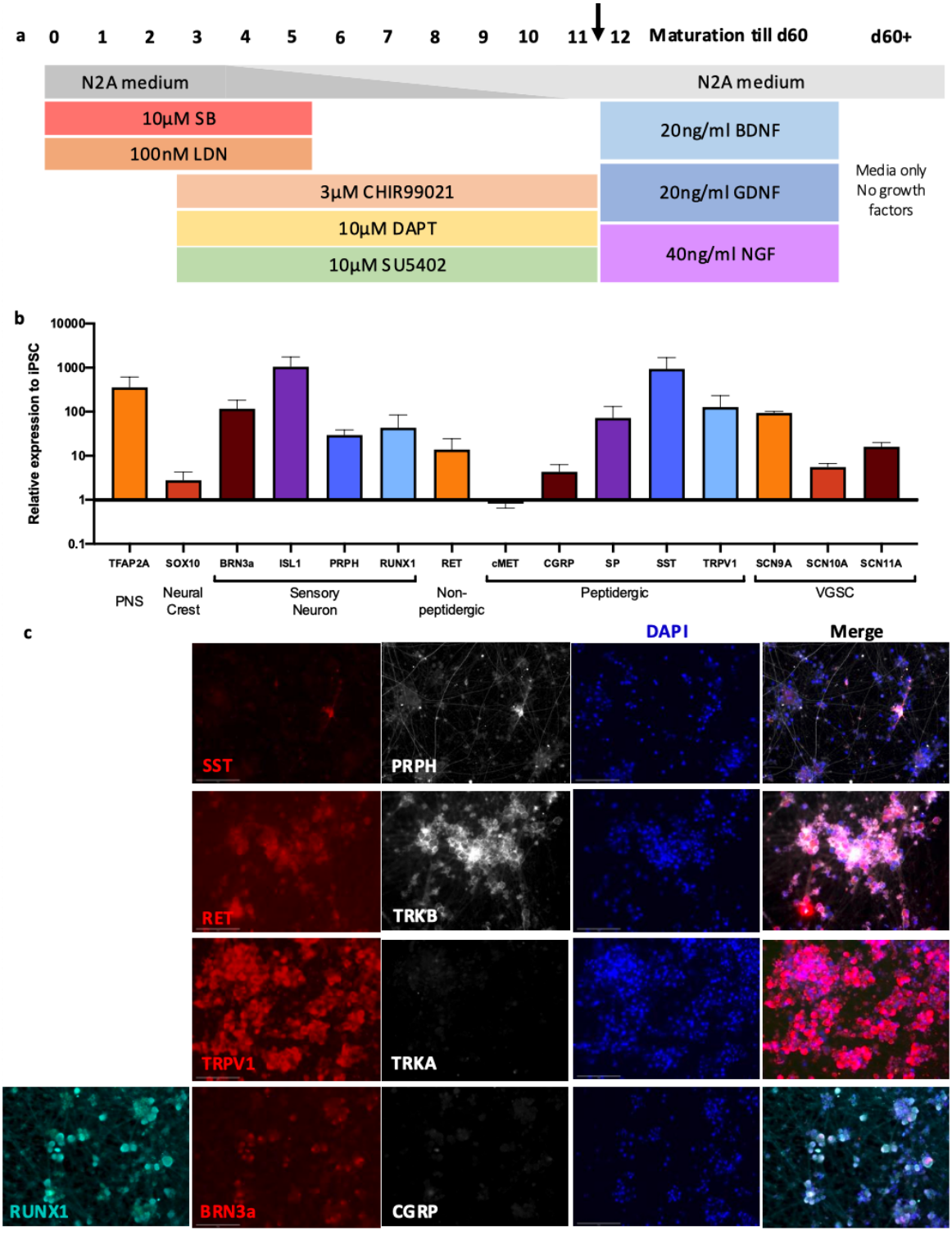


Figure 6: Confirmation of DRG iNociceptor identities by Chambers' method.
(a) Schematics of DRG non-peptidergic iNociceptor differentiation protocol. Arrow indicates the day to replate for maturation. (b-c) Markers expressed in d65 SBAD03 DRG iNociceptors demonstrating neural crest non-peptidergic identities confirmed by (b) RT-qPCR and (c) IF, n=3 independent differentiations. (b) Error bar standard deviations. (c) Scale bar 150µm.

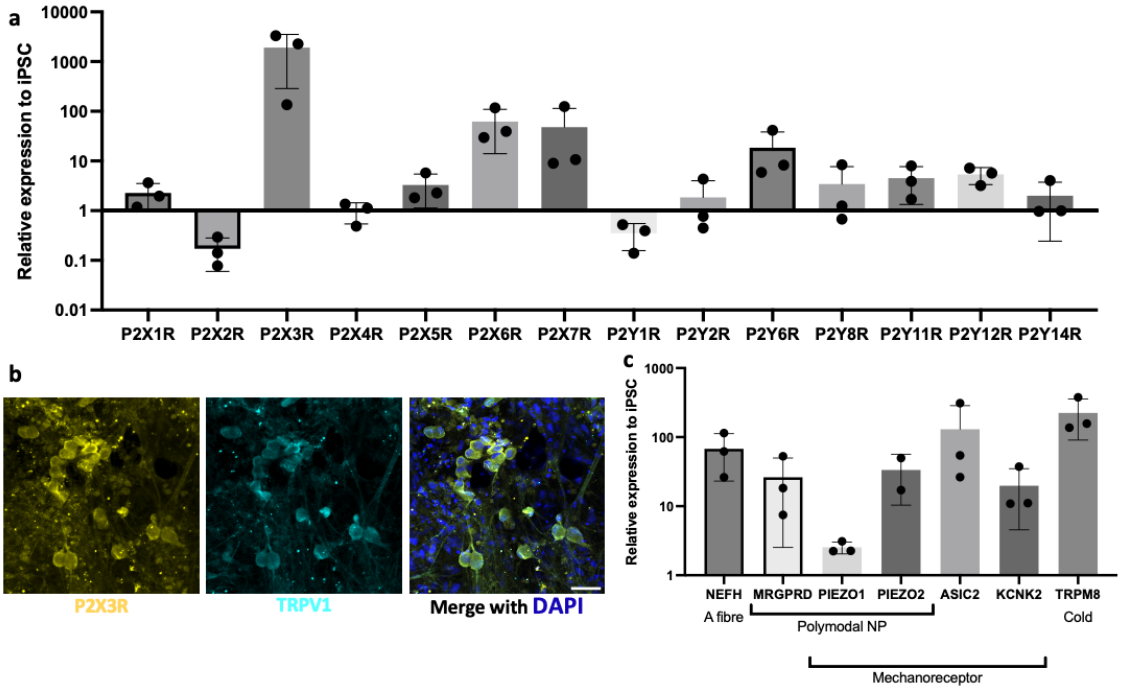


Figure 7: Selective expression of sensory neuron markers in SBAD03 DRG iNociceptor cultures. (a) Purinergic channel expression confirmed by RT-qPCR. (b) Co-expression of P2X3R and TRPV1 in mature SBAD03 Chambers' iNociceptors identified by IF. Scale bar 25µm. (c) Expression of identity markers of RUNX1+/RET+ subpopulations by RT-qPCR in SBAD03 DRG iNociceptors. For all panels, n=3 independent differentiations each. Error bar standard deviation in panel (a) & (c).

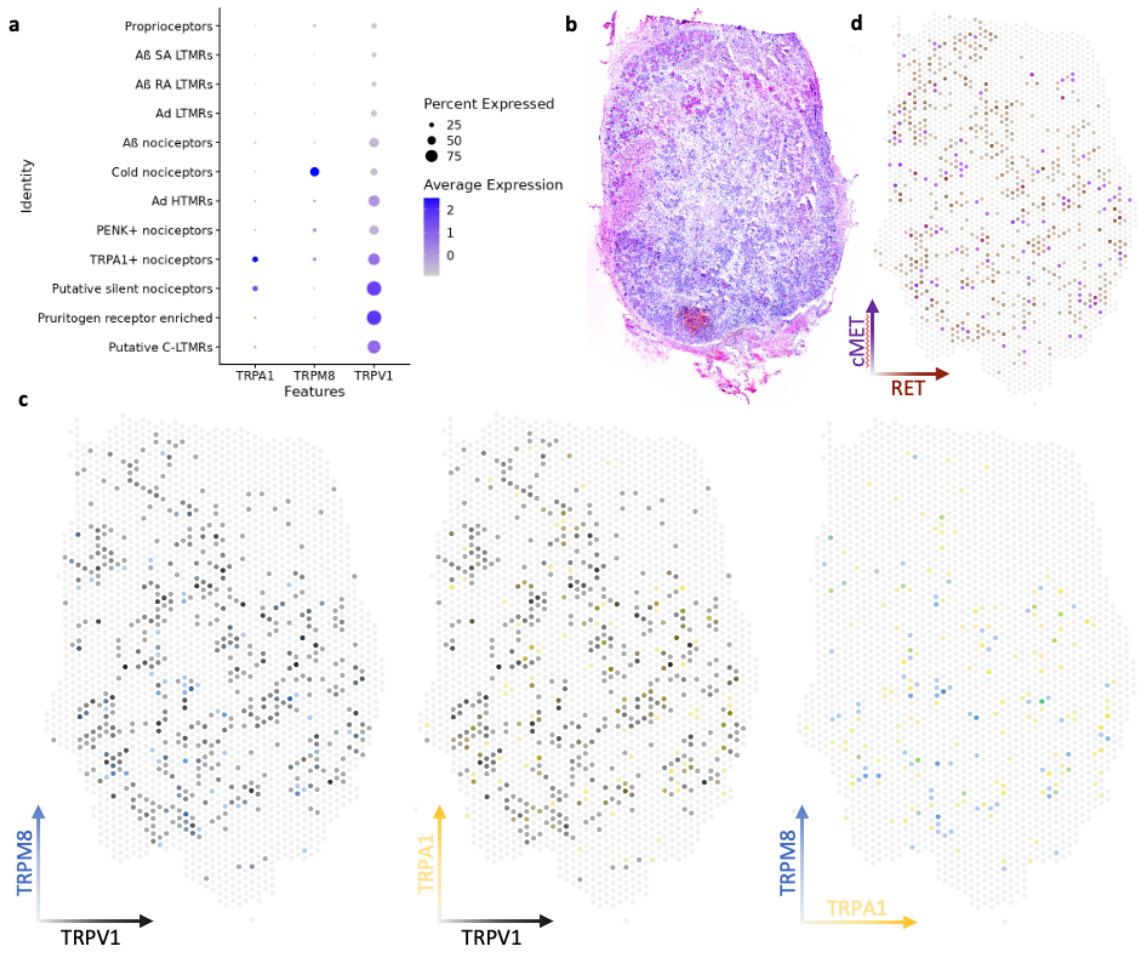


Figure 8: Representative distribution of TRP channels and conventional peptidergic/non-peptidergic markers in post-mortem human DRGs, identified by cluster-based spatial transcriptomics[4].
(a) Dot plot of the abundance and distribution of gene expression in sensory neuron clusters. (b-d) (b) Histological image, (c) TRP channel co-expression, and (d) retained competitive marker that determined peptidergic/nonpeptidergic cell fates of representative ex vivo human DRG section (Sample ID VM4-2).

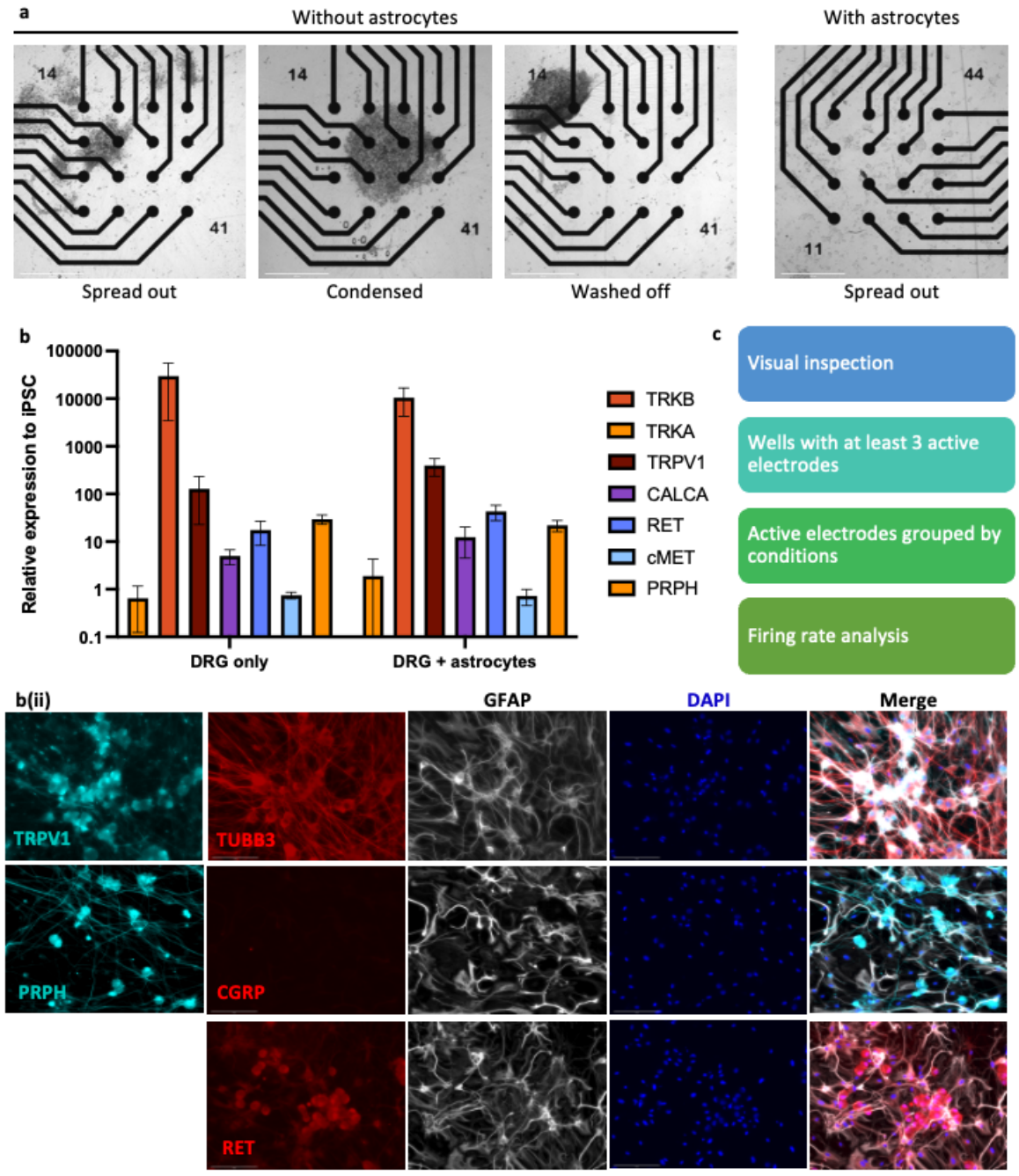


Figure 9: Phenotypic modulations of DRG iNociceptors in astrocyte co-cultures. (a) Representative brightfield images showing morphological changes of DRG iNociceptor colonies with and without primary neonatal rat cortical astrocyte co-cultures on MEA platform by d65. Scale bar 650µm. (b) Expression of identity markers in DRG iNociceptor-astrocyte co-cultures confirmed by (i) RT-qPCR and (ii) IF, n=3. (i) Primers specific to human. Simple effect determined by two-way ANOVA: gene of interest 50% total variation, $F(6,28)=6.626$, $p=0.0002$; the addition of astrocytes 1.785% of total variation, $F(1,28)=1.470$, $p=0.2354$; interaction 11.67% of total variation, $F(6,28)=1.525$, $p=0.2066$. (ii) Scale bar 150µm. (c) MEA analysis selection criteria.

Electrophysiological properties of DRG iNociceptors were verified by multi-electrode array (MEA, Figure 10). We supplemented primary neonatal rat cortical astrocytes to facilitate neuronal attachment to electrode surfaces, which can be significantly affected by cumulative disturbances of media change and handling (Figure 9a & S6). No dedifferentiation, adverse changes in morphology, or increased CGRP production were identified with the presence of astrocytes (Figure 9b). Co-culturing with SGCs[441] was not possible due to limited commercial availability.

We first optimised the culture conditions for spontaneous and evoked firing activities of SBAD03 DRG iNociceptors. Although action potentials could be detected by d35 (Figure S7), we conducted MEA assays after d65 to allow electrophysiological maturity[442].

The level of spontaneous activities was compared between iNociceptors cultured in Neurobasal-A (N2A) and BrainPhyz (BP) media, both with N2 and B27 (without vitamin A) supplements. Cultures were allowed at least 24 hours of adaptation after media exchange. Cells in Neurobasal A-based maturation media produced fewer spontaneous firings, similar to previous reports in human induced cortical neurons[443] (Figure S8).

Synaptic network activities were present in cells cultured in both media, which can be effectively removed by an acute application of non-selective glutaminergic synaptic inhibitor cyanquixaline (CNQX)[444,445]. CNQX was therefore added when examining selective channel responses for more accurate reports of cellular firings, with less interference from network activation.

It is conventionally understood that most Chambers' neurons do not respond to TRPV1 agonists despite high channel expression[411,417]. However, it is still unknown whether the lack of capsaicin-induced TRPV1 activities in Chambers' neurons is due to an innate deficit of the differentiation program or a consequence of suboptimal environmental factors. Attempts to optimise TRPV1 responsiveness have included temporally defined NGN1[418] or NGN2[446] expression along with chemical inductions, or concentration-dependent NGF pre-treatment before electrophysiological assays[418].

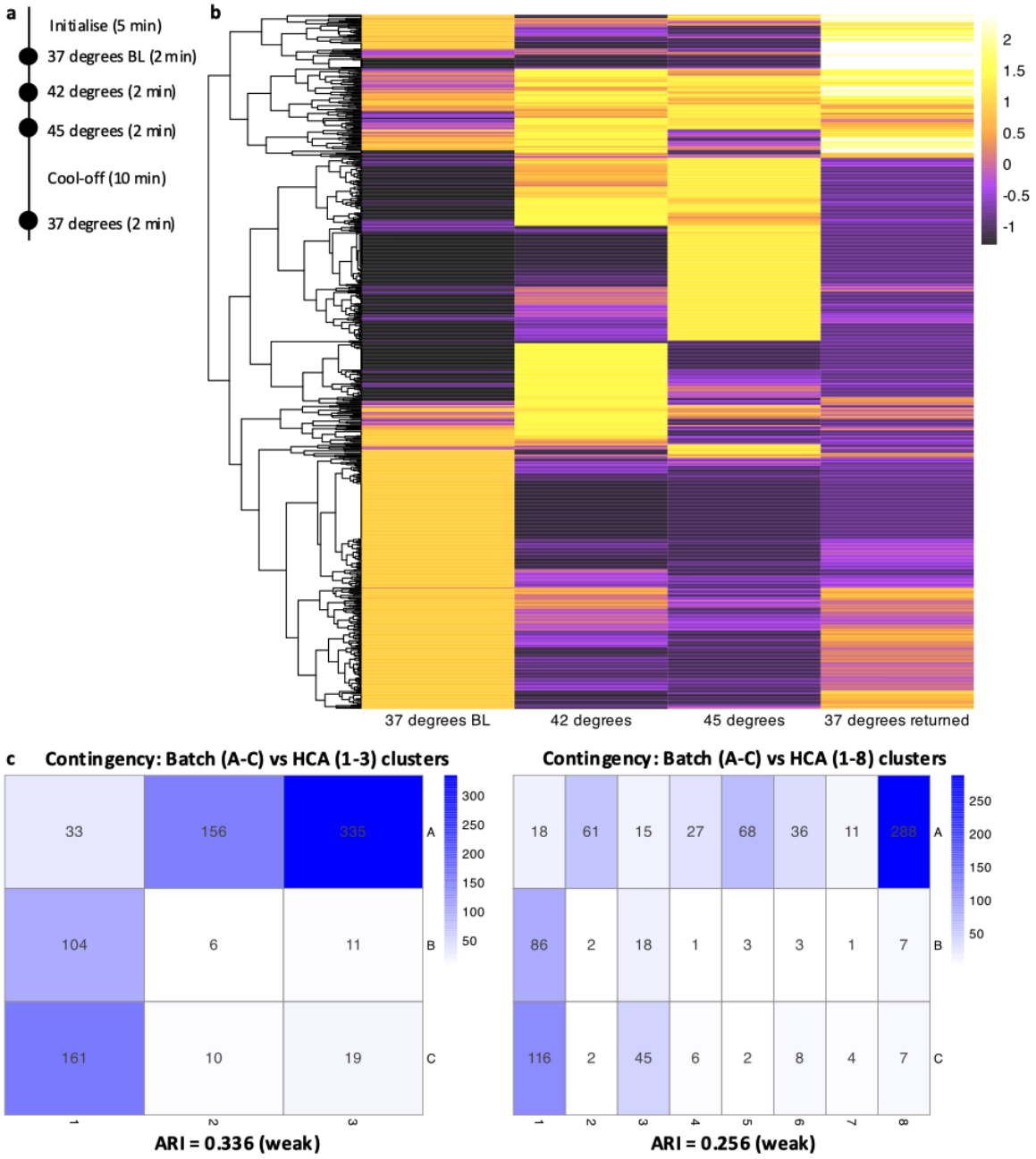
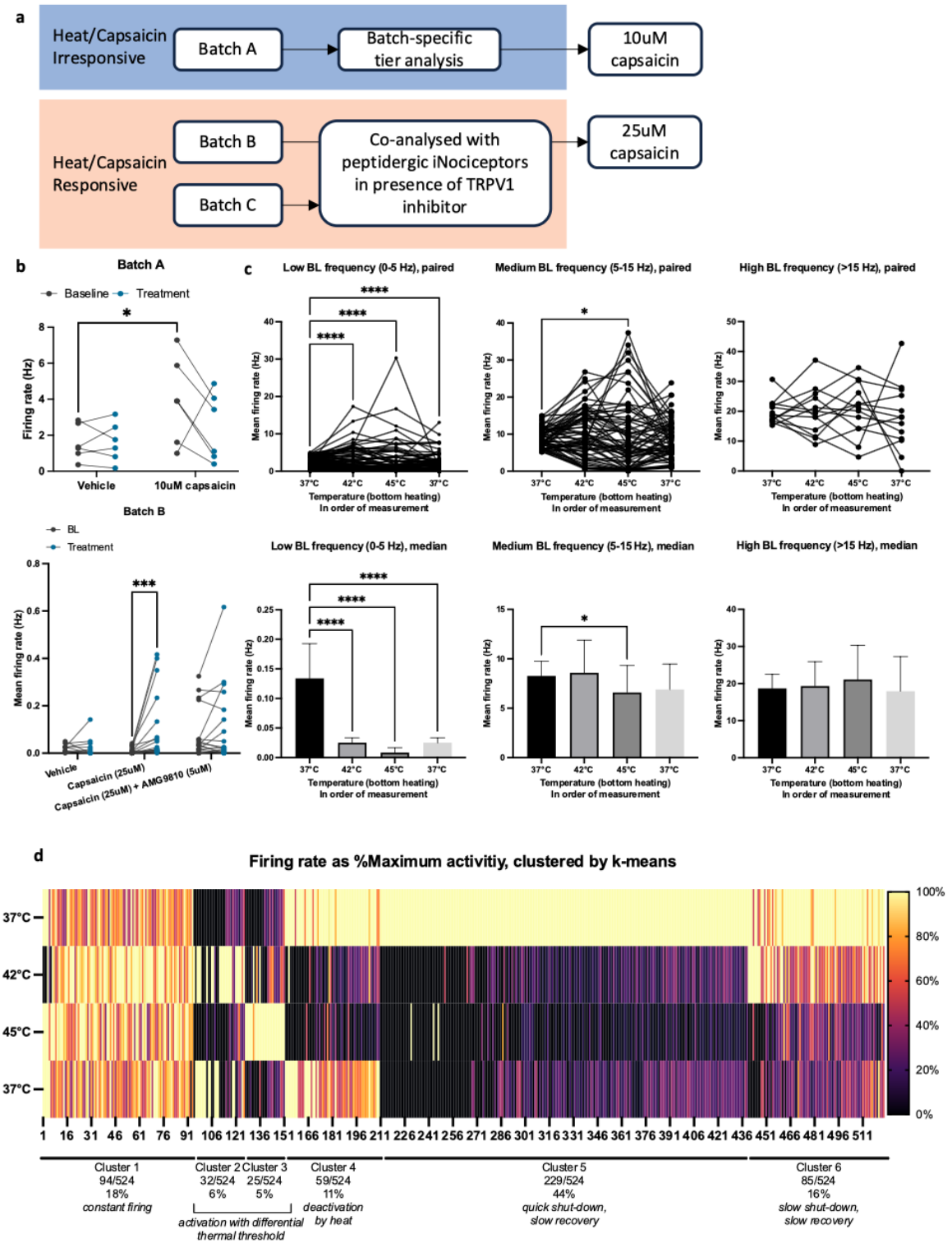


Figure 10: Responses to noxious heat in SBAD03 DRG iNociceptors.
(a) Schematics of heat sequence and the order of MEA measurement. (b) Hierarchy clustering analysis of all firing electrodes pooled from three individual batches perform in R, with Euclidean distance. (c) Heatmap of contingency tables comparing similarities between HCA and batch of origin of either k=3 or k=8 (arbitrarily chosen for batch effect comparison). Batch effect minimal but present. ARI computed by R.



(Caption see next page.)

Figure 11: Further experiments and analysis based on batch-differential heat responsiveness in SBAD03 Chambers' iNociceptors (figure see previous page).
(a) Schematics of further experiments based on heat response. (b) Differential responses to capsaicin in Batch A heat-irresponsive and Batch B heat-responsive Chambers' iNociceptors, TRPV1 involvement in the latter confirmed by selective antagonist AMG9810. For both panel, statistical significance determined by RM two-way ANOVA. (c-d) Changes in mean firing rates per electrode in Batch A, analysed as (c) tiers of BL firing rates or (d) %maximum activities ordered by k-means clustering. (c) Tier division by conventions. Statistical significance determined by Friedman (non-parametric) test with Dunn's multiple comparisons: Low BL frequency p<0.0001, medium BL frequency p=0.0002, high BL frequency p=0.8087. Error bars 95% confidence interval. (d) k-means clustering performed in R, graphed in cluster order in GraphPad Prism.

As TRPV1 is independently activated by heat and capsaicin (see Section 2.5.3 for literature review), we suspected that the lack of response to capsaicin does not necessarily imply the lack of responses to heat, knotted toxin (DkTx), other selective activators, or a combination of such. Therefore, we applied an ascending heat sequence to three independently differentiated plates of SBAD03 Chambers' neurons and measured their firing activities. Extreme heat above 48 degrees was avoided to prevent irreversible damage to cell viability.

The heat map of normalised activities revealed differential firing patterns of Chambers' iNociceptors in presence of noxious heat, ranked by non-biased hierarchy clustering analysis (HCA) cross-examined with batch of origin (Figure 10). Although the adjusted rand index (ARI)[447] between HCA and batches is weak, there was an uneven distribution of Batch A in certain clusters regardless of the number of clusters cut from the dendrogram, indicating non-trivial batch effects (Figure 10c). Batch A yielded about 11% neurons that produced more firing when noxious heat was applied (Figure 11 & 21). In comparison, the majority of electrodes in Batch B & C were reactive to noxious heat by increasing firing activities in a TRPV1-dependent manner (Figure 21). Electrophysiological responsiveness (or the lack of) to noxious heat also co-related with that to capsaicin in Batch A & B (Figure 11b).

further categorised firing patterns of electrodes in Batch A by tiered baseline activities (Figure 11c, cut-off chosen by convention) and k-clusters of normalised activities (Figure 11d, for easier interpretation). There was a significant reduction in firing activities in most low-frequency neurons from Batch A (Figure 10c-d), which has not been characterised previously in the literature. Electrodes of medium and high baseline frequencies were more resistant to temperature changes, likely representing big neuron clusters (into which bottom

heating was hard to penetrate) or cell types other than thermo-sensors. The cause of such batch variations remained inconclusive.

In conclusion, the Chambers protocol consistently yielded mostly non-peptidergic DRG iNociceptors due to the lack of cMET and CGRP, and the overriding presence of RET and TRKB over TRKA by d65. Although TRPV1 activities varied by batches, at least 10% were responsive to known agonists which was similar to previous reports.

2.3 Generation of TG CGRP+ peptidergic iNociceptors *in vitro*

2.3.1 Optimisation of the induction efficiency of sensory neurons of placodal identity

To bridge the gap of a reproducible CGRP+ TG iNociceptor model, we optimised a TP generation protocol[435]. We first confirmed the reproducibility of placodal induction on traditional 2D culture plates. TPs could be consistently reproduced in multiple lines, time of appearance varying slightly by cell lines (Figure S11 & S12a-b).

Compared to other sensory neuron cocktails such as Chambers', low neuronal induction rate appears to be a common caveat of TP protocols when the correct ectodermal patterning is prioritised (e.g.[433,435], summarised as Figure S10). Therefore, we identified and quantified subpopulations of sensory neuron progenitors by TRK receptor expression and distribution before attempts at enrichment. The majority of sensory neurons derived was nociceptors, as *TRKA* expression was prominent with minimal *TRKB* and undetectable *TRKC* transcripts (Figure S12c-d). Positive selection by sorting TRKA+ population from total cultures enriched *SIX1* and *ISL1* expression, with no difference in the level of *SOX10* expression. The ubiquitous level of expression of SOX10 in total and TRKA+ progenitor enriched populations indicates the presence of both neuronal and non-neuronal neural crest derivatives derived from the original TP protocol (Figure S12d).

As most cells of neural border origins were packed within the placodes (Figure S12b), TRKA+ nociceptor progenitors could be significantly enriched by manually isolating the placodes from the whole culture (Figure S12d). Prevalent bipolar MAP2+ neurite outgrowth from both SOX10+ and SIX1+ lineage was observed in manually isolated placodes after 24 hours of incubation with BDNF (Figure S12f).

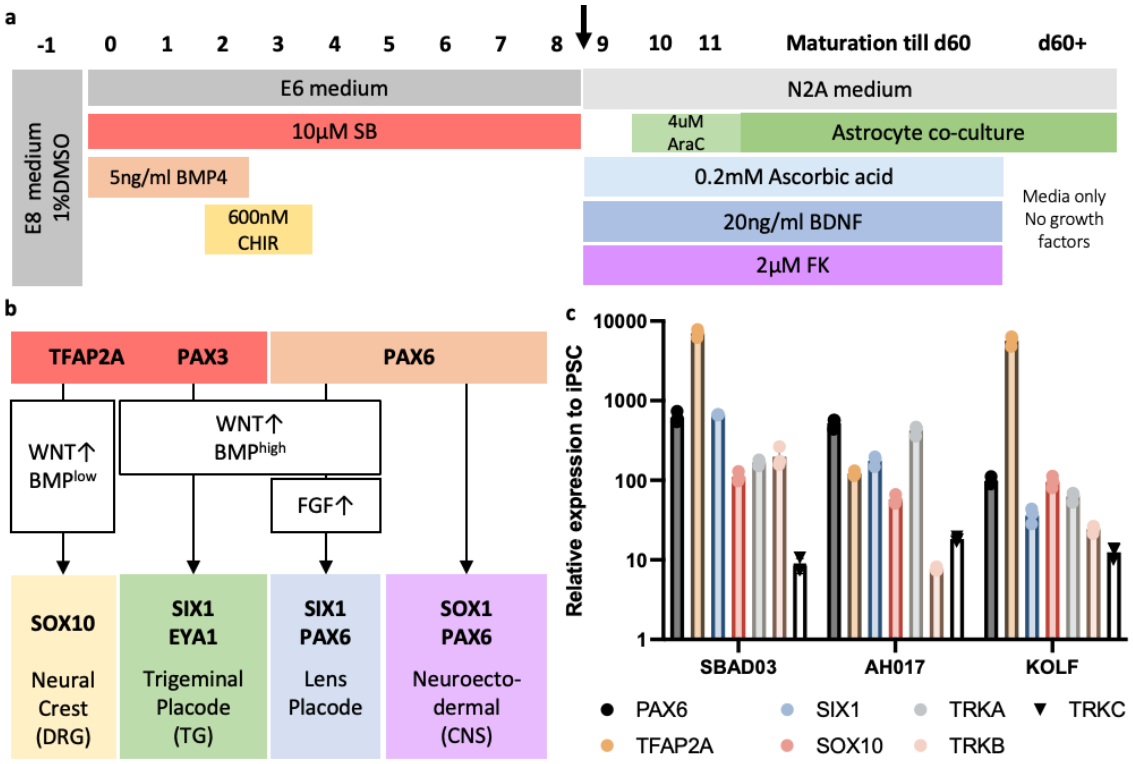


Figure 12: Differentiation of hiPSCs towards TP lineage.
(a) Schematics of TG peptidergic iNociceptor differentiation protocol. Arrow representing the day of subculturing for maturation. (b) Schematics of master signalling pathways that define competitive ectodermal cell fates. (c) Differential expression profiles of key transcription factors and TRP receptors of d8 TG iNociceptor progenitors. n=3 independent differentiations in 3 WT lines. Error bar standard derivations.

To fully take advantage of the intercellular communication and cell-autonomous organisation during placodal induction, we migrated the protocol to 3D cultures. Early embryoid body formation was introduced before the onset of directed differentiation, to bypass the challenge of even seeding and forceful 3D cellular organisation on a 2D surface (Figure 12).

We also compared the effect of DMSO pre-treatment[429,448] on improving neuronal induction for both culture formats. Susceptibility to DMSO appeared to be cell-line specific. Taking SBAD03 WT as an example, we noticed consistent cell death with DMSO supplementation higher than 1%, presented as lower starting cell count or slower expansion later in differentiation (Figure S13a-c). Therefore, we applied 1% DMSO during embryoid body formation for all relevant cell lines (Figure S13d, see also Section 2.3.4). Similar to 2D-derived TPs, *TRKA* transcript was significantly upregulated (Figure 12). TRKB+ mechanoreceptor progenitors were minimal (Figure 22c).

Cell-line dependent differences in TP induction were observed, including variations in the differentiation efficiency of TRKA+ progenitors (Figure 22) and placode morphology (Figure 22 & Figure S14). Therefore, we reconstructed the expression and organisation patterns of neural border derivatives of SBAD03 3D TPs, specifically examining the proportion and migration of SOX10+ neural crest and SIX1+ trigeminal placode progenitors (Figure 13 & S15).

Orthogonal reconstruction of z-stack images revealed typical drawbacks of single-photon confocal microscopy, including decreasing signal strength along z-axis and limited z-resolution for signal segmentation[449]. High cellular density further complicated the technical capacity of efficient 3D nuclear segmentation. Therefore, we compared relative signal areas of either transcription factor instead of counting positively labelled 3D segmented nuclei. Normalised signal areas of both SOX10 and SIX1 increased initially and stabilised from d6 (Figure 13a-c).

Similar to 2D placodal immunolabelling, most regions were of neither ectodermal identity (Figure 12 & S12). The presence of other embryological lineages coincided with RT-qPCR results (Figure 12c). Manders analysis revealed that the majority of signal co-localisation were due to noises or overlapping nuclear density (Figure S15). It can be concluded that there was minimal similarity of signal distribution between SIX1 and SOX10, suggesting mutually exclusive ectodermal development similar to *in vivo* (Figure 13d).

The distances to edge of both SOX10+ and SIX1+ regions increased during development as the diameter of organoids grew. During differentiation, both neural border markers appeared to aggregate in the limb-like outgrowing protrusions, suggesting active progenitor migration and cytoarchitecture remodelling (Figure 13a d6 and S14). By d9, SOX10+ neural crest and SIX1+ cranial placode progenitors displayed polarities in distribution, implying a tissue-autonomous internal axial definition. In 3D TPs, SIX1+ TP progenitors migrated further outwards, with SOX10+ progenitors remained in the core of TPs 13), which was not typical on 2D cultures (Figure S12). Quantitative analysis of pixel distances to edge did not reveal significant differences under most conditions, likely due to sample-based averaging and an underpowered number of samples.

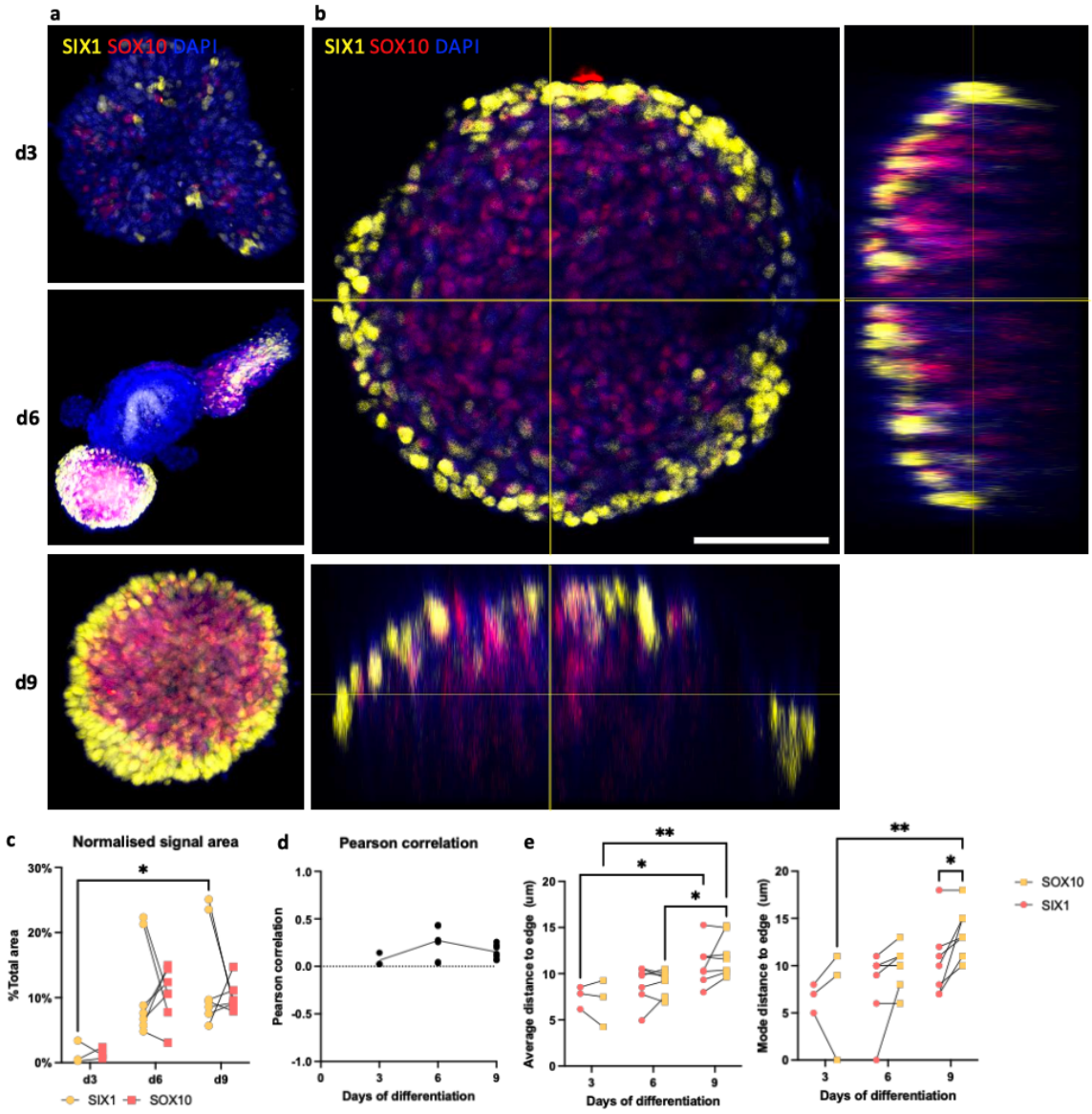


Figure 13: Temporal profiling of ectodermal transcription factor topology in developing SBAD03 TP organoids.
(a) 3D reconstruction of cellular organisation of SBAD03 3D TPs collected during early ectodermal induction, rendered via Arivis. (b) Representative orthogonal display of SIX1/SOX10 distribution in d9 SBAD03 TP organoid. Scale bar 50µm. (c) Comparison of normalised signal area during ectodermal induction. Statistical significance was determined by RM two-way ANOVA with Geisser-Greenhouse correction and Sidak's multiple comparison test: significance effect in time of induction [F(2,14)=8.976], p=0.0031, with significant multiple comparison labelled. (d) Pearson correlation of SIX1/SOX10 signal distribution across time by JaCoP in ImageJ. (e) Average and mode of distance to edge per organoid of SIX1 and SOX10 in SBAD03 3D TPs during early differentiation. Statistical significance determined by RM two-way ANOVA with multiple comparisons. For panel (c-e), n=3 at d3, 7 at d6&9.

2.3.2 Optimisation of maturation conditions for peptidergic cell fate specification in TG iNociceptors

Once ectodermal patterning was complete, the application of BDNF has led to extensive neuralisation within the placodes (Figure 14a-c). Both pseudounipolar and bipolar neurons could be identified (Figure 14c).

Although the original protocol[435] and a 3D adaptation[429] both applied NOTCH inhibition to increase neuronal content, there was no change in neuronal commitment with 120-hour DAPT treatment. Neurite outreach within the organoid structure was extensive and not affected by DAPT (Figure 14). There was no difference in the mean fluorescence intensity of TUBB3 signal with and without DAPT treatment (Figure 14d).

The application DAPT in sensory neuron differentiation *in vitro* could have several impacts. Besides promoting neuralisation, DAPT can inhibit glial differentiation and lead to glia detachment (see also Section S3.5). As glial progenitors were difficult to distinguish from bi-potential neural progenitors in d10 placodes, we continued growing TP organoids suspended in maturation media till d60 to identify any emergence of glia. The addition of DAPT did not alter the long-term expression of glial or neuronal markers (Figure 15b).

Preliminary work in our lab has identified the presence of glial cells spontaneously differentiated with neuron progenitors and its impact on cell fate specification[2], which we verified on 2D TP-derived TG iNociceptors (see Section S3.4.2). Similarly, we tested the effect of adding AraC and astrocytes on cell fate specification in iNociceptors derived from 3D TPs, by first digesting TPs to single cells and seeding the progenitors at 400k/cm^2 (Figure 15). The application of AraC triggered detachment and cell-death of still dividing non-neuronal cells co-developed the placode.

In iNociceptors derived from 2D TPs, the presence of non-neuronal cells significantly increased baseline CGRP secretion, either by spontaneous differentiation with the placodes or by supplementing rat astrocytes (Section S3.4.2). Surprisingly, all conditions grew as a high CGRP secretion phenotype when placodes were induced initially as 3D EBs (Figure 15b).

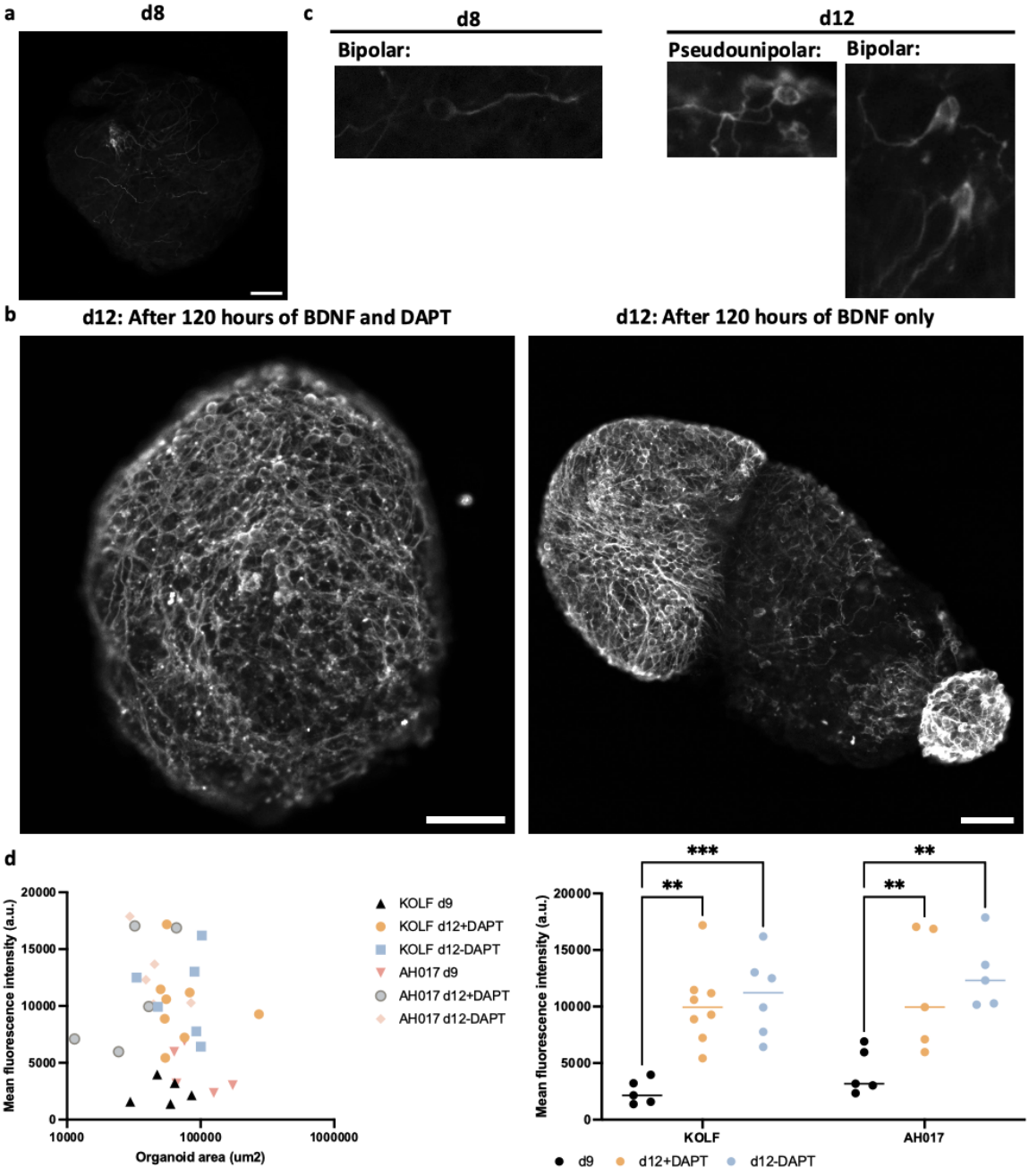


Figure 14: No effect of DAPT shock on neuronal commitment in 3D TPs.
(a-b) Demonstration of TUBB3+ neurite networks in (a) d8 and (b) d12 3D TPs in the presence of BDNF with/without DAPT. Scale bar 50µm. (c) Representative neuron morphologies. (d) Mean fluorescence intensity of TUBB3 within placodes as (i) distribution against placode sizes and (ii) comparison based on cell lines and treatments. Statistical significance of panel d(ii) determined by two-way ANOVA with Tukey's multiple comparisons: significant effect by DAPT treatment [$F(2,28)=19.32$, $p<0.0001$] but not by cell line or interaction.

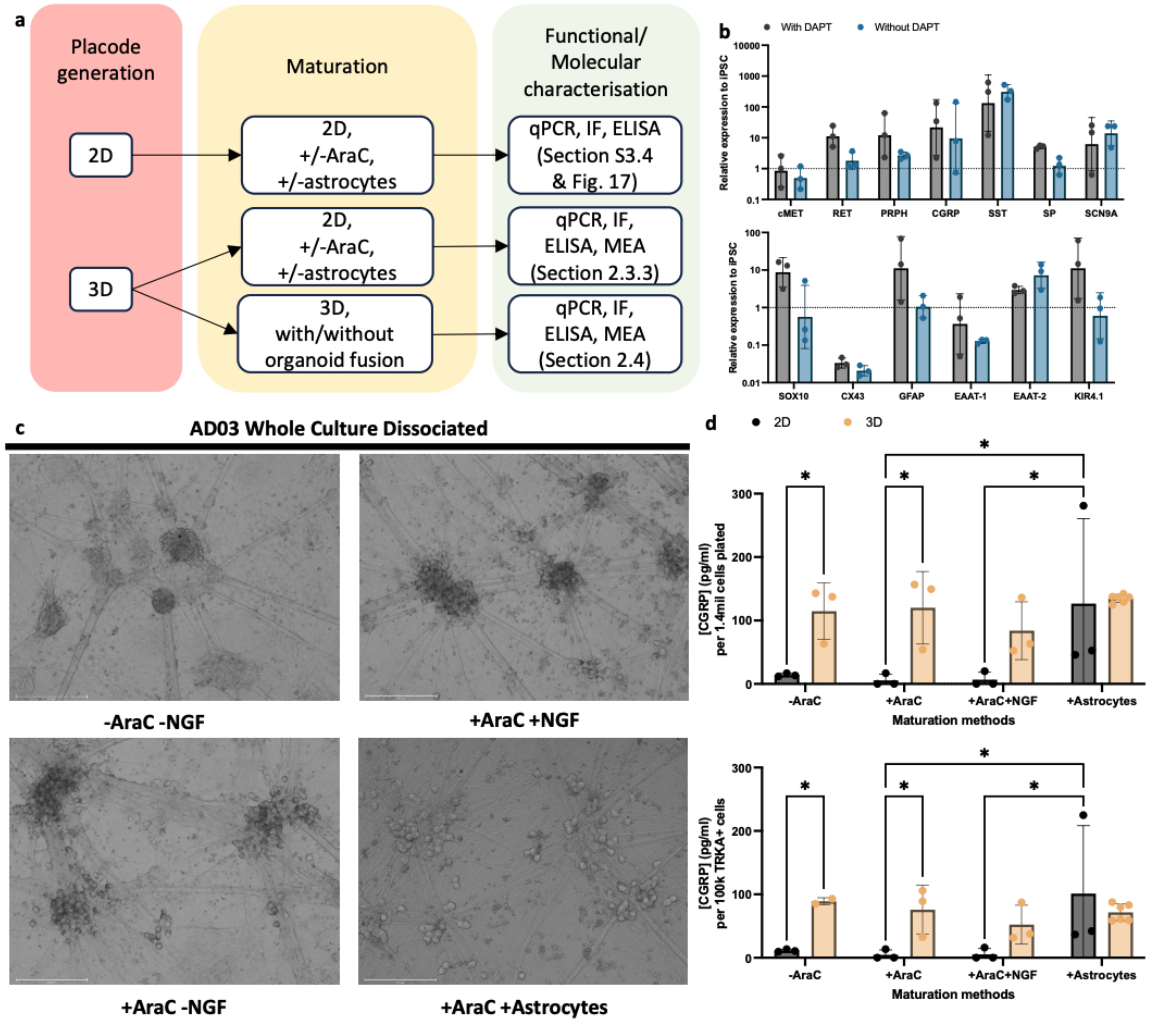


Figure 15: Maturation outcomes of SBAD03 TG iNociceptors modulated by the presence of glia. (a) Schematics of maturation methods based on culture platforms. (b) Effect of early DAPT treatment on long-term neuronal (top) or glial (bottom) marker expression in suspended SBAD03 TG organoids by RT-qPCR. (c) Representative brightfield images of d55 SBAD03 TG iNociceptor cultures via different chemical purification conditions. Scale bar 275µm, (d) Quantification of raw and %TRKA-normalised baseline CGRP secretion by culture supernatant ELISA in 2 WT cultures, n=3-6 per condition from 3 independent differentiations. Statistical significance determined by two-way ANOVA with Tukey's multiple comparison tests.

We proceeded to the functional characterisation of dissociated 3D TPs treated by AraC supplemented with astrocytes, as it provided the best viability and attachment over long-term culturing.

2.3.3 Functional characterisation of TG CGRP+ peptidergic iNociceptors

Sensory neuron markers were significantly upregulated in mature TG iNociceptors (Figure 16 & 23). Similar to the Chambers' protocol, we expected minimal presence of mature mechanoreceptors in mature TG cultures in vitro due to low *TRKB* induction. Although *TRKC* transcripts were detectable in 3D placodes (Figure 12c), minimal transcripts of proprioceptor marker (e.g. *PVALB*, C_T around 34 for 3ng cDNA input) could be amplified from mature TG iNociceptors (Figure 23).

Compared to Chambers' DRG iNociceptors, the most prominent difference was the retained expression of conventional peptidergic markers *TRKA* and *cMET* quantified by RT-qPCR (Figure 16a). In contrast to mature Chambers' iNociceptors that were exclusively RET+ (Figure 6 & 9), most TG iNociceptors observed were positive for cMET immunolabelling, with no detectable signal for RET (Figure 16c-d). In particular, cMET signals displayed both membrane and nuclear enrichment in TG iNociceptors, indicating active nuclear translocation for downstream signalling (Figure 16c). Although the functional relevance of cMET in mature nociceptors is currently unknown after the extinguishment of RUNX1, nuclear transport of the cytosolic component of cMET is known to regulate cell type-specific transcription, DNA repair, and initiation of intracellular calcium signalling in hepatocytes and cancer cell lines[450,451].

For *in vivo* comparison, we extracted the expression and distribution of cMET and RET from *ex vivo* multiomics datasets from published literature[4,5]. There was minimal overlap between spatial mapping of RET and cMET in human DRGs by cluster-based spatial transcriptomics (Figure 11d). Single-cell transcriptomics further identified most cMET+ cells in human TGs as non-neuronal (Figure 16e). We did not observe cMET+ non-neuronal cells in mature TG iNociceptor cultures *in vitro*, partially because most non-neuronal iPSC derivatives were effectively removed by AraC treatment.

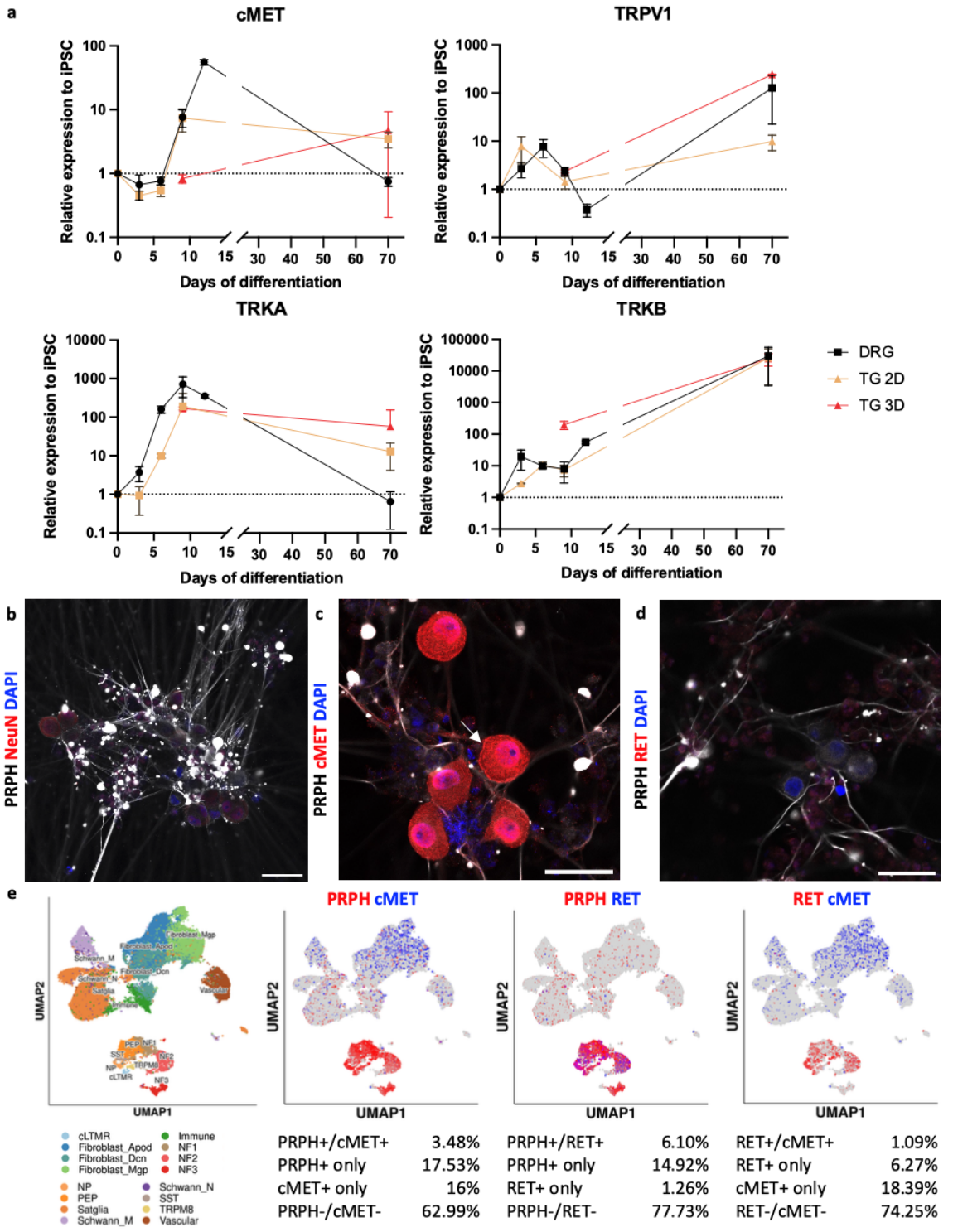
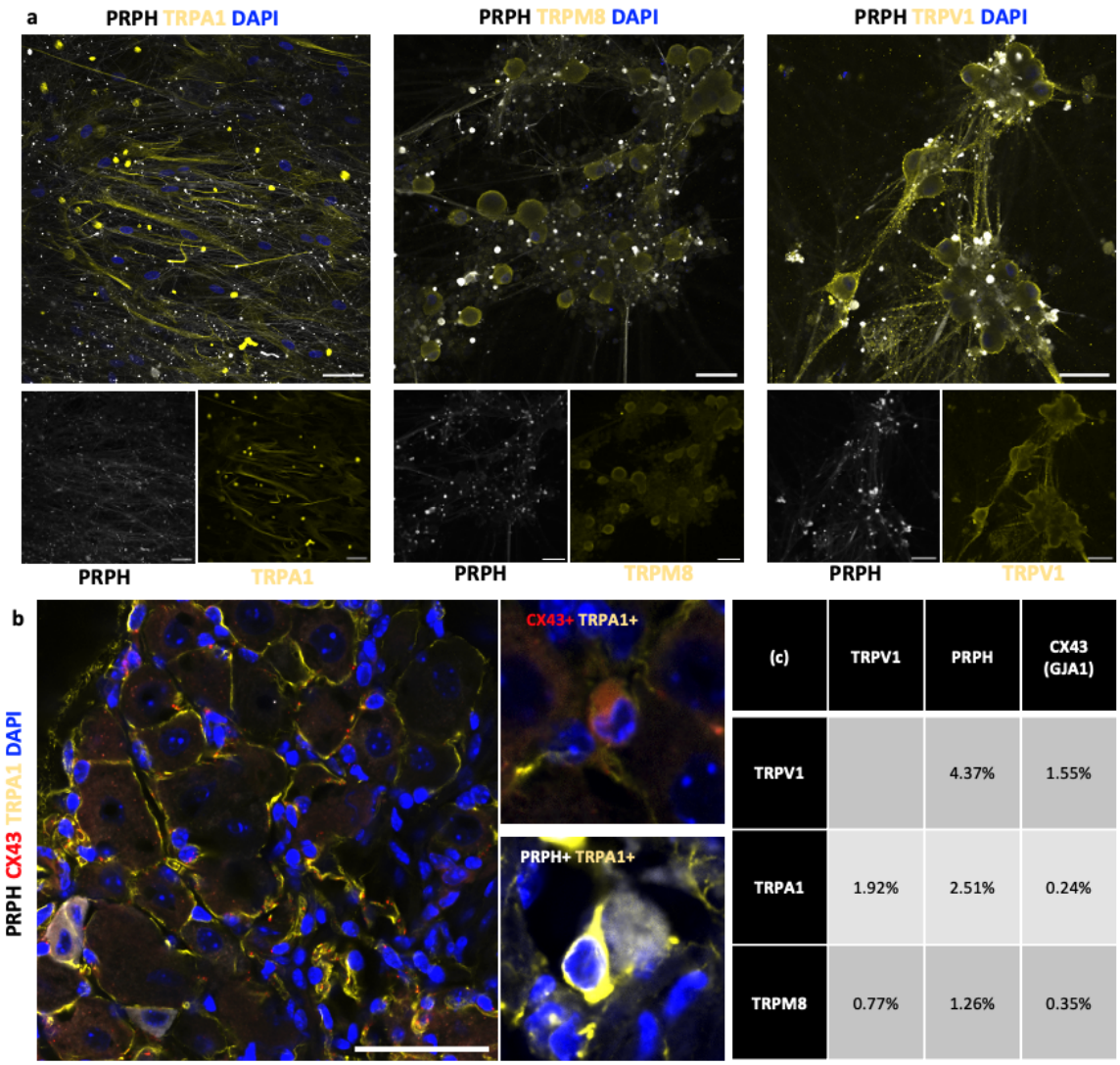


Figure 16: Directed differentiation of peptidergic TG iNociceptors.
(a) Comparison of major peptidergic marker expression in iNociceptors derived from Chambers', 2D TP, and 3D TPs by RT-qPCR before and after maturation. n=3 independent differentiations in SBAD03 iNociceptors. Primers human specific. Error bar standard deviations. (b) Uniform PRPH distribution in mature peptidergic TG iNociceptors. (c-d) Subcellular localisation of (c) cMET and (d) lack of RET in peptidergic TG iNociceptors. Arrow indicating membrane localisation besides nuclear translocation of intracellular cMET. For (b-d), scale bar 50µm, n=3 independent differentiations in 3 WT lines, panels for individual channels see Figure S17. (e) Transcriptomic expression patterns of cMET and RET co-expressed with PRPH in human post-mortem TG, data extracted from[5].



(c)	TRPV1	PRPH	CX43 (GJA1)
TRPV1		4.37%	1.55%
TRPA1	1.92%	2.51%	0.24%
TRPM8	0.77%	1.26%	0.35%

Figure 17: TRP channel expression in SBAD03 TG iNociceptors compared to primary human and mouse TGs.
(a) Identification of TRPA1, TRPM8, and TRPV1 immunoreactivities in SBAD03 TG iNociceptors co-cultured with rat astrocytes. n=3 independent differentiations. (b) Confirmation of glia-enriched TRPA1 immunoreactivities in ex vivo female murine TGs, with zoomed panels identifying individual TRPA1+ glia or small-diameter sensory neuron. Scale bar 50µm for (a-b). (c) Percentage of cells with TRP channels co-expression in human post-mortem TG, extracted from[5].

TRPV1 was widely expressed in mature TG iNociceptors (Figure 16-17). Immunolabelling also identified a membrane enrichment of TRPV1 and TRPM8 signals (Figure 17). Although *TRPA1* transcripts were detectable in RT-qPCR, anti-TRPA1 (Alomone) labelled glia instead of neurons, both *in vitro* and in *ex vivo* murine TGs (Figure 17).

Having confirmed the presence of peptidergic hallmark genes in mature TG iNociceptors, we proceeded to compared neuropeptide expression of TG nociceptors *ex vivo* and *in vitro*. CGRP immunoreactivities in *ex vivo* female murine TGs were enriched in perinuclear granules (Figure 51), typical of Golgi body appearances[452]. Co-labelling with NeuN (total neurons) and peripherin (soma of small diameter fibres[453]) allowed quantification and visualisation of CGRP+ neurons *ex vivo*. Despite using the same antibody, we identified a lower proportion of CGRP+ cells (around 20%, Figure 51) compared to previously reported (around 30%[452]). However, the distribution of CGRP+ soma sizes was comparable.

In comparison, all TG iNociceptors generated *in vitro* were PRPH immunoreactive (Figure 16b). Most iNociceptors derived from 2D TPs were also positive for CGRP (Figure 18). Interestingly, immunolabelling of mature CGRP peptides displayed vesicle-like puncta besides dispersed cytosol signals in mature TG iNociceptors (Figure 18a), which is unique compared to available literature. Both *CALCA* and *CALCB* transcripts were present in mature TG iNociceptors (Figure 23), similar to *ex vivo* human TGs (Figure 18c). Notably, no commercially available immunolabelling kits for IF and ELISA could distinguish between CGRP isoforms. A recent study has identified differential localisation patterns of CGRP isoforms in mouse TGs using genomic insertion of isotype-specific fluorescent tags, that only αCGRP could translocate to synapses[117]. Assuming similar feature conserved in human counterparts, we could at least confirm the expression of αCGRP as CGRP+ neurites could be identified (Figure 25). To determined whether βCGRP is actively translated and functional in TG iNociceptors will require genomic editing of locus-specific endogenous tags.

We then examined the distribution of other neuropeptides such as SP and SST *in vitro* (Figure 18b). Compared to the universal distribution of SST and CGRP, SP+ iNociceptors were considerably rarer. Signals for both SST and SP appeared more spread out within

the cytoplasm compared to that of CGRP due to the specific immunogen our antibodies recognise: Anti-SST (Proteintech) labels the precursor and both isoforms of SST, while anti-SP (Proteintech) labels TAC1 precursor. Axonal puncta of SST were identified (Figure 18d), which are likely packaged neuropeptide progenitors getting processed and trafficked down sensory nerves. CGRP/SST double positive neurites could also be identified (Figure 25).

Due to limited resources, we did not confirm neuropeptide immunolabelling and co-expressions of iNociceptors generated from 3D placodes co-cultured with astrocytes.

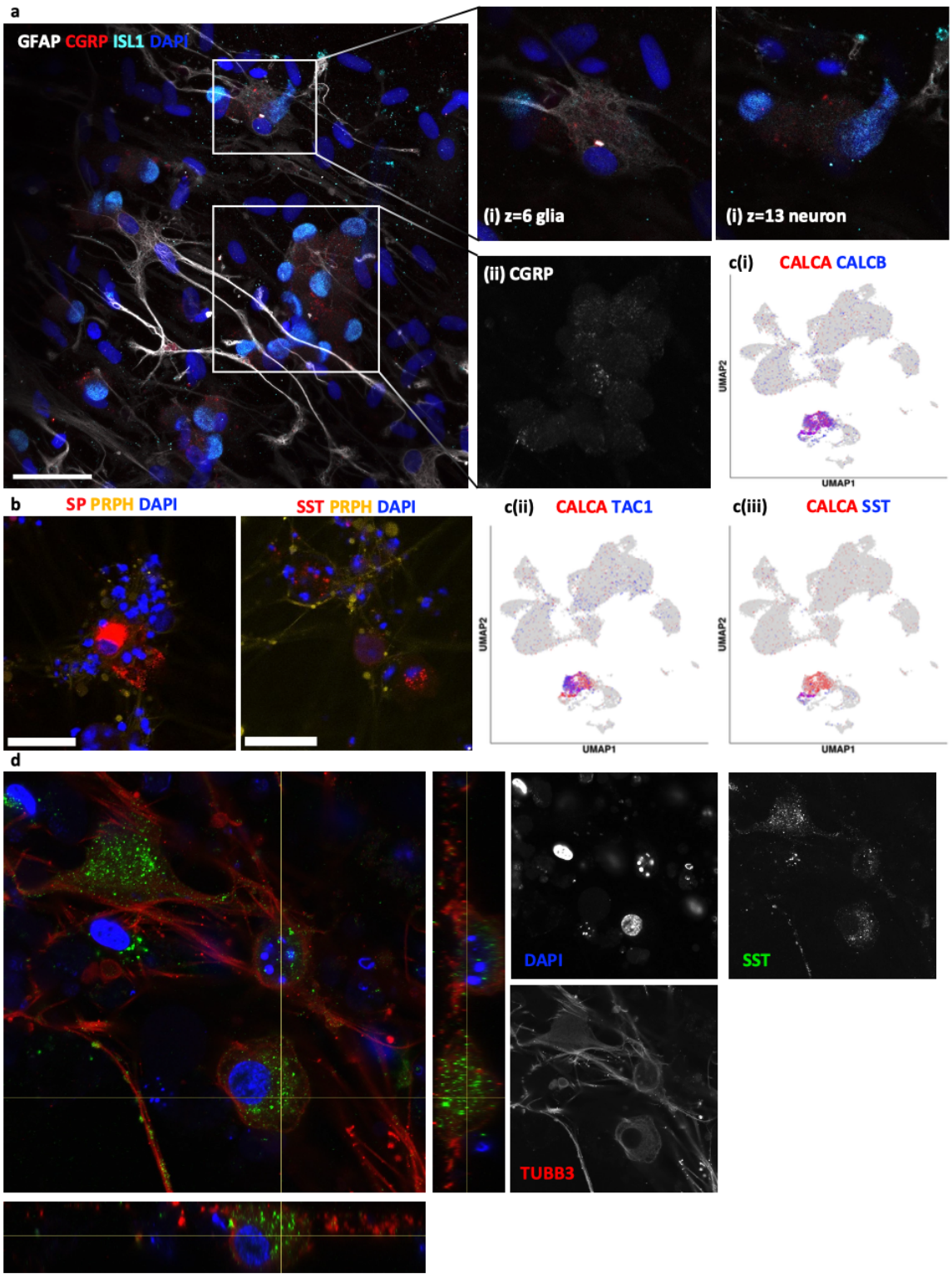


Figure 18: Confirming neuropeptide immunoreactivities in mature SBAD02 TG iNociceptors generated from 2D placodes.
(a-b) Representative confocal images of intracellular distributions of neuropeptides labelled by IF: (a) CGRP, zoomed panels showing (i) close association with supplemented astrocytes, (ii) neuropeptide-containing puncta; (b) SP in cytosol and SST both as dispersed cytosol signals and puncta. Scale bar 50µm, n=3 differentiations. (c) Transcriptomic distribution and co-expression patterns of neuropeptides in human post-mortem TG, data extracted from[5]*. (d) Representative orthogonal analysis of differential subcellular distribution patterns of SST in mature SBAD02 iNociceptors. For all panels, n=3 independent differentiations in SBAD02 iNociceptors.*

TG iNociceptors could be cultured for over 100 days with good viability, maintaining baseline CGRP secretion with some fluctuations (Figure 19a). CGRP release could be triggered by previously established stimulants such as FK and inflammatory soup in most wild type lines (Figure 19d). Using high-responder line AH017, we also compared the baseline and induced CGRP secretion in cells matured from either 2D or 3D-induced placodes. Mature AH017 iNociceptors derived from 3D placodes displayed less increment in CGRP secretion when exposed to stimulants (Figure 19b-c). Repetition with other lines will be required to confirm the source of the substantial differences in the extent of responsiveness observed.

We then characterised the expression of neuropeptide receptors in iNociceptor cultures compared to *ex vivo* human TGs (Figure 20). We used human-specific primers to avoid confounding from rat astrocytes in the co-culture. The expression of SP receptor *TACR1* could be identified in hiPSC-derived cells. In contrast, components of CGRP receptors from hiPSC-derived cells were lowly expressed and unlikely to be biologically meaningful. Co-expression between neuropeptides and matching receptors is reported in rats[452] but appears less common in human[454]. In *ex vivo* human TGs, genes such as *RAMP1*, *CALCRL*, *CRCP*, and *TACR1* displayed enriched expression in supportive cells, such as SCs, SGCs, and vasculature, rather than sensory neurons (Figure 20b).

As astrocytes are known for being physiological targets of CGRP[455], we tested whether the supplemented rat astrocytes could be a target of iNociceptor-derived CGRP using conditioned media, given that there are high sequence and structural homology between human and rat αCGRP[456]. Compared to positive control FK, no cAMP cascade was found in primary rat astrocytes after a 1-hour incubation with TG iNociceptor-conditioned media or purified CGRP (Figure S18).

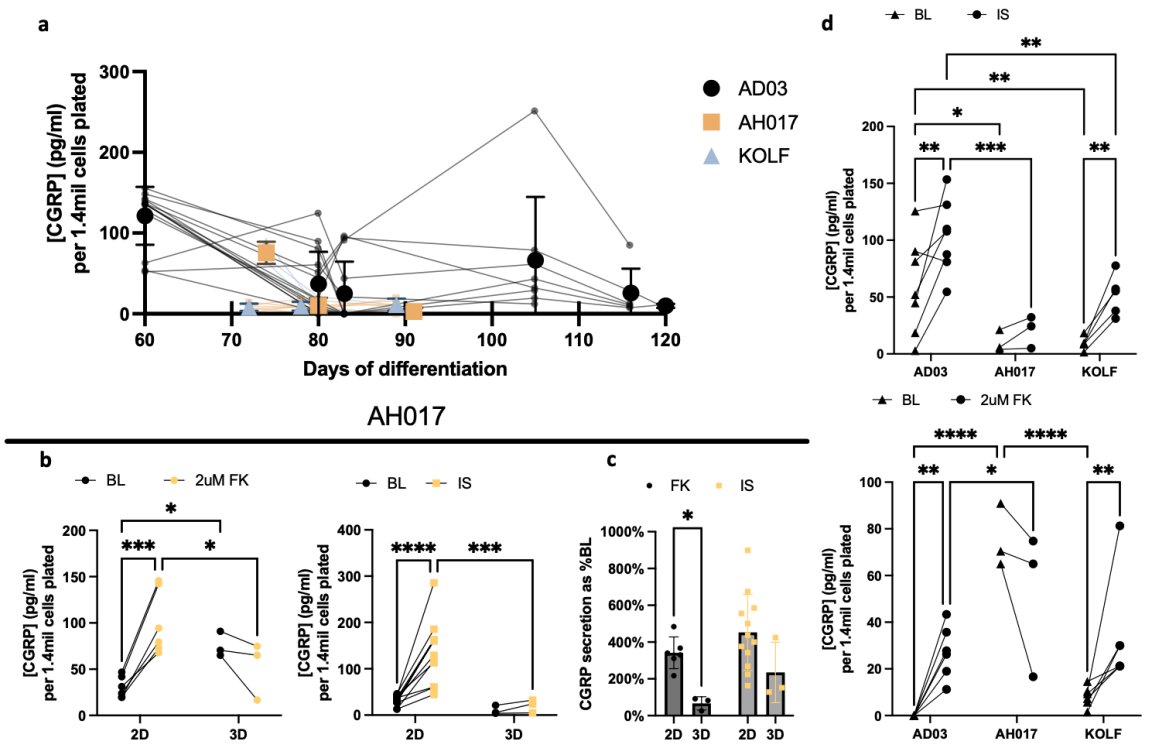


Figure 19: CGRP secretion in response to stimuli in mature WT TG iNociceptors. (a) Time course of paired, repetitive measurements of baseline CGRP secretion in mature TG iNociceptors from 3 WT lines, error bars standard deviations. n=2-12 for AD03, 3 for AH017, and 5-6 for KOLF, lowering number of replicates due to reduced viability over extended period of culturing. (b) Comparison of BL and chemically stimulated CGRP secretion in mature AH017 iNociceptors derived via 2D or 3D TPs. Statistical significance determined by RM two-way ANOVA with uncorrected Fisher's LSD for both panels: for FK treatment, significant effects by treatment [F(1,7)=6.876, p=0.0343] and interaction [F(1,7)=27.61, p=0.0012] but not growth format; for IS, significant effects by treatment [F(1,13)=10.01, p=0.0075], growth format [F(1,13)=10.11, p=0.0073] and interaction [F(1,13)=6.679, p=0.0219]. (c) Comparison of agonists responsiveness as CGRP secretion normalised to baseline in mature AH017 iNociceptors derived via 2D or 3D TPs. Statistical significance determined by ordinary two-way ANOVA with with uncorrected Fisher's LSD: significant effect by growth platform [F(1,20)=9.383, p=0.0061] but not type of agonists. (d) Responsiveness to IS (top) and FK (bottom) in 3 mature TG iNociceptors from 3 WT lines. Statistical significance determined by RM two-way ANOVA with uncorrected Fisher's LSD for both panels: for IS, significant effect by cell line [F(2,12)=10.60, p=0.0022] and present of agonist [F(1,12)=15.31, p=0.0021]; for FK, significant effect by cell line [F(2,12)=17.69, p=0.0003] and interaction [F(2,12)=8.179, p=0.0057] but not presence of agonist (as a major effect only).

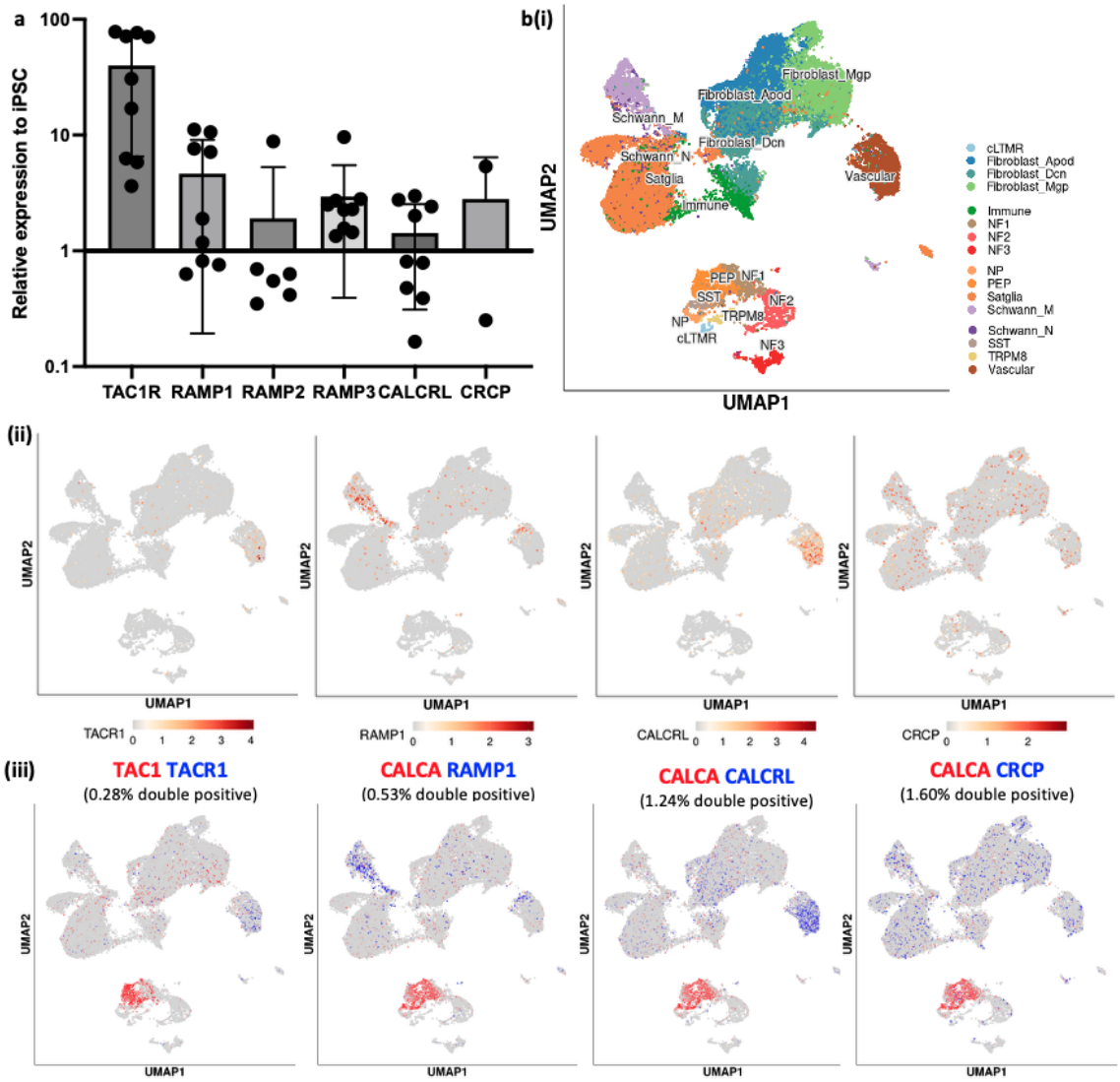


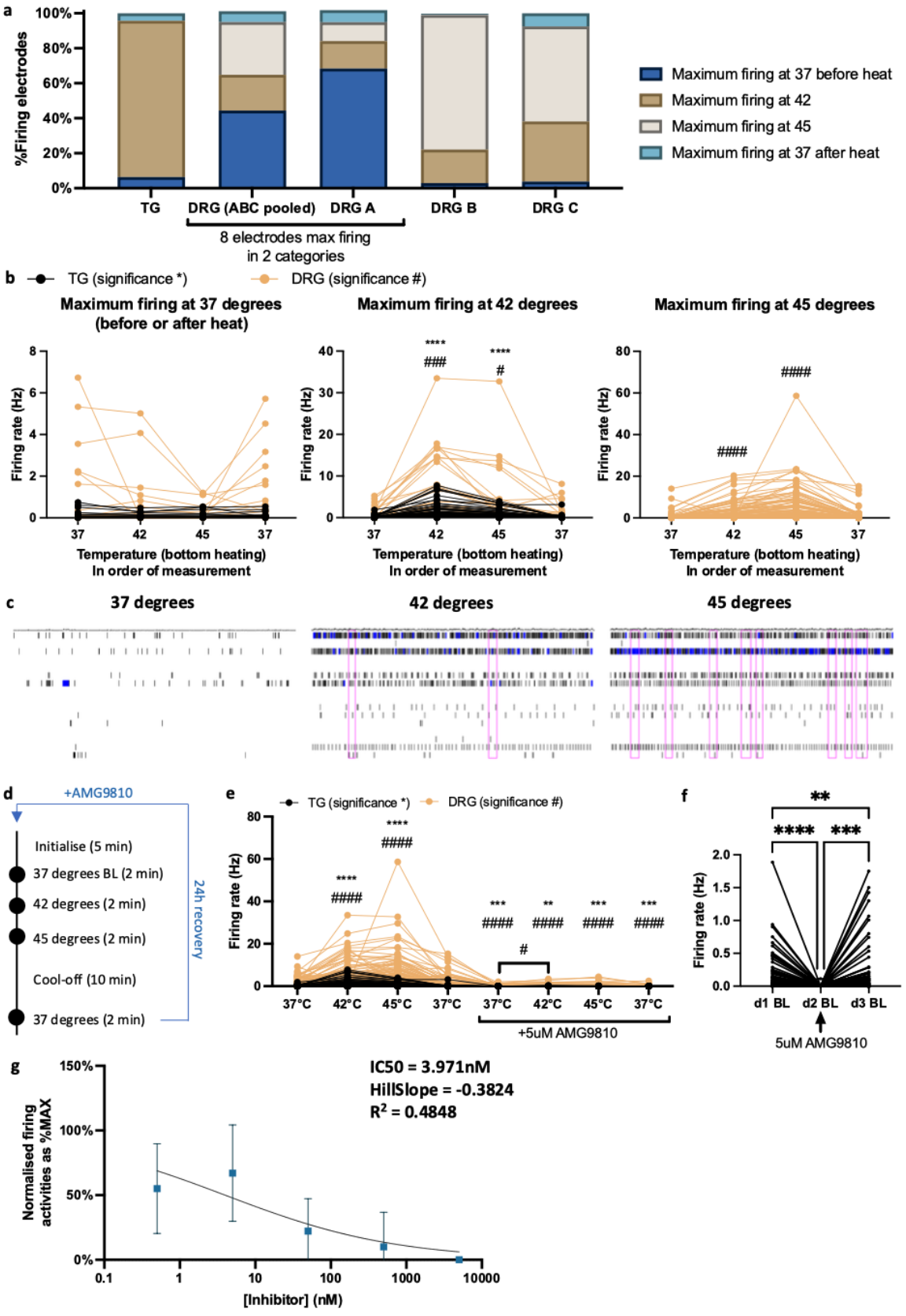
Figure 20: Expression and distribution of neuropeptide receptors in human TG in vitro and ex vivo. (a) Confirmation of neuropeptide receptor expression in mature TG iNociceptors by RT-qPCR, n=3 independent differentiations from SBAD03, MIG009, and MIG012 lines. Primers human specific. (b) Distribution of neuropeptide receptors in human post-mortem TG confirming glial enrichment, data extracted from[5]: (i) cluster labelling from the original publication, and (ii) distribution and level of expression of neuropeptide receptors, and (iii) minimal co-expression of neuropeptides with matching receptors.

We cultured TG iNociceptors on MEA to investigate the electrophysiological properties of mature sensory neurons *in vitro*. Unlike astrocytes which do not exhibit typical action potentials[457] (Figure S18c), firing activities of TG iNociceptors were detectable during development at d35 (Figure S7c). Compared to DRG iNocicieptors, TG cultures displayed fewer spontaneous activities at physiological temperature (Figure S7). More specifically, about 30% of electrodes in TG iNociceptors cultures did not display any baseline firing activities but could be evoked by stimulants such as heat, compared to 12% in DRG iNociceptors.

We repeated the heat sequence on mature TG iNociceptors by MEA (Figure 21) in comparison with Chambers' DRG iNociceptors. As most cells from Batch A DRG were not heat reactive, we proceeded further analysis with Batch B and C pooled (denoted as DRG in Figure 21b and hereinafter). Unlike Chambers' iNociceptors of heterogenous responsiveness to heat, the majority of thermally active TG iNociceptors exerted maximum firing activities at 42 degrees (Figure 21a-c).

TRPV1 dependency of thermal reactivities in iNociceptors was confirmed by repeating the heat sequence in presence of selective competitive TRPV1 antagonist AMG9810[458] (Figure 21d-e). Despite drastically reduced firing activities at all temperatures with AMG9810 applied, there was a statistically significant increment of firing activities at 42 degrees in DRG iNociceptors (meaan difference -0.02224, standard error 0.007700 p=0.0240, q=2.889, extracted from pre-determied groups of Dunnett's multiple comparisons, Figure 21e). The partial resistance to AMG9810 of thermal activation suggests potential functional redundancy with other thermo-sensors at 42 degrees specifically in DRG iNociceptors.

We also noticed a significant reduction in baseline activities when 5uM AMG9810 was applied in either cell type, which was reversible when AMG9810 was removed (Figure 21f). It is likely that some of the baseline activities without exogenous agonists could have been initiated via spontaneous or endogenous activation of TRPV1 in either culture.



(Caption see next page.)

Figure 21: Comparison between TRPV1-dependent noxious heat responsiveness in SBAD03 TG and DRG iNociceptors by MEA (figure see previous page).
(a) Relative quantity of thermally active electrodes categories by maximum responsice temperature in SBAD03 TG and DRG (individual and pooled batches) iNociceptors. (b) Paired firing analysis of TG and DRG iNociceptors grouped by maximum firing temperature. Statistical significance determined by RM two-way ANOVA with Geisser-Greenhouse correction with Dunnett's multiple comparisons tests (individual variances for simple effects within columns, compared against control mean at 37 degrees before heat) for (i) and (iii); Friedman test with Dunn's multiple comparison test for (ii) due to lack to TG counterparts. (c) Rastor plot of a representative well of TG iNociceptors in response to noxious heat. (d) Schematics of heat sequence with selective TRPV1 antagonist AMG9810. (e) TRPV1 dependency of heat responsiveness in SBAD03 TG and DRG iNociceptors by the addition of AMG9810. Statistical significance determined by RM two-way ANOVA with Geisser-Greenhouse correction with Dunnett's multiple comparisons tests (individual variances for simple effects within columns, compared against control mean at 37 degrees before heat on either day). (f) AMG9810-induced reversible reduction of firing activities at 37 degrees in SBAD03 TG iNociceptors. Statistical significance determined by Friedman tests with Dunn's multiple comparisons. (g) Dose-response curve of normalised firing activities at 42 degrees with increased concentrations of AMG9810 in SBAD03 TG iNociceptors. Parameters determined by non-linear curve fitting ([inhibitor] v.s. normalised response - variable slope) in GraphPad Prism. For all panels, glutaminergic synaptic blocker CNQX was present.

To rule out potential off-target effects at higher doses, we performed a dose-response curve of normalised firing activities at 42 degrees with a range of AMG9810 concentrations in presence of synaptic blocker CNQX. The IC_{50} of AMG9810 on TG iNociceptors *in vitro* was 3.971nM, within a comparable magnitude of reported values (15.8nM for heat[459]) in ectopic expression systems.

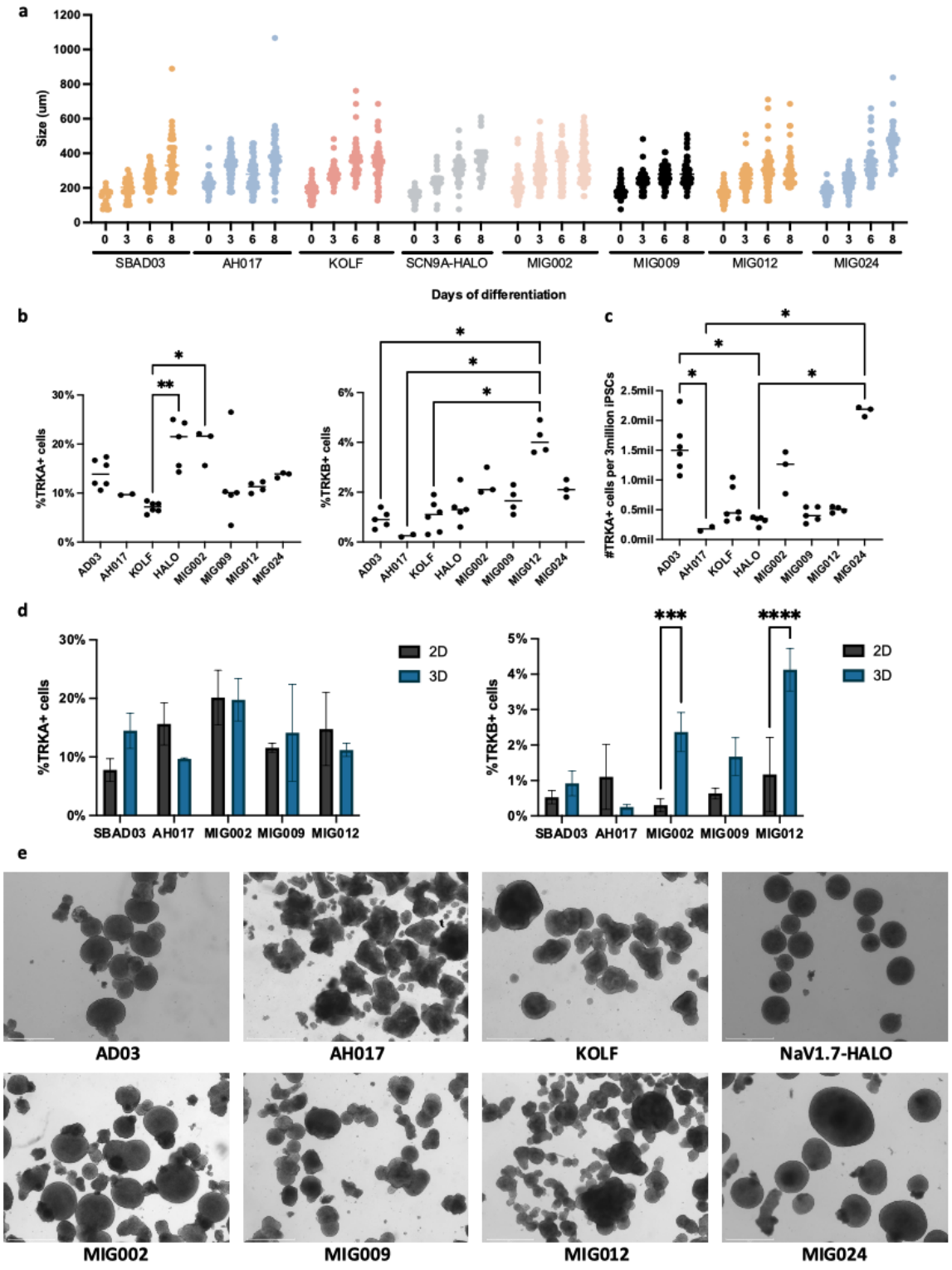
In conclusion, we have successfully generated a reproducible protocol for peptidergic TG iNociceptors that express conventionally markers such as cMET, TRKA & TRPV1 and secrete CGRP. The patterns of PRPH and CGRP immunoreactivities suggest biochemical resemblance of TG iNociceptors differentiated *in vitro* with conventional peptidergic C-fibres *in vivo*.

2.3.4 Applying TG CGRP+ peptidergic iNociceptor models to the study of migraine pathobiology

Trigeminal CGRP is known as a critical factor of migraine pathogenesis. Although the exact mechanism by which CGRP is involved in the development of migraine headaches is unknown, surges of CGRP secretion are associated with migraine attacks[460]. Intravenous infusion of CGRP directly triggers migraine-like headache attacks in more than half of the patients[461]. Monoclonal antibodies against CGRP have shown promising efficacies in clinical practice for migraine treatment[127–129].

Migraine susceptibility is partially contributed to the genomic background of patients, with heritability predicted around 40%-50% in one study[462] and 30%-60% in another report[463]. Associated risk variants include the locus of *CALCA/CALCB* that transcribes CGRP[462]). Genetic background also potentially predicts treatment efficacies[464]. As hiPSC technology preserves genomic information, we hypothesise that our TG iNociceptors that secrete CGRP in response to external triggers can be a model for migraine pathogenesis.

To examine whether our TG iNociceptor model could reflect certain clinical features of migraine pathobiology, we recruited six migraine patient-derived hiPSC lines, including three responsive to common treatments (such as triptans and topiramate) and three resistant. Although patient line hiPSCs underwent similar processes of quality control and maintenance, it was challenging to differentiate some lines into 2D placodes (Figure S11). In comparison, generation of embryoid bodies to induce 3D TPs achieved relatively high differentiation efficiencies in patient lines previously difficult to work with (Figure 22, also see Section S3.4.1). As all iPSCs formed uniformly sized embryoid bodies in AggreWell prior to differentiation, the expansion and size of 3D TPs could be a qualitative parameter to compare the progress of induction. Although significantly more TRKB+ cells were derived in some patient lines, the proportion of TRKB+ cells were still considerably less than that of TRKA+ progenitors (Figure 22d).



(Caption see next page.)

Figure 22: Generation of TPs from migraine patient-specific iPSC lines (figure see previous page). (a) Growth curve of 3D placode sizes of WT and patient lines. Statistical significance determined by ordinary two-way ANOVA with main effects only: significant effects in time of differentiation [F(3,1700)=301.7, p<0.0001, 32.95% of total variation] and cell lines [F(7,1700)=18.62, p<0.0001, 4.746% of total variation]. (b-c) (b) Percentage of TRKA+/TRKB+ cells by FC and (c) yield of TRKA+ nociceptor progenitors from WT and patient-specific 3D placodes at d8. Yield calculated by multiplying total cell counts with %TRKA+, both batch specific. Statistical differences determined by Kruskal-Wallis tests with Dunn's multiple comparisons: p=0.0014 for panel (b) %TRKA+, 0.0019 for panel (b) %TRKB+, and p=0.0003 for panel (c). (d) Comparison of %TRKA+ (left) and %TRKB+ (right) progenitors from WT and patient-specific TPs derived by either 2D or 3D methods, data compiled from panel (b) and Figure S12e. Statistical significance determined by ordinary two-way ANOVA with Sidak's multiple comparisons: for %TRKA+, significant effects by cell line [F(4,32)=4.871, p=0.0035] and interactions between cell line and platform [F(4,32)=2.905, p=0.0370] despite no significant multiple comparisons; for %TRKB+, significant effects by cell line [F(4,32)=16.42, p=<0.0001], platform [F(1,32)=33.02, p=<0.0001] and interactions [F(4,32)=11.41, p=<0.0001]. (e) Representative brightfield images of d8 3D placode morphologies. Scale bar 650µm.

3D TPs derived from migraine patient hiPSC lines could be matured in similar fashion to WT. Expression of markers specific to peptidergic nociceptors could be detected in patient line-derived mature iNociceptors, comparable to WT levels (Figure 23).

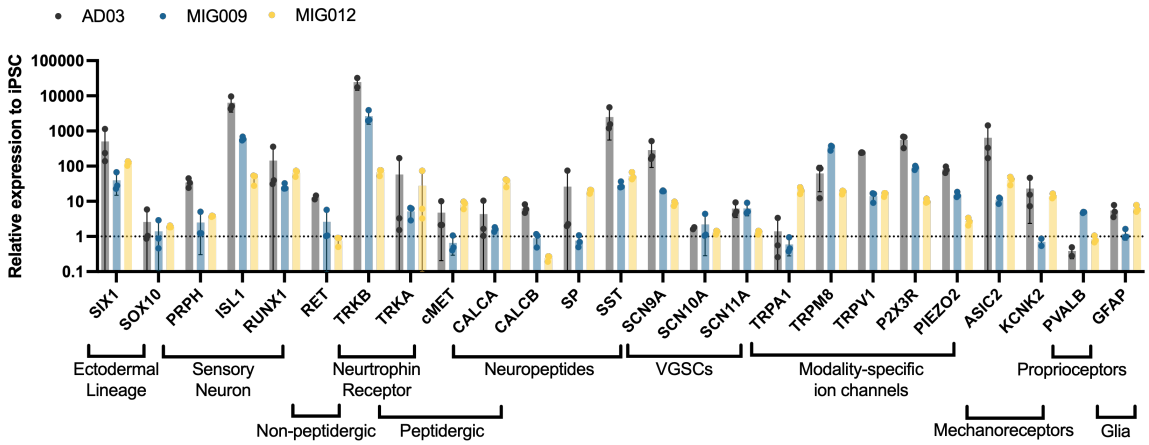


Figure 23: Confirmation of successful differentiation and maturation of d70 TG iNociceptors in WT and patient-derived lines by RT-qPCR.
n=3 independent differentiations per line. Missing data entry due to insufficient RNA recovered from certain batches.

Similar to WT counterparts, TG iNociceptors generated from patient lines secreted CGRP without external stimulation (Figure 24a).

Baseline CGRP secretion varied across lines as identified by the Kruskal-Wallis test, which is a non-parametric alternative for one-way ANOVA that examines whether the data from one group tends to be consistently higher or lower than that from other groups[465]. The

Kruskal-Wallis statistic was smaller when CGRP secretion was normalised by the number of TRKA+ cells seeded (H=11.47) compared to that when normalised by the number of total cells seeded (H=17.39). It suggests some variances arise the difference in the proportion of TRKA+ neurons from each line, which was statistical significant (Figure 22b).

Although the Kruskal-Wallis test identified significant differences among all lines (p=0.0016 for normalisation by seeding density, p=0.0218 for normalisation by the number of TRKA+ cells when seeded), Dunn's multiple comparisons only identified significant differences when normalised by seeding density. To capture cell line-specific variations, we recruited the more robust Cliff's delta effect size (CDE) comparison with neuron counts kept consistent[466]. Cliff's delta ranges from -1 to +1, indicating the normalised degree of overlap data distribution when a Group 1 cell line is compared to each of the Group 2 cell line (Figure 24b). For example, all values of baseline CGRP secretion in WT KOLF iNociceptors were lower than those derived from MIG012 (Δ=-1). In contrast, the median secretion of WT AD03 iNocicepotrs was similar to that of MIG012 iNociceptors (Δ=0.03). Therefore, we conclude that the varations in baseline CGRP secretion were not co-related with the clinical phenotype of migraine of the donor, but other cell line-dependent feature.

We then tested the responsiveness to stimulants in iNociceptors derived from migraine patient lines, using IF to mimic neuroinflammation during migraine attacks[467]. Unlike WT iNociceptors, no increments in secretive CGRP were detected in MIG009 and MIG012 TG iNociceptors when inflammatory triggers were applied. As only two patient lines were tested, it is unclear whether the lack of response to IS is a common feature of iNociceptors derived from migraine patient lines. Alternative migraine-like triggers will be also needed to induce CGRP surges *in vitro*, such as PACAP[467] and hormonal cycles[468].

In conclusion, our peptidergic TG iNociceptor protocol could be successfully reproduced with migraine patient-derived hiPSC lines. However, further experiments are needed to probe for environmental cues similar to migraine attacks.

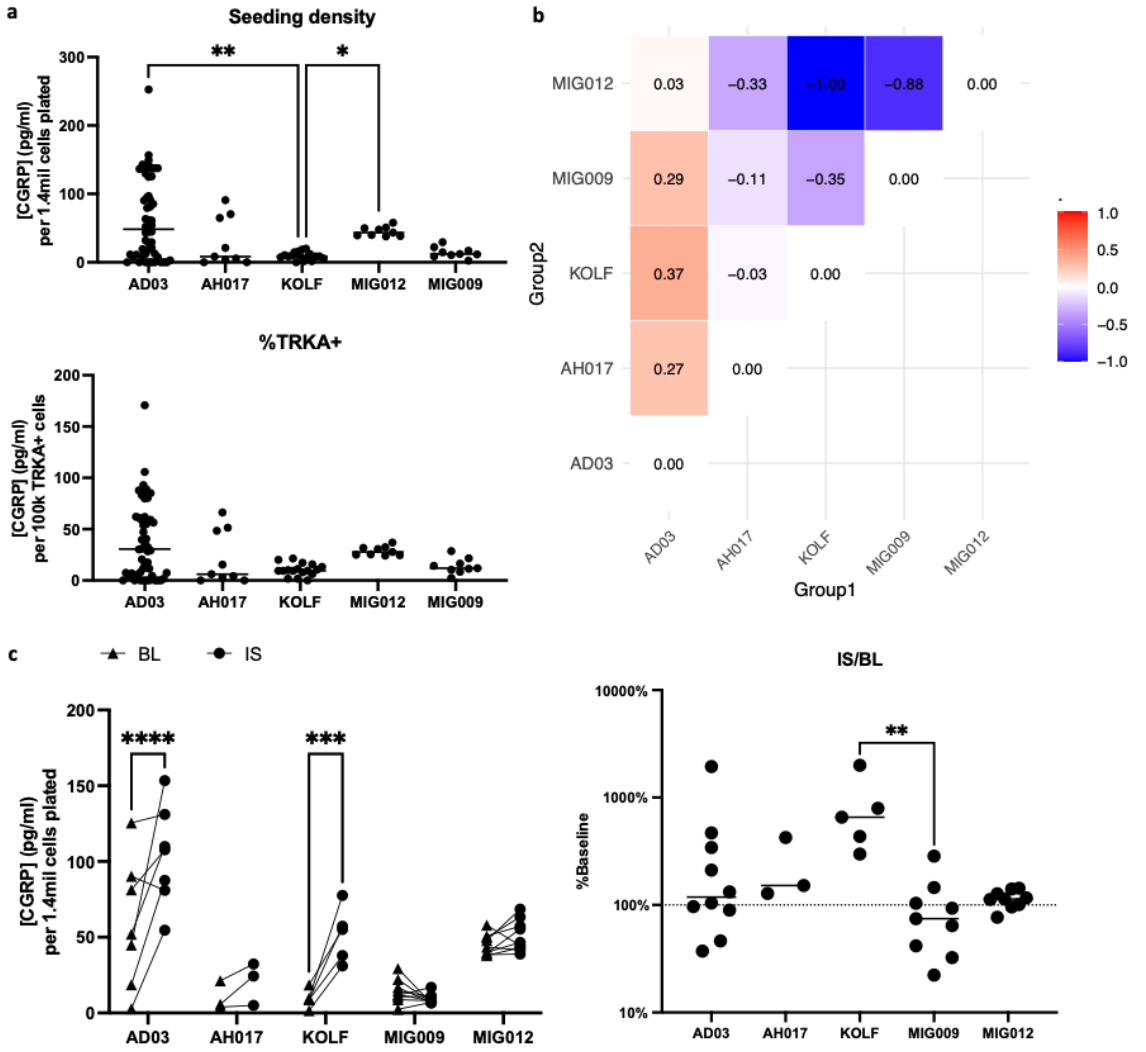


Figure 24: Baseline and stimulated CGRP secretion in mature TG iNociceptors in WT and patient-derived lines.
(a)Baseline CGRP secretion of WT and migraine patient-derived TG iNociceptors, normalised by seeding density (top) and %TRKA+ cells (bottom). Statistical significance determined by Kruskal-Wallis tests with Dunn's multiple comparisons: H = 17.39 & p=0.0016 for normalisation by seeding density, H = 11.47 & p=0.0218 for normalisation by the number of TRKA+ cells when seeded. (b) Heatmap of pair-wise CDE comparisons of CGRP secretion per 100k TRKA+ cells in all cell lines, computed in R. (c) Responsiveness to IS as paired (left) and normalised (right) CGRP secretions of WT and migraine patient-derived TG iNociceptors. Statistical significance determined by RM two-way ANOVA with uncorrected Fisher's LSD for paired analysis: significant effects by IS treatment [F(1,28)=23.99, p<0.0001], cell line [F(4,28)=20.48, p<0.0001], and interaction [F(4,28)=7.919, p=0.0002]; statistical significance determined by Kruskal-Wallis tests with Dunn's multiple comparisons for normalised analysis, p=0.0040..

2.4 Generation of a hiPSC-based neurovascular TG assembloid model

Supplementing vasculature to our TG model offers several advantages. The primary technical consideration is to allow nutrient exchange in larger and denser structures without necrosis[469]. Secondly, sensory ganglia are highly vascularised[470]. Supplementing vascular cell types reciprocates physiological tissue complexity and further promotes intercellular communication[471].

Integration of micro-vasculature is particularly relevant for preclinical TG modelling *in vitro*, as migraine is considered as a neurovascular disease[472]. Headache attacks can be directly triggered by the activation of the trigeminovascular system, through vasoactive signalling molecules secreted by trigeminal nociceptors[473].

Among major neuropeptides and neurotransmitters with known association in migraine attacks, CGRP is the strongest vasodilating neuropeptide[473]. Cells that constitute local vasculature in sensory ganglia are major reservoirs of CGRP receptors (Figure 20b). A recent GWAS meta-analysis has identified migraine-associated risk variants in vascular cell types, but not via mutations through CGRP receptor components[462]. Therefore, our CGRP-secreting TG model is a suitable candidate for the neuronal component of the assembloid model.

TG iNociceptors that continued maturation as suspended organoids maintained peptidergic cell fate (Figure 25a). Mature TG organoids were of high cellular density which has led to uneven penetration during staining and imaging (Figure 25b & d). Despite the technical challenges, we were able to identify bipolar sensory neurons (Figure 25c). Compared to d12 organoids (Figure 14), pseudounipolar neurons were more difficult to individually identify and trace. Axonal processes that were CGRP+/SST- or CGRP/SST double positive could be identified (Figure 25d).

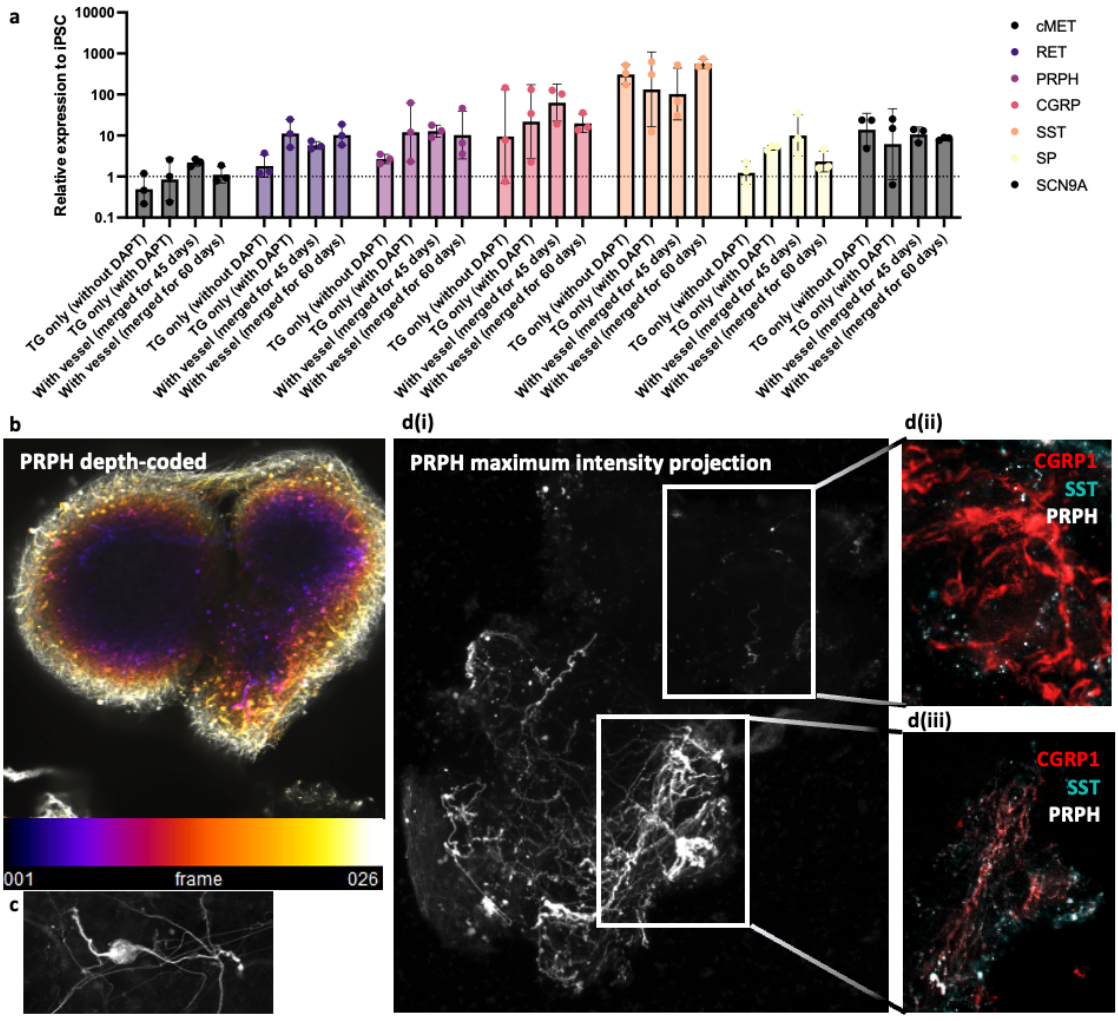


Figure 25: Confirmation of peptidergic cell fate in TG iNociceptor cultured as organoids without ArC treatment.
(a) Confirmation of retained pepetidergic marker expression in mature SBAD03 TG iNociceptors cultured as organoids by RT-qPCR, n=3 independent differentiations per condition. (b) Demonstration of the loss of staining and imaging penenetration in the centre of mature TG organoids. (c) Representative PRPH+ bipolar and pseudounipolar morphologies identified from mature SBAD03 TG organoids. (d) Representative peptidergic nociceptors in mature SBAD03 TG organoids: (i) Uneven distribution of PRPH immunoreactivities in maximum intensity projection of an irregularly shaped TG organoid; (ii-iii) axonal process positive for (ii) CGRP alone and (iii) CGRP with SST.

Neuron differentiation *in vitro* begins by introducing ectoderm lineages, bypassing mesoderm that embryologically derives to vasculature[469]. Minimal expression of early mesoderm marker *TBXT*+ was expressed in our TP protocol (Figure S12). Therefore, we differentiated endothelial cells separately from a vascular organoid protocol[474] (Figure 26) to prepare for neurovascular integration. After initial mesoderm induction, Matrigel domes allowed tube formation and extensions without limitations in directions in presence of vascularisation cues vascular endothelial growth factor-A (VEGF-A) and basic FGF (bFGF) (Figure 26b). Unlike neuronal differentiation, pre-treatment of hiPSCs with DMSO prior to differentiation did not further improve endothelial gene expression (Figure 26c). By d10, major markers for endothelia and pericytes were significantly upregulated (Figure 26c-d).

To visualise and compare between vessel density of primary sensory ganglia *ex vivo* and vascularture developed*in vitro*, we first reconstructed complete CD31+ topology in chemically cleared whole WT female DRGs (Figure 27). Vessel networks appeared to wrap around individual neuron-glia units *in vivo* (Figure 27b), similar to cell topology mapped by spatial transcriptomics[475] and cryo-EM imaging[476]. For quantitative comparisons, vasculature geometry of 7 whole mount DRGs was extracted via a published pipeline[477] (Table 5). Maximum intensity projections of unprocessed CD31 fluorescent signal and pipeline-extracted skeleton could be visualised for DRGs of a range of sizes (Figure 27c). Although we did not limit to any specific spinal region during tissue harvest, average branch sizes appeared uniform across the primary DRGs that we examined.

DRG	**1**	**2**	**3**	**4**	**5**	**6**	**7**
Total length (μm)	38171.5	47827.79	25346.81	12293.27	12998.04	7280.46	12123.92
Number of branches	1289	1585	757	419	414	207	407
Average branch length (μm)	29.61	30.18	33.48	29.34	31.4	35.17	29.79
Mean vessel cross-section (μm^2)	0.62	0.62	0.69	0.57	0.65	0.67	0.62
Mean vessel diameter (μm)	0.89	0.89	0.94	0.85	0.91	0.93	0.89
Total volume (μm^3)	23693	29866.27	17598.34	6948.02	8445	4903.00	7564.43

Table 5: Summary of mouse primary DRG vasculature based on CD31 geometry analysis.

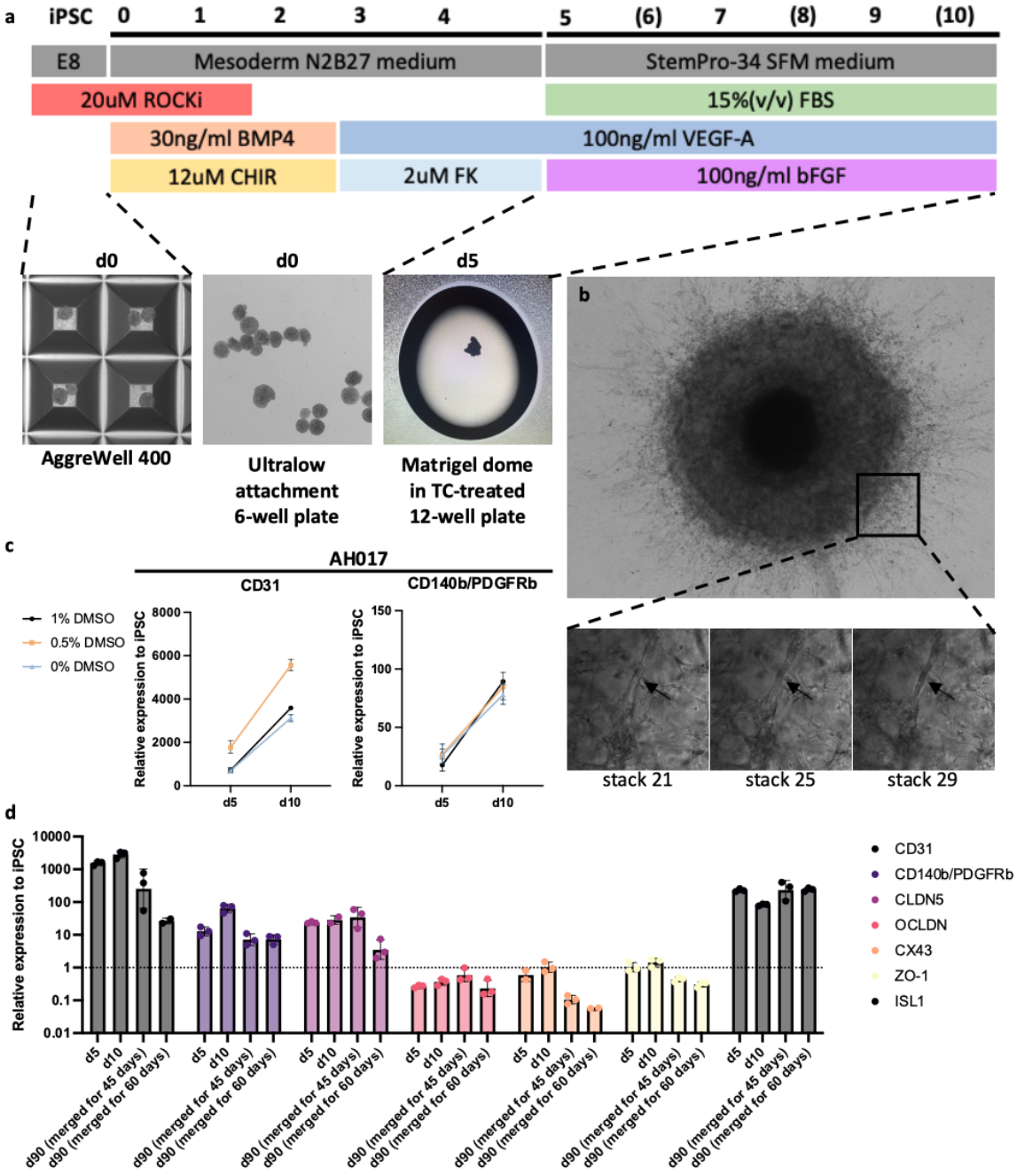


Figure 26: Optimisation of a 3D iPSC-derived vessel model
(a) Schematics of the development of an iPSC-derived vessel model, optimised based on published protocol[474]. (b) Representative brightfield images of cellular migration and branch outreach in the extracellular matrix. (c) Impact of DMSO pre-treatment on mesodermal cell fate induction by RT-qPCR, n=3 independent differentiations in AH017 vascular organoids. (d) Expression of vascular markers before and after merging with TG neurons by RT-qPCR, n=3 independent differentiations in SBAD03 assembloids.

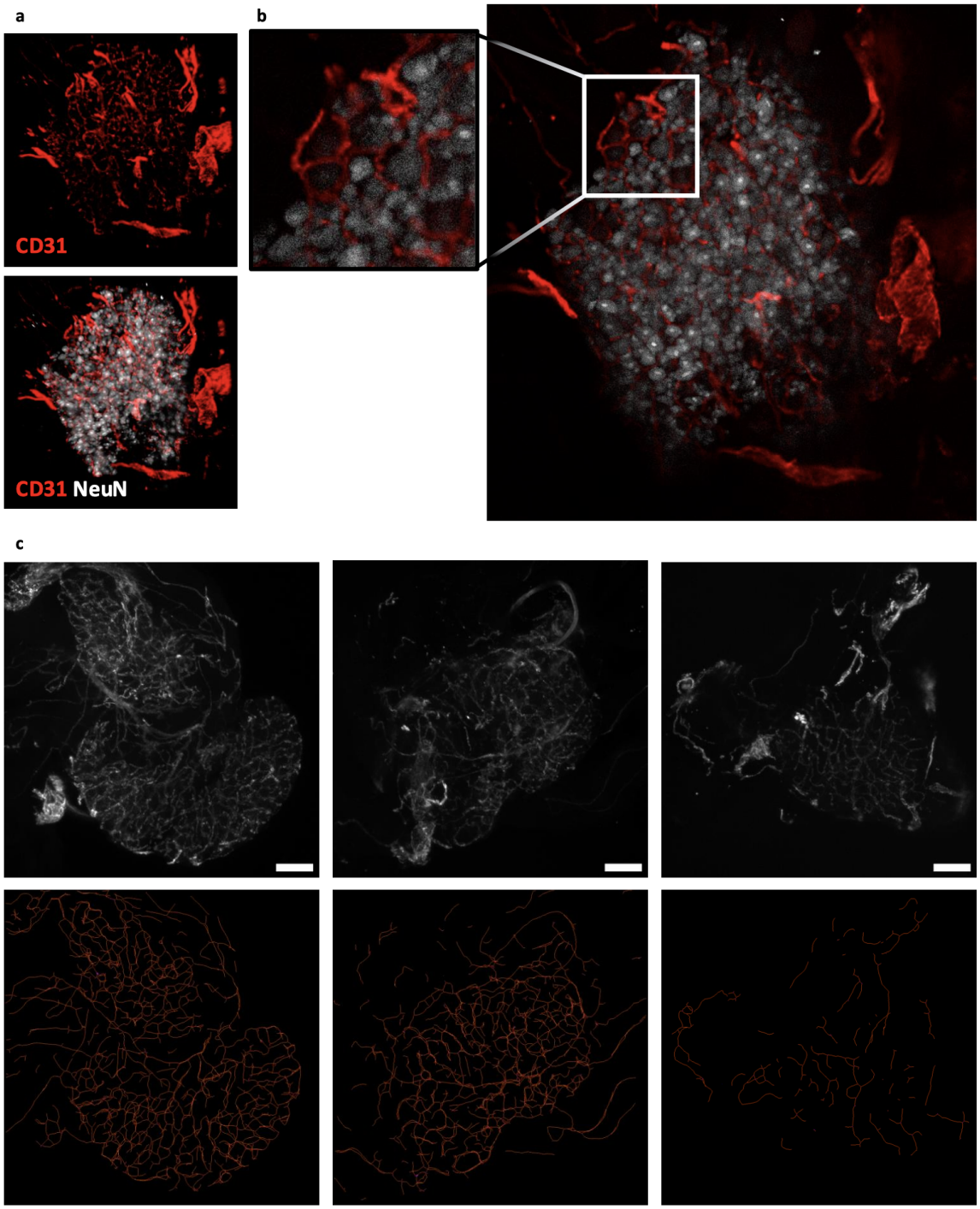


Figure 27: Extensive CD31+ endothelial network visualised in whole mount BL6 female DRGs. (a) 3D rendering of the complete CD31+ network from the confocal z-stack series covering the whole thickness of chemically cleared whole mount DRGs from female BL6 mice. (b) Representative slice extracted from z-stack. Zoom region shows CD31+ endothelial network wrapping up individual neurons. (c) Comparison between projections of original CD31 signal and vascular geometry extracted from pipeline[477] across a range of sample size and thickness. Scale bar 100µm.

We did not clear primary TGs due to challenges of bigger sizes and uneven cell distribution. However, sensory neurons, SGCs, endothelia and pericytes could be identified in proximity in cell-dense areas (Figure 28). CX43+ gap junctions were identified as glial contacts outlining neuronal soma[174] and within vasculature[478] (Figure 28b).

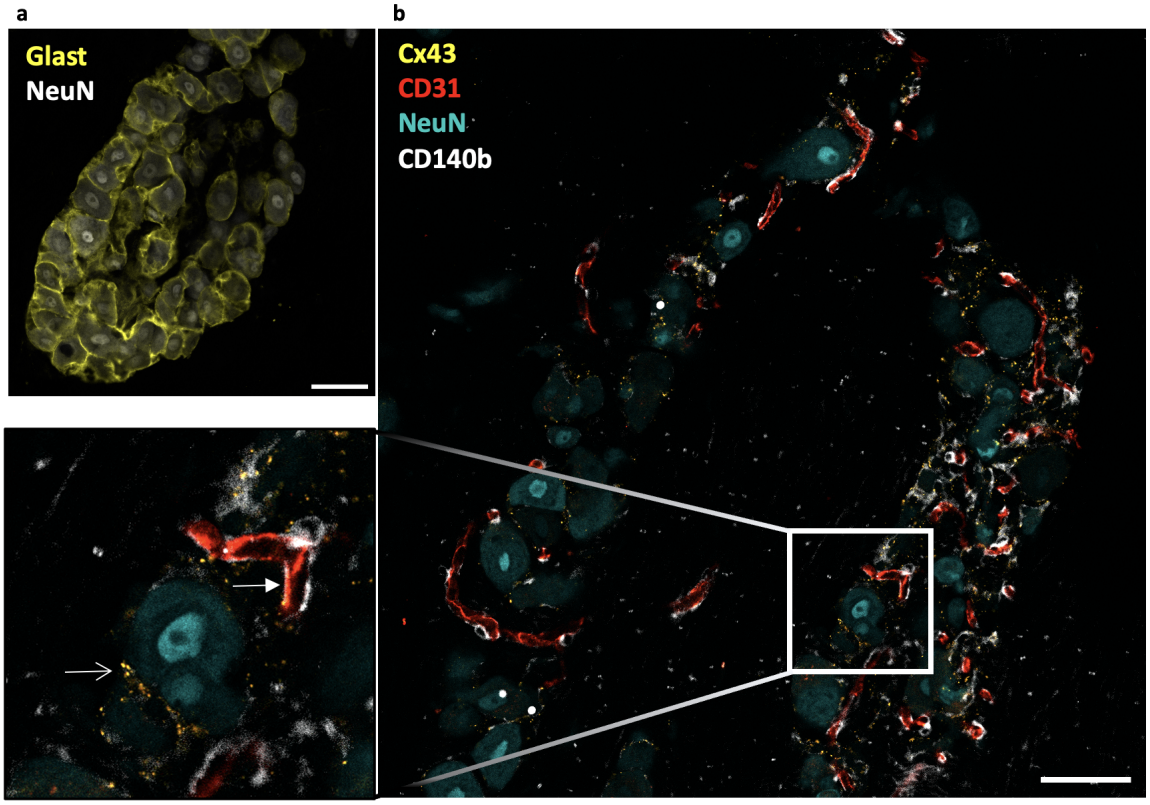


Figure 28: Visualisation of major cell types and spatial distribution in primary mouse TGs. (a) Demonstration of spatial distribution of major cell types in female WT mouse TGs, as (i) merged fluorescence labelling of all markers, (ii) corresponding brightfield, (iii) SGCs encapsulating neurons, and (iv) endothelial and pericyte network. (b) Identification of tight junctions encapsulating neurons (thin arrow) and within vasculature (thick arrow). Scale bar 50µm.

We then applied the same visualisation and quantification strategy to the tubular geometry of CD31+ cells in the iPSC-derived vascular model (Figure 29). CD31+ endothelial network *in vitro* was less organised, with smaller vessel branch lengths and diameters on average.

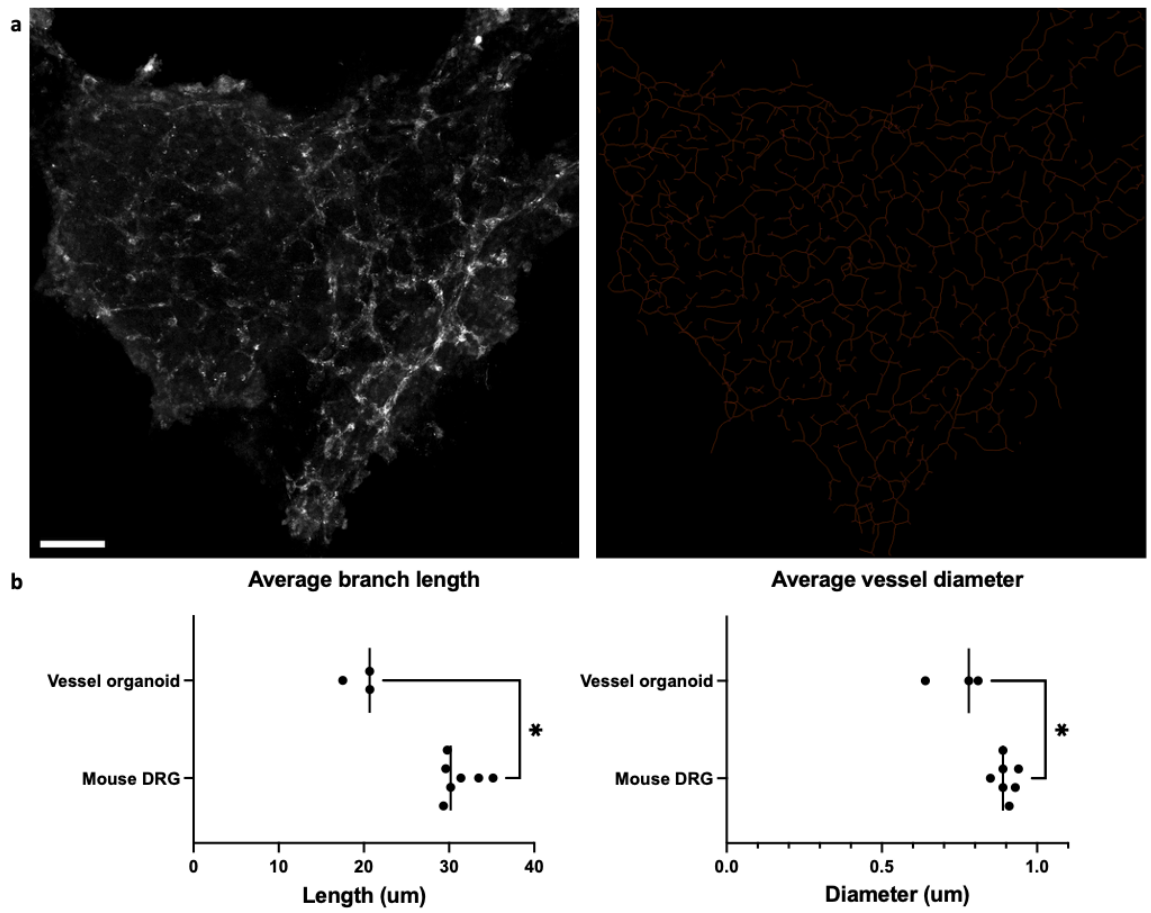


Figure 29: CD31 geometry in hiPSC-derived vessel organoids.
(a) Representative maximum intensity projection (left) and extracted reconstructed geometry (right) by pipeline[477] of CD31+ endothelial network in d10 SBAD03 vessel organoids. Scale bar 100µm.
(b) Comparison of vascular geometry parameters ex vivo and in vitro. n=3 for vessel organoids developed in vitro and 7 for murine DRGs ex vivo. Statistical significance determined by Mann-Whitney tests for both panels: p=0.0167 for branch length comparison, p=0.0167 for diameter comparison.

As the neuronal and vascular organoids were induced individually, we attempted to investigate mutual outreach, infiltration and migration by fusing the vascular half at different time points during iNociceptor maturation. No substantial differences were observed in marker gene expression for endothelia (Figure 26d) or neurons (Figure 25a). However, fusion by gravity in ultra low-attachment wells was insufficient to maintain strong physical contacts, given different cellular density between the neuronal half and the vascular half. Although we observed some close association between endothelial and neuronal somata (Figure 30), sample dissociation occurred during whole-mount sample washes for chemical clearing. It was mechanically difficult to locate structures with both halves retained, or to proceed with functional experiments.

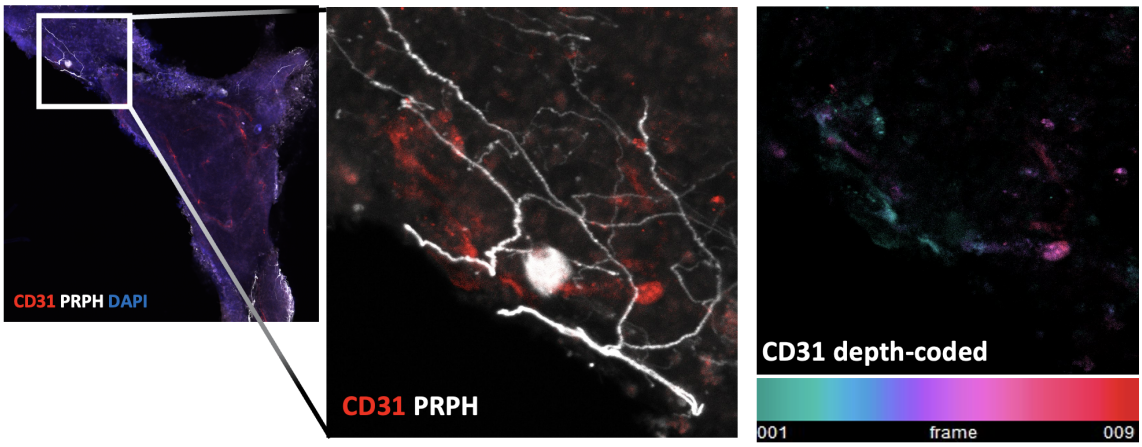


Figure 30: Representative confocal image of endothelial association in proximity to neuronal soma in the neurovascular assembloid, as maximum intensity projection (middle), and CD31+ vessel topology colour-coded by depth in z-stack.

It is noteworthy that, another similar protocol using the fusion-by-physical-contact method was able to identify nerve endings in close contact to endothelia in the assembloid[479]. However, as sensory nerve endings are extensive and remote from sensory ganglia themselves *in vivo*, sensory innervation of vasculature would be a more appropriate model for the pain-detecting periphery. It is unlikely that micro-vessels have direct physical contacts with neurons within sensory ganglia *in vivo*, as sensory somata are known to be physically enclosed by SGCs (Figure 28a). However, we could not visualise any GFAP+ glia by immunolabelling potentially co-developing from 3D TPs (data not shown), despite detectable transcripts (Figure 15b). As SGCs are transcriptionally diverse[173,174], alternative markers or high-throughput assays could potentially identify glial cells retained in such organoids. Overall, it can be concluded that the neurovascular assembloid protocol in the current project is a proof-of-principle model that requires further optimisation on cellular organisation, structural support, and functional characterisation. Although key marker expression was induced and maintained, consistent extracellular scaffold support such as hydrogel embedding[480] will be pivotal.

2.5 Discussion

2.5.1 Generation of neuropeptide secreting TG iNociceptors

The current project has successfully produced a protocol for peptidergic TG iNociceptors that are embryologically accurate, secreting high level of CGRP modulated by a range of chemical cues, and expressing thermally responstive TRPV1. Our protocol can be readily adapted to both 2D and 3D culturing platforms while preserving peptidergic cell fate. The adaptable maturation methods allow different kinds of functional assays and integration with protocols of other cell types.

The current project further confirmed that the TG iNociceptors derived from our protocol can produce multiple types of neuropeptides, in particular with SST and CGRP co-expressed, for the first time in the literature. A recent sequencing study identified a group of SST and CGRP double positive cells in human TG and their involvement in migraine[5], highlighting the potentials of our protocol for pathological modelling. Our protocol is also the first to demonstrate vesicle-like intracellular distribution of neuropeptides comparable to neuropeptide immunolabelling features *ex vivo*. Experimental outcomes of our protocol compared to similar studies in the literature are listed in Table 6.

One major limitation of the current TG protocol is the relatively lower induction efficiency of cranial placodal progenitors[435] and resulting neurons. Optimisation of enrichment methods was attempted in the current project, with varying success. Scalable production is possible but relatively costly.

PHENOTYPES	CURRENT PROJECTS	LITERATURE
Embryological origin	Placodal structure with mixed SIX1 and SOX10+ progenitors, matching with cell identidy *in utero*	Mostly neural crest
CGRP secretion	0-170.7pg/ml (median 17.18pg/ml, mean 28.41pg/ml, standard deviation 30.54pg/ml) per 100k secreting cells at BL, responsive to agonists (Figure 19 & 24)	<1pg/ml per 100k secreting cells at BL[434]
SST secretion	Untested due to kit incompatibility	No published data available
SP secreton	Untested due to kit incompatibility	<5pg/ml per 1 mil cells at BL[434]; 10pg/ml per 2 mil cells at BL[414]; 3pg/ml*hour, no density provided[422]
Co-expression	SST and CGRP double positive by IF (Figure 25)	No published data available
Subcellular localisation	CGRP granules, SST granules & cytosol signals, and SP cytosol signals visualised, restricted by antigen specificity from commericially available immunolabelling tools. Co-expression and SgII+[117,481] LDCV packaging theoretically possible, but limited by the scope of the current project.	Cellular resolution only, no vesicle appearance with IF.
TRPV1 responsiveness	Majority of firing cells noxious heat-responsive (Figure 21)	<30% in mouse counterparts by capsaicin-treated calcium imaging[424]

Table 6: Comparison of phenotypical outcomes between peptidergic iNociceptor protocols from the current project and available literature.
BL, baseline; IF, immunofluorescence.

2.5.2 Glia-facilitated survival and cell fate specification of iNociceptors

Supplementary glial co-cultures have been a common practice for iPSC-derived sensory neurons, for the benefits of more mature morphology[441] and firing activities[445].

Despite the obvious benefits of astroglial co-cultures, it begs the question of the unnatural configuration of direct contacts between peripheral ganglion-residing sensory somata and CNS-residing astrocytes. Although it is suggested that SGCs and astrocytes are functionally comparable[482], the lack of in-depth research on SGCs might overlook critical and unique glial biology that distinguish the two cell types[169]. Given the growing knowledge of different molecular signatures in TG and DRG[173,432], it is also logical to speculate spatially diverse neuroglial interactions.

Upregulation of conventional peptidergic markers such as SCN10A and TRPV1 was common in both Chambers' iNociceptors and our TG iNociceptors (Figure 6 & 23), suggesting that the classical definition of peptidergic neurons from murine studies is not directly applicable to classify iNociceptor identities. However, certain aspects of developmental trajectory were conserved from rodents to human. The retained expression of *cMET* and *TRKA* which predict functionally peptidergic identities in iNociceptors aligns with the current understanding from rodent studies.

Although neuropeptides were transcribed in both types of iNociceptors, translation and secretion were limited to the TG iNociceptors (Figure 18, 19 & 24). Therefore, it is expected that iNociceptors generated from the two protocols differentially regulate the translation, packaging, and sorting of neuropeptides. Local cytosolic factors such as pH and calcium levels are known to guide vesicle sorting from Golgi bodies[483,484]. However, it is currently unknown to what extent this process is determined by the genetic programs that diversifies specific nociceptor cell fates.

The striking contrast in terminal nociceptor subtypes and functional diversities between the Chambers' and our TG protocol suggest the following observation-based *hypotheses* on human nociceptor development:

- *Placodes (derived either via 2D or 3D) contain the necessary supportive cell types*

as part of the neural boarder induction, likely glia, because (1) baseline secretion of CGRP was reduced in iNociceptors derived from 2D placodes treated with AraC, which recovered when astrocytes were supplemented (Figure S16); (2) TGs induced and matured in 3D without AraC treatment or glial supplementation still produced CGRP+ iNociceptors (Figure 25).

- *Genomic and epigenetic programming for nociceptor subtype specification begins very early during differentiation, which requires specific spatial organisation*, because supplying astrocytes to Chambers' iNociceptors did not impact secretive CGRP (Figure 9); (2) supplying astrocytes to TG iNociceptors after d35 did not further increase CGRP secretion (data not shown); and (3) migrating TP induction to 3D platform largely increased the efficiency of neuronal induction and generated CGRP-secreting phenotypes regardless of the method of maturation (Figure 15).

- *The glia-facilitated CGRP secretion must require specific physical contacts and/or density*, as (1) sensory neurons *in utero* co-develop with glia from a communal pool of neural crest progenitors, which requires direct cell-to-cell contacts of markers in the NOTCH signalling pathway[73,485–487]; (2) astrocytes in both Chambers' and our co-cultures displayed the typical tiling morphology[488], suggesting active physical engagement with neurons (Figure 9 & S16f); and (3) pilot work in our lab demonstrated that astrocyte-conditioned media was not sufficient to induce CGRP-secreting iNociceptors during development[2].

It is worth noting that sensory neuron development and diversification is not a simple bifurcation[73,489]. Sensory neuron subtype segregation is a result of extensive internal genetic regulations and external cues depending on the destination of innervation[11]. The current project lacks the resolution to resolve the transition and specification temporally and to single-cell level, which is one possible direction for future experiments.

2.5.3 TRPV1 & Peripheral thermo-sensors

TRPV1 expression during development

Among the 28 members of TRP superfamily, TRPV1 is inarguably the most studied for its involvement in pain and thermoregulation[490]. In mice, early expression of TrpV1 marks all future TrpV1+ and TrpM8+ sensory neurons, and some Mrg-, TrpV2, and TrpA1-expressing neurons[12]. Mice with the TrpV1 lineage removed completely lost thermosensitivity and purinergic nociception. Some CGRP expression was retained[12], possibly from the RET-independent A fibres[88]. In the spinal cord of TrpV1-KO mice, multimodal wide dynamic range (WDR) neurons lost thermal but not mechanical coding[491].

Given the interspecies differences of TRPV1 distribution and the lack of understanding for human peptidergic neuron development, the impact of TRPV1 as an embryonic marker is inconclusive in human. A recent study of spatio-temporal map of developing human DRGs has identified relatively universal TRPV1 expression in multiple branches of sensory neurons from the second wave of neurogenesis by GW21[73]. Similarly, TRPV1 is upregulated by d10 (Figure 16a) in either iNociceptor protocol, long before action potential or capsaicin-induced calcium influx could be detected[411]. Therefore, it is theoretically possible that the early induction (or even the retained expression) of TRPV1 in iNociceptors reflects certain conserved developmental programs of human nociceptors besides functional thermo-regulation. However, it is still unknown whether embryological expression of TRPV1 has any functional relevance to cell fate specification *in utero* or *in vitro*.

Modes of TRPV1 activation

TRPV1 is a homotetramer with each subunit consisting of six transmembrane segments (S1-S6)[492]. Structural biology studies identified a dual gating system of the TRPV1 ion pole, granting it multiple and synergic modes of activation depending on the stimuli[15,18].

Directed mutagenesis studies and cryo-EM crystallography demonstrated independent TRPV1 activation mechanism by capsaicin and heat[493,494]. Capsaicin and conventional selective antagonists (e.g. AMG9810[458]) compete for the binding pocket at transmembrane

domain S3-4[16]. In cells canonically express TRPV1 such as human and rodent C-fibres, capsaicin-dependent axonal TRPV1 activation appears to elicit contradictory effects on excitatory post-synaptic currents *ex vivo*[495]. Capsaicin paradoxically induces a brief excitatory pro-nociceptive effects and then desensitises sensory neurons for a long period of time, by inhibiting further activation by a range of agonists via T-type calcium channel inactivation[496].

In contrast, noxious heat induces a series of stepwise conformational changes from and rearranges the outer pore[493,497]. Mathematical modelling indicates temperature changes introduce a shift of voltage-dependent activation curve[498].

The two activation pathways can interact allosterically in synergy, as low concentration of capsaicin did not elicit currents through TRPV1 expressed in oocytes, rather amplified heat-induced currents[493]. When inserted on a lipid surface more rigid than the plasma membrane, combined action of heat and capsaicin can rescue the ion passage which heat alone cannot fully open[15]. Irreversible TRPV1 channel opener DkTx quenches adjacent subunits at the out pore[15], which leads to heat insensitivity but synergy to capsaicin[493].

Functional genomics of TRPV1 and other potential thermosensing channels

TRPV1 is not the only heat-sensing channel in sensory neurons. The TRP family contains multiple thermo-sensitive members[499–502]: Besides TRPV1, TRPV2 and TRPM3 respond to noxious heat. TRPM8 and TRPA1 react to coolness and coldness. TRPV3, TRPV4, TRPM2, TRPM4, and TRPM5 are activated by non-noxious warmth.

Besides TRP channels, new heat pain-sensing subpopulations have also been identified in murine DRGs, such as zinc-finger CCHC domain-containing 12 (Zcchc12)-positive neurons[503]. Additionally, direct interaction between FGF13 and $Na_V1.7$ is found to partake in noxious heat detection in mice[504].

Clustering based on responsive thermal ranges, a recent paper has defined three sets of thermosensing neurons in murine DRGs and the corresponding relaying projection neurons using *in vivo* calcium imaging[33]: Besides the cluster (39.3%) that exclusively responds to cold (22 degrees) and extreme cold (8 degrees), there are two distinct groups of

heat-responsive sensory neuron & projection neuron pathways. About 50% of L4 DRG neurons respond to noxious heat about 43 degrees while a small population of neurons display tonic activities to skin temperature but also fire when higher temperature is applied. Similarly, thermosensors in mouse TGs were recruited in a graded manner, with a fraction of nociceptors response to full ranges between body temperature and extreme noxious heat up to 50 degrees[32].

Notably, crystallography and channel dynamics studies are usually conducted in ectopic expression systems, which might not reflect natural contexts for signalling pathways. Although it is conventionally understood that TRPV1 is activated between 42 and 45 degrees, TrpV1+ peptidergic neurons in mouse TGs typically react to body temperature and non-noxious warmth, as well as noxious heat[32]. The majority of thermosensors active under extreme heat belonged to non-canonical non-peptidergic subpopulations, instead of conventionally defined TrpV1+ peptidergic murine nociceptors[32]. All major classes of thermosensors identified in mouse TGs via *in vivo* calcium imaging have been confirmed to express TrpV1[5]. Consequently, TrpV1-KO mice displayed comparable nociceptive behaviours under noxious heat under 50 degrees, and impaired nocifensive responses at 52 degrees and beyond[491]. A similar discrepancy between *in vitro* and *in vivo* thermo-threshold was reported in TrpV3-KOs[501].

Combined, current evidence suggests redundancy of thermo-sensing channels over certain temperature ranges. One hypothesis for the mismatch of thermal ranges is naturally existing TRP heterodimers with altered thermal thresholds, which is lacking in *in vitro* ectopic systems.

Examining TRPV1 functions in nociceptors developed *in vitro*

Overall, current evidence strongly suggests functional redundancy and complex interactions between multiple temperature-sensing proteins in nociceptors *in vivo*. However, reports for heat-induced firing from nociceptors of any *in vitro* differentiation protocol are considerably rarer (e.g. in Chambers'[421], from commercially available kits[445], and other differentiation

programs[425]), all of which tested for responsiveness at one specific temperature. None of the reports confirmed the involvement of TRPV1 specifically via pharmacological or genomic intervention.

Instead, the current project tested multiple temperatures of non-detrimental noxious heat. We further confirmed the involvement of TRPV1 by applying selective antagonist AMG9810 in a dose-dependent fashion. Although AMG9810 acts via competitive binding with TRPV1 at the S3-4 binding pocket, AMG9810 can inhibit TRPV1 activation via other means of conformational change, including heat and protons[459].

Firing activities at physiological temperature without chemical triggers are conventionally regarded as spontaneous for iNociceptors *in vitro*. However, the reduction in baseline activities with AMG9810 in both Chamber's and TG iNociceptors suggests that part of the spontaneous firing detected at physiological temperature is partially TRPV1-dependent, potentially through tonic channel activation. Alternatively, the lack of tissue regulation (especially electric isolation by SGCs) *in vitro* can potentially lead to TRPV1 activation by innate agonists in the culture (e.g. protons[17], membrane lipds[17], voltage changes[494]).

The shift in maximum firing temperature between Chambers' and our TG iNociceptors further implies differential thermal regulation mechanisms in different subtypes of nociceptors. It is unclear whether TGs and DRGs *in vivo* also display a difference in peak activating temperature. One critical consideration is that thermal pain assays are applied over skin *in vivo* while *ex vivo* or *in vitro* experiments directly expose nociceptor somata to heat. Therefore, future experiments will require better cellular and thermal resolution.

3 Investigation of the Molecular Oscillations and Pain-Related Functional Relevance in iNociceptors

3.1 Overview

Cellular circadian experiments in human tissues are commonly carried out in fibroblasts[310,324,505–507], immortalised cell lines (e.g. HCT-116[508,509], U2OS[244,257,506,510–512] and HEK293 derivatives[285,512,513]), and primary hepatocytes[514–516]. In particular, mammalian fibroblasts are valuable models due to comparably easy sample acquisition and sustainable molecular oscillations *ex vivo*[310,324,505,517].

In comparison, the molecular circadian properties in hiPSC-derived neuronal models are less characterised. Undifferentiated pluripotent stem cells usually lack sustained circadian cycles (review see[518]). A few published works extensively investigated TTFL expression during and after the maturation of hiPSC-derived cortical neurons *in vitro*, most of which employs clock gene promoter-driven bioluminescence readouts[406,519,520].

The lack of central entrainment further demands alternative synchronisation methods to *in vivo* "native" time or sustained cycles *ex vivo*. As the impact of light/dark cycles does not apply to most cultured cells, robust circadian oscillations can be induced via environmental cues such as serum shocks[521], feeding-fasting entrainment[522], hypoxia[506], temperature[272,523,524], and chemical synchronisers FK[525] or Dex[526]. For assays where discrete time points are necessary, it is crucial to define an efficient routine with enough temporal resolution for sample collection and time series curve fitting[527]. Different clock gene paralogs might differentially respond to different entrainment cues[528]. Therefore, this chapter will address the best culture conditions (such as media composition, synchronisation method and sustainability of in-phase cycles) to obtain molecular oscillations.

Previous work in our lab has mapped oscillating naïve *BMAL1* promoter activities in mature Chambers iNociceptors using *BMAL1*::luciferase lentivirus[1]. As the rhythmicity

in transcription alone doesn't necessarily entail functionally oscillating protein products[529], we will focus on multiple ways to quantify and visualise clock genes, from transcriptional and translational abundance to subcellular distributions and functional associations, using normal human dermal fibroblasts (NHDF) and primary murine sensory ganglia as positive controls to optimise experimental design when appropriate.
Overall, this chapter aims to:

1. Identify culture conditions that induce clock gene oscillations in iNociceptors developed *in vitro* (Section 3.2.1).

2. Optimise experimental designs for clock gene quantification in vitro with known oscillator NHDFs (Section S3.6-S3.7).

3. Quantify changes of clock gene expression at transcriptional (Section 3.3) and translational level in chemically synchronised iNociceptors.

4. Identify diurnally differential pain-related gene expression and firing patterns in chemically synchronised iNociceptors (Section 3.4).

3.2 Transcriptional analysis of clock gene oscillations in Chambers' DRG iNociceptors

3.2.1 Quantifying chemically induced oscillations of clock gene transcription

Relative mRNA quantification via traditional RT-qPCR relies heavily on suitable reference genes as stable endogenous controls. Therefore, we extracted common choices for RT-qPCR references from mammalian circadian studies (Table 7).

GENE	**PRODUCT**[530–532]	**RNA abundance**[533]	**MODEL SYSTEM**
18S	Ribosomal RNA	Extremely high	*Mouse lungs*[530], *Mouse fibroblasts*[534]
bACTIN	Beta-actin	Relatively high	U2OS[182,257]
GAPDH	Glyceraldehyde-3-phosphate dehydrogenase	Relatively high	HEK[513], U2OS[271,506,512], Human fibroblasts[522]
HPRT1	Hypoxanthine phosphribosyl-transferase	Relatively low	Human adipose tissue[535]
RPLP0	Ribosomal protein, large P3	Medium	*Mouse lungs*[530]
TBP	TATA box binding protein	Relatively low	HEK[285], Human fibroblasts[507], Mouse lungs[530]
YWHAZ	Tyrosine 3-monooxygenase/tryptophan 5-monooxygenase activation protein, zeta polypeptide	Medium	Human adipose tissue (for hypoxia & differentiation)[535]

Table 7: Commonly used or preferred reference genes for RT-qPCR in mammalian circadian models (rodent example italicised).

There is no guarantee for concordance of rhythmicity between the production of mRNA transcript and that of protein product, for both technical (e.g. sampling intensity, choice of replicates) and biological reasons[527,529]. Therefore, we designed all primers for circadian assays based on mature mRNA sequences relatively close to the N-termini to limit the effect of C-terminal biased mRNA degradation. Primers for all genes of interest except for *bACTIN*

had single peaks from melt curve analysis (data not shown). *18S* was not included due to overwhelmingly high abundance of transcripts.

In conventional *ex vivo* and *in vitro* studies of circadian rhythmicity, the first cycle is considered as entrainment cue-driven and less reflective of the innate feedback-driven clock[257]. Therefore, we extended the total sampling time to 49h in NHDFs as a positive control (Figure S23-S25) and 36h in Chambers' iNociceptors (Figure 31-34). For Chambers' iNociceptors, we also compared the effect of two basal media with different concentration of glucose, ion balance, and osmolarity on the strength of synchronisation.

None of the reference candidates demonstrated circadian variations in raw C_T values (Figure 31 & S23). The raw C_T levels of the reference genes in Chambers' iNociceptors were significantly different in contrast to NHDFs (Figure S26), reflecting tissue-specific expression patterns. As reference gene stability was assessed separately for each cell type, the difference in housekeeping gene expression did not impact downstream calculations.

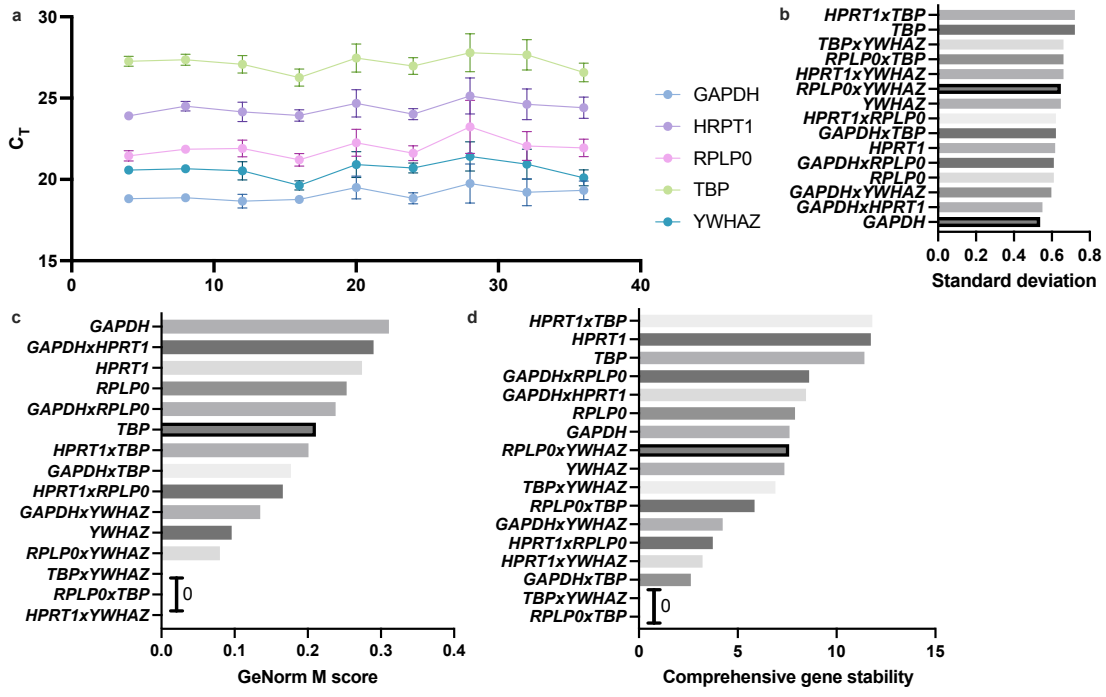


Figure 31: Evaluation of stable reference genes for mRNA relative quantification by RT-qPCR in SBAD03 DRG iNociceptors.
(a-b) (a) C_T values and (b) standard deviations of 5 different reference mRNA transcripts in SBAD03 DRG iNociceptors, n=12 technical replicates (pooled regardless of media composition or synchronisation methods) per time point for either protocol, 3ng cDNA per reaction. Error bars standard deviations per time point. (c-d) (c) GeNorm analysis and (d) comprehensive ranking of single and double reference gene stability in SBAD03 DRG iNociceptors.

Relative transcript quantification in hiPSC-derived cell types is conventionally done in relation to undifferentiated hiPSCs, usually to emphasise the trajectory of differentiation. As hiPSCs do not possess oscillating TTFL transcription[506] (Figure 37), we pilot tested the technical stability of TTFL transcript abundance across multiple samples of hiPSCs (Figure 32). Certain clock gene transcripts demonstrated large technical variations between RNA samples of the same hiPSC clones.

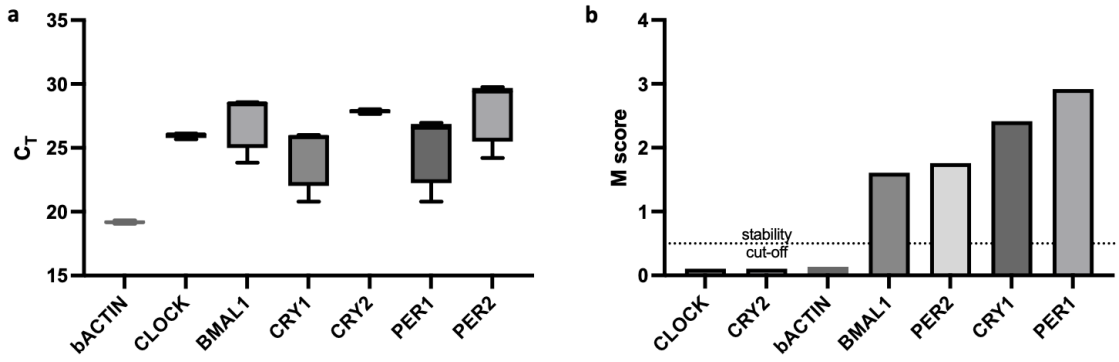


Figure 32: Challenges of using unsynchronised undifferentiated hiPSCs as the universal control sample for relative quantification.
(a-b) (a) Raw C_T distribution (n=4) and (b) stability ranking of TTFL transcripts in technical replicates of the same SBAD02 hiPSC clone.

Therefore, we used a pseudo-standard (C_T average of the first time point per treatment) for all $\Delta\Delta C_T$ calculations across multiple plates, including Chambers' iNociceptors and NHDFs.

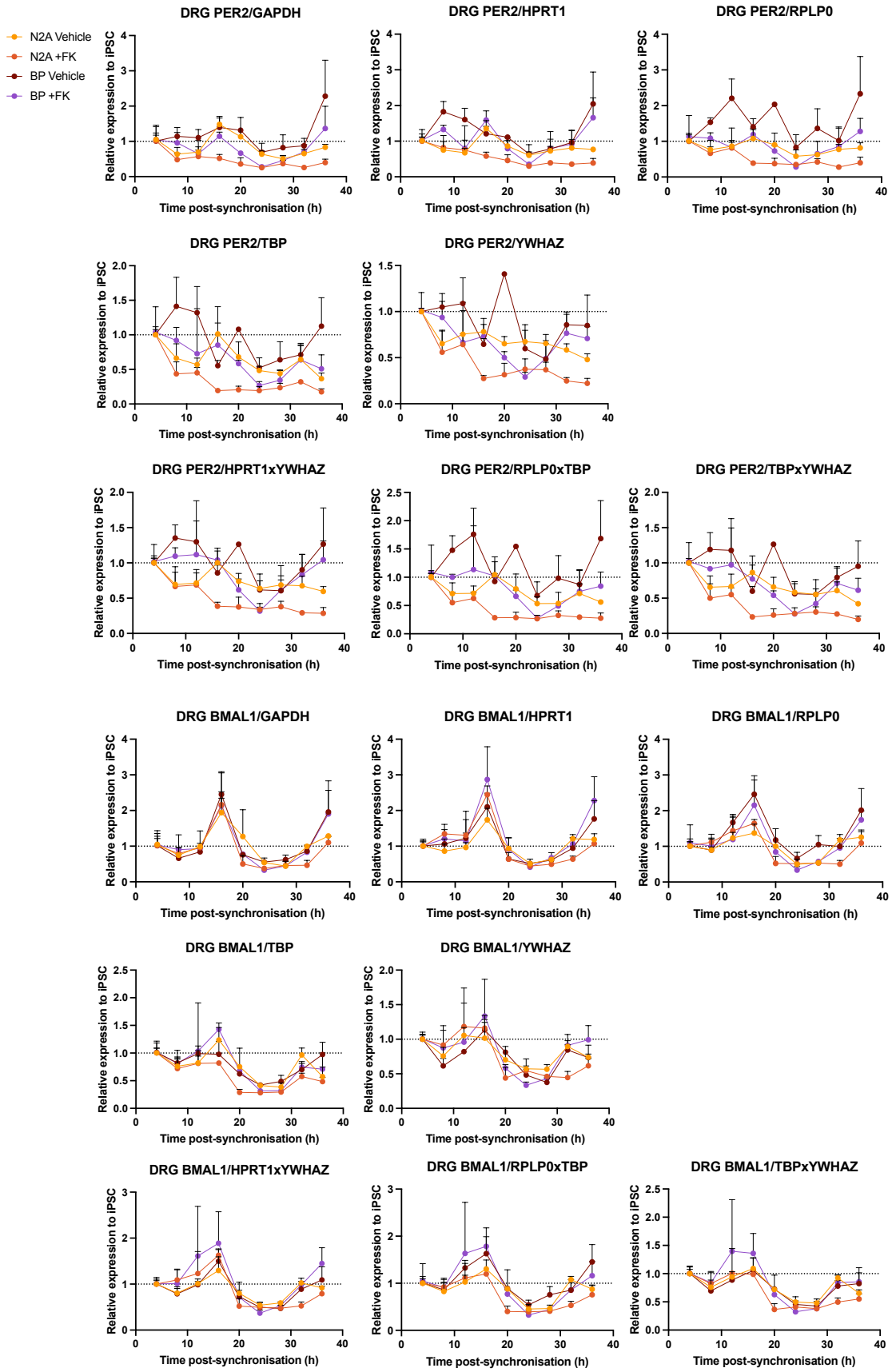


Figure 33: Relative expression of PER2 (top) & BMAL1 (bottom) in SBAD03 DRG iNociceptors normalised with different single or double reference genes. n =3 technical replicates per time point per synchronisation method. 3ng cDNA per reaction. Error bar standard deviation.

Reference gene stability was ranked by the GeNorm algorithm which compares total C_T values of each reference gene available via stepwise comparison and removal of the least stable until the two best candidates. Besides individual genes, we also used geometric means[536] of two genes as prospective dual reference candidates. GeNorm results were integrated with other published stability algorithm to produce a comprehensive gene stability score via the web-based stability tool RefFinder[537] for confirmation. In both NHDFs and iNociceptors, double reference systems appeared more stable than most single reference genes (Figure 31 & S23).

To demonstrate the impact of reference stability on circadian transcriptional analysis, relative abundance of *PER2* and *BMAL1* as fold changes was graphed against all five single and three most stable double reference candidates in DRG iNociceptors (Figure 33). We chose *HRPT1xYWHAZ* dual system as the reference for Chambers' iNociceptors based on stability and the visualisation of oscillation. We focused on *BMAL1*, *PER2* and *CRY1* which represent both arms of the core loop and major players of either repressor family.

Both N2A and BP media were sufficient to trigger *BMAL1* fluctuations over at least 24 hours without the addition of external synchroniser. The entrainment effect by media was likely exerted by the combination of glucose, amino acids, progesterone and corticosteroid present in the basal medium and supplements. FK synchronisation increased the amplitude but did not alter the phase of *BMAL1* oscillation.

The first 12 hours after synchronisation appeared more variable across technical replicates for the repressors. The peak of *PER2* appeared immediately after the entrainment with FK, as FK synchronises cells by inducing *PER* and *DBP* transcription after activating cAMP cascades[525]. In N2A media, the oscillation of *CRY1* was anti-phase to that of *BMAL1* from 12 hours post-synchronisation onward, with FK amplifying the peak fold change. BP media depleted *CRY1* transcription after 24 hours, possibly as a consequence of lower glucose[249]. Interestingly, *GAPDH*, a common choice for circadian stable reference, was moderately oscillating anti-sense to *BMAL1* in FK-synchronised Chambers' iNociceptors. Nonetheless, the M score for *GAPDH* temporal stability was lower than the conventional cut-off at 0.5, suggesting the oscillation was of small effect.

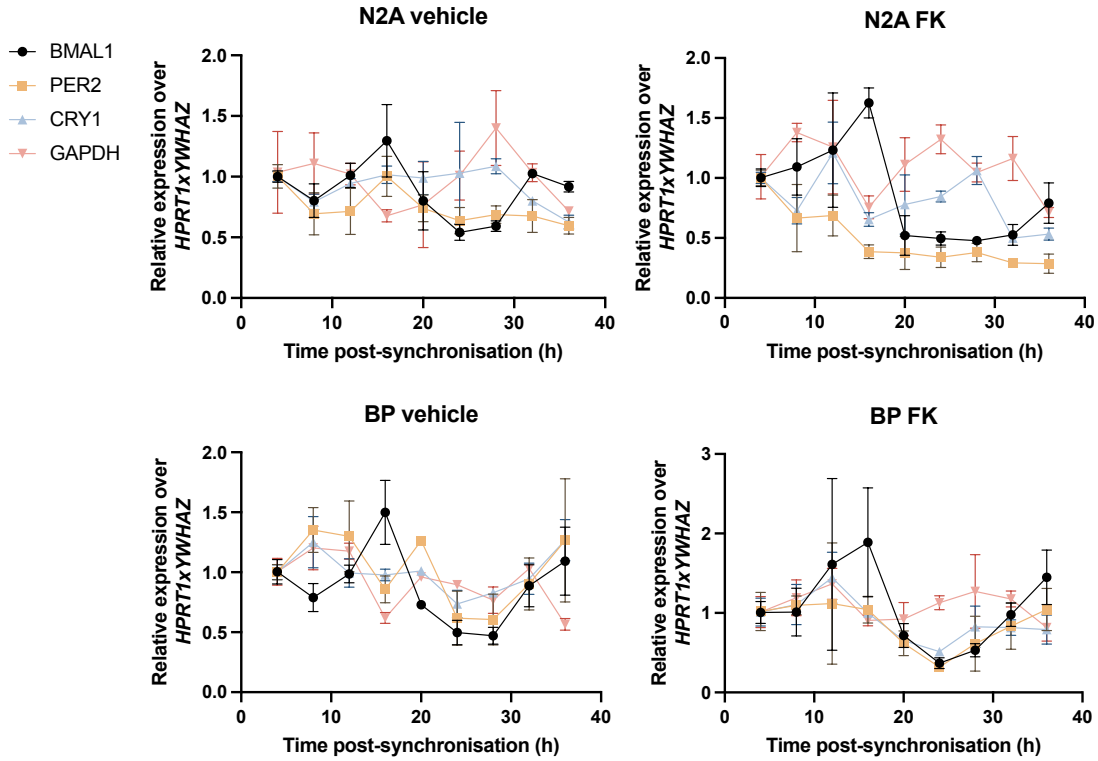


Figure 34: Transcriptional analysis of clock gene expression in chemically synchronised SBAD03 DRG non-peptidergic iNociceptors, grouped by synchronisation conditions. n=3 technical replicates per time point per synchronisation method. 3ng cDNA per reaction. Error bar standard deviation.

Given the potential interspecies differences, it is important to verify major TTFL players *in vivo*. We examined a published bulk transcriptomic dataset that compared absolute transcript abundance of clock genes in human and mice[6]. Although no information on time of death was reported in the study, tissue- and species-specific distribution of core clock genes were identified (Figure 35). Human DRGs displayed higher abundance *CRY2* and *PER1 in vivo* than other orthogonal courterparts in each repressor family. In comparison, relative expression for *CRY2* and *PER1* (both C_T above 32 at most circadian time) were too low to calculate circadian variations for Chambers' iNociceptors *in vitro*. The difference in detectable orthologs is likely a consequence of reduced sensitivity and specific primer designs of RT-qPCR. Future experiments will reduce technical variabilities by applying similar sequencing analysis to chemically synchronised Chamber's iNociceptors.

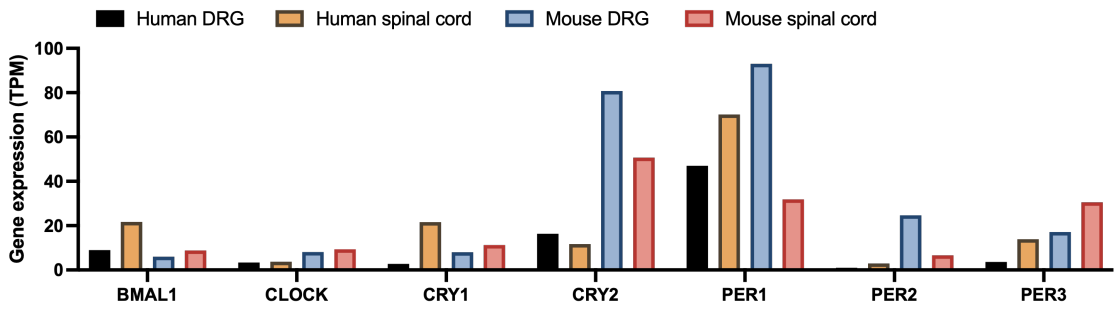


Figure 35: Demonstration of species- and location-dependent variations of core clock gene transcript abundance, extracted from[6].

Overall, we could conclude that transcriptional variations of core TTFL genes were inducible in Chambers' iNociceptors. The time for peak and trough for *BMAL1* transcripts matched with previous reports in Chamber's iNociceptors via *BMAL1* promoter-driven luciferase activities[1].

3.2.2 Temporal dynamics of the transcription of pain-related genes in iNociceptors

We extended the transcriptional analysis to candidate pain-related genes (Figure 36). Except for SP which demonstrated diurnal differences *in vitro* (Figure 36) and *ex vivo*[354], none of the other transcripts of interested displayed any particular temporal pattern.

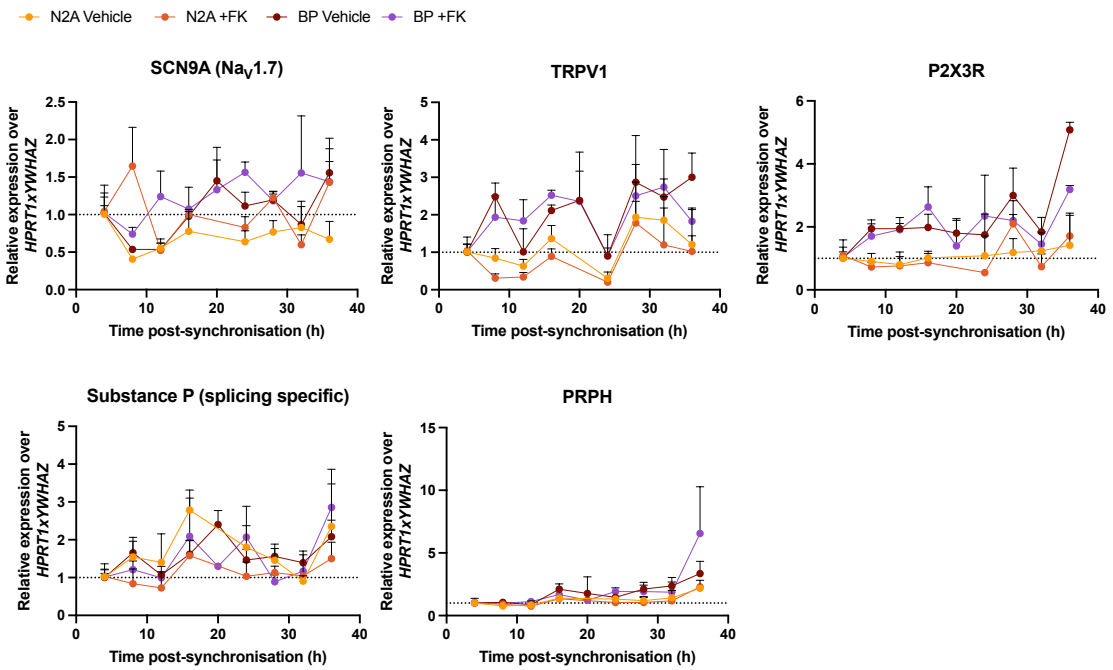


Figure 36: Circadian-driven variations of pain-related transcript abundances in SBAD03 DRG iNociceptors.
n=3 technical replicates per time point per synchronisation method. 3ng cDNA per reaction. Error bar standard deviation. Missing data points (N2A vehicle/FK +20) was due to insufficient RNA inputs.

3.3 Global changes of protein abundance in chemically synchronised Chamber's iNociceptors based on subcellular localisation

Net protein quantity is defined by the combined efficiency of production, PTMs, and degradation, which can be individually regulated by circadian machinery. As all circadian gene primers in Section 3.2 were designed based on post-transcriptionally processed mature mRNA transcripts, we expected reduced phase delays between transcriptional and translational oscillations. Although the translational and transcriptional efficiencies vary substainially in most cells[538,539], pilot tests on NDHFs provided moderate confidence of circadian concordance (see Section S3.6-S3.7).

Although we confirmed the lack of clock proteins in undifferentiated hiPSCs by IF (Figure 37), traditional immunolabelling methods were not as sensitive to quantify diurnal clock protein fluctuations in mature iNociceptors due to low expression levels (e.g. Figure 38). Therefore, we applied bulk proteomics to diurnally harvested Chambers' iNociceptors 4 and 16 hours after synchronisation via FK (Figure 39a). We recruited the open source multi-omics analysis and visualisation tool Omics Playground[540].

To minimise batch effects and technical variations, all samples were derived from the same differentiation and processed together for subcellular protein extraction, showing minimal technical variation in sample quality (Figure 39b & d). Peptides of lower intensity displayed typical vulnerability to inconsistency missningness[541], as proteins of smaller intensity were more likely to be missing in some but not all samples (Figure 39c). We removed missing values that did not reach 10% observations across samples as previously recommended[542]. Value imputation[541] was not performed as comparisons of statistical power and downstream bias between imputation methods were beyond the scope of the current project.

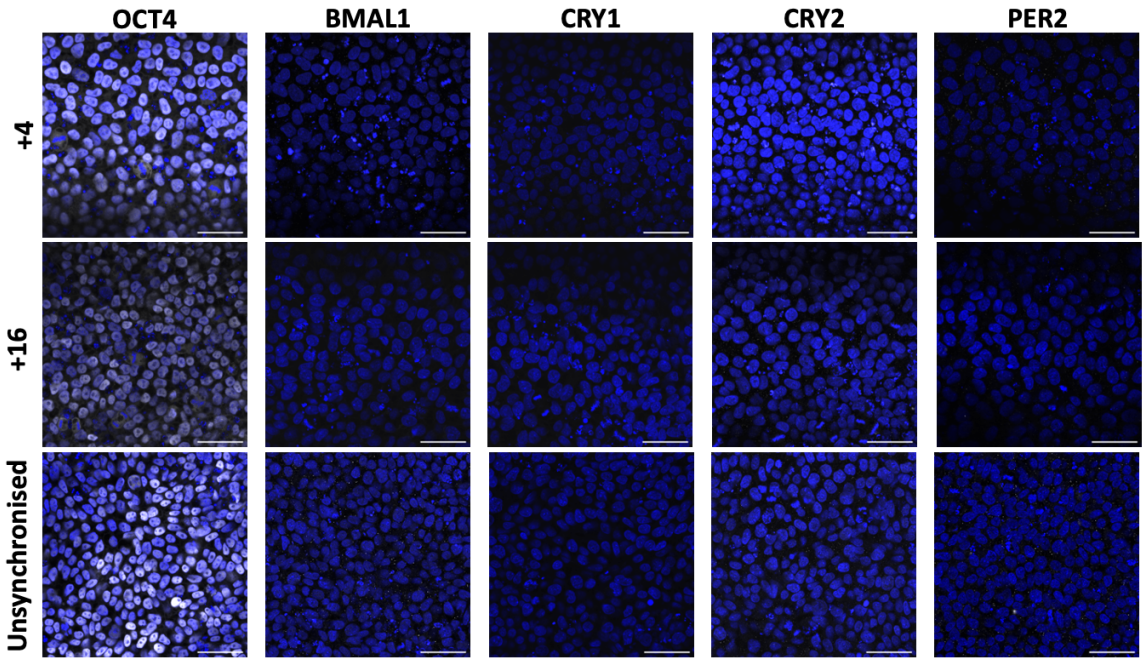


Figure 37: Lack of core TTFL protein immunoreactivities in chemically synchronised undifferentiated hiPSCs. Scale bar 50µm.

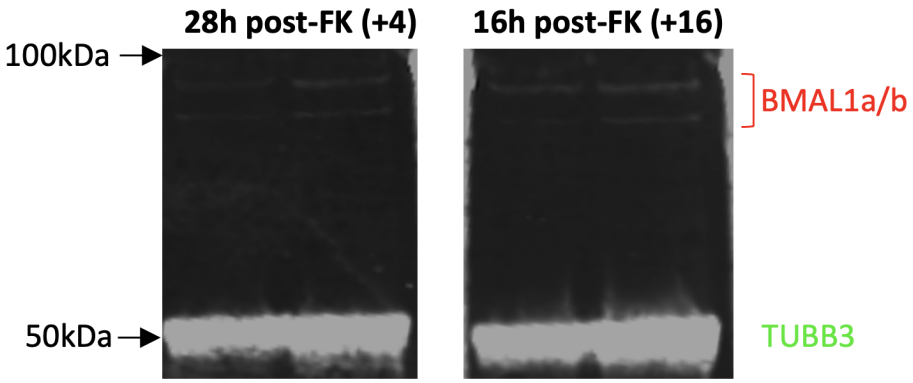


Figure 38: Confirmation of BMAL1 protein expression in chemically synchronised Chambers' iNociceptors by western blotting.
n=2 per time point. Uncropped image of the original blot see Figure S33.

Subcellular fractionation was performed with a commercially available kit, which separates soluble proteins and membrane-bound (including plasma membrane and membrane-bound organelles) via sequential partition phase separation[543]. As the kit exploited differential solubility in detergents determined by physiological hydrophilicity of individual proteins, complete phase isolation was not possible as a consequence of the transient interface[543]. We prioritised the enrichment of hydrophobic proteins with transmembrane domains which could potentially affect neuron firing and nutrient exchange.

We verified the efficacy of membrane protein extraction by identifying differentially expressed proteins (Figure 40a-c). Proteins most enriched in membrane fractions included mitochondrial proteins (AGK, LARS2, TIMM44, GFM1, ETFDH, PDK3, NDUFA9, GDP2, PYCR2), ion channels (TRPV2, SLC9A1, CLCN6), endoplasmic reticulum components (SEC63, SSR1), and secreted protein (LGI1). In comparison, proteins highly represented in the cytoplasmic fraction included proteasome components (PITHD1, ATXN3), protein folding (PFDN4), lysosome (RILPL1), nuclear protein shuttle (IPO11), proteostatis (TATDN1[544]), ribosomal RNA degradation (PUDP), transcription repressor (DR1), nucleotide regulation (IMPDH1), cell death/survival regulation (GSDME, NKIRAS1), microtubule dynamics (DOCK5), and other proteins with confirmed cytosolic localisation but no known functions in neurons (AAMDC, FTO, HTATSF1, HMBS). Cytoskeleton proteins did not show differential extraction in either fraction, including neuron-specific PRPH and more generic bACTIN (Figure 40d).

Besides proteins involved in common cellular processes, we examined hallmark genes that indicated successful induction of nociceptor cell fate. One of the most membrane-enriched protein LGI1 is a secreted protein highly expressed in human DRGs that regulates pain sensitivity[545]. Major VGSC Na_V 1.7 and non-peptidergic marker RET also displayed moderate membrane enrichment (Figure 40d), matching with IF results (see Section 2.2).

It is worth noting that a few verified hallmark genes such as ISL1, BRN3a, and TRPV1, as well as all core circadian proteins were missing in all samples of the current studies. Proteins missed in explorative high-throughput assays but otherwise detectable by target-specific methods represent coverage missingness, which is a typical drawback

of global proteomics[546]. The cause of coverage missingness can include threshold of detection, random losses, and other technical biases during liquid chromatography mass spectrometry[541,546]. Optimisation to recover or impute coverage missingness was therefore beyond the scope of the current project.

Both HCA by protein expression matrix (Figure S32) and uniform manifold approximation and projection (UMAP[547], Figure 40e) indicated a strong segregation between cytoplasmic and membrane samples regardless of circadian time, suggesting highly effective fractionation. Therefore, we proceeded to analyse circadian-driven differences separately in each subcellular fraction (Figure 41-44).

Proteins with differential expression (DE) in each fraction were extracted based on the aggregated statistical significance combining DESeq2 (Wald test)[548], edgeR (QLF test)[549], and limma-trend[550]. Statistically significant top hits ($q<0.05$, $|\log2FC|>0.5$) including 6 proteins from cytoplasmic fraction and 68 proteins from membrane fractions were summarised and annotated with known pain-related functions in Table 8 & 9.

To identify potential functional relevance of DE proteins in nociceptors, we first validated the transcriptional enrichment of each hit in human *ex vivo* sensory neurons using a published human TG single-cell transcriptomic database[5]. Although Chambers' iNociceptors were of neural crest lineage that embryologically resemble more of human DRG[411] than TG, we did not use published DRG datasets here because available resources either lacked true single-cell resolution[4] or examined substantially fewer nuclei (e.g. 1837[28] compared to 38028[5] neuronal nuclei).

We also cross examined proteins with diurnal changes in expression with previously known hits with DE identified from rodent models of neuropathic pain[551], as well as potential interacting partners of Na_V 1.7 based on a published interactome in mouse CNS[552].

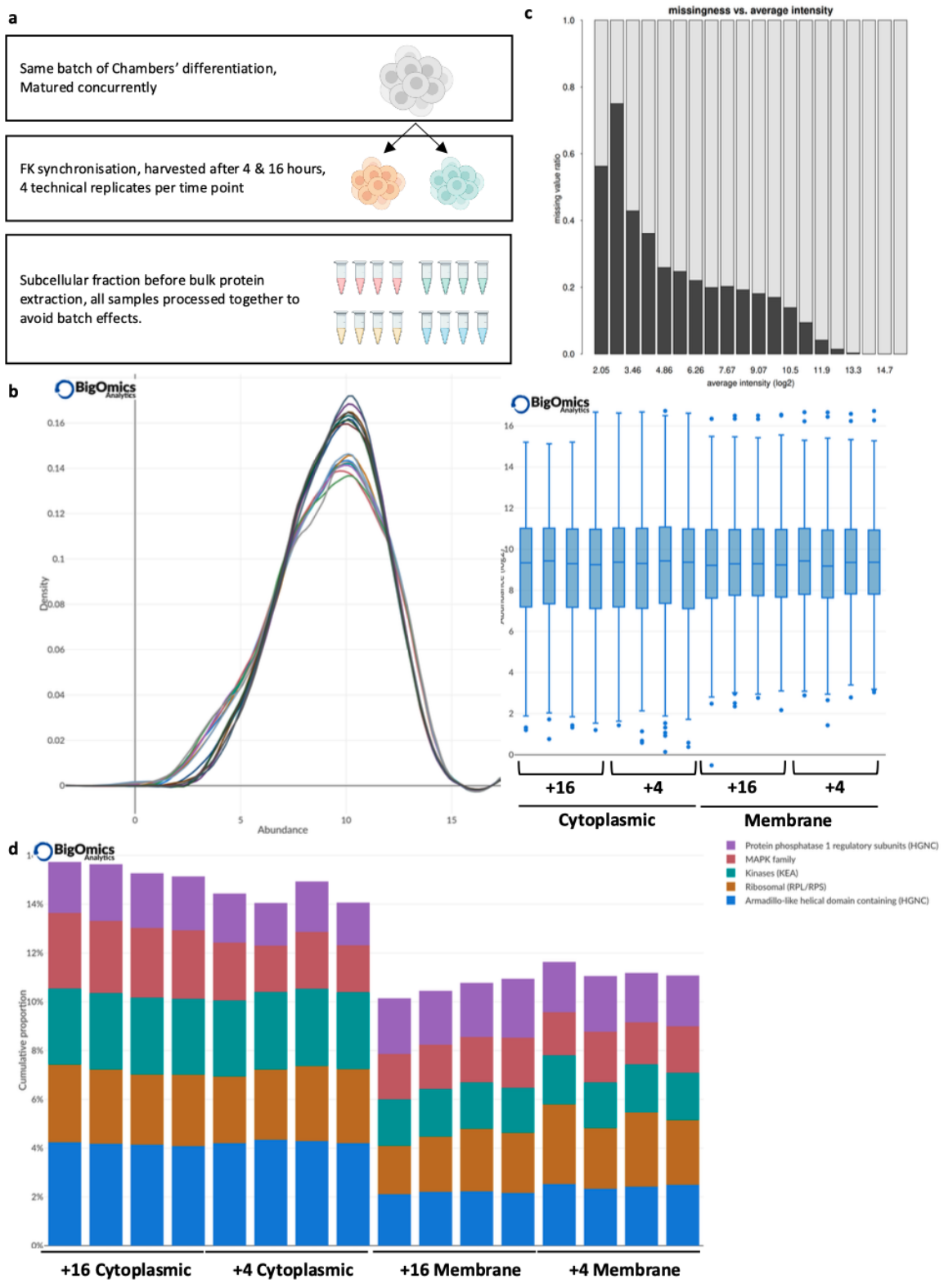


Figure 39: Sample preparation and quality check prior to proteomics analysis.
(a) Schematics of cell culture preparation. (b) Sample quality check presented as signal histogram (left) and box plots (right). (c) Overall quality check presented as missing value distribution across sampling intensity prior to sample clean-up. (d) Proportions of major protein classes detected per sample. Panel (b-d) extracted from Omics Playground[540].

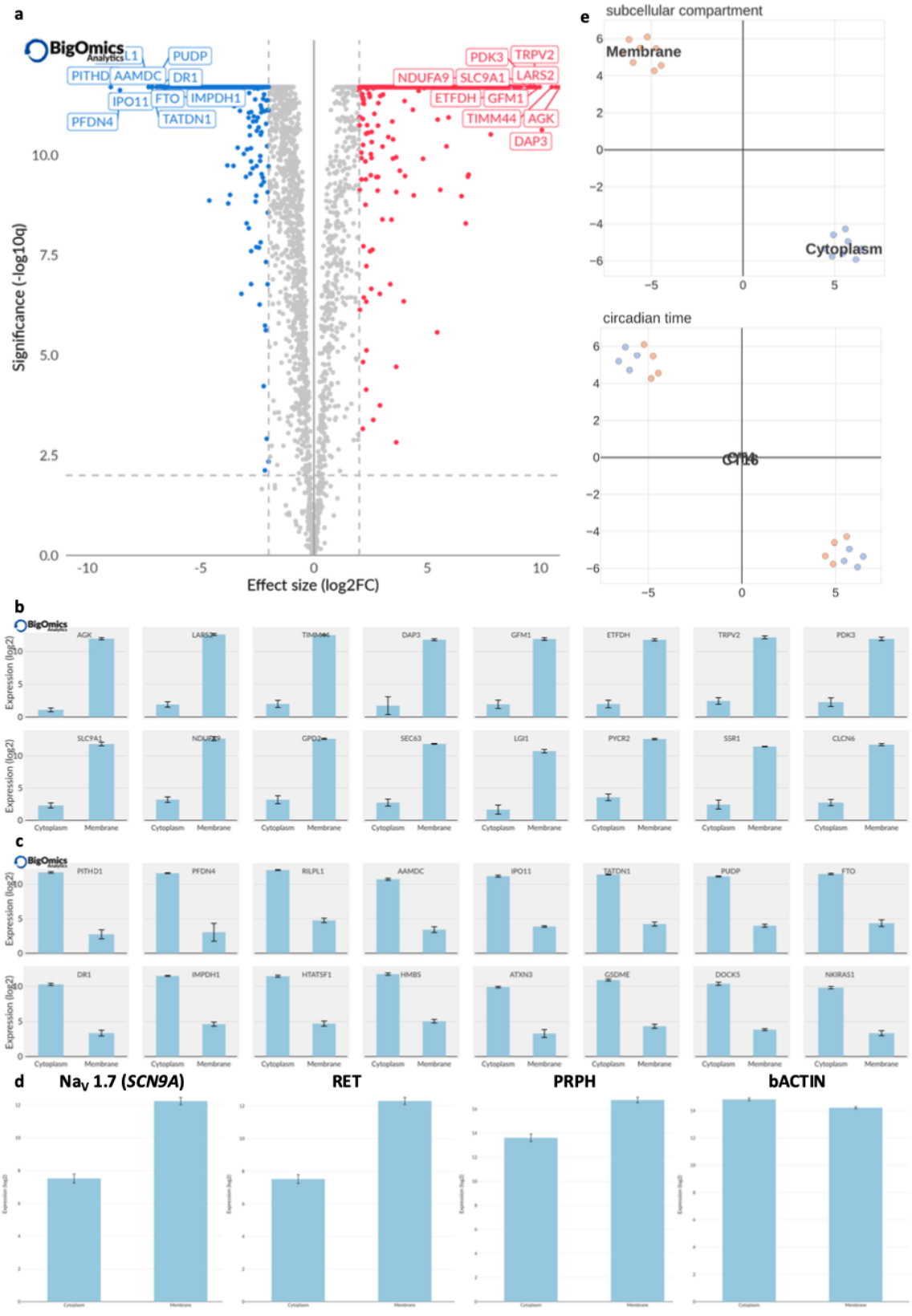


Figure 40: Efficacy of membrane/cytosol fractionation.
(a-c) Differential protein expressions by subcellular fractionation as (a) volcano plot, with the 16 most enriched proteins in (b) the membrane fraction and (c) the cytosolic fraction ranked by |log2FC|. (d) Expression level of hallmark genes of nociceptor identities. (e) Dimensionality reduction UMAP indicating strong sample clustering based on subcellular fraction instead of circadian time. All panels extracted from Omics Playground[540]. False discovery rate cut-off 0.01, effect size (log2FC) cut-off set as 2.

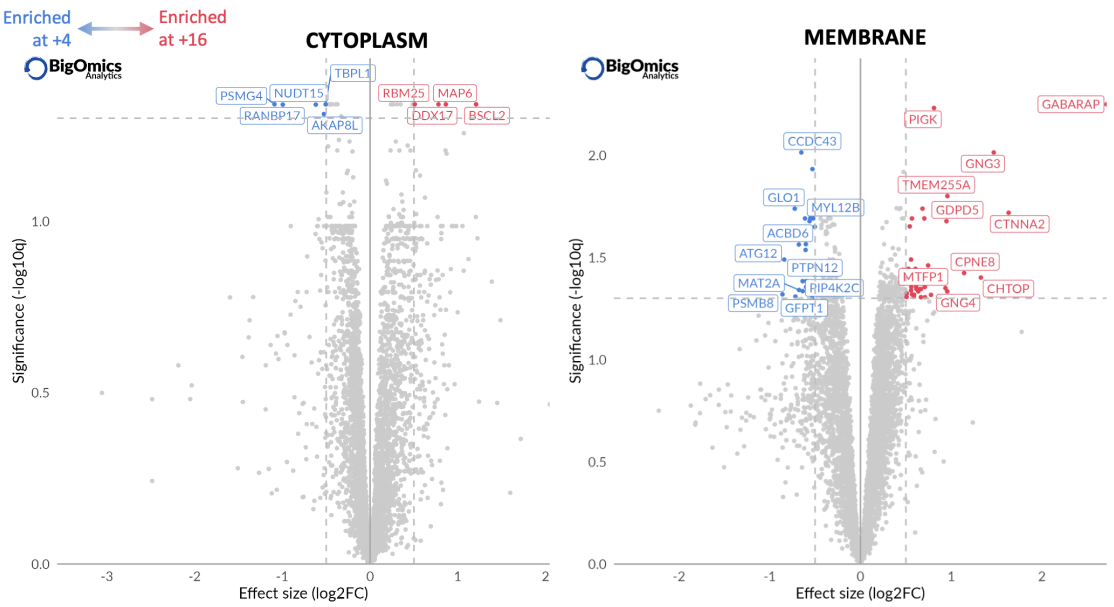


Figure 41: Top hits with diurnally differential expressions in cytoplasmic and membrane fractions of chemically synchronised Chambers' iNociceptors, extracted from Omics Playground[540]. Significance presented as a meta q value by combining DESeq2 (Wald test)[548], edgeR (QLF test)[549], and limma-trend[550]. False discovery rate cut-off 0.05, effect size (log2FC) cut-off set as 0.5.

Of the 74 total hits with diurnal DE, several proteins were involved in metabolism (e.g. BSCL2, GLO1, AHCY, ACBD6), mitochondrial function (e.g. MRPL16, MTFP1, FUNDC2, COA6, ATP5PO), autophagy (e.g. ATG12 & HS1BP3), translation (e.g. ATXNL2 & XPOT), and proteasome (e.g. ARDM1, PSMG4, PSMB8) activities . It suggests that the coupling between fundamental cellular processes such as metabolism and survival and circadian time is conserved in Chambers' iNociceptors, consistent with observations in other primary cell types[285–287].

From the 74 differentially expressed proteins, 20 hits have been previously identified to be differentially regulated after nerve injury in rodent DRGs[551]. Notably, the neuropeptide ADCYAP1 (alternatively named PACAP) has been found as to be enriched in the membrane fraction (Figure 42) with membrane-specific diurnal DE ($\log^2$FC = 0.5570 at +16 compared to +4, q=0.032327).

Among proteins associated with neuropathic pain, several hits contribute to the regulation of sensory neuron thresholds by modulating ion channel activities, such as GABARAP which modulates TRPV1 activities[553] and GLO1 which activates TRPA1[554–559]. Additionally, three proteins (STXBP1, HSP90AB1, and PKM) were recognised as part of Na_V 1.7

interactome in mouse brains[552].

In particular, we identified significant DE in HSP90AB1 (log^2FC = -0.5505 at +16 compared to +4, q=0.037808) and chaperone protein CDC37L1 (log^2FC = -0.5993 at +16 compared to +4, q=0.044030) only in the membrane fraction, despite overall higher expression in the cytosol (Figure 42). HSP90 typically constitutes about 1%-2% of total soluble proteins in the cytosol, where it serves as critical chaperones facilitating protein folding[543,560]. In contrast, membrane-bound HSP90 exerts unconventional functions such as axonal extension and polarisation, neurotransmitter release, membrane protein stabilisation, and synaptic receptor cycling in CNS neurons[560,561]. Additionally, HSP proteins are known modulators in chronic pain, exerting dual functions of opioid-dependent neuroprotection and pro-inflammatory neuro-immune communications in both peripheral and central neurons in the pain pathway[562–564]. Consistent with such observation, HSP90 was found to be upregulated and amplifying calcium signalling in DRGs in a estrogen-dependent manner in a chronic inflammatory pain model[565]. Together, the pattern of subcellular compartmentalisation-specific DEs of HSP90 components observed here implicates the potential functional relevance of membrane-bound HSP90 in nociceptors similar to CNS neurons[565].

Besides the potential involvement of HSP90 components, we also identified multiple proteins known for axonal and cytoskeleton organisation (e.g. MAP6, DDX17, GABARAP, CTNNA2, RHOB).

Overall, DE analysis of the current proteomics experiment identified changes in proteins that regulate ion channel activities and axon structures. Gene ontology (GO) pathway analysis also identified multiple processes involved in axonal organisation and ion transport (Figure 43-44). The convergence of proteins with diurnal variations in expression, ion channel modulation, and pathological pain involvement indicates the possibility of circadian regulated membrane excitabilities and firing activities in Chambers' iNociceptors.

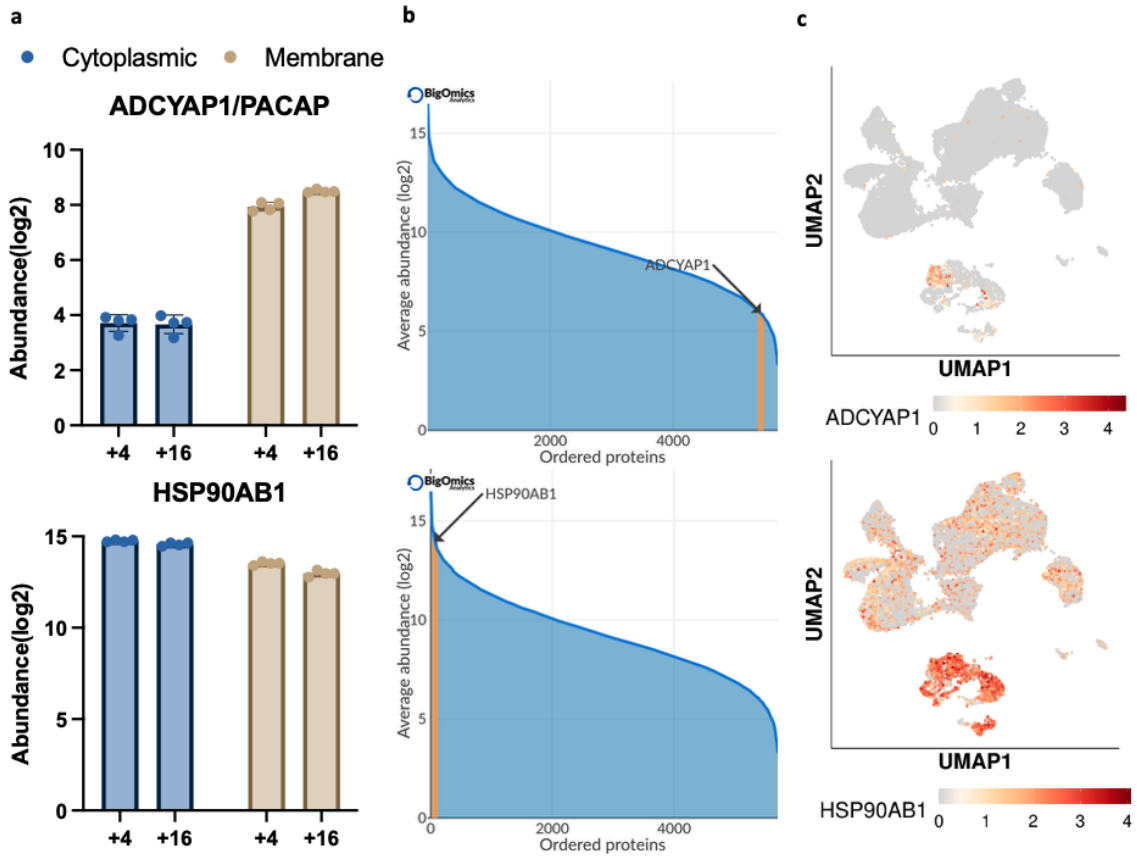


Figure 42: Representative proteins identified with diurnally differential expressions in chemically synchronised Chambers' iNociceptors with known functions related to pain.
(a-b) (a) Grouped quantification and (b) rank among total proteins detected of key pain-related proteins with diurnal DEs in Chambers' iNociceptors. (c) Ex vivo cell type-specific expression patterns of pain-related hits with diurnal DEs identified in vivo, extracted from single-cell human TG seuqencing[5].

GENE	TITLE	logFC	meta.q	PAIN-RELATED FUNCTIONS
BSCL2	BSCL2 lipid droplet biogenesis associated, seipin	1.2089	0.04552	Enriched in human TG sensoryne urons[5], with no known nociceptor-specific functions.
PSMG4	Proteasome assembly chaperone 4	-1.0890	0.04552	
MAP6	Microtubule-associated protein 7	0.8631	0.04552	Altered nociception and opiate sensitivity in global MAP6 KO mice due to elevated endogenous alkaloid morphine[566]
DDX17	DEAD-box helicase 17	0.7794	0.04552	Associated with dendrite morphogenesis in *C. elegans* sensory neurons[567].
NUDT15	Nudix hydrolase 15	-6188	0.04561	Differentially expressed in rodent DRGs after neuropathic pain[551]
AKAP8L	A-kinase anchoring protein 8 like	-0.5262	0.04860	
RBM25	RNA binding motif protein 25	0.5098	0.04552	
TBPL1	TATA-box binding protein like 1	-0.5063	0.04552	
RANBP17	Ran-binding protein 17	-0.9949	0.04561	

Table 8: List of top hits with diurnally differential expressions in cytoplasmic protein fractions of FK synchronised Chambers' iNociceptors.
Data extracted from Omics Playground[540], with q<0.05 and |log2FC|>0.5: hits enriched in +16 samples labelled red, hits enriched in +4 samples labelled blue. For proteins previously identified to be differentially expressed in rodent neuropathic pain models based on[551], only significant hits after correction were included.

GENE	TITLE	logFC	meta.q	PAIN-RELATED FUNCTIONS
GABARAP	GABA type A receptor-associated protein	2.7112	0.005620	Modulation of TRPV1 expression, surface clustering, sensitivity, and desensitisation[553]; microtubule interactions[568]; differentially expressed in rodent DRGs after neuropathic pain[551].
PIGK	Phosphatidylinositol Glycan Anchor Biosynthesis Class K	0.8097	0.005859	
GNG3	G protein subunit gamma 3	1.4680	0.009671	Enriched in human TG sensory neurons[5],no known nociceptor-specific functions; differentially expressed in rodent DRGs with neuropathic pain[551].
CCDC43	Coiled-coil domain containing 43	-0.6515	0.009671	
GPHN	Gephyrin	-0.5289	0.011668	GABAergic synapse organiser typically present in CNS postsynaptic membrane[569], absence in small diameter afferent terminals in mice[570] and most CGRP+ sensory neurons in human TG[5].
TMEM255A	Transmembrane protein 255A	0.9573	0.015810	
ADRM1	Adhesion-regulating molecular 1, 26S proteasome ubiquitin receptor	-0.5314	0.017128	Identified as part of Na_V 1.7 interactome in mouse brains[552].
GLO1	glyoxalase I	-0.7239	0.018216	Enzyme for toxic glycolysis byproduct metabolism, substrate accumulation leading to activation of TRPA1, increased Na_V 1.8 activities and neuropathies[554–559].
ATXN2L	Ataxin 2 like	0.6832	0.018216	Regulation of selective and temporally sensitive translation of core clock genes[182], functional relevance in nociceptors currently unknown.
CTNNA2	Catenin alpha 2	1.6320	0.019072	Actin neurofilament binding activities[571]; SNP associated with chronic pain[572,573]; differentially expressed in rodent DRGs with neuropathic pain[551].
RAF1	Raf-1 proto-oncogene, serine/threonine kinase	-0.5489	0.019072	Involvement in the development of oxaliplatin-induced neuropathic pain via interaction with OIP5[574].

CD47	CD47 molecule	0.7031	0.020343	Confirmed expression in nociceptors, potential involvement with immune cell via CGRP positive feedback loops[575]; identified as part of Na_V 1.7 interactome in mouse brains[552].
MYL12B	Myosin light chain 12B	-0.6114	0.020343	Differentially expressed in rodent DRGs with neuropathic pain[551].
C2CD4C	C2 calcium dependent domain containing 4C	0.5668	0.020343	Significance downregulation in rat trigeminal ganglia after the induction of inflammatory oral facial pain with Complete Freund's Adjuvant injection[576]; differentially expressed in rodent DRGs with neuropathic pain[551].
COPS7A	COP9 signalosome subunit 7A	-0.5542	0.020343	
PPP6C	Protein phosphatase 6 catalytic subunit	-0.5202	0.020343	Involved in the STING pathway which is a critical component of neuro-immune interactions of nociception[577,578]
GDPD5	Glycerophosphodiester phosphodiesterase domain containing 5	0.9474	0.020981	
ARPP19	cAMP regulated phosphoprotein 19	-0.5606	0.020981	
PTGFRN	Prostaglandin F2 receptor inhibitor	0.5426	0.022250	
AHCY	Adenosylhomocysteina	-0.5028	0.022344	
NAE1	NEDD8 activating enzyme E1 subunit 1	-0.6015	0.027191	
ACBD6	Acyl-CoA binding domain containing 6	-0.6788	0.027291	
PPP6R1	Protein phosphatase 6 regulatory subunit 1	-0.6047	0.029022	Involved in the STING pathway which is a critical component of neuro-immune interactions of nociception[577,578]
ATG12	Autophagy related 12	-0.8392	0.032327	
ADCYAP1/PACAP	Adenylate cyclase activating polypeptide 1	0.5570	0.032327	Encoding for neuropeptide PACAP involved in axonal regeneration and pain signalling[579–581], also contributing to pathogenesis of migraine[582]; differentially expressed in rodent DRGs with neuropathic pain[551].
NTNG2	Netrin G2	0.7447	0.034546	
RMDN3	Regulator of microtubule dynamics 3	0.6055	0.035899	
RHOB	Ras homolog family member B	0.5284	0.035899	Confirmed expression in sensory neurons[5,583]; differentially expressed in rodent DRGs with neuropathic pain[551].

OGFR	Opioid growth factor receptor	-0.5331	0.036091	
STXBP1	Syntaxin binding protein 1	0.6628	0.036983	Enriched in human TG sensory neurons[5,6]; differentially expressed in rodent DRGs with neuropathic pain[551]; identified as part of Na_V 1.7 interactome in mouse brains[552].
CPNE8	Copine 8	1.1412	0.037651	Enriched in human TG sensory neurons[5,6],no known nociceptor-specific functions.
HSP90AB1	Heat shock protein 90 alpha family class B member 1	-0.5505	0.037808	Regulation of inflammatory pain by ectopic expression in nociceptors[565], also involved in opioid-induced modulation of nociception in spinal cord and brain[563,564]; differentially expressed in rodent DRGs with neuropathic pain[551]; identified as part of Na_V 1.7 interactome in mouse brains[552].
HS1BP3	HCLS1 binding protein 3	-0.5007	0.038504	
CHTOP	Chromatin target of PRMT1	1.3263	0.039615	
SLC35G2	Solute carrier family 35 member G2	0.6654	0.039615	Differentially expressed in rodent DRGs with neuropathic pain[551].
PTPN12	Protein tyrosine phosphatase non-receptor type 12	-0.6377	0.041252	
PANK4	Pantothenate kinase 4 (inactive)	-0.5975	0.041252	
MRPL16	Mitochondrial ribosomal protein L16	0.5365	0.041270	Differentially expressed in rodent DRGs with neuropathic pain[551].
DCK	Deoxycytidine kinase	-0.5023	0.041270	
TOR1A	Torsin family 1 member A	0.6132	0.043865	
TAF15	TATA-box binding protein associated factor 15	0.7068	0.043963	
PPP1R16A	Protein phosphatase 1 regulatory subunit 16A	0.7090	0.044030	
CDC37L1	Cell division cycle 37 like 1, HSP90 cochaperone	-0.5993	0.044030	Chaperone of HSP90 alpha (see HSP90AB1 above)
ATRNL1	Attractin like 1	0.5594	0.044030	Enriched in human TG sensory neurons[5]
MTFP1	Mitochondrial fission process 1	0.9360	0.044609	Differentially expressed in rodent DRGs with neuropathic pain[551].
TXNDC15	Thioredoxin domain containing 15	0.6158	0.045036	Drosophola ortholog likely involved in thermal nociception[584], however lowly expressed in human TG sensory neurons[5]

SPRED2	Sprouty related EVH1 domain containing 2	0.6653	0.045101	
FUNDC2	FUN14 domain containing 2	0.6555	0.045101	
FBLL1	Fibrillarin like 1	0.6199	0.045101	Differentially expressed in rodent DRGs with neuropathic pain[551].
XPOT	Exportin for tRNA	-0.5036	0.045101	Enriched in human TG sensory neurons[5]
MAT2A	Methionine adenosyltransferase 2A	-0.6773	0.045554	
ADRA2A	Adrenoceptor alpha 2A	0.5570	0.045805	Differentially expressed in rodent DRGs with neuropathic pain[551], however lowly expressed in human TG sensory neurons[5].
RAD23A	RAD23 homolog A, nucleotide excision repair protein	-0.5234	0.045805	
PIP4K2C	Phosphatidylinositol-5-phosphate 4-kinase Type 2 Gamma	-0.6362	0.046139	Identified to be genetically associated with nociception or hypersensitivity[585], despite no significantly different pain phenotypes in murine KO models[586].
GNG4	G protein subunit gamma 4	0.9559	0.046294	
COA6	Cytochrome c oxidase assembly factor 6	0.6364	0.046294	
CACNA1A	Calcium voltage-gated channel subunit alpha1 A	0.5098	0.047355	Mutations causding familial hemiplegic migraine[587]; differentially expressed in rodent DRGs with neuropathic pain[551].
PSMB8	Proteasome 20S subunit beta 8	-0.8593	0.047859	Differentially expressed in rodent DRGs with neuropathic pain[551].
MAT2B	Methionine adenosyltransferase 2 non-catalytic subunit beta	-0.5757	0.047859	
EPB41L1	Erythrocyte membrane protein band 4.1 like 1	0.5688	0.047859	
ATP5PO	ATP synthase peripheral stalk subunit OSCP	0.5905	0.048066	
INPP4A	Inositol polyphosphate-4-phosphatase type I A	0.7771	0.048143	
GFPT1	Glutamine fructose-6-phosphate transaminase 1	-0.7169	0.049062	Differentially expressed in rodent DRGs with neuropathic pain[551].
SDC2	Syndecan 2	0.5882	0.049290	

MGST3	Microsomal glutathione S-transferase 3	0.5077	0.049290	Enriched in human TG sensory neurons[5], with no known nociceptor-specific functions
CALB1	Calbindin 1	0.7109	0.049404	Differentially expressed in rodent DRGs with neuropathic pain[551], minimal expression in nociceptors in human TG[5].
PKM	Pyruvate kinase M1/2	0.6655	0.049404	Differentially expressed in rodent DRGs with neuropathic pain[551], involved in neuropathic pain in rat spinal cord[588].
BIRC6	Baculoviral IAP repeat containing 6	-0.5323	0.049900	

Table 9: List of top hits with diurnally differential expressions in membrane protein fractions of FK synchronised Chambers' iNociceptors.
Data extracted from Omics Playground[540], with q<0.05 and |log2FC|>0.5: hits enriched in +16 samples labelled red, hits enriched in +4 samples labelled blue, ranked by significance. For proteins previously identified to be differentially expressed in rodent neuropathic pain models based on[551], only significant hits after correction were included. For proteins identified in Na_V 1.7 interactome in mouse brains by liquid chromatography mass spectrometry, hits were extracted from repository PXD004926 at the ProteomeXchange Consortium corresponding to Kanellopopulos et al. (2018)[552].

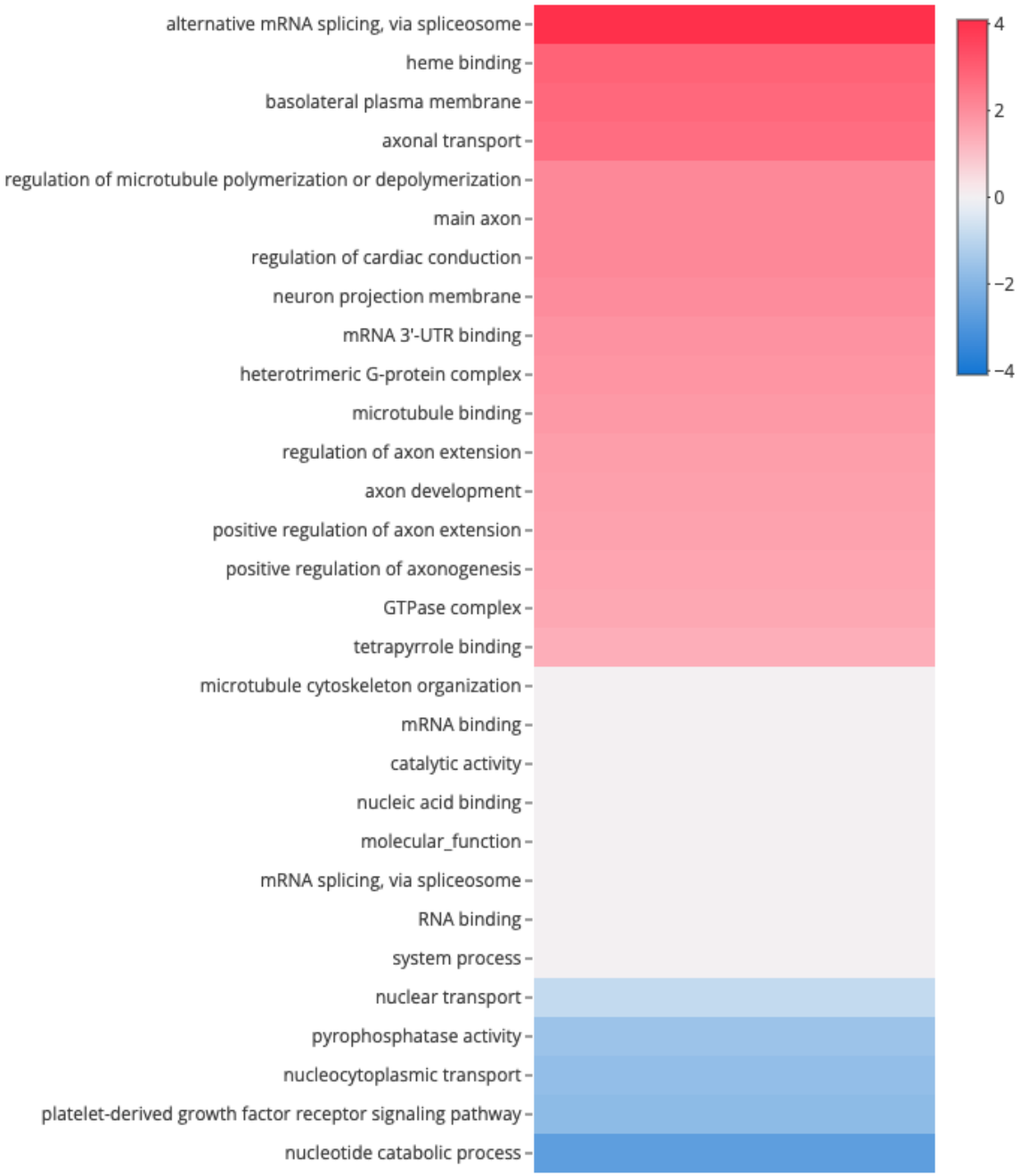


Figure 43: Activation matrix of GO pathways enriched at +16 compared to +4 in cytoplasmic protein fractions of chemically synchronised Chambers' iNociceptors, extracted from Omics Playground[540].

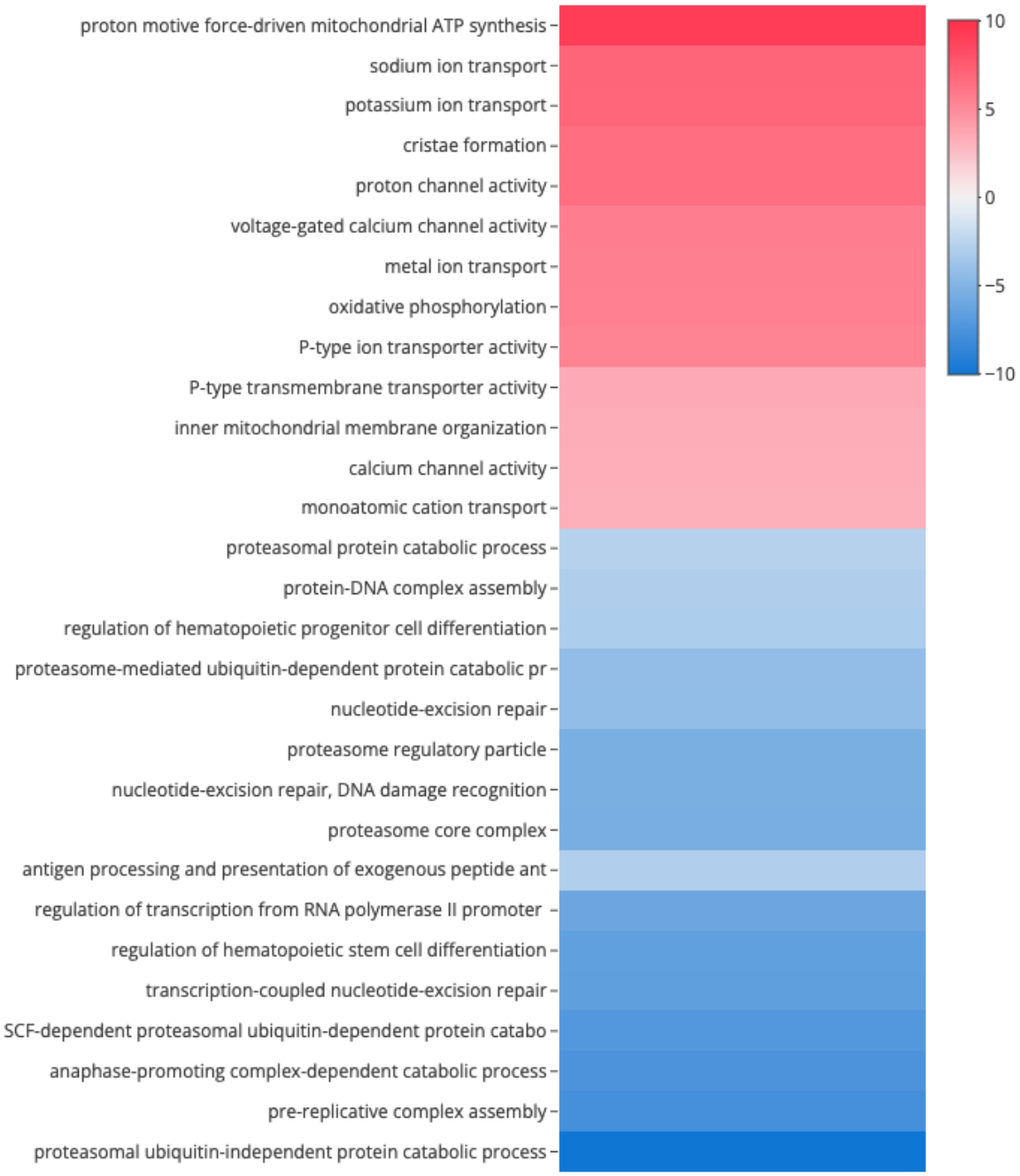


Figure 44: Activation matrix of GO pathways enriched at +16 compared to +4 in membrane protein fractions of chemically synchronised Chambers' iNociceptors, extracted from Omics Playground[540].

3.4 Functional relevance of circadian properties in peripheral sensory neurons

3.4.1 Diurnal firing patterns in iNociceptors

As the proteomics data indicates a strong possibility of diurnal differences in sensory neuron excitabilities, we examined the firing activities of iNociceptors by MEA. In mature SBAD03 TG iNociceptors, differential firing activities at baseline and by thermal activation could be introduced with media changes without additional chemical synchronisation (Figure 45).

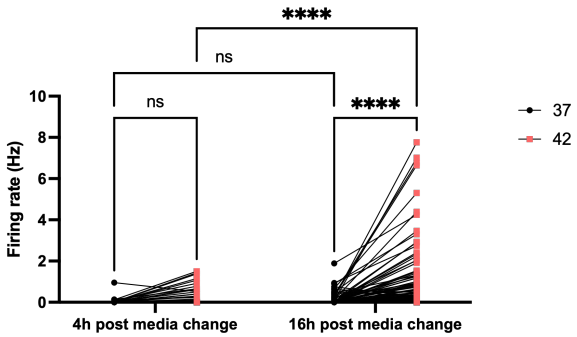


Figure 45: Diurnal responsiveness to selective TRPV1 antagonist AMG9810 in SBAD03 TG iNociceptors, synchronised by media only.
Differential activities were diminised by 5µM AMG9810. Statistical significance determined by two-way ANOVA with uncorrected Fisher's LSD, significant effects by circadian time, temperature, and interactions.

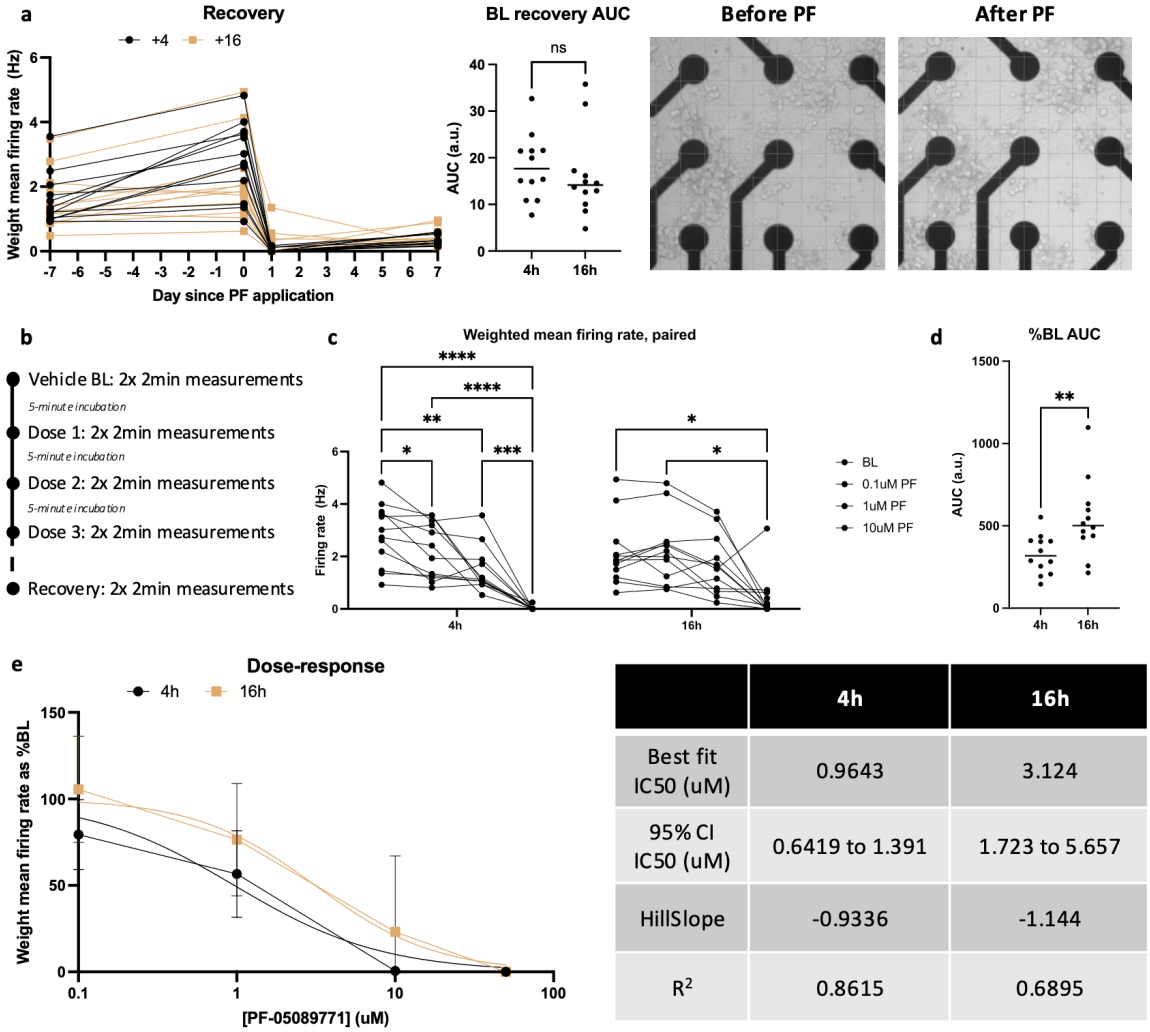
In comparison, the diurnal differences of baseline firing activities in Chambers' iNociceptors were less distinct and required chemical synchronisation (Figure S9). However, pilot experiment in our lab did confirm a diurnal differential responsiveness to agonists such as ATPγs and OD1[1]. In particular, the temporal difference in the potency of selective $Na_V1.7$ activator OD1 suggested a correlation to the circadian time-dependent availability of active $Na_V1.7$ in Chambers' and primary murine DRG neurons. Therefore, we expanded the experiment by inspecting the diurnal differences in the susceptibility of mature Chambers' iNociceptors to the selective $Na_V1.7$ inhibitor PF-05089771[41].

PF-05089771 exhibits slow onset and slow dissociation with only partially reversible inhibition[42], which can be demonstrated with the gradual and partial return of BL firing activities (Figure 46a). Morphological examination indicates that the loss of firing activities

was not due to cell death or detachment from electrodes, although confirmatory assays for viability should be included in future experiments. There was no difference in the speed of recovery based on circadian time when PF-05089771 was applied.

Consequently, we repeated firing activity measurements in presence of increasing concentrations of PF-05089771 (Figure 46b-e). Three doses of PF-05089771 at 0.1μM, 1μM, and 10μM were applied consecutively without media change in-between. We normalised antagonist-reduced firing activities and calculated the area under the %BL-against-[PF-05089771] curve per well. A significantly higher AUC at 16 hours post-FK synchronisation demonstrated a small potency of PF-05089771 at this circadian time point (Figure 46d, Mann-Whitney U=24, p=0.0045).

Together with a vehicle control and a terminating dose (50μM), a dose-response curve was plotting using normalised firing rates. PF-05089771 is known to present a staggering three-magnitude difference in affinity in favour of inactive $Na_V1.7$: IC_{50}=11nM for heat inactivated human $Na_V1.7$ compared to IC_{50}=25μM for active counterparts in single-cell patch experiments)[42]. Therefore, a lower IC_{50} of PF-05089771 at 4h post-FK synchronisation suggested a higher abundance of inactive $Na_V1.7$ relative to that at 16h post-FK synchronisation, coinciding with reduced baseline firing activities at +4 (Figure S9).



	4h	16h
Best fit IC50 (uM)	0.9643	3.124
95% CI IC50 (uM)	0.6419 to 1.391	1.723 to 5.657
HillSlope	-0.9336	-1.144
R^2	0.8615	0.6895

Figure 46: Diurnal responsiveness to selective $Na_V1.7$ antagonist PF-05089771 in SBAD03 DRG iNociceptors.
(a) Confirmation of the partial reversibility and slow recovery of PF-05089771, independent of circadian time of application, without obvious morphological alterations on SBAD03 DRG iNociceptors. Grid size 100µm. (b) Schematics of stacked PF-05089771 applications. (c-d) (c) Paired analysis of weighted mean firing rates per well and (d) Area under the %BL curve (AUC) analysis of stacked PF-05089771 concentrations. (c) Statistical significance determined with two-way ANOVA with Tukey's multiple comparisons for paired analysis: significant major effect on doses [42.35% variation, F(1.993, 43.86) = 41.37, p<0.0001]. (d) Statistical significance determined with Mann-Whitney test for AUC analysis: p=0.0045. (e) Dose-response curves for diurnal differential potency of PF-05089771, determined by non-linear curve fitting ([inhibitor] v.s. normalised response - variable slope) in GraphPad Prism.

3.4.2 Diurnal regulations of Na_V 1.7 localisation

Electrophysiological assays demonstrated circadian variations of the relative proportion of active Na_V 1.7 in iNociceptor, which could potentially arose from PTMs, changes in channel dynamics, or axonal distribution.

As the transcriptional (Figure 36) and the translational abundance of Na_V 1.7 [abundance ratio (CT16/CT4) 0.975 in membrane fraction & 1.146 in cytoplasmic fraction] were stable across circadian time, we further characterised the axonal distribution of Na_V 1.7.

Immunofluorescence identified a circadian time-associated axonal pattern of Na_V 1.7 pucnta in both FK synchronised Chambers iNociceptors (Figure 49) and primary cultures of murine sensory neurons (Figure 47-48). The distribution of Na_V immunulabelling was unlikely a result of myelination in primary culture as TrpV1 immunolabelling was used to distinguish murine peptidergic nociceptors that are mostly unmyelinated C-fibres[11]. The pattern of axonal fluorescent signals in our study also differed from nodal Na_V 1.7 immunolabelling in myelinated sciatic nerves[589]. Reported size of Schwann cells, nodes of Ranvier, and internode areas[590] were also notably larger than the distance we observed between peaks.

We hypothesised that the puncta reflected aggregation of Na_V 1.7 molecules either as vesicle contents during trafficking or as clusters inserted into axonal membrane, as the distance between signal peaks observed in our experiment was similar to that of reported Na_V 1.7 nanoclusters *ex vivo*[63]. Axonal clusters and transport vesicles of VGSCs have been reported in rodent primary cultures[63–65]. Findings from the current project suggested that it is plasible that similar regulatory patterns are also biologically relevant in human. However, available studies did not report on information of circadian times for validation and comparison.

Although the pattern of distribution can be qualitatively evaluated, post-hoc quantification of axons displaying Na_V 1.7 puncta was technically demanding. Automation of axonal labelling was challenging in dense iNociceptor cultures without apparent directions of axonal outreach, with additional complications of axonal thickness and overlaps. It was also beyond the resources of the current project to extensively map complete axons to avoid double-counting in randomly selected views.

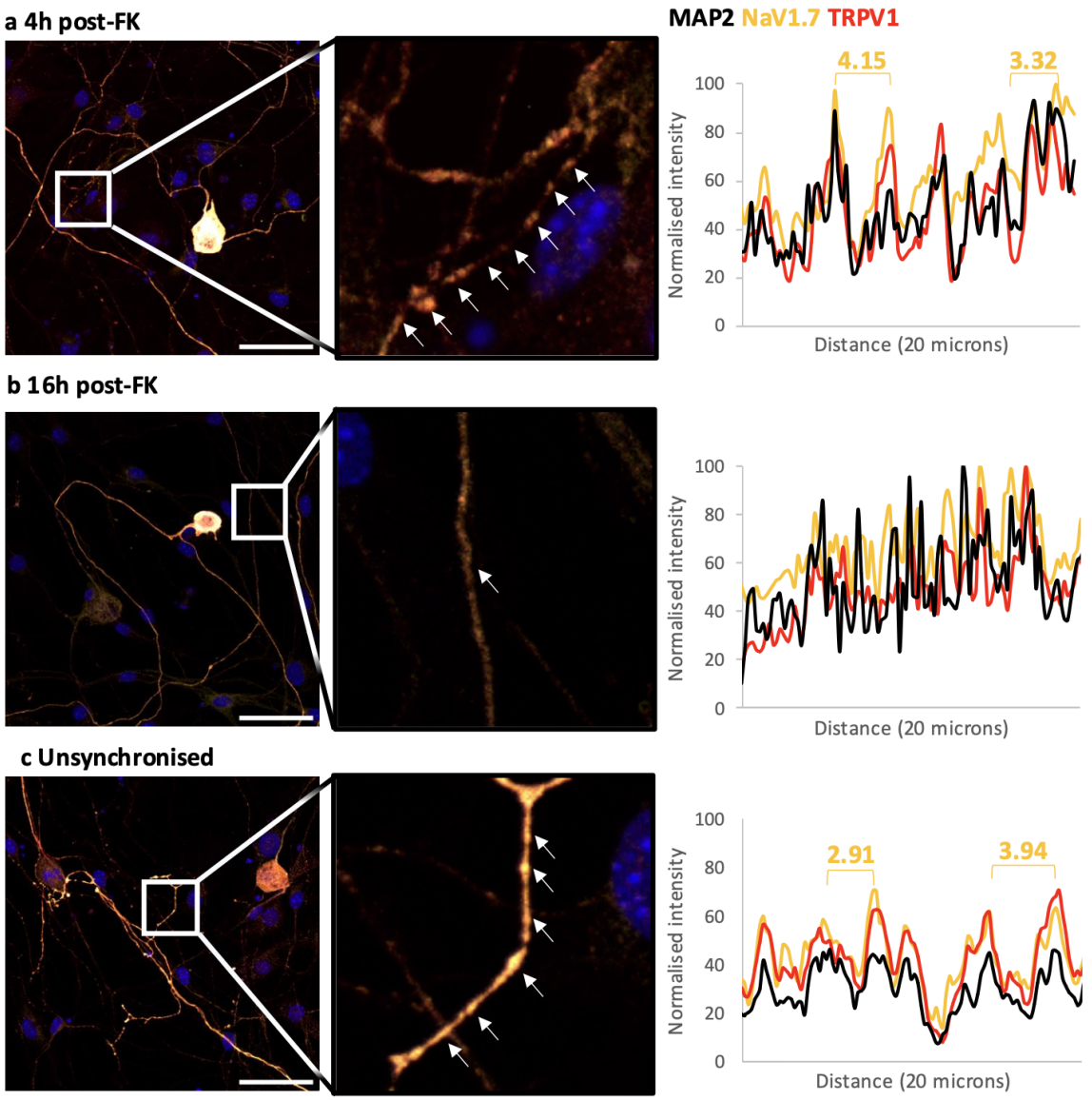


Figure 47: Axonal distribution of Na_V 1.7 in chemically synchronised primary murine DRG cultures.
Representative confocal images of Na_V 1.7 immunolabelling in TrpV1+ murine DRG neurons (a) 4 hours and (b) 16 hours after FK synchronisation, in comparison to (c) unsynchronised counterparts. Line profile of normalised fluorescent intensities measured by ImageJ for zoomed-in panels along axonal TRPV1 signal, distance between distinct local maxima labelled. Scale bar 50 µm.

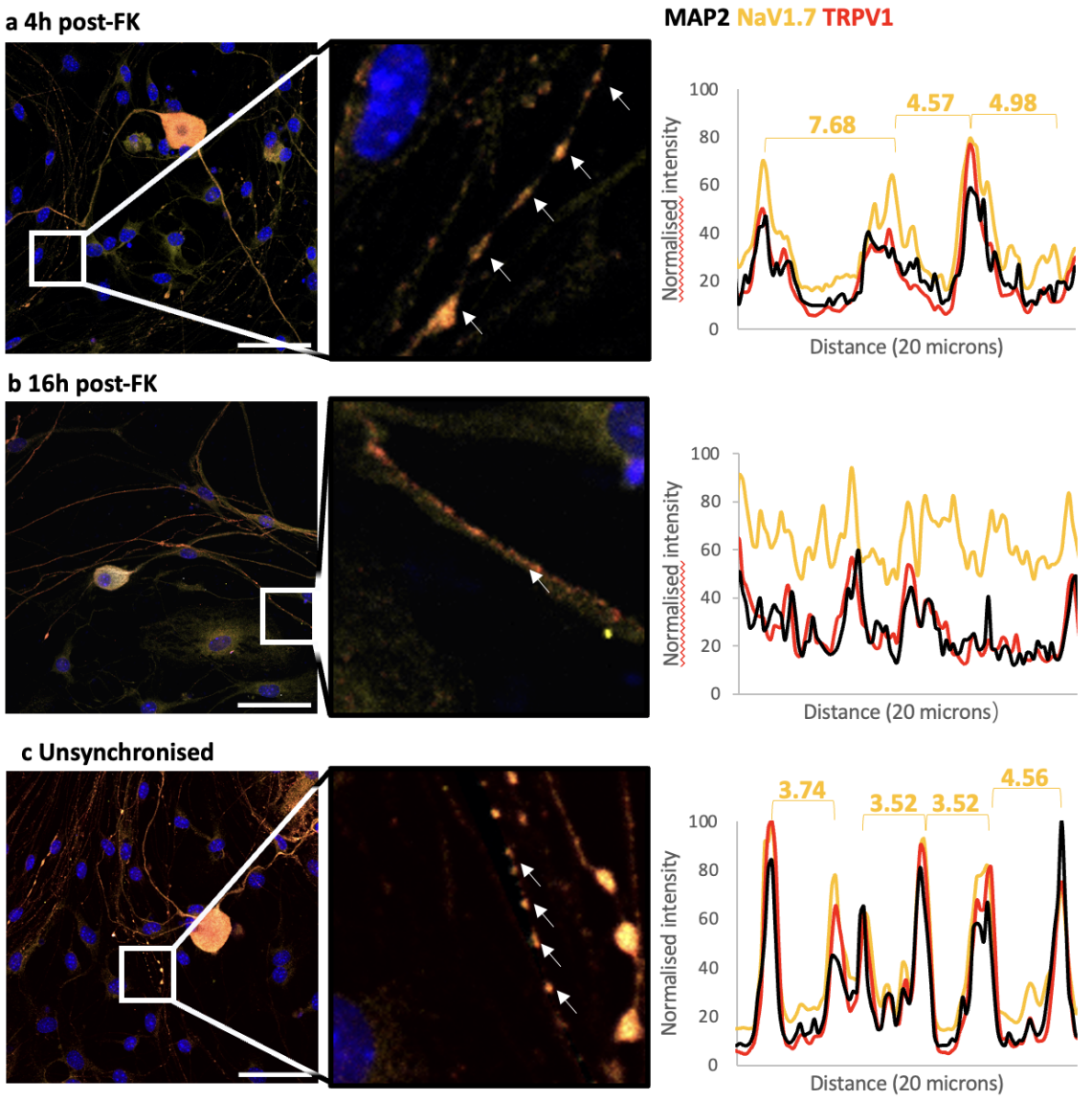


Figure 48: Axonal distribution of Na_V 1.7 in chemically synchronised primary murine TG cultures. Representative confocal images of Na_V 1.7 immunolabelling in TrpV1+ murine TG neurons (a) 4 hours and (b) 16 hours after FK synchronisation, in comparison to (c) unsynchronised counterparts. Line profile of normalised fluorescent intensities measured by ImageJ for zoomed-in panels along axonal TRPV1 signal, distance between distinct local maxima labelled. Scale bar 50 µm.

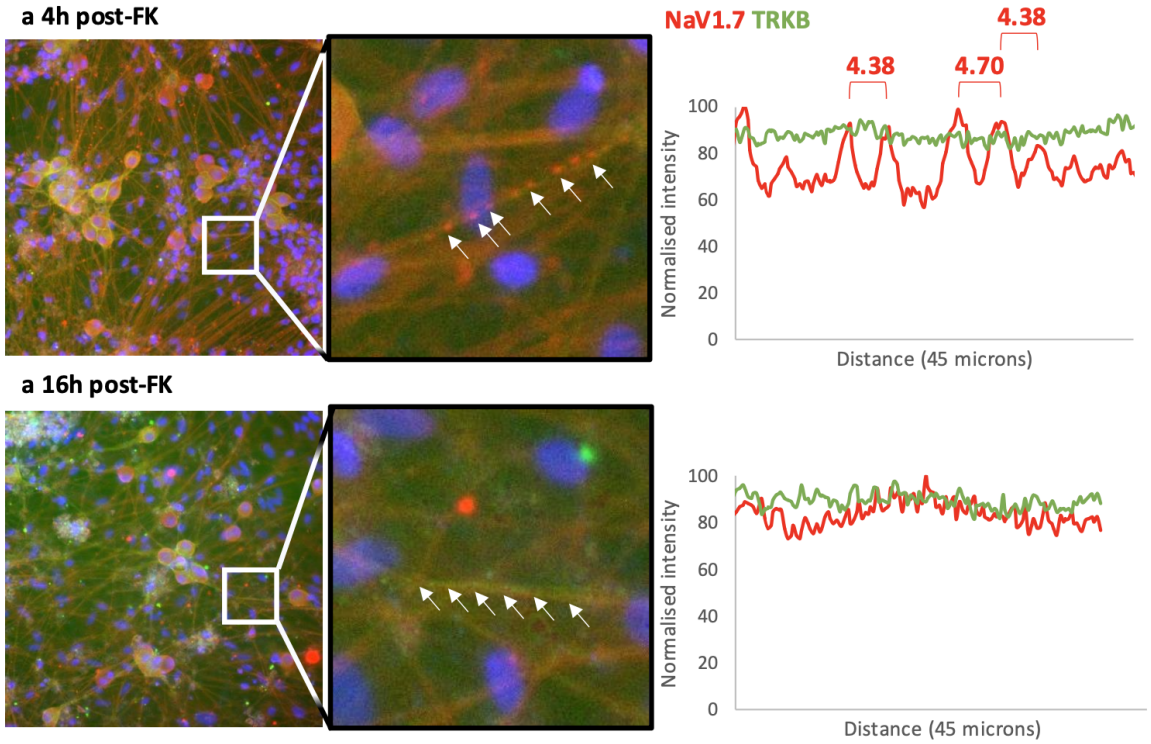


Figure 49: Axonal distribution of Na_V 1.7 in chemically synchronised Chambers' DRG iNociceptors.
Representative confocal images of Na_V 1.7 immunolabelling in nonpeptidergic Chambers' DRG iNociceptors (a) 4 hours and (b) 16 hours after FK synchronisation, with TRKB as a membrane label. Line profile of normalised fluorescent intensities measured by ImageJ for zoomed-in panels along axonal TRKB signal, distance between distinct local maxima labelled.

3.4.3 Diurnal regulations of Na_V 1.7 phosphorylation

We examined the phospho-proteomics profiles of the samples from Section 3.3 and focused specifically on the changes in phospho-peptides of Na_V 1.7 (Figure 50). A total of 34 non-redundant phosphosites was detected, with 31 modified serine and 3 modified threonine. All phosphosites detected in our experiments were densely distributed in three regions of flexible structure unresolved by crystallography[591]: Residue 449-706, 1039-1065, 1858-1953. About half (18 out of 34) were exclusive to membrane-bound Na_V 1.7. Four of the phosphosites identified in our studies have been previously reported by liquid chromatography-mass spectrometry: S530, S535, S691, and S1950[592]. Although N-terminal phosphorylation of Na_V 1.7 has been identified to be associated with plasma membrane insertion[593], the current experiment did not capture any phosphosite in residues closer to the N-terminus until the first cytoplasmic loop (L1) which connects domain I and II.

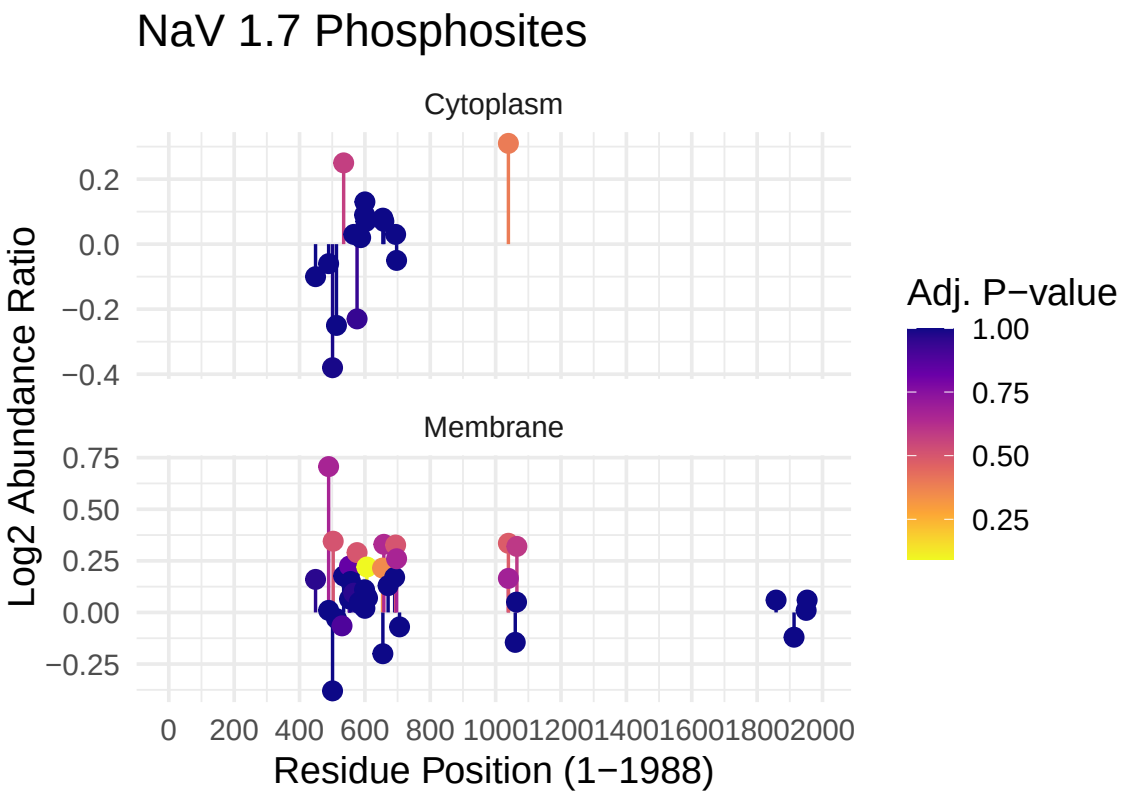


Figure 50: Diurnally differential phosphorylation status of Na_V 1.7 in chemically synchronised Chambers' iNociceptors based on subcellular localisation, Lollipop graph graphed in R.

Additionally, we cannot fully rule out the possibility that the puncta were resulted from the

fluctuation of cAMP concentration without any circadian mechanism. However, attempts to reproduce such pattern directly in cryopreserved *ex vivo* tissues were unsuccessful due to challenges of amplifying single-channel signals along nerves regardless of myelination (data not shown). Although puncta were seen in unsynchronised cultures, future experiments should validate the correlation of circadian time using alternative synchronisation methods (see Section 3.5.1).

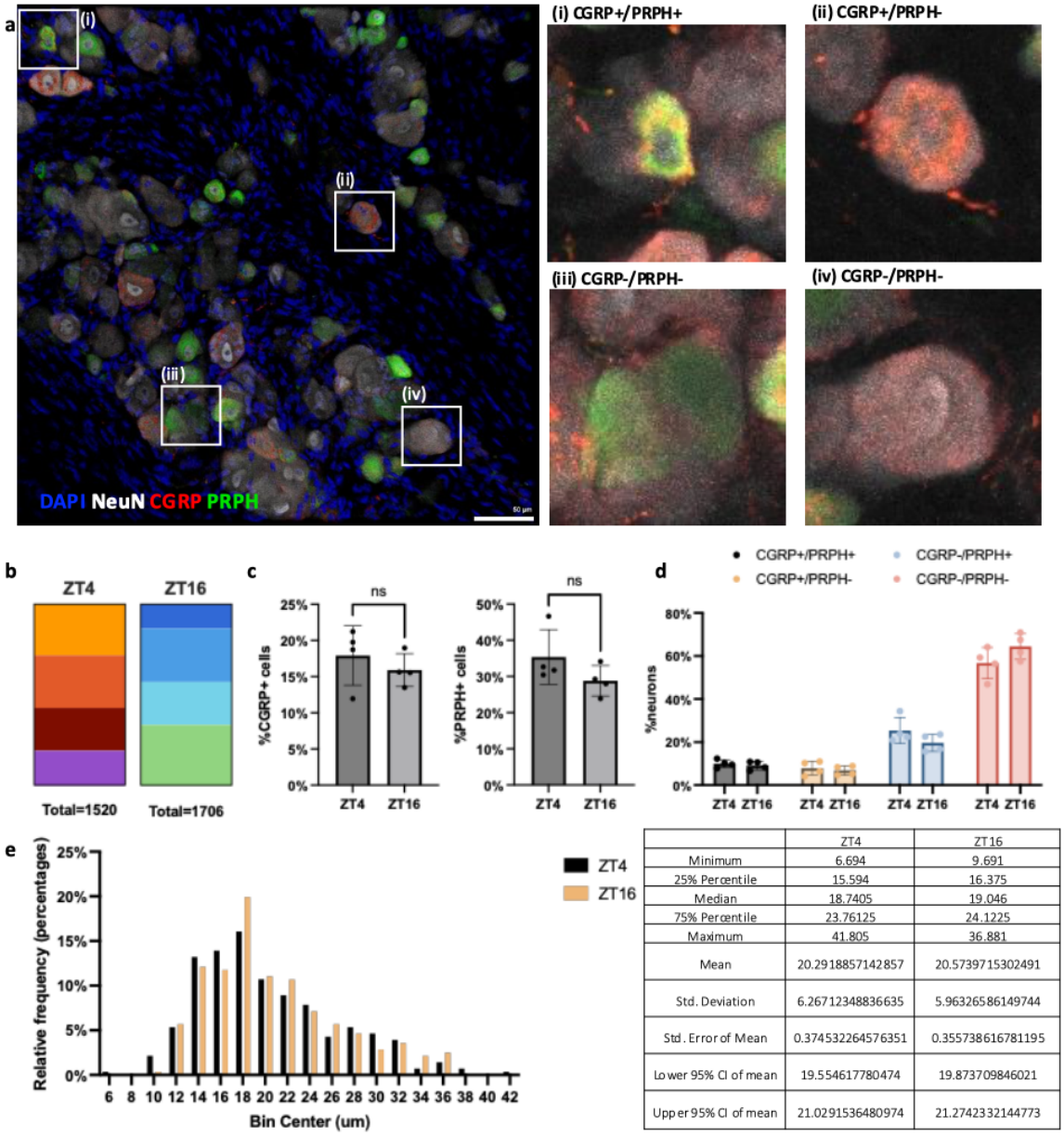
Among all phospho-sites detected, only three were statistically significant enriched at +16 compared to +4: S489 (adjusted p-value 0.0002 in membrane fraction, unavailable in cytoplasmic fraction), S576 (adjusted p-value 0.0033 in membrane fraction, 0.9411 in cytoplasmic fraction), and S1039 (adjusted p-value 0.0427 in membrane fraction, unavailable in cytoplasmic fraction). None of the diurnally differentially modified sites from the current experiment have been previously reported.

As phosphorylation of Na_V 1.7 has been recognised to be a critical modulator in pain detection[594], the binding partner and functional relevance of diurnally variable phosphosites could bring further insights to the circadian regulation of Na_V 1.7 activities. Together with proteomics and electrophysiological results, observations from our study implicates Na_V 1.7 as a potential key node connecting molecular clocks and nociception in sensory neurons.

3.4.4 Diurnal distribution of neuropeptides

Global proteomics only detected PACAP (Figure 42) and no other neuropeptides in FK synchronised Chambers' iNociceptors. Besides the confirmed lack of CGRP expression in Chamebers' iNociceptors, the lack of detection of other neuropeptides such as SP was likely a consequence of screwed missingness for smaller peptide sequences. Therefore, we verified diurnal immunoreactivities of CGRP in primary mouse tissues.

Although serum CGRP was found to be varying on a circadian basis[595–597], there is scarcely any report on the diurnal expression profile of CGRP within mammalian sensory ganglia. Therefore, we quantified the number of CGRP+ cells in diurnally harvested WT female murine TGs (Figure 51). We reconstructed CGRP immunolabelling signals in 20um z-stacks to locate, which were used to identify positive cells. Overall, there was no circadian-based difference in the relative quantity of CGRP+ cells. Future experiments will examine whether quantitative diurnal differences in CGRP abundance or CGRP secretion are evident.



	ZT4	ZT16
Minimum	6.694	9.691
25% Percentile	15.594	16.375
Median	18.7405	19.046
75% Percentile	23.76125	24.1225
Maximum	41.805	36.881
Mean	20.2918857142857	20.5739715302491
Std. Deviation	6.26712348836635	5.96326586149744
Std. Error of Mean	0.374532264576351	0.355738616781195
Lower 95% CI of mean	19.554617780474	19.873709846021
Upper 95% CI of mean	21.0291536480974	21.2742332144773

Figure 51: CGRP distribution in primary TGs from diurnally harvested female WT mice. (a) Representative 3D reconstruction of 20µm TG sections showing a variety of CGRP/PRPH co-distribution patterns, cut-out panels demonstrating the maximum intensity projections of examples of each category of quantification for panel (d). (b) Sources of total neurons counted (n=4 per time point), each colour representing the proportion of NeuN+ cells from an individual biological replicate. (c) Quantification of total %CGRP+ and total %PRPH+ in NeuN+ cells diurnally harvested TG sections. Statistical significance determined by Mann-Whitney test: %CGRP: p=0.4857, %PRPH: p=0.2000.. (d) Diurnal co-distribution pattern of CGRP and PRPH. Statistical significance determined by three-way ANOVA, no significance found in factors associated with circadian time. (e) Frequency distribution and descriptive statistics of CGRP+ soma diameters.

3.5 Discussion

3.5.1 Reflections on the methodology of circadian research in iNociceptors

Choice of methodologies for *in vitro* circadian research

The choice of methods for quantifying and/or visualising circadian markers depends on the target (Table 10). Based on initial success of live monitoring of BMAL1::luciferase in Chambers' iNociceptors[1], the current project extended the characterisation of neuronal circadian activities from variations in promoter activities to transcriptional (Section 3.2), translational (Section 3.3), and functional modulations (Section 3.4).

For the current project, transcriptional quantification of RT-qPCR was an economic but labour-intensive choice. Temporal resolution of transcriptional oscillations by relative quantification was highly dependent on the method of synchronisation, media conditions, RNA quality, primer design, stable references, and the method of fold change calculation. The current project provided a workflow that could identify more robust oscillators, such as *BMAL1* and surprisingly *GAPDH*. Consequently, the current project was unable to detect certain repressor orthologs that were prominently expressed in sensory neurons according to previous reports of absolute transcript quantification.

The current project applied multiple methods of protein quantification, particularly focusing on the complementary nature of high-throughput methods (e.g. proteomics) and target-specific traditional immunolabelling methods (e.g. IF & western blotting).

Global proteomics is highly robust and quantitative, particularly useful for identifying new targets of interest (e.g. Figure 41-42, Table 8-9). The efficiency of proteomics and phosphoproteomics in our study has been strongly influenced by the efficacy of subcellular fractionation. The kit used in the current study[543] generated three fractions of increasing protein hydrophobicity, of which the hydrophilic and hydrophobic fractions were processed further as cytoplasmic and membrane extractions in Section 3.3. However, the residual insoluble fraction could potentially retain highly lipophilic proteins that could not be released from bilipid membrane layers with the pre-determined detergent strength. We also lacked resolution to further distinguish the source of lipid-associated proteins from the plasma

membrane, storage and trafficking vesicles, or other membrane-bound organelles.

Another major category of missing values was transcription factors (such as all core clock components, sensory neuron markers ISL1, BRN3a, and TFAP2A). There is insufficient information to determine whether the missingness was a consequence of biased loss of nuclei acid-associated proteins during extraction, missingness of lowly expressed protein during quantification, or other technical factors. One way to validate missing values of total proteins in proteomics is by immunogen-specific labelling, in sacrifice of quantitative power. Mass spectrometry identifies multiple peptide fragments of the same master protein, with variable coverage depending on protein properties and sequending depth. Although major VGSC Na_V 1.7 displayed moderate membrane enrichment, the complete lack of phospho-peptide detection in more structurally ordered regions closer to transmembrane area[598] or the N-terminus[593] suggests potential detection bias. Analysis of potential bias in sequence coverage of proteins of interest across all samples or in each subcellular fractionation could potentially provide further insights.

In comparison, traditional protein quantification methods recruit antibodies or genetically engineered tags to trace the changes in highly specific targets. For example, the current project attempted to identify the axonal distribution of Na_V 1.7 in iNociceptors and primary cultures of rodent sensory neurons. Considering the technical challenges of axon quantifications, follow-up experiments need to incorporate several methodological optimisations. Axonal morphology can be improved with specialised axon-guidance culture platforms which limits the density and direction of axon outreach. To allow live tracking and increase specificity, we will also recruit hiPSC lines with endogenous reporters (e.g. Na_V 1.7-HALO, examples of trial differentiation see Figure 22)[65]. Live tracking provides the opportunities to examine the internal reproducibility of Na_V 1.7 clusters with different synchronisation methods in the same iNociceptor populations.

Overall, despite technique-specific drawbacks, the current project has exploited complementary assays that confirmed innate, functionally relevant molecular oscillations in sensory neurons derived *in vitro*.

METHOD	TARGET	ADVANTAGES	DISADVANTAGES
Bioluminescence	Promoter activities	Continueous & non-destructive live reporting.	Genetic modification required for construct expression; Indirect reference of naïve promoter activities, complicated with cell density[599], epigenetic silencing[310], the dynamics of luciferin transport, luciferase protein level and enzymatic kinetics[232,510].
RT-qPCR	Transcript abundance	Economic for multiple genes of interest investigated at once; Design freedom of primer annealing location	Relative quantification requiring suitable reference; Consideration over sampling intensity[527] and optimisation; Potential mismatch of phase, abundance, and rhythmicity between mRNA transcripts and protein products.
Translating ribosomal affinity purification (TRAP[600])	Active translation of mRNA transcripts in ribosomes	High cell-type specificity; Absolute quantification by sequencing.	Genetic modification required for ribosome labelling.
Live-cell fluorescence imaging	Tagged protein abundance & localisation	Direct, continuous, and non-destructive reporting; Spatial information; Semi-quantitative; Single-cell resolution; Option for pull-down or purification	Genetic modification required for construct expression; Potential interference with target protein dynamics[244], including folding, translocation, protein-protein interactions (PPI), half-life.
Western blot	Protein abundance	High target specificity; Detection of PPI & subcellular localisation coupled with other techniques.	Relative quantification requiring suitable reference; Consideration over sampling intensity[527]; Outcome handicapped by antibody availability and total/target protein abundance; Tedious procedure and anecdotally a normality of failure.
ImageSteam	Protein abundance & localisation	High throughput[601]; Quantitative; Single-cell resolution; Spatial information; Fewer cells required.	No temporal continuity in most cases due to suspension, fixation, and sample loss; Consideration over sampling intensity[527]; Currently available circadian reports focusing on quantification of metabolites without directly tracking core clock components but(e.g.[602–604]).
Proteomics	Protein abundance & localisation (combined with fractionation)	High throughput and explorative; Absolute quantification; Robust.	Biased missingness[541,542]; Power dependent on fractionation efficacy (if applicable); Analysis and visualisation dependent on bioinformatics.

Table 10: Comparisons between common methods for quantifying the circadian oscillations of clock genes.

Sampling intensity & synchronisation methods

Given that iNociceptors are less robustly oscillating than conventional circadian models, the challenges of common circadian assays[527] are expected if not more formidable. Therfore, unsaid effort went into the housekeeping conditions and maintenance before a robust synchronisation was achieved. For example, for all cultures subject to circadian assays, we maintained a consistent feeding schedule every 3 days, ideally around the same time of day. Samples for collections at discrete time points were grown on separate plates to avoid temperature fluctuation during handling. Fixation was done at 37 degrees instead of the conventional room temperature to prevent protein complex dissociation due to thermal shock.

The choice of the number and density of discreet circadian time points was a compromise between cost, labour, resources, and temporal resolution. The current project fully understood the risk that significant temporal variations could be misleading and might not necessarily co-relate to biologically relevant, externally reproducible cycles, without a concurrent continuous live monitoring assay. Therefore, all assay-specific sampling densities were determined based on previously determined *BMAL1* bioluminescence cycles in a different batch of Chambers' iNociceptors[1]. We chose 4-12 time points for target-specific assays (Section 3.2,S3.6-S3.7). For electrophysiological evaluations (Section 3.4.4), high-through experiments (Section 3.3 & 3.4.1) and validations with *ex vivo* tissue (Section 3.4.2), the choice was reduced to diurnal time points that previously displayed the biggest functional variations. Some argue that denser sampling with fewer replicate is more advantageous over sampling less frequently in duplicates as the former option condenses resources to prioritise temporal continuity[527]. However, we maintained 3-4 technical replicates for each time points in most assays to confirm internal validity of consistent iNociceptor differentiation (also see Section 4.2).

We chose FK as the major synchronisation cue for most assays due to comparably high efficacy, unless feeding alone could induce molecular oscillations (e.g. Figure 34 & 45). Compared to another common option such as DEX, FK induced higher amplitude in *BMAL1* promoter activities[1]. FK induces PER expression by elevating cAMP level[605]. Therefore,

any biological effects determined at different time points after FK treatment should be validated by alternative synchronisation methods to rule out accumulative effects from cAMP cascade[324]. In particular, our current proteomics data did not include any synchronisation control due to limited resources. Future experiments will either recruit unsynchronised or vehicle-synchronised samples or *ex vivo* mammalian sensory ganglia harvested at different zeitgeber times for contrast and validation.

3.5.2 Circadian rhythmicity in iNociceptors

Onset

The gradual acquisition of circadian rhythmicity appears to be tightly coupled to cell fate specification *in utero* and *in vitro*[606]. Neither early mammalian embryo[607–609] or iPSC[506] expresses oscillating clock genes. Expression of circadian oscillators is traceable in cortical neural progenitors *in vitro*[406,608], via spontaneous[406] or directed[519,520] differentiation. Although transcripts of core clock genes can be detected, it remains inconclusive whether transcriptional alone is sufficient to implicate a functional and oscillating genetic network. Similarly, proper transcriotional oscillation was not detected in iNociceptors until d60[1], significantly later than what is conventionally considered as mature (d35 by action potential characterisation[437]). The current project has observed similar patterns only in mature sensory neurons derived *in vitro*, further suggesting a more universal regulatory pathways that directs the sequential events of the loss of pluripotency marker expression and gaining circadian rhythmicity[606].

Functional relevance of circadian rhythmicity in iNociceptors

The current project has confirmed the diurnal variations in iNociceptor firing activities by direct electrophysiological assays (Section 3.4.4) and by identifying potential contributing biomarkers (Section 3.3 & 3.4.1). Although the exact mechanism for tissue-specific induction of clock-controlled gene expression and function modulation is unknown, elements

of the core TTFL cycle displays differential tissue expression (e.g. Figure 35). It is, therefore, speculated that individual clock components could exert unconventional cell type-specific functions that connects circadian rhythmicity to functional oscillation.

The current project has confirmed previous observation of the temporal variations in the relative abundance of active and inactive Na_V 1.7 in plasma membrane by electrophysiological experiments. We further identified the diurnally differential and membrane association-specific phosphorylation which could potentially alter Na_V 1.7 permeability. The majority of phosphosites detected in the current experiment resided with in the serine- and threonin-rich L1, which contains known sites for kinase-specific activities in close sequence proximity to phospho-acceptor residues we have identified (e.g. p38[593]). Previous work in the lab has identified the involvement of cryptochrome in the diurnal modulation of Na_V 1.7 via pharmacological interventions[1]. However, the current project lacked the technical measures to confirm direct or indirect interactions between cryptochrome members and Na_V 1.7. Future experiment can adopt similar methods of interactome prediction and point mutagenesis to validate the potential co-correlation of individual phosphosites with channel dynamics and membrane insertion of Na_V 1.7.

As the current project identified axonal regulation as a critical pathway, we further hypothesise the involvement of BMAL1 in nociceptor functional modulations. Among the core transcriptional oscillators, *BMAL1* is the only one observed to display regular axonal trafficking in cortical and sensory neurons[199,212–214]. Casein kinase 1δ is also known to regulate neuron-specific filaments such as beta-tubulin[610] and microtubule associated protein 2[611] by direct phosphorylation. Therefore, we hypothesised that a circadian-regulated axonal organisation of ion channels further contributed to the diurnal differential firing activities we observed. The protein fractionation method exploited in the current experiment could not distinguish ion channel inputs from soma plasma membrane, axonal termini, or storage vesicles. Therefore, synaptome-specific protein fractionation (e.g.[612]) could be used in further experiments.

4 Conclusion & Discussion

4.1 Conclusion

The current project has fulfilled its major aims:

1. We developed a novel protocol to generate reproducible neuropeptide-secreting sensory neurons *in vitro*, which can be maintained both as 2D conventional cultures and as 3D organoids/assembloids. The resulting neurons from our protocol has functionally complemented those derived from the benchmark method of sensory neuron differentiation (Chambers'[408]), with differential transcriptional, neuropeptide, and electrophysiological profiles. Together, the two protocols functionally represent multiple subtypes of human sensory neurons.

2. We optimised the conditions and methods to characterise multiple aspects of the molecular clock in sensory neurons generated *in vitro*, which can be readily adapted to different types of *in vitro* cell models.

3. We have confirmed the presence of an oscillating molecular clock in iNociceptors that can be sychronised with chemical cues, as an integrating component of differentiation programming and cell fate specification.

4. We have identified relevant biomarkers that co-relate molecular clock oscillations with sensory neuron excitability *in vitro*, which provides directions and insights for future experiments with more target specificity.

Overall, the findings of the current project strongly support the *Distributed Hypothesis* of circadian pain, as molecular oscillations in sensory neurons differentiated *in vitro* do not

rely on central guidance and entrainment. In the following sections, we will further discuss the limitations, biological implications, and future directions based on the results we have obtained.

4.2 Reflection on using iNociceptors as a pain model system as major methodologies in the current study

For more than a decade, hiPSC-derived models of reproducible sensory neuron differentiation have served as a great complement to rodent models in pain study[613]. The specific cell fate achieved by directed differentiation provides opportunities to study tissue-specific molecular pathways, including circadian oscillations. In this section, we will focus on the detailed discussion of precautions, limitations, and potential improvement of such model system.

Variations and quality control of undifferentiated hiPSCs

Variations in culture maintenance and differentiation outcomes are affected by the genetic background, method of generation, and culturing quality of iPSCs[613]. Even within the same culture, varying stages of cell cycle progression at the time of differentiation initiation can impact batch-specific production efficiency[614].

Methods of differentiation

Many published hiPSC differentiation protocols has been engineered for directed differentiation to generate target cell types of high specificity and purity. Defined chemical guidance can reduce batch effects and improve reproducibility. It is well recognised that the human origin of iPSCs bridges the potential interspecies differences at the expense of multi-tissue interactions and integrated behavioural responses[404]. Consequently, there has been growing attention on the importance of biophysical scaffold and intercellular communications during cellular development *in vitro*[615]. The choice of directed/spontaneous differentiations, combined with specialised physical support and extracellular matrix supplementation, is dependent on the balance between the needs of experimental design, types of assays for specific target biomarkers of interest, and resource availability.

Maturation

There is no single defined cut-off for sensory neuron maturity and functional competency. Many published papers using iNociceptor models define the generation of overshooting action potentials as the sole indicator of maturity (e.g.[437]), thereby providing no investigation of long-term (>45 days) neuronal characteristics. Some protocols intentionally aim for accelerated differentiation (e.g.[437,616]).

Following developmental cell fate specification, epigenetic barriers help set the pace of neuronal maturation and progressive functional development[617]. The current project has observed dynamic cellular functions rising as different time points during maturation (Figure 52). A recent study has identified a relative late membrane insertion of Na_V 1.7 to sensory neuron plasma membrane *in vitro*, coupling with a temporal development of firing activity[442]. We have confirmed a similar experimental timeline (>60 days) that involved acute functional modulation of Na_V 1.7, such as subcellular phosphoproteomics and MEA.

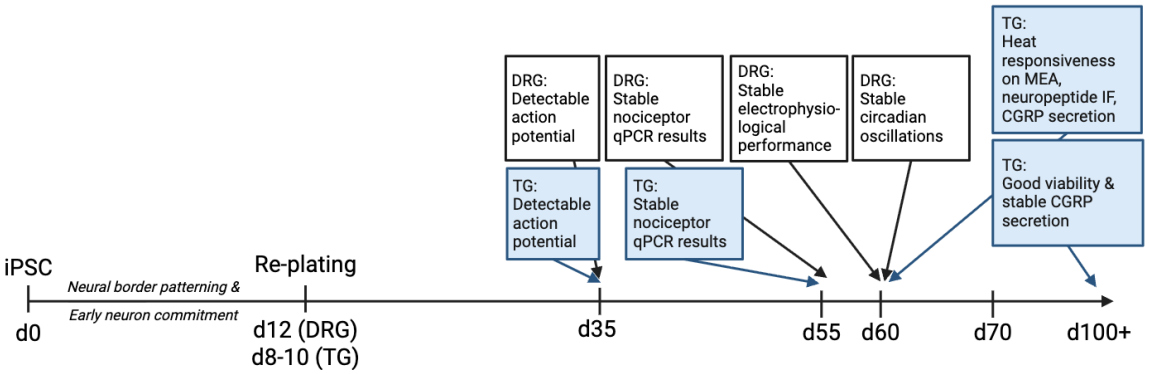


Figure 52: Schematics of experimental timelines during iNociceptor maturation. Illustrated in Biorender.

The maintenance of hiPSC-derived cultures is inarguably costly and labour-intensive. Although iNociceptors derived from our novel protocol could be maintained functionally competent above 100 days in culture, intensive and rigurous handling was applied to prevent mechanical disturbance, contamination, and accumulative cell death. Overall, these observations highlight the necessity of validating the minimal culturing time appropriate for specific biological targets.

Authenticity

Cell fate specification by directed differentiation begs the question of functional resemblance to *in vivo* human tissues. Therefore, published protocol frequently recruit high-throughput global profiling methods to compare transcriptomic profiles between sensory neurons developed *in vitro* and *ex vivo* (e.g.[73,411,429]).

Functional comparisons are usually limited to channel-specific electrophysiological activities by selective chemical regulations (e.g. Table 3) or using specialised biophysical equipments (e.g. for mechnosensitivity[618]). For channels for which no selective agonists or antagonists are available, functional relevance could be alternatively validated through genomic interventions. The establishment of genetically modified cell lines requires further quality checks to confirm efficient and functionally relevant modifications without off-target effects or mosaicism[619].

One particular contrast of neuronal function *in vitro* and *ex vivo* is the status of baseline firing without external stimuli. Spontaneous activities are minimal in sensory neurons under physiological conditions *in vivo*, yet paradoxically considered as a measurement of maturation *in vitro*. A variation of Chambers' protocol reported 70% neurons capable of spontaneous activities[417], which is a potential consequence of reduced tissue complexity and support from other cell types. Therefore, it is common to supplement primary glia to improve neuronal viability and axonal signal conduction[441,620]. Furthermore, CNQX was able to remove more than 90% activities during MEA measurements in our experiment (Section S3.3), and the residual signals could be from AMPA-independent electric synaptic activities or gap junction communications[444]. Our experiments further identified that some of the baseline activities were due to TRPV1 activation by innate factors within the culture (Figure 21).

Overall, synaptic connectivity is spatially unregulated and potentially circulating between multiple cells in simplified *in vitro* experiments. Less regulated network firing is therefore a representative drawback that remains critically different than sensory neuron physiology *in vivo*.

4.3 Discussion on the major biological findings of the current project and future directions

4.3.1 Development & cell fate specification of sensory neurons

As previously discussed in Section 2.5.2, sensory neuron diversification *in vitro* does not solely rely on directed differentiation using small molecules with defined concentration and application. In particular, the current project has identified the critical dependency of non-neuronal cells spontaneously emerging during early ectodermal induction. Bipotential neural crest progenitors commit to sensory neurons by cell-autonomous WNT signalling, which promotes surrounding cells to glia by direct cell-to-cell contact at the NOTCH synapse *in vivo* and *in vitro*[485,621,622]. In support of early neuroglial communication, the current project has identified the presence of hiPSC-derived glia from our TG cultures by bulk RT-qPCR. It will be beneficial for future studies to apply alternative methods such as lineage tracing or endogenous tags of glial markers to identify the spatio-temporal dynamics of neuroglial interaction during development *in vitro*.

The current project also confirmed the correlation between the retained expression of cMET/TRKA and neuropeptide-secreting phenotypes in mature iNociceptors, consistent with previous reports using murine and chick embryos[10,90]. Additionally, the early expression of TRPV1 in iNociceptors warrants further investigation into its human-specific functions during development, particularly with respect to the potential contribution of TRPV1 in thermo-sensor specification[12]. Together, these results provide insight on identifying conversed and species-specific features in the sensory neuron specification pathways during human development.

4.3.2 Profiling & stratification of sensory neurons

Although we have been referring to the iNociceptors generated in the current project as "peptidergic" (Section 2.3) and "non-peptidergic" (Section 2.2), this traditional binary categorisation is less applicable to the transcriptionally diverse human sensory neurons

in vivo (Section 2.5.1). It is likely that simplified chemical induction *in vitro* produces iNociceptors that correspond to only a narrow subtype of sensory neurons *in vivo*. Therefore, rigorous molecular characterisation of iNociceptors demands single-cell or single-nucleus RNA sequencing, which was beyond the scope of the current project. High-throughput transcriptomic profiling is necessary to provide information on the developmental trajectory, cell type diversity and heterogeneity, and transcriptional similarities of our protocol compared to *ex vivo* human sensory neurons.

It is also important to note that the molecular and functional profiles of mature sensory neurons *in vivo* are diversified depending on embryological origin (e.g. TG v.s. DRG[432]), anatomic location (e.g. cervical DRGs v.s. lumber[623]), innervation destination (e.g. trigeminal nociceptors innervating muscles v.s. skin[11,624]). Reproducing the dynamic contextual cues and biophysical scaffold is challenging for hiPSC-based models with established axial identity. However, proof-of-concept studies have applied artificial chemical gradients to approximate regionalisaion[625,626]. It suggests the prospects of modifying currently available protocols to generate iNociceptors representative of distinct anteroposterior locations for pathobiology modelling or regeneration therapies.

4.3.3 Sexual dimorphism

The current project did not study the impact of donor sex due to the limited number of cell lines involved. However, innate sexual dimorphism has been identified in both hormone-dependent[468] and independent[374,627–629] aspects of the physiology of pain. Certain types of pathological pain also exhibit biased prevalence in males (e.g. cluster headaches[630]) and females (e.g. migraine[631], also see sections below). The impact of donor sex should be considered for future hiPSC-based pain research.

4.3.4 Circadian properties of sensory neurons

The current project has established the correlation between the diurnal variation of sodium channel dynamics and that of firing activities in iNociceptors through pharmaceutical interventions. However, it is important to validate whether such functional association is genuine or merely a consequence of generic downstream effect of cAMP cascade activated by FK. Alternative synchronisation approaches can be done using a different synchronisation agent such as DEX in vitro, or by extracting *ex vivo* murine tissues with intact systemic entrainment.

The proteomics and phosphoproteomics analysis of the current study also raises several open questions for further investigation. Although no diurnal difference was detected in the expression or membrane translocation of TRP channels themselves, established modulators of TRP channel activities were identified as hits with significantly differential expression. It will be crucial to confirm that the electrophysiological properties of relevant TRP channels are diurnally different as a consequence. Furthermore, we would like to elucidate the importance of diurnally differential site-specific phosphorylation of Na_V 1.7, including the functional consequences, responsible kinases, and binding parpters involved in the regulation of these modifications.

4.3.5 Reflection on understanding migraine pathology with stem cell technologies

With a one-year prevalence of 15%, migraine is the second largest cause of disability in the world[472,632]. Migraine is understood as a complex neurological pathology that heavily involves the activation of the trigeminovascular system[472]. In particular, the release of nociceptor-derived CGRP to local vasculature is highly correlated with migraine headache attacks, which induces vasodilation by nitric oxide induction[460,461,473].

The mechanism of migraine pathogenesis and chronisation remains largely unknown. Mouse models of migraines commonly induce episodic and chronic migraine via single or consecutive daily injections of nitric oxide stimulant nitroglycerin, which provides limited representation of the female-biased prevalence and polygenic association of

migraine in human[633]. Consequently, there exist few mechanism-based treatment options, which are further convoluted by heterogeneity in clinical phenotypes and treatment efficacies. Common pharmacological treatments include nonsteroidal anti-inflammatory drugs (NSAIDs), triptans for acute attacks, and preventative medicines such as topiramates[632]. Meta-analysis also identified monoclonal antibodies for CGRP as a safe and efficacious prophylactic option[128,634,635].

The current project is a proof-of-concept study that demonstrates the relevance of hiPSC-based trigeminovascular assembloids as suitable preclinical models to study the pathogenesis of migraine. Our protocol allows the direct investigation of interactions between a CGRP-producing cell type and a CGRP-responsive cell type, preserving the human origin and patient-specific genetic background. The donors of patient lines used in the current project exhibit differential responsiveness to common treatment, which can be potentially reproduced *in vitro* using our protocol.

Migraine is also a representative pain pathology that has clear daily patterning of symptoms. One genetic association study has identified that mutations in casein kinase 1δ–an enzyme related to PER2 functions–lead to familial migraine and advanced sleep phase[371]. A recent study has shown the downregulation of several clock genes (including *PER2*) was associated with chronic migraine headache induced by nitroglycerin in rats[636]. Circadian-based regulation have also been found in the regulation of a few biological markers related to migraine, such as PACAP[582], vasoactive intestinal peptide (VIP)[582], and plasma CGRP[595–597]. As the current project has established the circadian regulation of healthy iNociceptor activities *in vitro*, it is a powerful tool to identify migraine-related biomarkers that are potentially circadian-regulated.

Supplementary Information

S1 Material & Methods

Materials

TYPE	MATERIAL	SUPPLIER	CATALOG
Buffers & Chemicals	16% Paraformaldehyde (PFA)	Alfa Aesar	043368.9M
	Dimethyl sulfoxide (DMSO)	Merck	D2650-100ML
	DPBS, no calcium, no magnesium	Thermo Fisher Scientific	14190094
	HBSS, no calcium, no magnesium-100 mL	Thermo Fisher Scientific	14170120
	L-Ascorbic acid	Merck	A4544-25G
	L-Cystine (L-Cys)	Merck	2470
	Sodium bicarbonate	Merck	S8875
	Sucrose	Merck	S8501-5KG
Electro-physiology reagents	AMG9810	Bio-Techne (R&D systems)	2316/50
	ATP disodium salt (ATP)	Bio-Techne (R&D systems)	3245/50
	Bradykinin (Brad)	Bio-Techne (R&D systems)	3004/5
	Capsaicin	Merck	21750-100 MG-F
	CNQX	Bio-Techne (R&D systems)	0190/50
	Histamine dihydrochloride	Bio-Techne (R&D systems)	3545/50
	Noradrenaline bitartrate (Nora)	Bio-Techne (R&D systems)	5269/50
	PF 05089771	Bio-Techne (R&D systems)	5931/10
	Prostagliandin E2 (PGE2)	Bio-Techne (R&D systems)	2296/10
	Sumatriptan	Bio-Techne (R&D systems)	3586/10
	Topiramate	Bio-Techne (R&D systems)	3620/10
Enzymes	Collagenase Type II	Thermo Fisher Scientific	10739473
	Dispase II	Thermo Fisher Scientific	11510536
	DNase I	Thermo Fisher Scientific	18047019
	Papain	Thermo Fisher Scientific	416760100
Medium	BrainPhys	STEMCELL Technologies	05790
	DMEM/F-12, no glutamine	Thermo Fisher Scientific	21331020
	Essential 6 (E6)	Thermo Fisher Scientific	A1516401
	Essential 8 (E8)	Thermo Fisher Scientific	A1517001
	Knockout DMEM	Thermo Fisher Scientific	10829018
	mTeSR1	STEMCELL Technologies	85850
	Neurobasal	Thermo Fisher Scientific	21103049
	Neurobasal A	Thermo Fisher Scientific	10888022
	StemPro-34 SFM	Thermo Fisher Scientific	10639011
Small molecules	AraC	Merck	C6645
	BDNF (human/mouse)	PeproTech	450-02-10UG
	bFGF	PeproTech	100-18B-50UG

TYPE	MATERIAL	SUPPLIER	CATALOG
	BMP4	Proteintech	HZ-1045
	CHIR99021 Hydrochloride	Stratech Scientific	S2924-SEL-5mg
	DAPT	Merck	D5942-5MG
	FK	Merck	F6886-10MG
	GDNF (human)	PeproTech	450-10-50UG
	GDNF (mouse)	PeproTech	450-44-50UG
	LDN-193189 (LDN)	Stratech Scientific	S2618-SEL-5mg
	NGF (human)	PeproTech	450-01-20uG
	NGF (mouse)	PeproTech	450-34-20UG
	ROCK inhibitor (ROCKi), y-27632 dihydrochloride	Abcam	Ab120129-100mg
	SB 431542 hydrate (SB)	Merck	S4317-5MG
	SU5402 (SU)	Merck	SML0443-5MG
	VEGF-A	Proteintech	HZ-1038
Supplement	2-Mercaptoethanol (50 mM, b-ME)	Thermo Fisher Scientific	31350010
	B27	Thermo Fisher Scientific	17504044
	B27 without vitamin A	Thermo Fisher Scientific	12587010
	Fetal bovine serum (FBS), heat-inactivated, qualified	Thermo Fisher Scientific	10500064
	GlutaMAX (100x)	Thermo Fisher Scientific	35050062
	Knockout serum replacement (KSR)	Thermo Fisher Scientific	10828028
	MEM Non-essential amino acids (100x)	Merck	M7145-100ML
	N2	Thermo Fisher Scientific	17502048
	Pen/Strip (10,000U/ml)	Thermo Fisher Scientific	15140122
Tissue culture reagents	0.25% trypsin-EDTA, phenol red	Thermo Fisher Scientific	15200056
	Accutase	STEMCELL Technologies	7920
	Anti-adherence Rinsing solution	STEMCELL Technologies	07010
	Cell Recovery Solution	Corning	354253
	EDTA, 0.5M, pH 8.0	Invitrogen^{TM}, Thermo Fisher Scientific	AM9260G
	Matrigel hESC-qualified	Corning	354277
	Matrigel Matrix for organoid, phenol red-free	Corning	356255

Table S1: List of supplier and catalog information of materials used in the current study.

Tissue culture housekeeping

Unless otherwise specified, all cell cultures were maintained in sterile incubators at 37 degrees, with 5% carbon dioxide, 95% air, and 95% humidity settings.

All AggreWell and ultra-low attachment plates were pre-treated with anti-adhesion solutions according to manufacturer's instructions.

Cultivation & Maintenance of hiPSCs

Healthy human iPSC lines SBAD02-01, SBAD03-01, and AH017 were obtained from STEMBANCC. Healthy human iPSC line KOLF2.1J was obtained from the Jackson Laboratory. The SCN9A-HALO line[63] was a kind donation from Prof. Sulayman Dib-Hajj at Yale University.

Migraine patient samples were collected under ethics regulation of the Oxford Radcliffe Biobank, converted to iPSC from peripheral blood mononuclear cell (PBMC)-derived erythroblasts, and undergone quality control by Oxford StemTech. The experimenter was blinded for patient drug susceptibility prior to all tissue culture, wet lab and electrophysiology experiments and analysis. As the experimenter is required to stay blinded for patient line information, only the demographic backgrounds of all non-patient iPSC lines are summarised in Section S2.1.

Undifferentiated hiPSCs were maintained feeder-free on Matrigel (human embryonic stem cell-qualified for all cultures, unless specified otherwise) and grown in mTeSR1 or E8 media, as required per differentiation protocol. Cells were passaged when reaching around 90% confluency, by lifting as single cells using 0.5mM EDTA and split at 1:3 ratio.

Routine quality control (QC) includes morphological examination, pluripotency marker expression, karyotyping, and CMV partition analysis every 5 passages (see Section S3.1).

Cultivation & Expansion of NHDFs

Commercially available adult NHDFs (Sigma) were thawed and seeded 3.5k/cm^2 onto uncoated t75s according to manufacturer's instructions. NHDFs were fed with DMEM/F12 every 2-3 days, supplemented with 5% FBS. When reaching 70%-90% confluency, cells were detached with 0.25% trypsin-EDTA and seeded at 3.5k/cm^2 for passaging.

Cultivation & Expansion of primary neonatral rat astrocytes

Commercially available neonatal rat cortical astrocytes (Thermo Fisher Scientific) were thawed and seeded in 0.5-1mil per uncoated t75s in in-house astrocyte media (85% DMEM/F12, 15% FBS, and 1x GlutaMAX). Media was changed every 3-4 days. The first feeding contained 1% pen/strip. Cells were detached with 0.25% trypsin-EDTA when 90%-100% confluent and passaged 1:3 until cell proliferation slowed down, usually by Passage 4. Fully expanded astrocytes were cryopreserved until needed.

Differentiation of DRG non-peptidergic iNociceptors

The differentiation of hiPSC-derived DRG nociceptors followed a published protocol (Figure 6a)[408,438]. In short, confluent iPSCs were detached as single cells with Accutase and seeded at 80k/cm^2 onto Matrigel-coated 6-well plates. Cells were allowed 24h recovery in mTeSR1 supplemented with 10μM ROCKi until reaching 40%-50% confluency.

Differentiation (d0) began with the addition of DRG KSR medium (Knockout DMEM, 15% KSR, 1% non-essential amino acids, 1x GlutaMAX, 100μM b-ME). From day 4, N2 medium (Neurobasal medium, N2 supplement, B27 supplement without vitamin A, 1x GlutaMAX) were added in 25% increments every other day until reaching 100% by d12. The media was supplemented with 10μM SB and 100nM LDN from d0 to d5, and with 3μM CHIR99021, 10μM SU5402 and 10μM DAPT from d2 to d11. For experiments investigating the impact of glial presence, DAPT was opted out for certain cultures (See Section S3.5).

On d12, cells were detached with Accutase and replated 80k/cm^2 for maturation, supplement with 10μM ROCKi. Maturation media included N2A medium (Neurobasal medium A, N2, B27 without vitamin A, 1x GlutaMAX) with 20ng/ml BDNF, 20ng/ml GDNF and 40ng/ml NGF. On day 14, cells were incubated with 4μM AraC in addition for 24h to remove non-neuronal contaminations. Astrocytes were supplemented at 20k/cm^2 density if needed.

Differentiation of TG peptidergic iNociceptors

The differentiation of hiPSC-derived TG nociceptors began by deriving TPs according to a published protocol (Figure 12a)[435].

For placodal induction on 2D platforms, single-celled iPSCs were seeded 250k-300k/cm^2 in 6-well plates to reach 100% confluency within 24h in E8 medium with 10μM ROCKi. Whereas for 3D TP generations, embryoid bodies were generated at 3mil/well in an AggreWell 800 in E8 medium with 10μM ROCKi and 1% DMSO for 24h.

Starting from d0, the following was supplemented in E6 medium: d0-1 10μM SB and 5μMg/ml BMP4; d2 10μM SB, 5μg/ml BMP4, and 600nM CHIR99021; d3 10μMM SB and 600nM CHIR99021; d4 10μMM SB till placodes were induced.

The day of placodal appearance on 2D platforms varied slightly depending on the line, ranging between d7 and d15. Two days after appearance, placodes were gently flushed with media for physical detachment from the basal layer. Suspended placodes were let stand for a few minutes till settling down by the pull of gravity (Figure S11b). Supernatant containing pieces of the basal layer and single cells were removed. Placodes were washed and gently resuspended to estimate counts. Otherwise, whole cultures derived from 2D or 3D platforms were lifted as single cells by Accutase and replated at assay-dependent concentrations for maturation.

Cells were matured in N2A medium till d70, supplemented with 20ng/ml BDNF, 2μM FK, and 200nM ascorbic acid. Two days after plating, 4μM AraC was added for 48h to remove non-neuronal contaminations. A day after removing AraC, 20k/cm^2 rat astrocytes were added unless specified.

Differentiation of vasculature organoid

The differentiation of hiPSC-derived vascular organoid followed a published protocol[474]. Embryoid bodies were generated at 1.2mil/well in an AggreWell 400 in E8 medium with 20μM ROCKi for 24h.

Organoids were cultured in suspension with gentle rocking, in Mesoderm N2B27 medium

(50% Neurobasal medium, 50% DMEM/F12, N2 supplement, normal B27 supplement, 1x GlutaMAX, 100μM b-ME) between d0 and d4. 20μM ROCKi was retained in the culture for the first 24 hours of differentiation. Between d0 and d2, 30ng/ml BMP4 and 12μM CHIR99021 were supplemented to Mesoderm N2B27 medium. Between d3 and d5, 2μM FK and 100ng/ml human VEGF-A were added.

On d5, organoids were allowed to pellet by gravity and cultured in Matrigel domes by mixing equal volume of Matrigel (organoid-specific) with media with organoids. Matrigel domes were submerged in StemPro-34 SFM medium supplemented with 15% FBS, 100ng/ml human VEGF-A, and 100ng/ml bFGF until d10. Organoids were released from Matrigel domes using Cell Recovery solution based on manufacturer's instructions..

Assembloid fusion

TG and vasculature organoids derived separately based on previous sections were fused by contact in ultra-low attachment 96-well plates. Each well contained one TG organoids and several vasculature organoids due to differences in size and cell density. Days *in vitro* were counted based on the progress of TG protocol.

Mice

Animal housekeeping and experiments were conducted under the project licence PP0010096. C57BL6/J (BL6) mice were kept under either normal (7AM-7PM light on) or alternative (9PM-9AM light on) light cycles for at least two weeks to allow for circaidan adaptation. Mice were kept with sibling littermates in individually ventilated cages. There was otherwise no difference in food & water supply (*ad libitum*), temperature, and home cage husbandry setups.

Dissection of primary murine sensory ganglia

Animals were culled with carbon dioxide, confirmed by cervical dislocation per Schedule 1 requirement. Eyes were then removed immediately after Schedule 1 culling to avoid light

contamination.

Identification and extraction of murine DRGs[637] and TGs[638] followed published protocols. For DRGs, a sagittal cut along the midline of the back was made to expose the vertebra. Although there was no preference to spinal segments, we focused on extracting thoracic and lumbar DRGs due to the ease, and to avoid damage from cervical dislocation. Muscles and other tissues were scraped off as much as possible. Another sagittal cut was made to open the vertebra, and both pieces were relocated to ice cold PBS under a dissection microscope for easier identification. Gentle pulling on the spinal cord revealed dorsal roots, from which the bulbs of ganglia, either alone or with certain length of nerve, were excised depending on the purpose of dissection.

TGs were extracted by craniotomy, removal of the brain, and excision at surrounding nerves.

Primary sensory neuron cultures

The protocol for the dissociation and culturing of primary sensory neurons from freshly dissected ganglia was modified from the literature[637]. Briefly, whole DRGs and roughly minced TGs were kept in ice cold Ca^{2+}/Mg^{2+}-free HBSS until ready for enzymatic dissociation. Most nerves were removed from the bulb to reduce the level of debris. Once ganglia settled by gravity, HBSS was removed and replaced with pre-warmed papain (40U/ml) in Ca^{2+}/Mg^{2+}-free HBSS with saturated $NaHCO_3$ (1:500) and L-Cys (1mg/1.5ml). Ganglia were incubated for 20 min at 37 degrees and pelleted at 200g. Papain solution was replaced by collagenase II (4mg/ml) and dispase II (4.6mg/ml) in Ca^{2+}/Mg^{2+}-free HBSS. Ganglia were incubated at 37 degrees for 20-30 min with gentle trituration in-between.

Digested cells were pelleted at 400g and treated with 100ug/ml DNase I in dissociation media (DMEM/F12, 10% FBS, 1x GlutaMAX, 1% pen/strip) for 5 min. After DNase I (20U/ml) treatment, an equal volume of dissociation media was added and the whole volume was passed through 70μm cell sieves (Falcon). Cells sieved through were pelleted at 1000g, seeded in dissociation media with 10μM ROCKi and 100ug/ml DNase I. Once attached (2 hours after seeding), liquid was replaced with pre-warmed growth media (Neurobasal A,

normal B27 supplement, 1x GlutaMAX, 1% Pen/Strip, 50ng/ml mouse NGF, 20ng/ml mouse GDNF, and 10μm ROCKi for the first feed) and changed every other day. Primary cultures were grown and stabilised for at least 7 days before proceeding to chemical synchronisation.

Cell counts & viability check with trypan blue

Freshly prepared cell suspensions were thoroughly mixed with an equal volume of 0.4% Trypan Blue (Thermo Fisher Scientific), 10μl of which was loaded onto each side of Countess cell counting chamber slides. Cell count and viability quantification were performed on a Countess 3 FL automated cell counter according to manufacturer's instructions.

Tissue culture synchronisation

All relevant cultures were synchronised by either one-hour chemical treatment of 10uM FK or vehicle (equal volume of DMSO) in maturation media without growth factors.

FC & FACS

In-house FACS staining buffer contained 5% FBS and 2mM EDTA in PBS, filtered through 0.22μm filter to maintain sterility. No additional sodium azide was supplemented for fixed samples.

For the examination of pluripotency marker expression, 90%-100% confluent hiPSCs were dissociated with Accutase and fixed in suspension with 4% PFA for 10 min at room temperature. Permeabilisation was done with 0.1% tx-100 for 15 min at room temperature, followed by blocking for 45 min. Cells were then stained with conjugated primary antibody against TRA-1-60 and NANOG with DAPI (1μg/ml) for 45 min at room temperature, ready for flow measurement after thorough washing.

For live cell TRK-typing FC and sorting, d8-d9 TG and d12 DRG iNociceptor progenitors were detached with Accutase for 10 min at 37°C. Single cell suspension was then blocked

with anti-human Fc receptor (eBioscience, Invitrogen, Thermo Fisher Scientific) at 4°C for 20 min. Cells were stained with monoclonal human TrkA-allophycocyanin (APC)/TrkA-phycoerythrin (PE) and human TrkB-Alexa Fluor 488 antibodies (both Bio-Techne, clone 165131R and 72509, respectively) at room temperature for 1h, in dilutions suggested by the manufacturer. Fluorophore-specific isotype controls [Ms IgG1-APC (400120, Biolegend), MS IgG1-PE (40011, Biolegend), and Ms-IgG1-Alexa Fluor 488 (400129, Biolegend)] and no-stain controls were co-developed for each run. All samples were washed with 1ml FACS staining buffer and reconstituted at a concentration less than 10 mil/ml. DAPI was applied at 1μg/ml 5 min prior to flow measurements as live/death gating. Cells were counted for viability as previously stated after detachment, staining and sorting. Flow cytometry efficiency of TRK genes was validated by RT-qPCR (Figure S12d).

FC was performed on a BD LSR Fortessa X20 while FACS was performed on a BD FACSAria III (Becton Dickinson). Analysis and visualisation of flow data, including cell cycle quantification, were achieved with the open source online platform floreada.io..

ImageStream

Sample preparation

Chemically detached single cell suspensions (unsynchronised mature TG iNociceptors in Section S3.4.4 and synchronised NDHFs in Section S3.7) were fixed with 4% PFA for 10 min at 37 degrees, followed by a 10-min permeabilisation with 0.05% tx-100 in PBS at room temperature. Immunolabelling of neuropeptides and clock proteins was identical to IF sections below.

Flow operation

Imaging flow cytometry was operated on a Cytek Amnis ImageStream X Mk II imaging flow cytometer with the 60x objective. EDF was applied for the detection of neuropeptide vesicle.

Analysis

Technical replicates of the same staining combinations of all relevant time points (if any) were pooled with negative controls for analysis in the IDEAS 6.4 software. Quality control process was detailed in Section S3.7.

RNA extractions & RT-qPCR

Cells were washed with PBS to remove media and directly treated with Trizol (Thermo Fisher Scientific). Total RNA was extracted with Direct-zol RNA kit (Zymo) following manufacturer's instructions. RNA concentration was quantified by absorbance spectroscopy (Nanodrop, Thermo Fisher Scientific). Unless otherwise specified in Section S3.6, total RNA was retrotranscribed with HiScript III RT Supermix (Vazyme) on a T100^{TM} Thermal Cycler (Bio-Rad). RT-qPCR was carried out with Taq Pro Universal SYBR qPCR Master Mix (Vazyme) according to manufacturer's instructions on a StepOnePlus Real-Time PCR System (Applied Biosystems). The cycling programs was as follows: initial denaturation at 95°C for 10 min, 40 cycles of denaturation (95°C, 15s) and annealing (60°C, 1 min), and a melt curve analysis. Primers were lab designed or sourced from PrimerBank and published literature (see Section S2.2), all confirmed for human specificity, annealing location and melt curve analysis. Relative quantification for differentiated cells compared to iPSC was calculated via the ddCT method against housekeeping gene *GAPDH* unless specified otherwise.

Reference gene stability analysis

Raw C_Ts of candidate reference genes were obtained from RT-qPCR as stated above. C_Ts from different synchronisation methods across all time points were grouped for the same gene for NHDFs and iNociceptors, respectively. GeNorm was accessed through the online tool RefFinder[537], analysed per cell type.

Period analysis of transcriptional circadian analysis

For circadian gene oscillations in NHDFs, sine wave fitting for each clock gene transcript was done with the curve fitting app in MATLAB. Circadian period was calculated as the average difference between local maxima/minima of the same curve. Phase difference between genes was calculated as the average difference in the time of occurrence of the first local maxima between two curves.

IF sample preparation & staining

Cultured cells grown on acid-treated glass coverslips or chamber slides (Ibidi) were washed with PBS to remove media, followed by a 10-min fixation with 4% PFA at 37 degrees (to preserve thermal stability of macrocomplexes of clock proteins) for circadian-related IF experiments, or at room temperature otherwise.

Immersion fixation of mouse sensory ganglia was done in ice cold 4% PFA for 1.5 hours, followed by thorough washes in PBS. Cryoprotection was performed by 24h immersion in 10%, 20%, and 30% surcrose consecutively. Once embedded in OCT solutions (VWR), tissues were cryosectioned at 25μm thickness and air-dried for 1h before proceeding.

Blocking was done for 1h at room temperature with 5% donkey or goat serum in PBS, species matching with corresponding secondary antibodies of choice. For intracellular/nuclear markers, 0.1% tx-100 was added in addition to serum during blocking.

For conventional two-step staining, primary antibodies were diluted according to Section S2.3 in blocking solution and incubated at 4 degrees overnight. Washes were followed by secondary antibodies (1:500, see Table S5). For one-step staining, primary antibodies were pre-treated with FlexAble 2.0 conjugation kits (Proteintech) according to manufacturers' instructions.

Samples were incubated in DAPI (1μg/ml) for 10 min at room temperature. Final washes were done with PBS for 5 min thrice at room temperature. Prior to imaging, slides were mounted with VectaShield anti-fade mounting medium.

IF staining for cleared 3D tissues was part of the clearing protocol according to

manufacturer's instructions.

Tissue clearing

Whole mouse DRGs and 3D assembloids were fixed as stated previously. Clearing was done with CytoVista Tissue Clearing kit (Thermo Fisher) or CytoVista 3D Culture Clearing kit (Thermo Fisher) according to manufacterer's instructions.

Image acquisition

For each sample, 3 fields of view were randomly selected for imaging. Fluorescence background was determined by secondary-only or isotype controls, depending on whether the conjugation kits were applied.

Brightfield & Widefield IF imaging

Brightfield and widefield fluorescence imaging were carried out on an EVOS^{TM} M7000 Imaging System (Thermo Fisher Scientific). Objectives used were as follows: EVOS^{TM} 4X Objective, fluorite, LWD, phase-contrast, 0.13NA/10.58WD; EVOS^{TM} 10X Objective, fluorite, LWD, phase-contrast, 0.30NA/7.13WD; EVOS^{TM} 20X Objective, fluorite, LWD, 0.45NA/6.23WD; EVOS^{TM} 40X Objective, fluorite, LWD, phase-contrast, 0.65NA/1.79WD (Thermo Fisher Scientific).

Confocal IF imaging

Confocal IF imaging was carried out on Zeiss LSM 780 or 880 Airyscan microscopes. Objectives used were as follows: 10x/0.3 DICI, 20x/0.8 DICII, and 63x/1.4 Oil DIC.

Image analysis

Image processing for visualisation

Multichannel pseudo-colouring, average fluorescence intensity across regions of interests, line intensity profiling, Pearson correlation, distance to edge, z-stack maximum intensity projection, z-stack depth coding by colour gradients, and z-stack orthogonal analysis were done in ImageJ. Brightness/Contrast adjustment was made only for visualisation purposes if necessary. All quantifications were done in unaltered original images, captured under the same imaging conditions.

Brightfield placode quantification (for 2D platforms only)

Three wells of independent differentiation per line were used for quantification, of which two randomly selected fields each were imaged. Brightfield images were loaded into ImageJ. For each image, automatic threshold was applied such that placodes had maximum intensity and basal layer none. Following watershed, Analyze Particles function was applied to count the number of placodes in the field, with Exclude on Edges. Size parameter was set as the area of smallest placodes (manually measured in ImageJ) to infinity, with 0-1 circularity. Incorrect watershed divisions were identified during size measurement, and the counting result was manually corrected. Numbers per cm^2 was scaled by a factor of 14.29 as the dimension of the original 4x image was 0.12 inches x 0.09 inches.

Diameter measurement

Sizes of TPs (Figure 22 & S11) and soma diameter (Figure 51) measurements were done by straight line labelling in ImageJ.

Z-stack 3D reconstruction

3D reconstruction of z-stack images (e.g. Figure 51 & 27a) was done in arivis 4D viewer.

CGRP & PRPH distribution quantification in primary murine TG sections

Three randomly selected areas from TG sections of 4 animals per circadian time were recruited for CGRP distribution (Figure 51). Experimenter was blinded for the section number, biological replicate, and time of harvest during quantification.

CD31 geometry

For vasculature network in whole mount mouse DRGs and hiPSC-derived vascular organoids, CD31 fluorescence signal was extracted as from the multi-channel hyperstack images via ImageJ and applied to the 3D Tubular Network Analysis workflow[477] on Arivis Cloud.

MEA

D12 DRG were dot plated at 25k/well or fully plated at 55k/well on Matrigel-coated MEA plates (Cytoview MEA 48, Axion Biosystems). Two days after plating, 4μM AraC was applied in culture media for 24h. 20k/cm^2 astrocytes were added after AraC treatment.
D8-9 single-cell suspension from 3D placodes were plated at 100k/well on Matrigel-coated MEA plates (Cytoview MEA 48, Axion Biosystems). No AraC was added to prevent detachment. 20k/cm^2 astrocytes were supplemented 2 days after seeding.
As a negative control, 20k/cm^2 astrocytes were seeded on Matrigel-coated MEA plates (Cytoview MEA 12, Axion Biosystems).
For both protocols, maturation methods were as entailed in previous sections. Visual inspections of cell attachments and colony morphology were performed before measurements. Unless specified for assays with a defined circadian-time, a fresh complete media change was applied 16-20 hour before measurements. BrainPhyz media exchange supplemented with N2 and B27 supplements without vitamin A was carried out at least 24 hours before an experiment to allow adaptation. Pretreatment of antagonists was added at least 30 min before measurement. Chemical agonists were added live during recording. Noxious heat sequence (Figure 21) was applied continuously for the heating period without the removal of plate to prevent redundant setting time.

Each MEA recordings were carried out for two consective 2-min sessions after a 5-min setting time as baseline on the MEA reader (Axion Biosystems). The plate was maintained at 37°C unless noxious heat was applied via bottom heating.

Spike detection was carried out in the AxIS software (Axion Biosystems) as previously described[438]: A spike was coined when an amplitude at least six standard deviations above background appeared; single-electrode bursts were recorded when at least five consecutive spikes showed up with intervals less than 100 ms. Spike sorting was done in the AxISmetrics plotting tool (Axion Biosystems). Plate maps of Mean Firing rates and Numbers of active electrodes and raster plots with spike histograms were derived from NeuralMetric Tool.

Prior to analysis, the following selection criteria were applied: (1) wells with visibly washed off colonies were excluded; (2) wells with less than 2 active electrodes in all conditions across a group of test conditions (e.g. before and after an agonist treatment, or at both +4 and +16 circadian time) were excluded. An example can be seen in Section S3.3. Firing rates were extracted and manually paired for baseline-stimulus analysis in GraphPad Prism for variance-based analysis or R for clustering.

CGRP ELISA

TP cultures were replated at d8-10 as single-celled whole cultures at 400k/cm^2 in 12 well-plates, or as placodes diluted accordingly to total cell counts that was batch- and cell line-specific. Two days after plating, cells were treated with 4μM AraC for 48h except for no AraC controls. Cells were matured as previously entailed unless specified otherwise. Growth factors were removed from cultures from d60. Feeding with N2A media alone were continued for another 10 days before proceeding to ELISA sample collections.

Cells were treated with 1ml/well media containing vehicle and individual stimuli for 24h each consecutively unless specified otherwise. IS included 500nM Nora, 50nM Brad, 500nM PGE2, 1uM Histamine, and 2uM ATP. Cells were allowed at least 24-hour recovery between each group of baseline-stimulus, or baseline-stimulus-treatment.

All media collected were immediately centrifuged at 2000g for 10 minutes to remove cells

and debris, then snap-frozen with proteinase inhibitors (Thermo Fisher Scientific) at -80°C till use. No repeated freeze-thaw cycle was applied to prevent degradation.

Human CGRP (Bertin) ELISA assays were done with commercially available kits according to manufacturer's instructions. All standards, samples, quality controls, and blank were loaded in pairs. Absorption/Optical density (OD) was measured using a FLUOstar Omega Microplate Reader (BMG Labtech), averaged, and normalised against blank. Standard curves were calculated as sigmoidal 4PL to calculate sample concentrations.

Intracellular cAMP ELISA

Primary rat astrocytes were treated with TG iNociceptor-conditioned media (CGRP determined by ELISA as stated above), 100pg/ml purified human CGRP, 5μM FK, or vehicle control for one hour. Intracellular cAMP level was quantified by a commercially available ELISA kit (Abcam) according to manufacturer's instructions. All standards, samples, quality controls, and blank were loaded in pairs. Absorption/Optical density (OD) was read with a FLUOstar Omega Microplate Reader (BMG Labtech), averaged, and normalised against blank. Standard curves were calculated as sigmoidal 5PL to calculate sample concentrations.

Protein extraction

Bulk protein extraction was done by direct treatment of radioimmunoprecipitation assay (RIPA) buffer supplemented with protease and phosphoprotease inhibitors (Thermo Fisher Scientific), according to manufacturer's instructions. Extracted proteins were snap frozen and stored at -80 degrees until use.

Western blots

Protein quantity was determined with the Pierce BCA kit according to manufacturer's instructions (Thermo Fisher Scientific). A total 10μg sodium dodecyl sulfate (SDS)-reduced protein per sample was run on NuPAGE 4-12% Bis-Tris Gels with Precision Plus Protein

Dual Color Standards (Bio-Rad) in MOPS running buffer (Bio-Rad) for 50 min at 200V constant. Size-separated protein samples were transported to western blots with the default transfer program on Bio-Rad Trans-Bot Turbo Transfer System (Bio-Rad).

Staining of BMAL1 (1:1000 Proteintech 14268-1-AP) against loading control TUBB3 (1:10000 Sigma T8578) and fluorescent secondary antibody labelling (1:5000 for Donkey anti-Ms IRDye 800 LI-COR 926-32212 and Donkey anti-Rb IRDye 680 LI-COR 926-68073) were done overnight at room temperature using the iBind Flex FD system (Invitrogen, Thermo Fisher Scientific).

Fluorescently labelled western blots was imaged on the LI-COR ODYSSEY Clx system, exposure automatically determined by ladder signal intensity.

No relative quantification was performed for the blots included in the current study.

Analysis & visualisation of functional genomics and protein crystal structures

Genomic sequences of genes of interest were imported from GENCODE[639] database to analyse in web-based R&D software Benchling (RRID:SCR_013955). Protein crystal structure and complex interactions were retrieved from Protein Data Bank and visualised in PyMol (The PyMOL Molecular Graphics System, Version 1.2r3pre, Schrödinger, LLC).

Multi-omics analysis

Transcriptomic profilings of human DRG and TG[4–6] and Chambers' iNociceptors[7] were directly retrieved from R shiny-based online database.

For iNociceptor subcellular proteomics, mature SBAD02 iNociceptors were synchronised with FK and harvested with the Mem-PER Plus membrane protein extraction kit (Thermo Fisher Scientific). Liquid chromatography-mass spectrometry was performed by collaborators from Department of Biochemistry and Molecular Biology at the University of Southern Denmark. Raw proteomics data were analysed using the open source multi-omics analysis and visualisation tool Omics Playground[540], which included all necessary coding for data quality control, sample clustering, DE identification, and GO analysis. No

imputation, batch correction, or outlier detection algorithm was performed.

Phosphoproteomics data for NaV_V 1.7 was extracted and graphed by R.

Graphing & Statistical analysis

Unless specified, data graphing, standard curve fitting, and statistical analysis were done in GraphPad Prism. Individual test methods and significance (if relevant) were specified in corresponding figure legends.

R codes for MEA clustering and contingency table computing (Figure 10), CDE statistical computing (Figure 24), and phosophoproteomics labelling (Figure 50) can be provided upon request. Raw data and source codes from BigOmics analysis for proteomics in Section 3.3 are confidential until publication.

Illustrated schematics were made in Biorender under the university licence. Panel arrangement was done with Microsoft PowerPoint.

S2 Supplementary tables

S2.1 HiPSC lines

LINE	SEX	AGE AT SAMPLING	CELL TYPE	KNOWN DISEASE	RRID
AH017	Female	67Y	Fibroblast of skin	N/A	CVCL_RB85
KOLF2.1J	Male	55-59Y	Fibroblast of skin	N/A	CVCL_B5P3
SBAD02	Male	51Y	Fibroblast of skin	N/A	CVCL_ZX54
SBAD03	Female	36Y	Fibroblast of skin	N/A	CVCL_ZX55

Table S2: Demographic and clinical information (if relevant) of WT HiPSC lines used in this project.

S2.2 Primers

GENE	FORWARD	REVERSE	SOURCE
ASIC2	GAGTGCCGATCCTCAGAGATG	CAATGTAGCGGGTCTCACAGT	PrimerBank
bACTIN	GACCCAGATCATGTTTGAGACCT	GAGGCGTACAGGGATAGCAC	Lab design
BMAL1	AAGGGAAGCTCACAGTCAGAT	GGACATTGCGTTGCATGTTGG	PrimerBank
BRN3a	GGGCAAGAGCCATCCTTTCAA	CTGTTCATCGTGTGGTACGTG	PrimerBank
CALCA	TCTAAGCGGTGCGGTAATCTG	TGTTGAAGTCCTGCGTGTATG	PrimerBank
CALCB	ACCCGGCCACACTCAGTAA	GGGCACGAAGTTGCTCTTCA	PrimerBank
CALCRL	CTCCTCTACATTATCCATGG	CCTCCTCTGCAATCTTTCC	Literature[640]
CD31	GAGTATTACTGCACAGCCTTCA	AACCACTGCAATAAGTCCTTTC	Lab design
CD140b	AGCACCTTCGTTCTGACCTG	TATTCTCCCGTGTCTAGCCCA	Lab design
CGRP	TCTAAGCGGTGCGGTAATCTG	TGTTGAAGTCCTGCGTGTATG	PrimerBank
CLDN5	GCGTGCTCTACCTGTTTT	CAGCTCGTACTTCTGCGA	Lab design
CLOCK	TGCGAGGAACAATAGACCCAA	ATGGCCTATGTGTGCGTTGTA	PrimerBank
cMET	AGCAATGGGGAGTGTAAAGAGG	CCCAGTCTTGTACTCAGCAAC	PrimerBank
CRCP	AGAGCAGCGTAAAGAAAGTGG	CTGACAATTTCAGGACTCTGGTG	PrimerBank
CRY1	CTCCTCCAATGTGGGCATCAA	CCACGAATCACAAACAGACGG	PrimerBank
CRY2	TCCCAAGGCTGTTCAAGGAAT	TGCATCCCGTTCTTTCCCAAA	PrimerBank
CX43	GGTGACTGGAGCGCCTTAG	GCGCACATGAGAGATTGGGA	PrimerBank
EAAT-1	AGCAGGGAGTCCGTAAACG	AGCATTCCGAAACAGGTAACTTT	PrimerBank
EAAT-2	CCTGACGGTGTTTGGTGTCAT	CAAGCGGCCACTAGCCTTAG	PrimerBank
EYA1	CACCACAGATTTACCCTTCCAAC	GTACGTGGCATAGGCTGTAGC	PrimerBank
GAPDH	GTCTCCTCTGACTTCAACAGCG	ACCACCCTGTTGCTGTAGCCAA	Lab design
GFAP	GTCCCCCACCTAGTTTGCAG	TAGTCGTTGGCTTCGTGCTT	Lab design
HPRT1	CCTGGCGTCGTGATTAGTGAT	AGACGTTCAGTCCTGTCCATAA	PrimerBank
ISL1	GCGGAGTGTAATCAGTATTTGGA	GCATTTGATCCCGTACAACCT	PrimerBank
KCNK2	ATAGTGGCAGCAATAAATGCAGG	TTCTGTGCGTGGTGAGATGTT	PrimerBank
KIR4.1	CCAAGGTGTATTACAGTCAGACC	CTGCGACCATCTTTTGTCAGG	PrimerBank
MRGPRD	AGCCCCTGGTCAATACCACT	TCAACCCGTTCATCAGGAGAC	PrimerBank
NEFH	GCAGTCCGAGGAGTGGTTC	CGCATAGCGTCTGTGTTCA	PrimerBank
OCLDN	GACTTCAGGCAGCCTCGTTAC	GCCAGTTGTGTAGTCTGTCTCA	Lab design
P2X1R	GGCTGACTACGTCTTCCCAG	GCGCAGTAGCCTTGAGTCT	PrimerBank
P2X2R	AGCTGGGCTTTATCGTGGAGA	TTGGGGTTGCACTCCGATG	PrimerBank
P2X3R	AGTCGGTGGTTGTGAAGAGC	AGCCTTCTCGTGCAAGAAAAC	PrimerBank

GENE	FORWARD	REVERSE	SOURCE
P2X4R	CTACCAGGAAACTGACTCCGT	GGTATCACATAATCCGCCACAT	PrimerBank
P2X5R	CTGTCGCTGTTCGACTACAAG	CCCATACGACCAGGTACGC	PrimerBank
P2X6R	GAACCCCAGTTTTCCATCATCA	GGCGTCACAAGGAAGTTGGT	PrimerBank
P2X7R	TATGAGACGAACAAAGTCACTCG	GCAAAGCAAACGTAGGAAAAGAT	PrimerBank
P2Y1R	AGCTCCTATGTGCCCTACCA	GCGGCCATGTAGAGTAGAGG	PrimerBank
P2Y2R	CACTGCTCTACACTGTCCTGT	AGTGGTCCTGTTCCCAGTTTG	PrimerBank
P2Y6R	AATCTAGCCGCAACATATTCAGC	GTCTGACTCTTTGTGTAGGGGAT	PrimerBank
P2Y8R	GGGATGCCATGTGTAAACTGC	CGCTGATACAGATCGCATTCTT	PrimerBank
P2Y11R	CGTGGCCTACAGCTCAGTC	GTGACGTGGAATGGCAGGAA	PrimerBank
P2Y12R	GTGTCTACCGCGAGAACTTCA	CCAGAGCAAGGTTTAGGGTGTA	PrimerBank
P2Y14R	CGCACCGATCTCACCTACC	GATGGTGGCCGTGTAACAAG	PrimerBank
PAX6	AGTGCCCGTCCATCTTTGC	CGCTTGGTATGTTATCGTTGGT	PrimerBank
PER1	GCCAACCAGGAATACTACCAGC	GTGTGTACTCAGACGTGATGTG	PrimerBank
PER2	GACATGAGACCAACGAAAACTGC	AGGCTAAAGGTATCTGGACTCTG	PrimerBank
PIEZO1	GGACTCTCGCTGGTCTACCT	GGGCACAATATGCAGGCAGA	PrimerBank
PIEZO2	ATGGCCTCAGAAGTGGTGTG	ATGTCCTTGCATCGTCGTTTT	PrimerBank
PRPH	GGGTGGGTAATTCTTGGGGA	GGGCATATGATGGGCACAAG	Lab design
RAMP1	AAGCTGGGCTGCTTCTGG	ACACAATGCCCTCAGTGC	Literature[640]
RAMP2	TCCTATCGAAAAGGATTGGTGC	GTTGGCAAAGTGGATCTGGTG	PrimerBank
RAMP3	TCGTGGGCTGCTACTGG	CTCACAGCAGCGTGTCG	Literature[640]
RET	AAAGTGGCATTGGGCCTCTAC	GCAGGGCATGGACGTACAG	PrimerBank
RPLP0	AGCCCAGAACACTGGTCTC	ACTCAGGATTTCAATGGTGCC	PrimerBank
RUNX1	CTGCCCATCGCTTTCAAGGT	GCCGAGTAGTTTTCATCATTGCC	PrimerBank
SCN9A	AGAGGGGTACACCTGTGTGAA	CCCAGGAAAATCACTACGACAAA	PrimerBank
SCN10A	AGCAATGGCACCAGAGGGGACT	CCTCACTCAGGGGCTCAGTGCT	Lab Design
SCN11A	CCCTTCACTTCCGACTCTCTG	AGGCTGGGGTACTTCTCCTG	PrimerBank
SIX1	ACAAGAACGAGAGCGTACTCA	CTCCACGTAATGCGCCTTCA	PrimerBank
SOX10	CCTCACAGATCGCCTACACC	CATATAGGAGAAGGCCGAGTAGA	PrimerBank
SP	CGACCAGATCAAGGAGGAACTG	CAGCATCCCGTTTGCCCATT	Literature[641]
SST	CCCAGACTCCGTCAGTTTCT	CCATAGCCGGGTTTGAGTTA	Literature[642]
TAC1R	TCTTCTTCCTCCTGCCCTACATC	AGCACCGGAAGGCATGCTTGAA GCCCA	Literature[643]
TBP	CCACTCACAGACTCTCACAAC	CTGCGGTACAATCCCAGAACT	PrimerBank

GENE	FORWARD	REVERSE	SOURCE
TBXT	CCCGAAAGATGCAGTGACTT	CATCTCCACAGTTGGGTTCA	Literature[644]
TFAP2A	GACTCGGAGACCTCTCGATCC	GACGGCATTGCTGTTGGAC	PrimerBank
TRKA	CCCCATCCCTGACACTAACA	GCACAAGGAGCAGCGTAGAA	Lab design
TRKB	ACAGTCAGCTCAAGCCAGACAC	GTCCTGCTCAGGACAGAGGTTA	Literature[413]
TRKC	CTTTGCCCAGCCAAGTGTAGT	CGTGATGTTGATACTGGCGTT	PrimerBank
TRPA1	GGAAAGCCACCCCTCTCCACCT	GCTCCCTGGGTGGCAGCAAAAT	Lab design
TRPM8	CAGAAGGAATGACACTCTGGAC	TCACCAAGTCGCTTTCACTGT	PrimerBank
TRPV1	GACCACTCTTCTCCCACACG	AGTGTGCAACCAGCTAGACG	Lab design
YWHAZ	TGCTTGCATCCCACAGACTA	AGGCAGACAATGACAGACCA	Literature[535]
ZO-1	AGGCGGATGGTGCTACAAGTG	AGAGGACCGTGTAATGGCAGACT	Lab design

Table S3: Primer sequences used in the current project.

S2.3 Antibodies

TARGET	IMMUNOGEN if relevant	HOST	CONC.	USE	SUPPLIER	CATALOG
BMAL1	441-610aa canonnical	Ms	1:500	FC	Santa Cruz	sc-365645
BMAL1	1-303aa canonical	Rb	1:500	FC	Proteintech	14268-1-AP
BRN3a		Rb	1:500	IF	Millipore	Ab5945
CD31		Rb	1:500	IF	Proteintech	11265-1-AP
CD31-CL594		Rb	1:100	IF	Proteintech	CL594-98258 -100UG
CD31-CL647		Rb	1:100	IF	Proteintech	CL647-98258 -100UG
CD140b-CL647		Rb	1:100	IF	Proteintech	CL647-98207 -100UG
CGRP	Whole molecule and 23-37aa fragments	Gt	1:100	IF	Abcam	Ab36001
CGRP	*Properitary information*	Ms	1:100	IF	Abcam	Ab81887
cMET	965-1085aa (cytoplasmic)	Rb	1:200	IF	Proteintech	25869-1-AP
CRY1	236-586aa	Rb	1:500	FC & IF	Proteintech	13474-1-AP
CRY2		Rb	1:50	IF	Proteintech	13997-1-AP
CX43/GJA1		Rb	1:500	IF	Proteintech	26908-1-AP
GFAP		Ck	1:500	IF	Abcam	ab4674
GLAST/EAAT1		Rb	1:100	IF	Abcam	ab416
ISL1		Rb	1:500	IF	Abcam	ab20670
MAP2		Ms	1:500	IF	Proteintech	67015-1-Ig
MAP2		Ms	1:500	IF	Abcam	ab32454
NANOG-AF647		Rb	1:100	FC	Cell Signaling Technology	5448S
Na_V 1.7		Rb	1:150	IF	Alomone	ASC-008
NeuN-AF488		Rb	1:500	IF	Abcam	ab190195
OCT4		Rb	1:500	IF	Abcam	ab19857
P2X3R		Rb	1:500	IF	Proteintech	17843-1-AP
PAX3		Ms	1:500	IF	DSHB	PAX3
PAX6		Rb	1:500	IF	Biolegend	901301
PER2	740-839aa canonical	Ms	1:500	FC & IF	Proteintech	67513-1-IG
PRPH		Gt	1:500	IF	Santa Cruz	sc-7604
PRPH		Ms	1:500	IF	Santa Cruz	sc-377093
RET		Rb	1:500	IF	Alomone Lab	ANT-025
RUNX1		Gt	1:500	IF	Santa Cruz	sc-8563
SIX1		Rb	1:500	IF	Sigma	HPA001893
SOX10		Gt	1:500	IF	R&D	AF2864
SOX10		Rb	1:500	IF	Abcam	ab155279
SST	64-81aa	Rb	1:500	IF	Proteintech	17512-1-1AP
TAC1-CoraLite 488		Rb	1:500	IF	Proteintech	CL488-13839
TFAP2A		Ms	1:500	IF	DSHB	3B5
TRA-1-60-AF488		Ms	1:125	FC	Biolegend	300613
TRKA-APC		Ms	$10\mu L/10^6$ cells	FC	R&D	FAB1751RA-100
TRKA-PE		Ms	$10\mu L/10^6$ cells	FC	R&D	FAB1751RP-100
TRKB-AF488		Ms	$10\mu L/10^6$ cells	FC & IF	R&D	FAB3971G

TARGET	IMMUNOGEN if relevant	HOST	CONC.	USE	SUPPLIER	CATALOG
TRPA1		Rb	1:100	IF	Alomone Lab	ACC-037
TRPM8		Rb	1:100	IF	Novus	NB200-145
TRPV1	Intracellular	Rb	1:100	IF	Alomone Lab	ACC-030
TRPV1	Extracellular	Rb	1:100	IF	Alomone Lab	ACC-029
TUBB3		Ms	1:500	IF	Sigma	T8578
TUBB3		Rb	1:500	IF	Abcam	ab18207

Table S4: List of primary antibodies (with conjugation and differential epitopes if applicable) used in this project.
For circadian immunogen labelling, "canonical" indicates the canonical isoform that carries full circadian function homologue to murine counterparts: Isoform b for hBMAL1, Isoform 1 for hPER2. Abbreviations: AF, Alexa Fluor; CL, CoraLite; Ck, chicken; FC, flow cytometry including ImageStream; IF, immunoflureoscence; Gt, goat; Ms, mouse; Rb, rabbit.

HOST	TARGET	ISOTYPE	FLUOROPHORE	SUPPLIER	CATALOG
Dk	Gt	IgG(H+L)	Alexa Fluor 488	Invitrogen	A-11055
Dk	Gt	IgG(H+L)	Alexa Fluor 594	Invitrogen	A-11058
Dk	Gt	IgG(H+L)	Alexa Fluor 647	Invitrogen	A-21447
Dk	Ms	IgG(H+L)	Alexa Fluor 488	Invitrogen	A-21202
Dk	Ms	IgG(H+L)	Alexa Fluor 594	Invitrogen	A-21203
Dk	Ms	IgG(H+L)	Alexa Fluor 647	Invitrogen	A-31571
Dk	Rb	IgG(H+L)	Alexa Fluor 488	Abcam	ab150073
Dk	Rb	IgG(H+L)	Alexa Fluor 555	Abcam	ab150074
Dk	Rb	IgG(H+L)	Alexa Fluor 594	Abcam	ab150064
Dk	Rb	IgG(H+L)	Alexa Fluor 647	Abcam	ab150061
Gt	Ck	IgG(H+L)	Alexa Fluor 647	Invitrogen	A-21449
Gt	Ms	IgG(H+L)	Alexa Fluor 488	Invitrogen	A-11001
Gt	Ms	IgG(H+L)	Alexa Fluor 594	Invitrogen	A-11005
Gt	Rb	IgG(H+L)	Alexa Fluor 488	Invitrogen	A-11008
Gt	Rb	IgG(H+L)	Alexa Fluor 594	Invitrogen	A-11012
Rt	Ms	IgG1	FITC	Biolegend	406606
Rt	Ms	IgG1	Alexa Fluor 594	Biolegend	406634
Rt	Ms	IgG1	Alexa Fluor 647	Biolegend	406618
Rt	Ms	IgG2a	Alexa Fluor 647	Biolegend	407116

Table S5: List of secondary antibodies used in this project. Ck, chicken; Dk, donkey; Gt, goat; Ms, mouse; Rb, rabbit; Rt, rat.

S3 Supplementary information & figures

S3.1 HiPSC Quality check

Quality check and verification of migraine patient lines

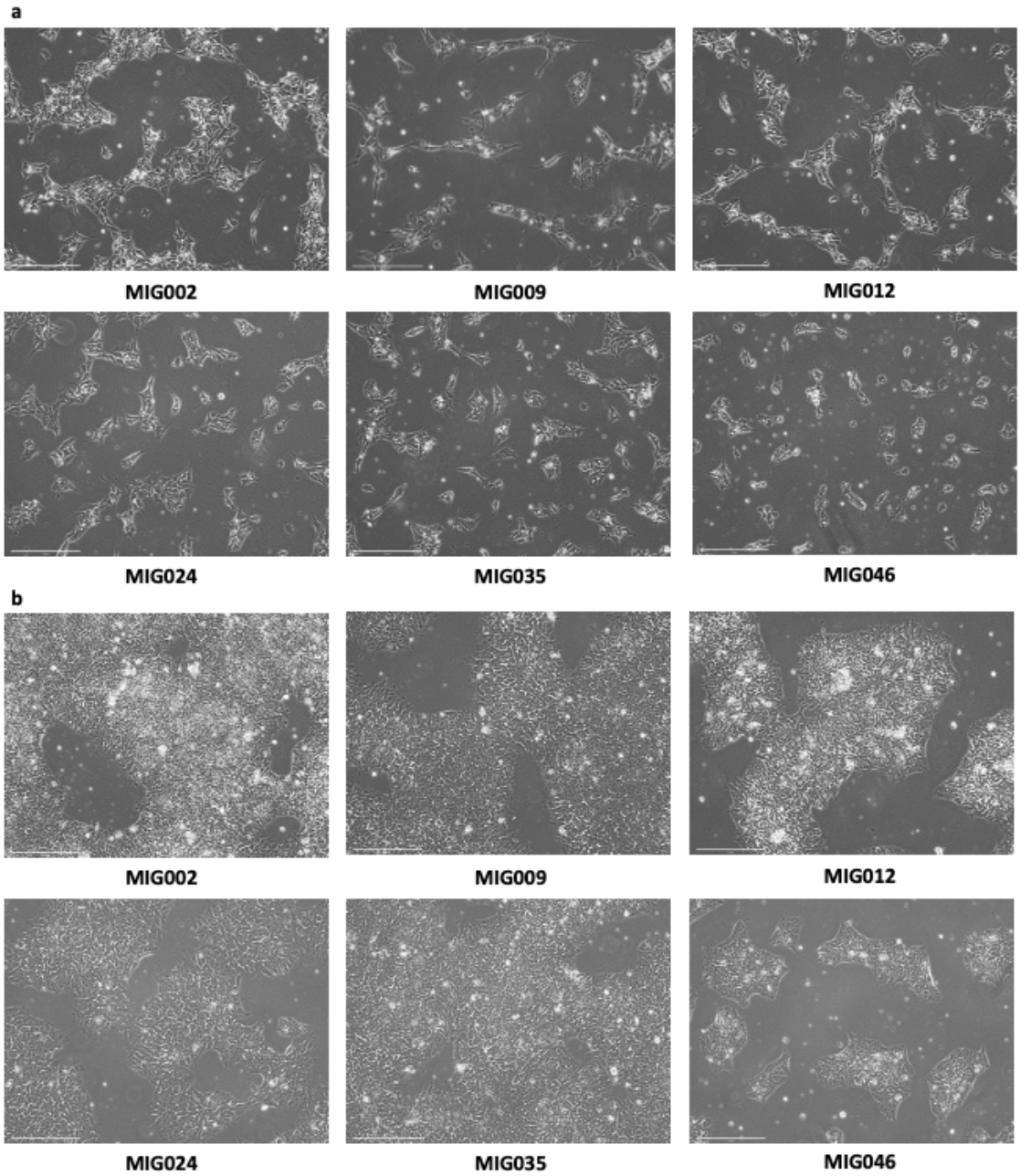


Figure S1: Representative brightfield morphology of iPSCs from patient-dervied lines, (a) 1- and (b) 3-days post-thawing. Scale bar 275µm.

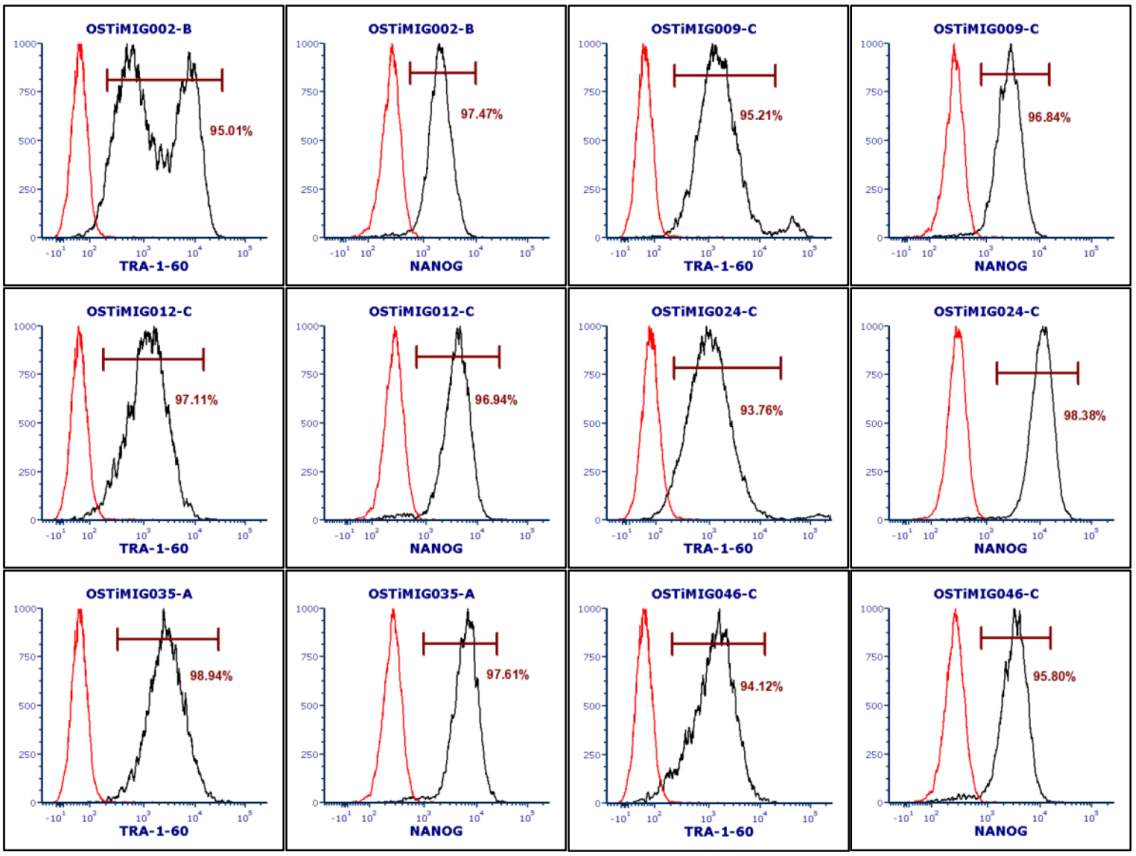


Figure S2: FC analysis of the expression level of pluripotency markers TRA-1-60 and NANOG in patient-derived iPSCs, extracted from Oxford StemTech reports.

Quality check and verification of the Na_V 1.7-Halo lines

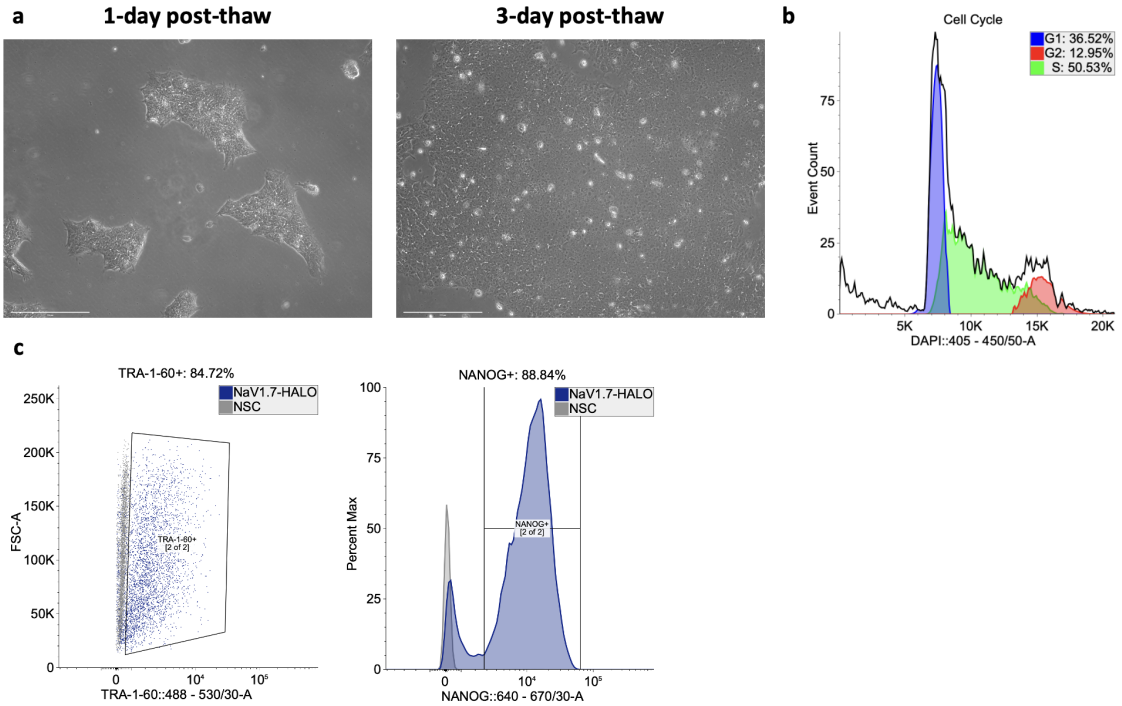


Figure S3: Quality control of Na_V1.7-HALO iPSC line.
(a) Representative brightfield morphology of Na_V1.7-HALO iPSCs 1- and 3-days post-thawing. Scale bar 275µm. (b-c) FC analysis of (b) cell cycle via DNA content quantification by DAPI staining, and (c) the expression level of pluripotency markers TRA-1-60 and NANOG in Na_V1.7-HALO iPSCs.

S3.2 Supplementary information on the optimisation of Trk-typing in DRG and TG iNociceptor progenitors

FC and FACS can reduce viabilities in live cells due to mechanical stress and lack of survival support during extended period of suspension[413]. We quantified the porportion of viabile cells during the sample preparation and measurement process of FC and FACS using low concentration of DAPI which does not penetration live cell membrane (Figure S4). Repetitive centrifugation and resuspension did not introduce a higher proportion of apoptotic cells (Figure S4b). In contrast, rapid cell death could be identified during the cytometry procedure particularly in DRG iNociceptors progenitors (Figure S4c). A 20% drop in viability is typical during sorting according to the manufacturer (Figure S4d).

Since RT-qPCR demonstrated adequate *TRKA* expression (Figure 16a) despite early presence of TRKB+ cells (Figure S21c), selection for TRKA+ Chambers' DRG progenitors was deemed unnecessary.

In iNociceptor progenitors from either protocol, DAPI-negative population P6 was distributed in a scattered fashion in cruelly estimated live cell population P1 and single cell population P2 (light blue population Figure S5a). TRKA+ (P3) and TRKB+ (P5) populations were selected against the background set in no-stain control (NSC, Figure S5b-c), as the efficiency of NSC compared to conjugated isotype control was comparable shown in pilot tests (Figure S5d).

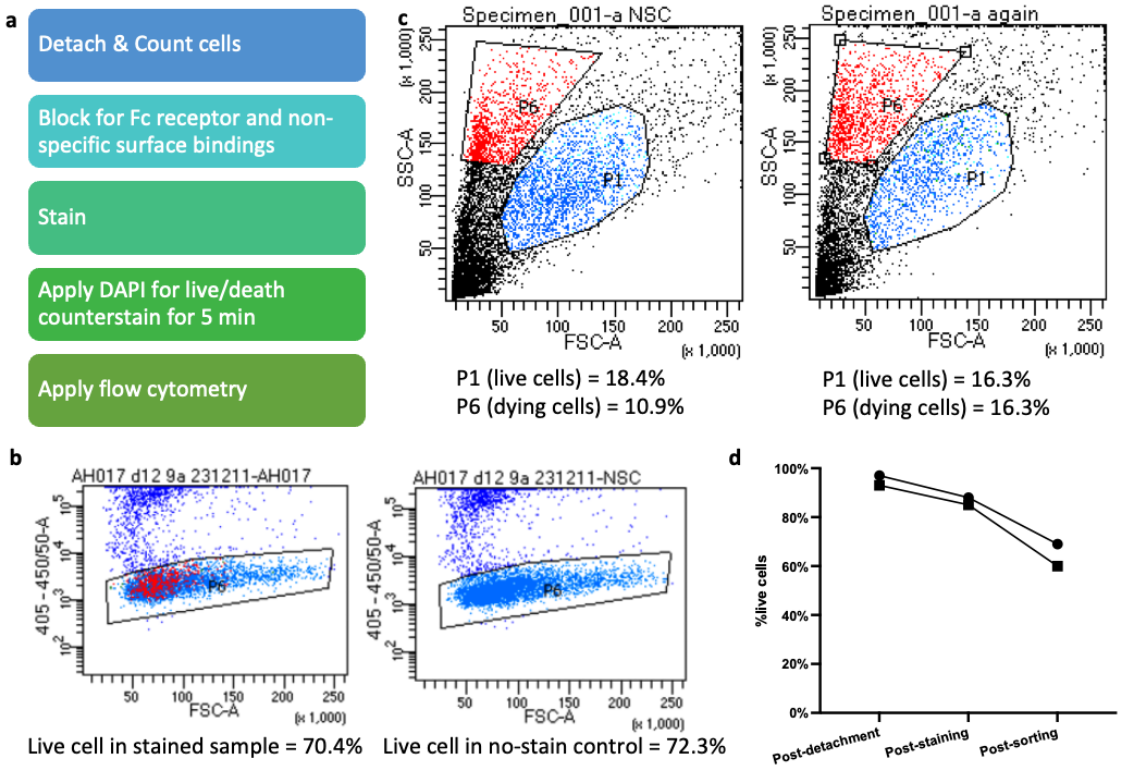


Figure S4: Trk-typing of DRG/TG iNociceptor by FC.
(a) Schematics of Try-typing workflow by FC. (b) Representative DAPI analysis in d12 AH017 TG iNociceptors. (c) A representative case of rapid loss of cell viability during FC in d12 SBAD03 DRG iNociceptors. P1 and P6 representing populations of live single cells and dying cells, respectively. Increased abundance of P6 observed from the same sample after 5 minutes of idle time. (d) Changes in viability in TG iNociceptors after detachment, staining, and sorting during Trk-typing.

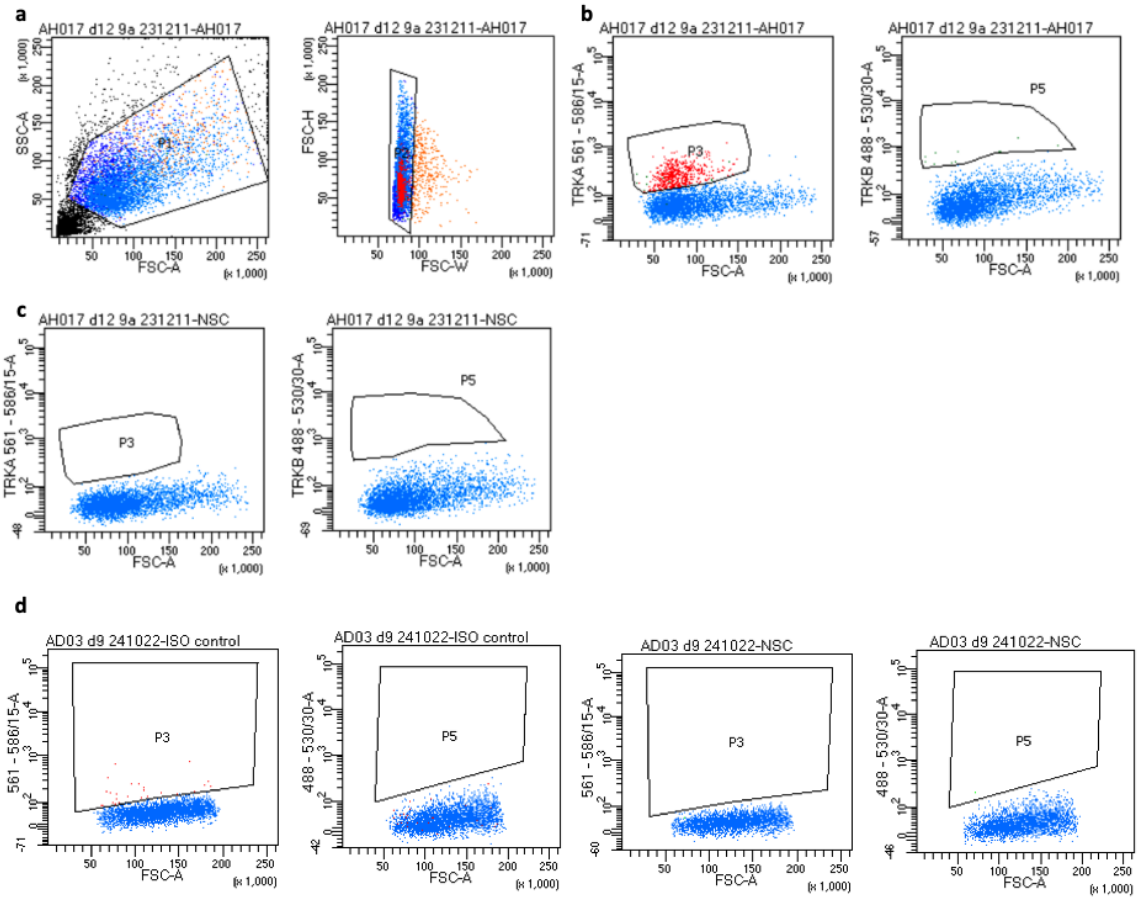


Figure S5: Gating strategy of Trk-typing of DRG and TG iNociceptor progenitors. (a) Conventional FSC and SSC analysis of a representative flow cytometry result using d12 AH017 TG iNociceptors. (b-c) Representative TRKA (left) and TRKB (right) fluorescence signals in (b) d12 AH017 TG iNociceptors in comparison to (c) no-stain control (NSC). (d) Demonstration for lack of non-specific antibody binding between negative controls by isotype labelling (left) and by NSCs (right) for both TRKA-PE and TRKB-488 signals using d9 SBAD03 TG iNociceptors.

S3.3 Supplementary information on the optimisation of iNociceptor MEA

S3.3.1 Sample data selection process for MEA analysis

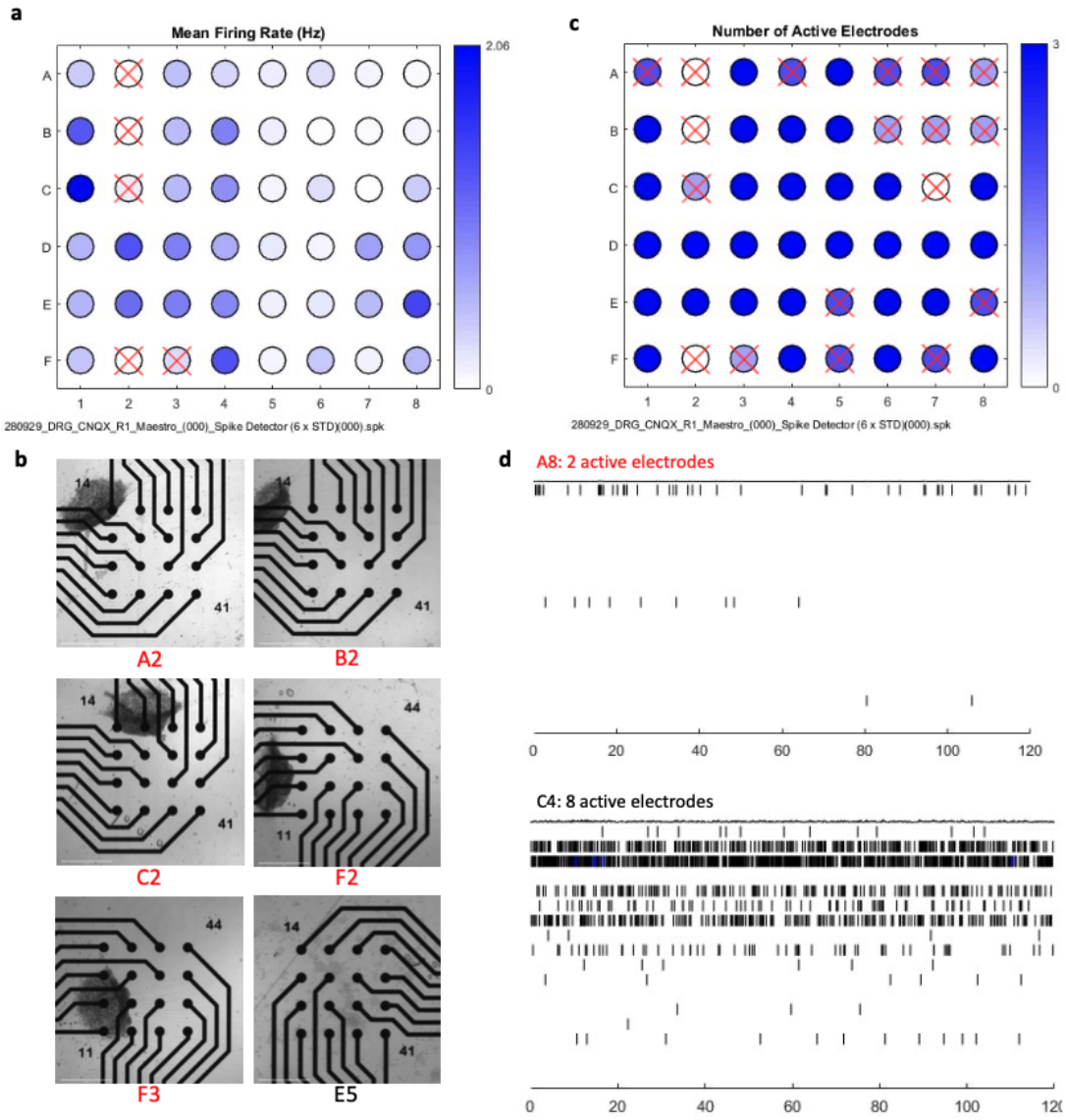


Figure S6: Demonstration of sample selection prior to MEA analysis.
(a-b) Elimination of inactive wells by morphology (red). (a) Plate map of mean firing rate (Hz) showing activity distribution across the sampler MEA plate. (b) Representative wells with major peel-offs or low density observed via brightfield microscopy in comparison to normal neuronal spread. (c-d) Elimination of inactive wells by the number of electrodes with threshold activities (red). (c) Plate map of the number of active electrodes per well. (d) Representative raster plots comparing wells with sufficient and insufficient number of active electrodes.

S3.3.2 Optimisation for the time frame of development and media composition

It is widely accepted that the firing activities of cells derived from the Chambers' protocol are detectable as early as at d20, peak around d35, and lower to a stable spontaneous activity by d60[442]. The exact range of stable baseline activities varies by seeding density and the size of neuronal clusters, if any. However, the majority of firing electrodes of Chambers' iNociceptor cultures gained more activities during development in our study. Given that Na_V 1.7 is only inserted into the membrane after 50 days of maturation[442], it is possible that the peak activity at d35 is led by other VGSCs typical of immature neurons such as Na_V 1.3[645]. Electrodes of which the activities were lost over time were mostly due to detachment and condensation of the clusters of neurons.

As of AD03 TG iNociceptors on MEA, spontaneous activities remained relatively low as seeding density was difficult to match on par with that of DRG due to the large proportion of non-neuronal cells before the application of AraC. A larger proportion of TG iNociceptors displayed firing acitivites only when a noxious heat was applied (e.g. Figure 21).

It is of note that the comparison for firing activities over time was only to demonstrate the temporal course of maturation and specific to individual plates. The proportion, well-to-well distribution, and firing rates of active electrodes would not be consistent as seeding density and long-term attachment naturally vary by batches.

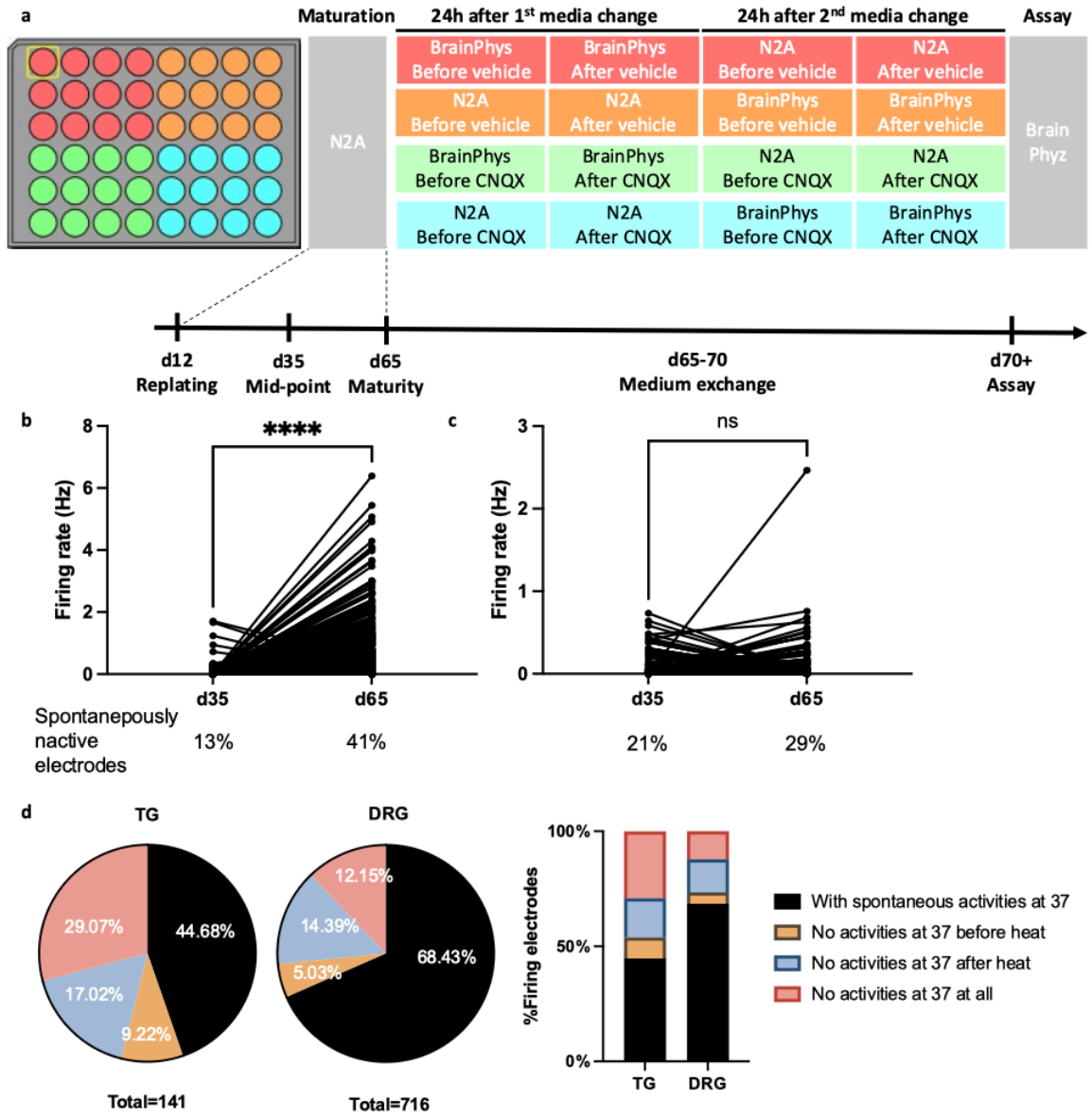


Figure S7: Timeline of MEA experiments in mature iNociceptors.
(a) Schematics of experimental time frame and sample allocations for media exchange. (b-c) Paired firing activities per electrode from one example plate in SBAD03 (b) Chambers' DRG iNociceptors and (c) TG iNociceptors at different time points of maturation. Statistical significance done by Wilcoxon test, with electrodes not spontaneously active (no firing at either time point) removed from paired analysis: p<0.0001 for DRG and p=0.2446 for TG. (d) Comparison of the proportion of spontaneous activity from the total pool of thermally active electrodes at physiological temperature in mature SBAD03 TG and DRG iNociceptors, relating to Figure 10 & 21.

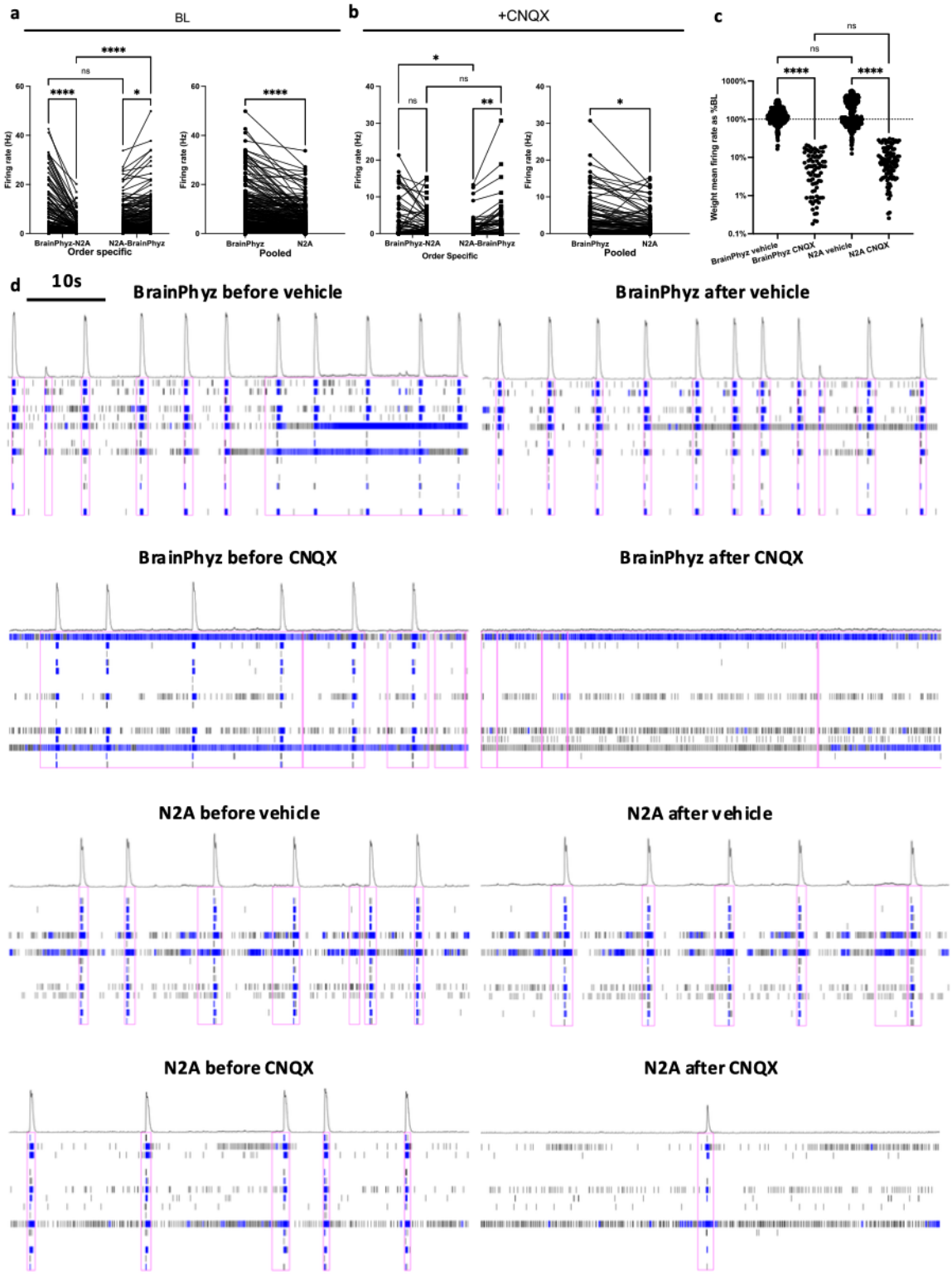


Figure S8: Optimisation of test conditions for SBAD03 DRG iNociceptor firing activities. (a-b) Mean firing rates (Hz) paired per electrode in different media compositions (a) at BL and (b) with CNQX. Order-specific: RM two-way ANOVA with uncorrected Fisher's LSD; pooled: Wilcoxon (non-parametric) test. (c) Change in mean firing rate (Hz) as %BL by CNQX, pooled by media. Outliers removed by the ROUT method, Q=1%. Statistical significance determined by Kruskal-Wallis (non-parametric) test with Dunn's multiple comparisons. (d) Representative raster plots demonstrating synchronised network firings efficiently removed by acute application of CNQX. Each pair of before & after treatment was from the same wells. A 60-second segment of network bursts and spike histogram was shown from the standard set of 2 x 120s measurements.

S3.3.3 Pilot tests of diurnal firing activities in mature SBAD03 Chambers' DRG iNociceptors

To estimate statistical power for diurnal firing activities, we performed a pilot test by dividing one MEA plate into four quadrants with 2 media each at 2 time points after FK synchronisation, without any CNQX.

Although wells were randomly allocated, the number of active electrodes were drastically different: N2A +4 (n=8), N2A +16 (n=19), BP +4 (n=18), BP +16 (n=48). The differential numbers of active electrodes could potentially reflect the compounded effect on excitabilities by media and circadian time: at the same time points, more electrodes in BP were active than those in N2A; regardless of media, more electrodes were active and of higher firing rate at +16 than +4.

The pilot data further imposed challenges on the method of statistical analysis (Figure S9). Due to variations in the number of electrodes and the nature of firing rates being asymmetrical, no normal distribution or even variance could be assumed. Therefore, we performed a normality test which all groups either failed or appeared ambiguous for (see Table S6). In this particular pilot run, data appeared to be lognormal which allowed the application of parametric two-way ANOVA. However, the lognormality was ambiguous in at least one group depending on the test chosen and could not be generalised for further experiments. We compared the significance of major effects by pooling data based on media types or time points (Figure S9d). The diurnal differences in firing activities (Mann-Whitney $U=223.5$, $p<0.0001$) were masked by media types (Mann-Whitney $U=836$, $p=0.6441$).

Overall, we decided to proceed with N2A to avoid potential effects of glucose deprivation for circadian experiments.

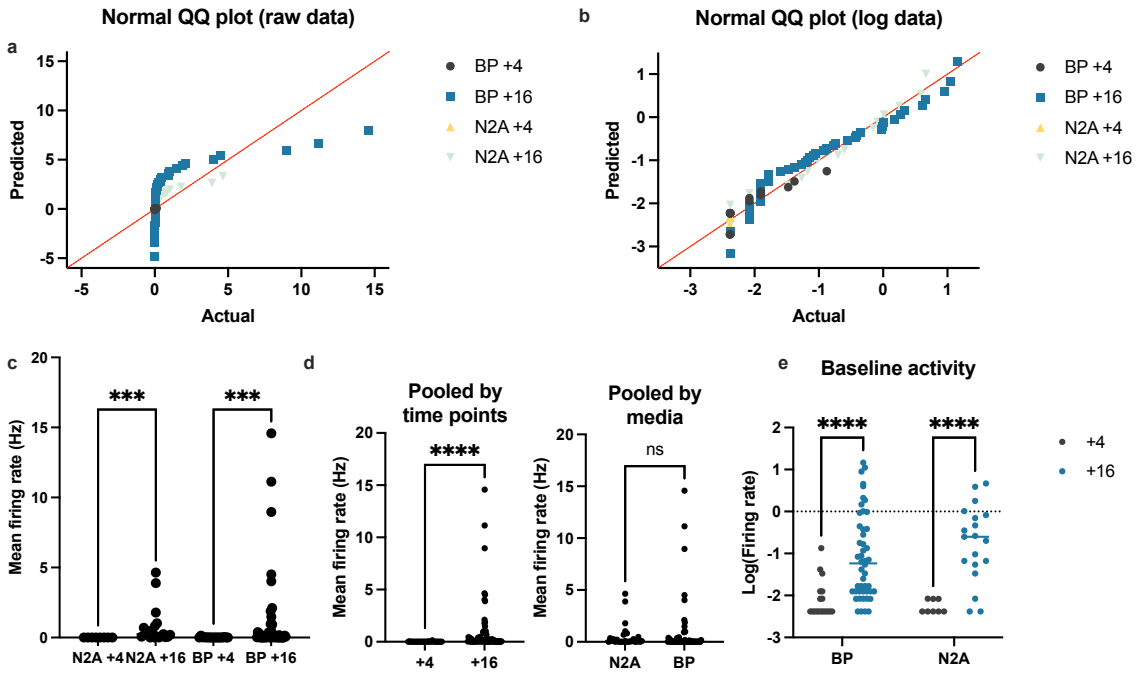


Figure S9: Optimisation of media composition and synchronisation method for diurnal spontaneous activities in SBAD03 DRG iNociceptors by MEA.
(a-b) Normality test on (a) raw and (b) log data of diurnal baseline network activities in SBAD03 iNociceptors in different media by MEA. Normality and lognormality tests done in GraphPad Prism, full comparison see Table S6. (c-e) Comparison of statistically significantly different diurnal firing rates by (c) non-parametric one-way ANOVA, (d) non-parametric t-test (for pooled data) or (e) two-way ANOVA. (c) Statistical significance determined by Kruskal-Wallis test with preselected pairs of conditions of either the same media or the same time. (d) Statistical significance determined by Mann-Whitney tests. (e) Statistical significance determined by two-way ANOVA on lognormal data: significant effect by time [F(1, 89)=33.44, p<0.0001], no statistically significant differences due to media [F(1,89)=0.1305, p=0.7187] or via interaction [F(1,89)=1.218, p=0.2727]. Only significant pairs of multiple comparisons shown.

		N2A +4	**N2A +16**	**BP +4**	**BP +16**
Raw data	Probability normal	2.696e-009%	0%	29.93%	2.938e-009%
	Probability lognormal	100%	100%	70.07%	100%
	Likelihood ratio	2.696e-011	5.836e-057	0.4271	2.938e-011
	Likely distribution	Lognormal	Lognormal	Lognormal	Lognormal
	KS distance	0.3438	0.1699	0.3903	0.1035
	P value	<0.0001	0.0014	0.0007	>0.1000
Log(data)	Probability lognormal	Impossible	Impossible	Impossible	Impossible
	Likely distribution	Normal	Normal	Normal	Normal

Table S6: Normality testing of diurnal firing rates of chemically synchronised SBAD03 DRG iNociceptors by MEA.
KS, Kolmogorov-Smirnov test.

S3.4 Supplementary information on the TG peptidergic iNociceptor protocol

S3.4.1 Supplementary information on improving the reproducibility & consistency of TP generation

We identified two major streams of TP induction methods available from the literature, either by sSMADi[435] or dSMADi[433] (Figure S10).

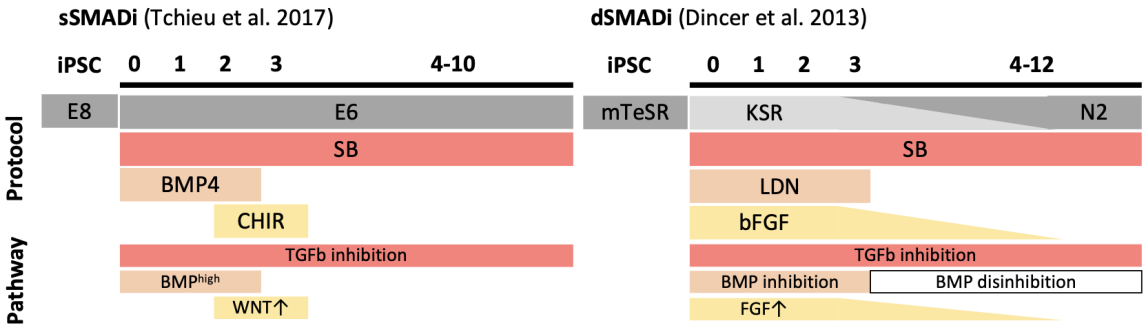


Figure S10: Available methods of deriving placodes from the literature.

Although previous work in our lab has confirmed that the dSMADi method could make CGRP-secreting neurons[2], several caveats were encountered such as the following:

1. cell line variations in successful seeding density, likely a combined consequence of innate WNT activities and differential stemness in each cell line;

2. batch inconsistencies likely due to thermal instability of bFGF during media percentage exchange;

3. high *PAX6* induction due to combined dSMADi and bFGF actions.

Therefore, we focused on improving the sSMADi method[435] which demonstrated more consistency in initial seeding densities and more ease of deriving placodes (Figure S11).

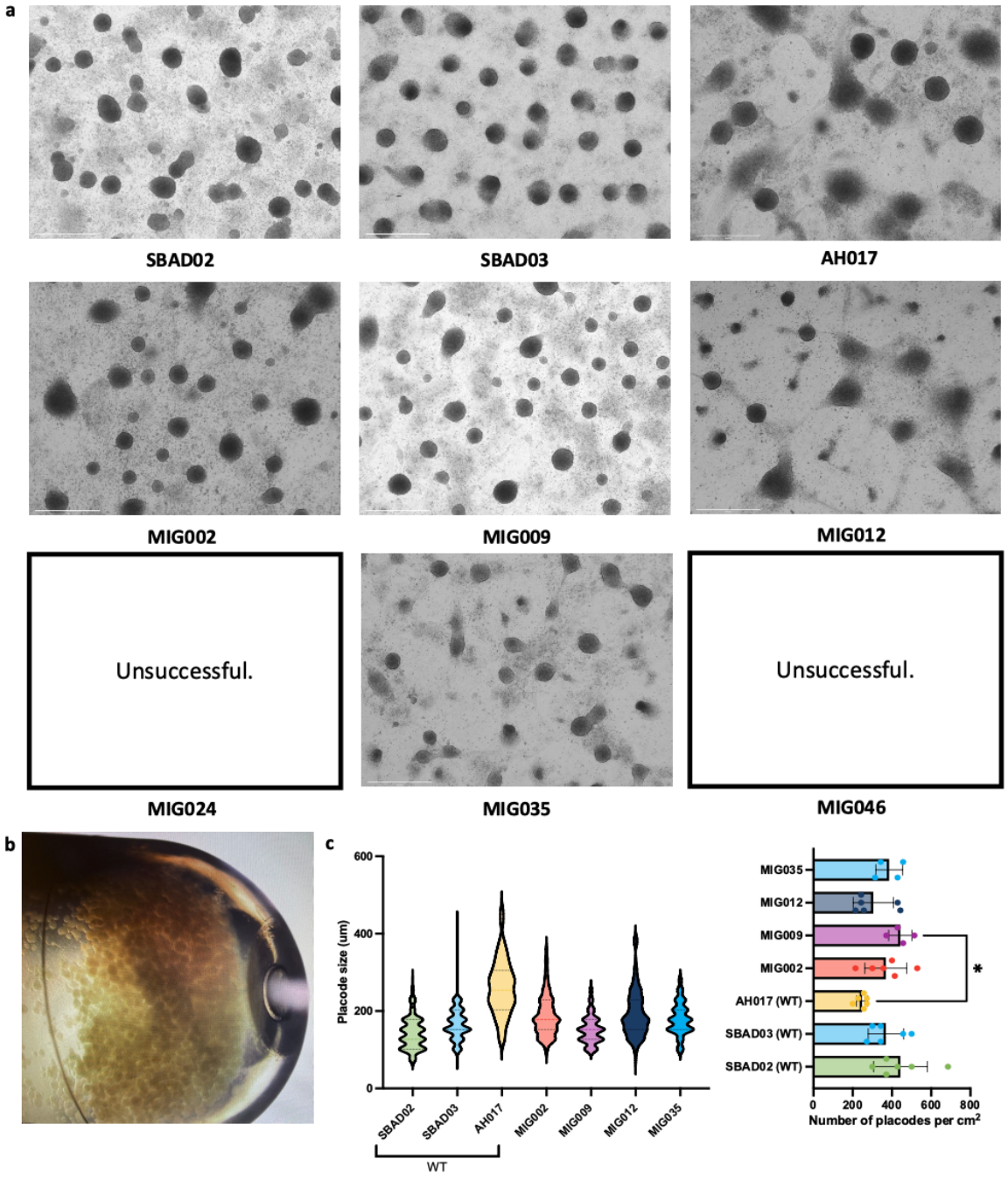
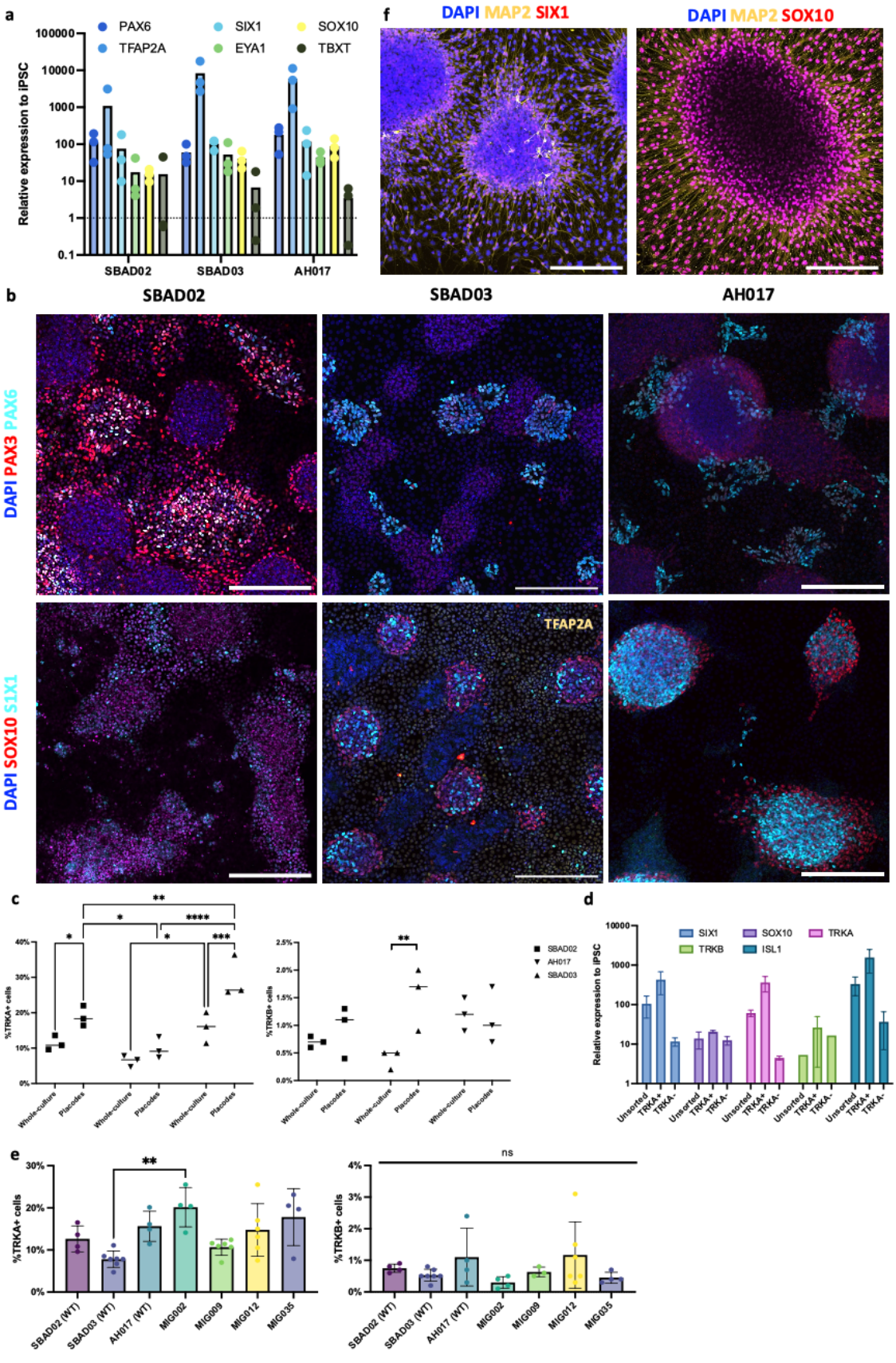


Figure S11: Morphological consistencies of growing sSMADi TPs on 2D platforms. (a) Representative brightfield images of reproducible placodal structures in healthy control and some but not all migraine patient-derived hiPSC lines. Scale bar 650µm. (b) Demonstration of gravity isolation of placodes. (c) Comparison of size and density of placodes across healthy and migraine patient cell lines. Statistical significance determined by Kruskal-Wallis (non-parametric) test with Dunn's multiple comparison tests: Left panel Kruskal-Wallis constant 256.7, p<0.0001, multiple comparisons not shown due to lack of space; Right panel Kruskal-Wallis constant 15.50, p=0.0167, significant multiple comparisons labelled. Error bar standard deviations.



(Caption see next page.)

Figure S12: Investigating on placodal contents dervied from the sSMADi TP protocol on 2D platforms (figure see previous page).
(a) Expression profiles of key transcription factors of d10 TG iNociceptor progenitors. n=3 independent differentiations in 3 WT lines. Statististical significance determined by two-way ANOVA: gene of interest 41.02% total variation, F(5,36)=7.132, p=0.0001; cell line 2.980% of total variation, F(2,36)=1.295, p=0.2863; interaction 14.59% of total variation, F(10, 36)=1.268, p=0.2843. (b) Representative IF image of regionally expressing ectodermal markers in three WT lines. Scale bar 250µm. (c-d) (c) TRK-typing of d10 2D WT TG iNociceptor progenitors from whole cultures detached or placodes manually isolated, verified by (d) RT-qPCR. (c) Statistical significance determined by two-way ANOVA, with Tukey's multiple comparisons: %TRKA sifnigicant effects by isolation methods [26.05% of total variation, p=0.0004, F(1,12)=23.67] and cell lines [54.06% of total variation, p<0.0001, F(2,12)=24.58]. (d) Error bars standard deviation. (e) TRK-typing of d10 2D TG iNociceptor progenitors from WT and successful migraine patient lines. Statistical differences determined by Kruskal-Wallis (non-parametric) test with Dunn's multiple comparison tests: Left panel Kruskal-Wallis constant 18.17, p=0.0058, significant multiple comparisons labelled; Right panel Kruskal-Wallis constant 11.12, p=0.0846. (f) Robust neuralisation demonstrated by MAP2+ outgrowth in manually isolated AH017 placodes after 24h incubation with BDNF of both PNS ectodermal lineages. Scale bar 250µm. For all panels, error bar standard deviations.

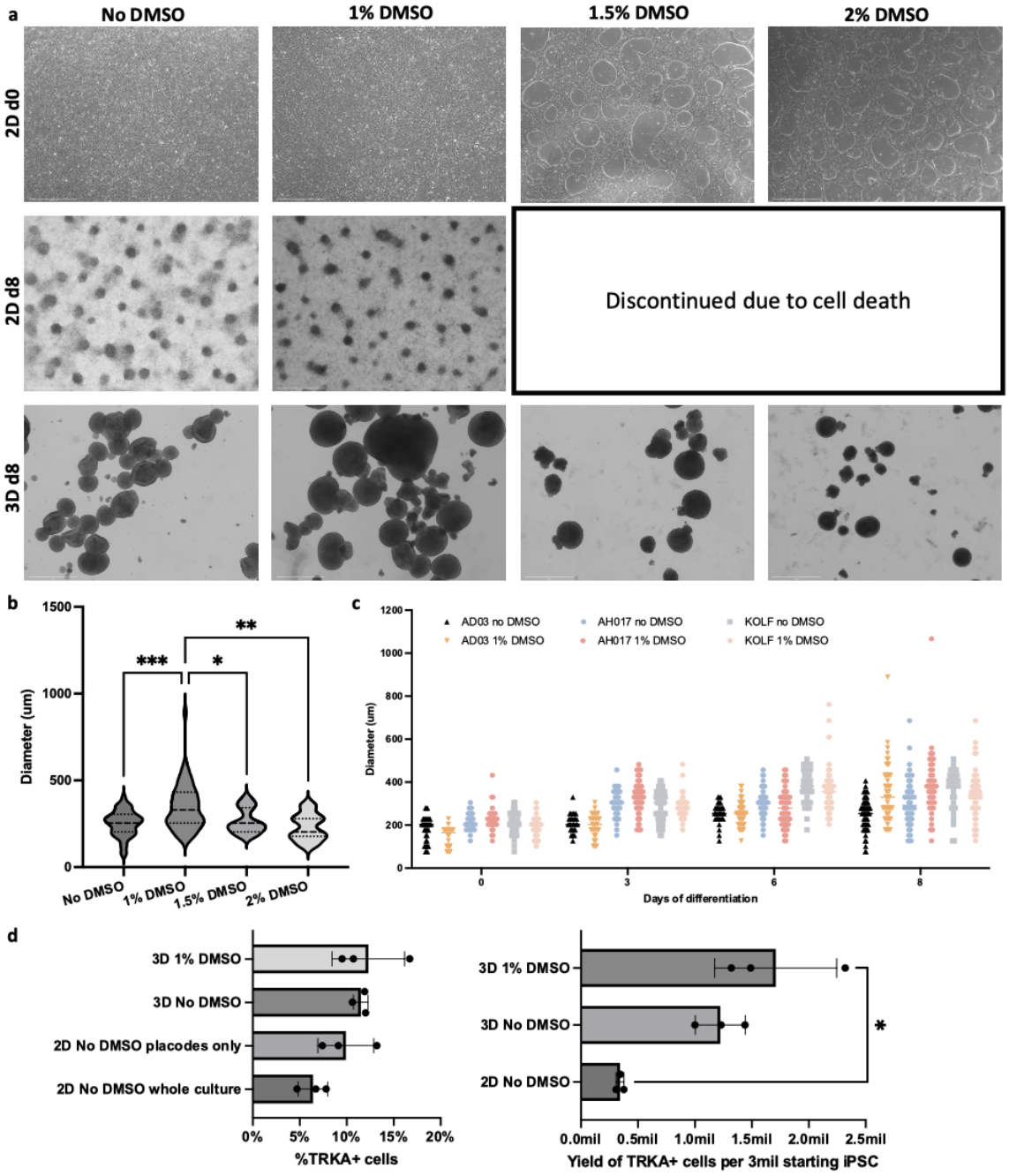


Figure S13: Titration of DMSO pre-treatment for TP induction.
(a) Representative brightfield images of cytotoxicity of high doses of DMSO pre-treatment with SBAD03 WT iPSCs. Scale bar 650µm. (b) Differential sizes of d8 SBAD03 3D TPs with titrated DMSO pre-treatment. Statistical difference determined by Kruskal-Wallis (non-parametric) test with Dunn's multiple comparison tests: Kruskal-Wallis constant 22.13, p<0.0001, significant multiple comparisons labelled. (c) Growth curve of 3D TPs with or without 1% DMSO pre-treatment from 3 WT iPSC lines. (d) Comparison of differentiation efficiencies by trk-typing FC and yield (%TRKA+ multiplied by total cells harvested). Statistical significance determined by Kruskal-Wallis tests: p=0.0918 for %TRKA and p=0.107 for yield; significant multiple comparisons via Dunn's method labelled.

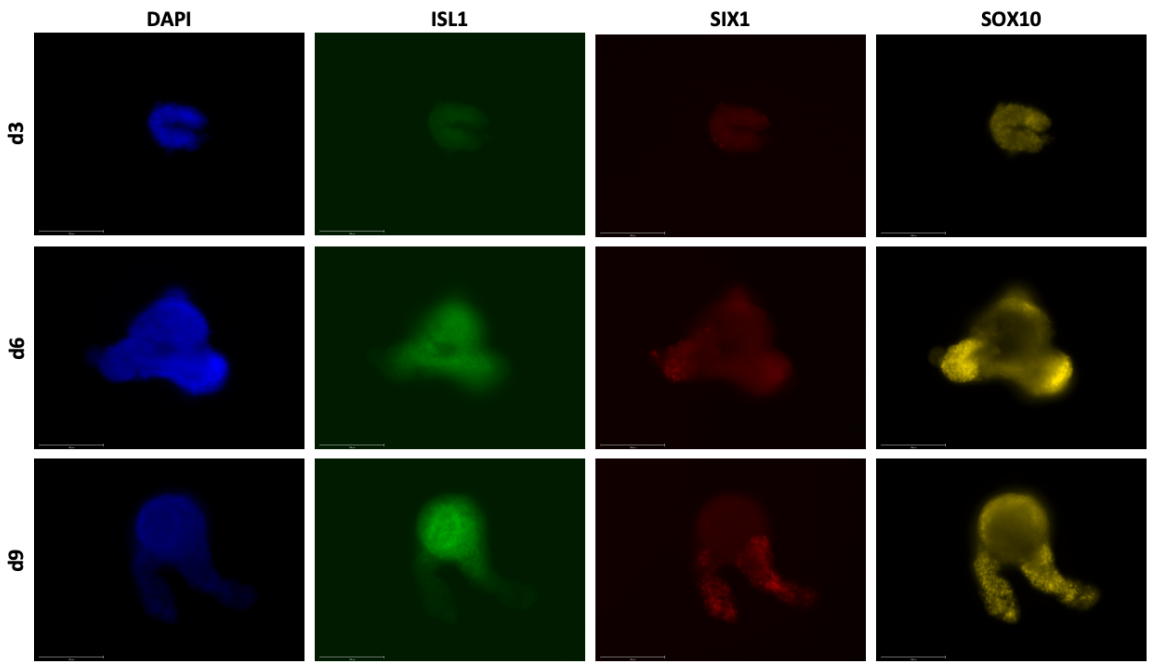


Figure S14: Temporal profiling of ectodermal transcription factor topology in developing SBAD03 TP organoids by IF, scale bar 150µm.

To apply quantitative parameters to ectodermal transcription factors, we attempted to quantify the distribution and co-localisation patterns of SIX1 and SOX10 immunolabelling (Figure S15a). As both proteins of interest are transcription factors, proper signal should be nucleus-shaped and overlap with DAPI. Artefacts and noises could thus be easily identified and manually corrected if necessary (Figure S15b).

Manders co-localisation analysis identified some degree of overlap across all samples analysed. However, most double positive region appeared to be a result of noise or high nuclear density (Figure S15c). Although signal-to-noise identifying methods such as Pixel classifier[646] are available, exquisite training and imaging de-noising is beyond the capacity of this project.

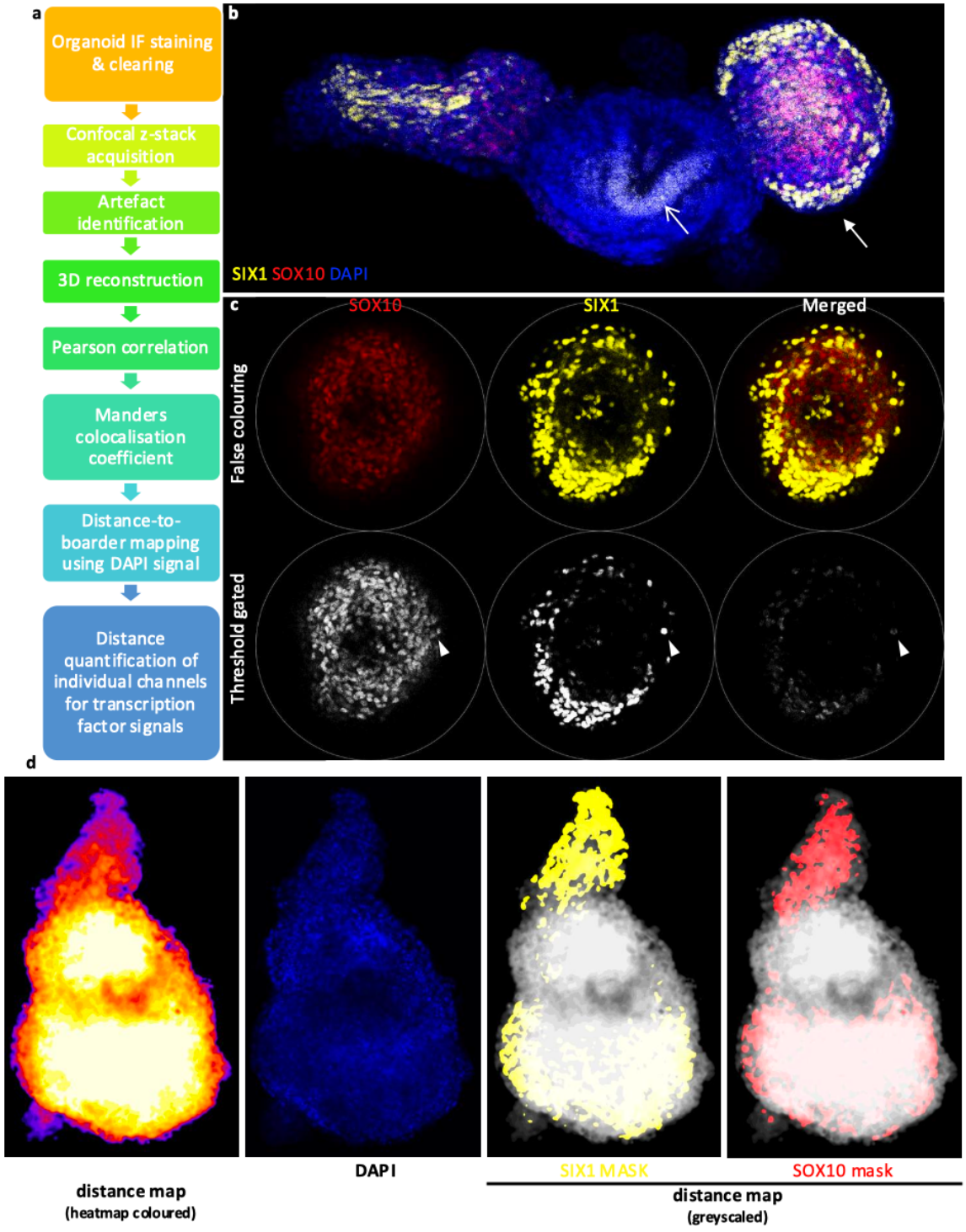


Figure S15: Workflow of the quantification of expression and distribution of immunolabelled transcription factors in 3D TPs.
(a) Schematics of workflow for confocal image processing. (b) Representative 3D reconstructed organoid showing real signal (thick arrow) and artefact due to antibody trapped in cavity (thin arrow). (c) Representative slice from stacked Manders analysis report, with false positive ovelap labelled (triangle arrow). (d) Representative slice from stacked distance-to-boarder map based on DAPI signal, with threshold masks of individual channels overlaid.

S3.4.2 Supplementary information on TG iNociceptor maturation

Starting with the 2D cultures, we optimised the method to best enrich and mature nociceptors that produce and secrete neuropeptides. Non-neuronal cells from the placodal culture could be grossly categorised as fast dividing AraC-sensitive (Figure S16a, thick arrow) and -resistant (Figure S16a, thin arrow). Purification thereby could thus be done by physical isolation of placodes (Figure S11b) or chemical removal via AraC when replated.

Preliminary work in our lab has identified the presence of glial cells spontaneously differentiated with neuron progenitors and its impact on cell fate specification[2]. Astrocytes were identified as an effective substitute. Therefore, we compared the phenotypical outcomes of TG iNociceptors growing in presence of all or a selective subset of the non-neuronal population, or when supplemented with astrocyte co-cultures.

As it is hard to estimate cell counts when preserving placode integrity was preferred, we matched seeding density in wells with placodes by approximating with dilution factors: for example, if one well from a 6-well plate yielded 4.5 mil cells in total (typical for SBAD03 and AH017), of which 1.4 mil (400k/cm^2 in 12-well plates, about a third from the original harvest) was plated for ELISA, then placodes manually isolated from a well in a 6-well plate were split 1:3; total cell counts varied more in SBAD02 per differentiation, for which we modified the dilution factor specific to batches. Despite the ease of physical isolation, washes did not always fully exhaust patches of basal layers as excessive pipetting would destroy placode integrity and reduce neuronal viability. Non-neuronal areas could still appear. The presence of non-neuronal cells from all no-AraC conditions generally improved neuron attachment and health when visually inspected for neurite morphology, which can be partially compensated by supplementing NGF (Figure S16a).

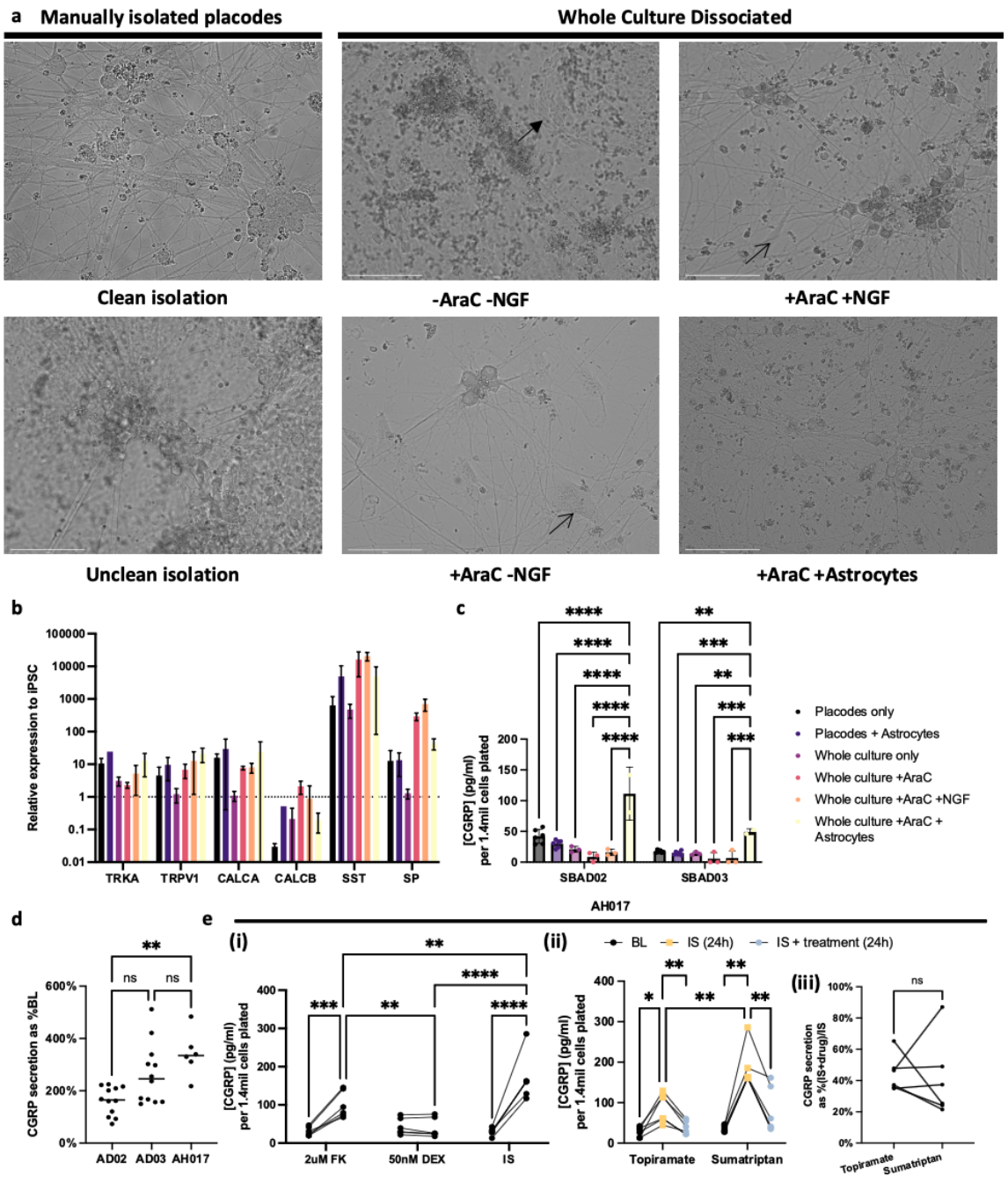
All conditions gave rise to CGRP-expressing mature peptidergic iNociceptors by d70 (Figure S16b-c). Although βCGRP could be produced in murine TGs[117], minimal *CALCB* transcripts were detected. There was also prominent upregulation of *SST* and *SP* (splice variance specific). Non-neuronal cells did not directly contribute to the expression or secretion of neuropeptides, rather diluting neuronal transcripts in relative quantification. Basal secretion of αCGRP was detected in all conditions. Astrocytes alone did not contribute

to neuropeptide secretion (Figure S18), but boosted neuronal CGRP release in the co-culture.

Beyond baseline secretion, we also tested chemically triggered release of CGRP. Given insufficient information of donor chronotype and pain pathology, we first confirmed differential responsiveness of 3 WT lines to cAMP agonist forskolin (FK, Figure S16d).

We proceeded with the high achiever line AH017 as a proof-of-concept pilot run for other CGRP secretion experiments [Figure S16e(i)]. Pro-inflammatory signals [administrated as an artificial Inflammatory Soup (IS), recipe see Section S1) and FK both stimulated CGRP secretion. In contrary, anti-inflammatory glucocorticoid dexamethasone (Dex) did not, as expected[647]. It is of note that, despite being common circadian synchronisers (see Chapter 3), both FK and Dex were administrated at a lower concentration, as ELISA sample collection required extended incubation period compared to a high dose synchronisation. AH017 also responded to common migraine treatment topiramate and sumatriptan, with reduced CGRP release despite IS stimulation [Figure S16e(ii)-(iii)].

Physical interactions via tight junctions were identified between mature iNociceptors and astrocytes, suggesting active bidirectional neuroglial communications (Figure S16f).



(Caption see next page.)

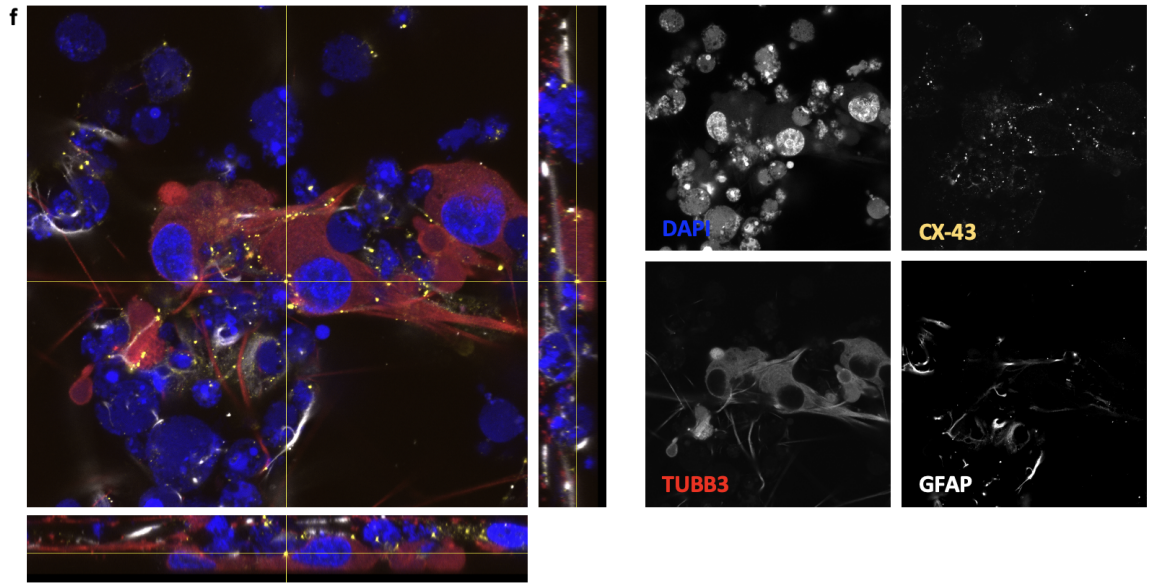


Figure S16: Maturation outcomes of TG iNociceptors derived from 2D platforms modulated by the presence of glia.
(a) Representative brightfield images of d55 TG iNociceptor cultures via different maturation methods. Thick arrow indicates fast dividing non-neuronal contaminations sensitive to AraC. Thin arrows indicate remaining flat glia-like cells resistant to AraC. Scale bar 150µm. (b) Expression of conventional peptidergic markers under different maturation conditions with RT-qPCR, n=3 independent differentiations from SBAD02 TG iNociceptors. Primers human specific. (c) Quantification of baseline CGRP secretion by culture supernatant ELISA, n=6 for placodal conditions, 3 for dissociated whole cultures, from 3 independent differentiations for each line. Seeding density 400k/cm^2 for single-celled whole culture and batch- and line-corresponding dilution of placodes (typically 1:3) per well. Outliers identified and removed via the ROUT method, Q=1%. Statistical significance determined by two-way ANOVA with Sidak's multiple comparisons: Significant effect of cell line [15.28% of total variation, p<0.0001, F(1,34)=38.72], maturation method [61.33% of total variation, p<0.0001, F(5,34)=31.08], and interaction [10.54% of total variation, p=0.0010, F(5,34)=5.341]. (d) Demonstration of cell line variations of stimulus responsiveness by normalised CGRP secretion to 24 hours of 2uM FK. Statistical significance determined by Kruskal-Wallis test with Dunn's multiple comparison tests: Kruskal-Wallis statistic 11.62, p=0.0030. (e) Pilot tests of triggered CGRP release. (i) Responsiveness to circadian synchronisers and inflammatory signals, statistical significance determined by RM two-way ANOVA with Tukey's multiple comparison test. (ii) Responsiveness to common migraine treatment as paired raw values of secretion, statistical significance determined by RM two-way ANOVA with Geisser-Greenhouse correction and Tukey's multiple comparison test. (iii) Responsiveness to common migraine treatment as normalised reduction rate of CGRP release under IS stimulation with/without treatment, statistical significance determined by Wicoxon test (p=0.8438). Error bar standard deviations. (f) Orthogonal analysis of physical interactions between TG iNociceptors and astrocytes via neuroglial tight junctions, n=3 independent differentiations in SBAD02 iNociceptors.

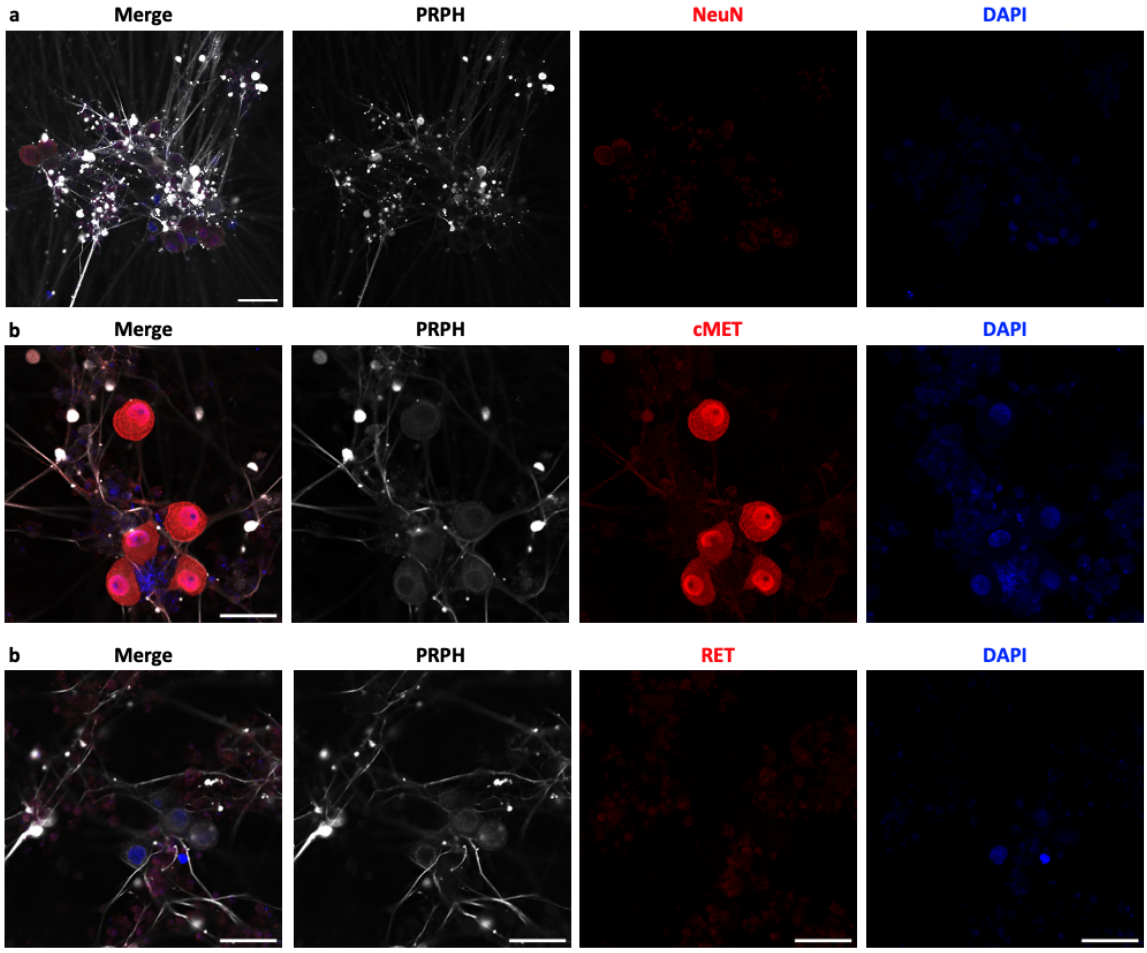


Figure S17: Expression of cMET and RET in mature peptidergic TG iNociceptors, as supplementary information for Figure16b-d.
(a) Uniform PRPH distribution in mature peptidergic TG iNociceptors. (b-c) Subcellular localisation of (b) cMET and (c) lack of RET in peptidergic TG iNociceptors. Arrow indicating membrane localisation besides nuclear translocation of intracellular cMET. For (a-c), Scale bar 50µm, n=3 independent differentiations in 3 WT lines.

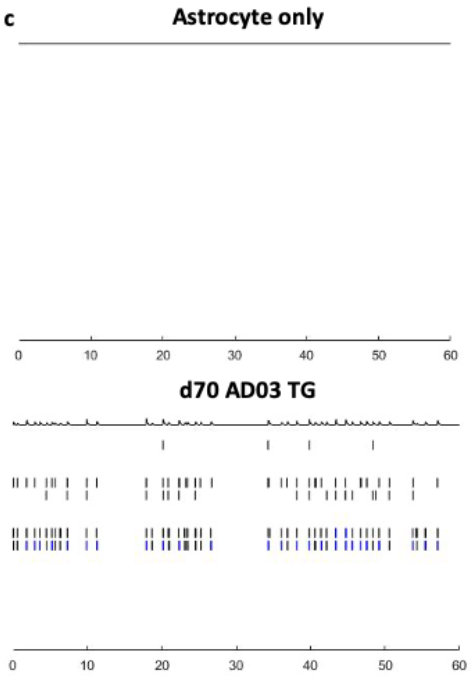
S3.4.3 Astrocytes

To ensure that the astrocytes in co-cultures direct neuron cell fate specification without its own CGRP secretion or firing activities, we repeated ELISA and baseline MEA experiments on astrocytes alone in consistent test conditions (Figure S18).

We also tested astroglial responsiveness to CGRP present in the media by intracellular cAMP ELISA. A positive control of 5μM/ml FK was beyond the detection range of the kit, presented as the maximum value of sensitivity only for reference.

a

Sample	Absorbance After blank
15.6 pg/ml positive control (below sensitivity)	-0.004
31.3 pg/ml positive control (in range of sensitivity)	0.019
Astrocyte 1	0.02
Astrocyte 2	-0.005
Astrocyte 3	-0.004
Astrocyte 4	-0.005
Astrocyte 5	0.004
Astrocyte 6	0.002



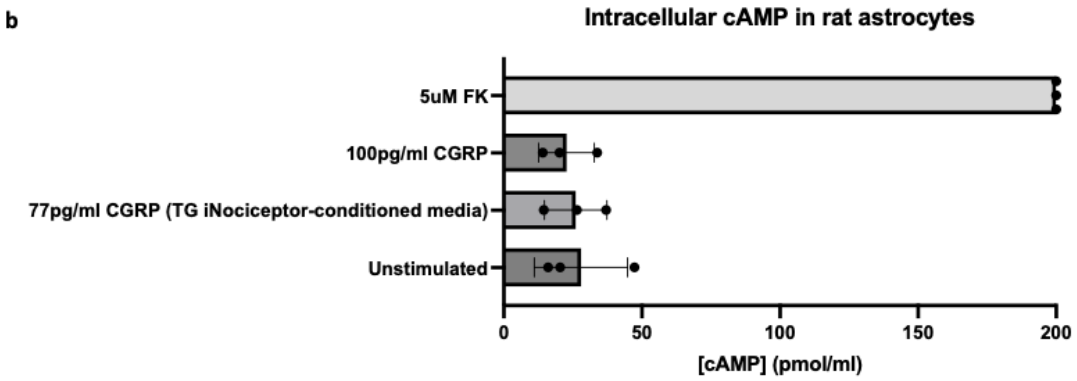


Figure S18: Neuropeptide and cAMP ELISA in rat astrocytes.
(a-b) Quantification of (a) CGRP, (b) intracellular cAMP in rat astrocytes. (c) Lack of firing activities of astrocytes on MEA platforms demonstrated as representative rastor plots, compared to d70 AD03 TG iNociceptors in astroglial co-cultures. Seeding density and test conditions consistent with astrocytes as co-cultures contributing to Figure S16. Error bar standard deviations.

S3.4.4 Optimisation of normalisation for secretive and intracellular CGRP quantification

Consideration of normalising secretory neuropeptides by ELISA included the following aspects:

SAMPLING TIME	REFERENCES	REASONS	CONCERNS
Pre-ELISA	Seeding density	Easy and consistent among cell lines for detetable level of secretory CGRP.	Differential TRKA+ progenitor purity from TP induction of each line.
	%TRKA+ cells by conventional FC	Theoretically the only cell type that contributes to CGRP secretion; ease and speed of application allowing batch-specific readouts.	Well-to-well and day-to-day variations, partially a consequence of uneven seeding and unpredictable variations of survival rate; over-estimating with no prediction of long-term cell behaviours.
Post-ELISA	%CGRP+ cells by conventional IF	Single cell resolution.	Less quantitative; a snapshot which cannot account for recently depleted cellular stocks, reflected by internal variations of each well; separate wells for ELISA and IF.
	%CGRP+ cells by ImageStream	Single cell resolution; same wells repurposed and matched.	Technical challenges making estimation by average readouts the only economic option; cell loss and cell death during preparation underestimating counts; a snapshot which cannot account for recently depleted cellular stocks, reflected by internal variations of each well; equipment not as common compared to normal flow cytometer.

Table S7: Choice of references for normalising secretive CGRP.

A trial run of neuropeptide vesicle quantification via ImageStream exposed tremendous difficulties in the preparation of single cell suspension. With avilable cells harvested and stained, we compared different imaging methods. The normal depth field captures a slice of intracellular environment in parallel to the direction of flow, which is suitable for dispersed signals such as full-length SST. In comparison, the Extended Depth of Field (EDF) function detects a thicker section of the cell, better capturing a small spherical structure. Although it is possible to distinguish different cytoplasmic environments (Figure S19) for similarity bright detail score (SBDS[648]) analysis for signal co-localisation, the potentially uneven loss

of neurons during detachment deemed the benefit of absolute quantification less virtuous. Therefore, we normalised CGRP secretion by %TRKA+ cells seeded before maturation (Figure 24). We included baseline results from repeated measurements of the same wells and all batches tested to account for internal variations for each line (Figure 24). Entries with no detectable CGRP were also included.

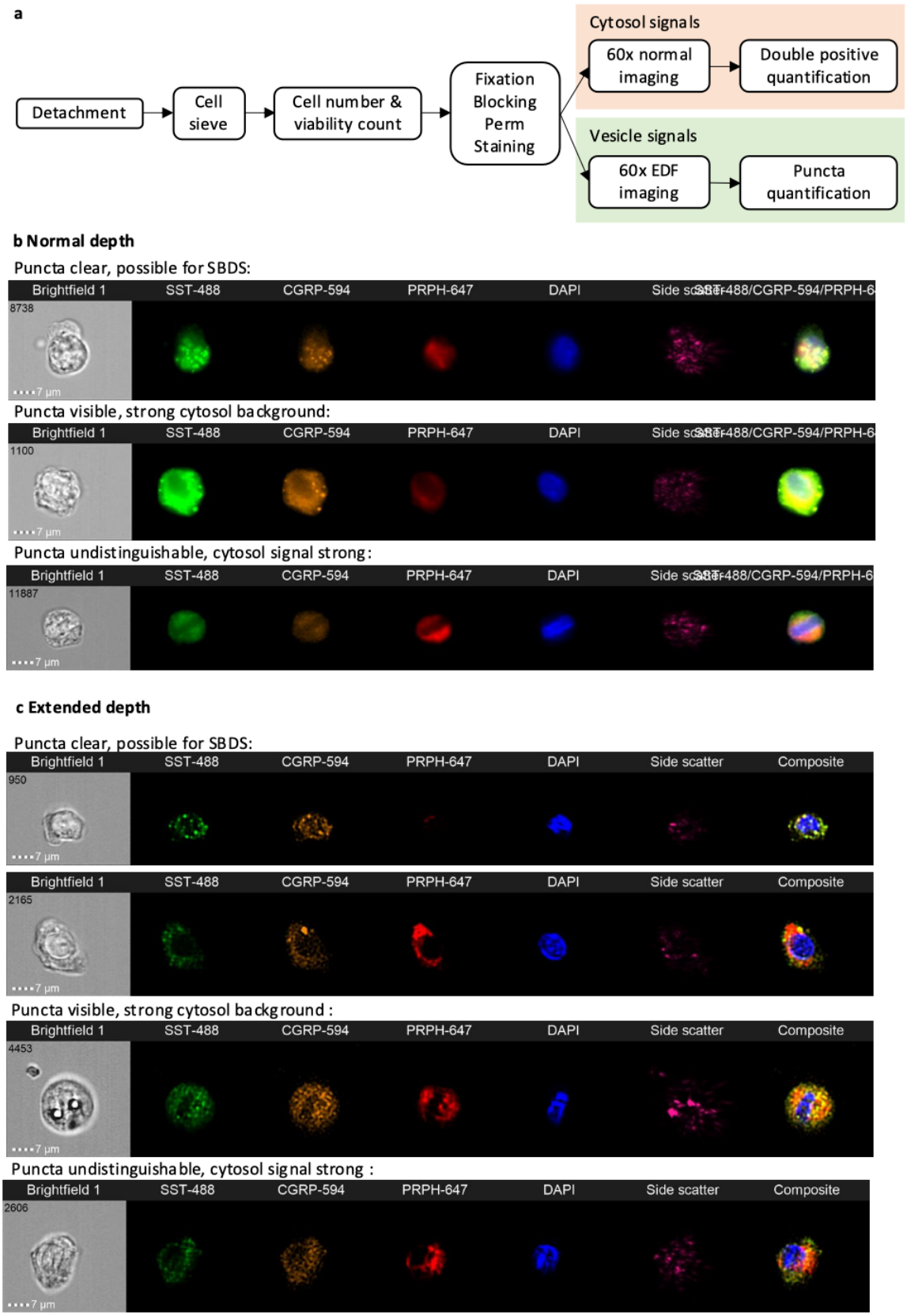


Figure S19: Optimisation of imaging conditions when applying neuropeptide ImageStream in mature TG iNociceptor-astrocyte co-cultures.
(a) Schematics of workflow using ImageStream to quantify neuropeptide-containing LDCVs. (b-c) Comparison of impact between (b) normal and (c) extended field depth on clarity of cytosol (SST) and vesicle (CGRP) signals. SBDS, similarity bright detail score.

S3.5 Supplementary information on the impact of DAPT in the Chambers' cocktail on the induction efficiency of neuronal progenitors in the Chambers' protocol

To improve purity, sensory neuron cell fate *in vitro* is often modulated by the addition of NOTCH inhibitor DAPT[622], as of the Chambers' cocktail. As NOTCH pathway initiates neuron/glia cell fate diversification, we compared the developmental outcome of DRG iNociceptors with and without DAPT.

The impact of DAPT was apparent as early as day 8 of differentiation via Chambers' protocol (Figure S20). Empty areas could be observed due to the elimination of pre-mitotic progenitors by DAPT in the original protocol. Unlike TG cultures on 2D platforms, elongated cellular processes characteristic of immature neurons were apparent in both prior to replating.

We thereby quantified the purity and yield of TRKA+ and TRKB+ sensory neuron progenitors from the original and modified Chambers' protocol by FC compared to 2D TG iNociceptors (Figure S21). The yield of sensory neuron progenitors was based on total cell counts per unit of differentiation (one well in a 6-well plate, surface area 9.6cm^2). Both purity and yield were considered as the original Chambers' and the 2D TG protocols employed very different starting densities (80k/cm^2 for 50% confluency in 24 hours and 250k/cm^{2}2 for 100% confluency in 24 hours, respectively) and ended with drastically different total numbers of cells.

As expected, the original Chambers' protocol contained the highest proportion of sensory neurons, with %TRKA close to reported 60%[408]. Despite starting with the same seeding density, the original Chambers' protocol generated three times the number of TRKA+ cells in the final culture compared to the no-DAPT cultures (Figure S21). Without accelrated neurogenesis with DAPT, the altered DRG protocol yielded comparable amount of TRKA+ neurons to that of the 2D TG protocol. Yet the difference in non-neuronal cell counts led to variations in the relative abundance of TRK signal in FC.

It has been hypothesised the number of neurons would cap in sensory ganglia regardless of glial presence during development based on murine embryos with congenital Notch deficiency[487].

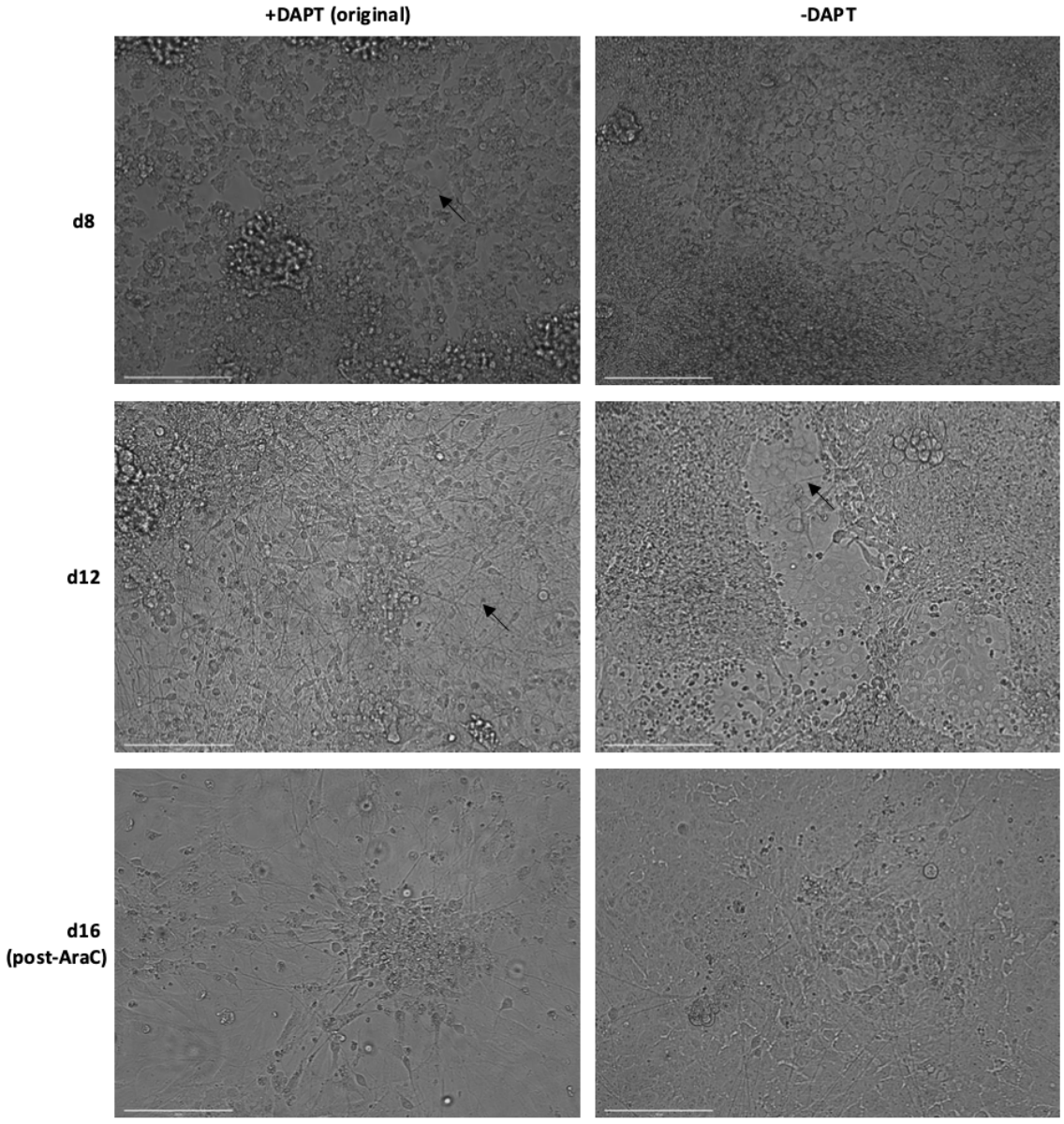


Figure S20: Representative brightfield images of DRG iNociceptors differentiated with and without DAPT, at d8, d12, and d16 (post-AraC treatment). Thin arrow indicating neuronal cellular processes prior to neurotrophin addition. Scale bar 150µm.

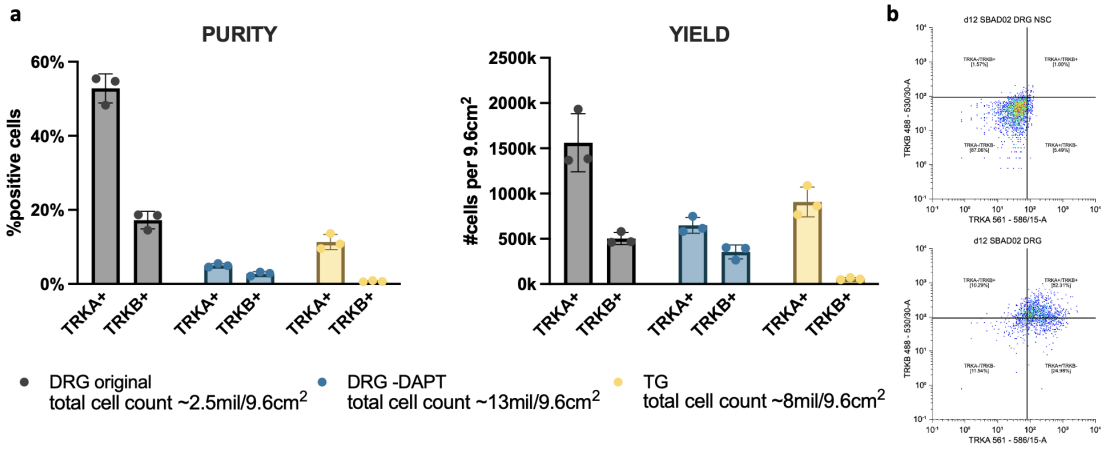


Figure S21: Trk-typing of SBAD02 DRG grown with/without DAPT and TG iNociceptor progenitors at the time of detachment prior to maturation on 2D platforms.
(a) TRK-typing by FC, n=3 wells of the same batch of differentiation per protocol. Error bars standard deviations. Total cell count batch specific. Statistical analysis by two-way ANOVA with Tukey's multiple comparison test: Left panel significant effect by differentiation protocol [63.07% of total variation, F(2,12)=423.9, p<0.0001], sensory neuron marker expression [20.38% of total variation, F(1,12)=273.9, p<0.0001], and interaction [15.65% of total variation, F(2,12)=105.2, p<0.0001]; Right panel significant effect by sensory neuron marker expression [55.63% of total variation, F(1,12)=97.99, p<0.0001], differentiation protocol [23.64% of total variation, F(2,12)=23.64, p<0.0001], and interaction [10.72% of total variation, F(2,12)=9.438, p=0.0034].
(b) Confirmation of TRK/TRKB distribution in SBAD02 DRG and TG iNociceptor progenitors via IF.

Naturally, one might assume that the extra nociceptors derived from the original Chambers' protocol in presence of DAPT were forced into neuralisation from a cohort of communal pool of neuronal/glial progenitors. We therefore compared the temporal expression profiles of known markers for sensory neuron commitment (Figure S22), grouped into (a) ectodermal lineage, (b) sensory neuron progenitors, and (c) NOTCH pathway which particularly contributes to neuron-glia restriction by RT-qPCR. The relative change of relative *NOTCH* transcript was minute with or withour DAPT in Chambers' iNociceptor progenitors. We also validated the early transcriptional trajectory of our Chambers' iNociceptor with the published database NOCICEPTRA[7]. The match between the temporal trends of absolute and relative transcripts in Chambers' DRG was mediocre, thus of minimal referring values. The extra non-neuronal cells in the modified Chambers' protocol tiled the bottom of the plate soon after replating, which could not be removed by AraC treatment (Figure S20 d16) and quickly choked out neurons. It is likely that WNT activation gave rise to non-

neuroectodermal lineages (such as smooth muscle[408]) with the complete lack of neuralisation by DAPT. However, such impact was not seen in the original Chambers' protocol, in which differentiation without DAPT only altered the ratio of Nestin+/TUJ1+ cells. Nor was the relatively high presence of TRKB+ cells characterised originally. We suspected that it was due to our prior optimisation on reducing the starting differentiation[438]. Therefore, we did not proceed the no-DAPT culture beyond d20.

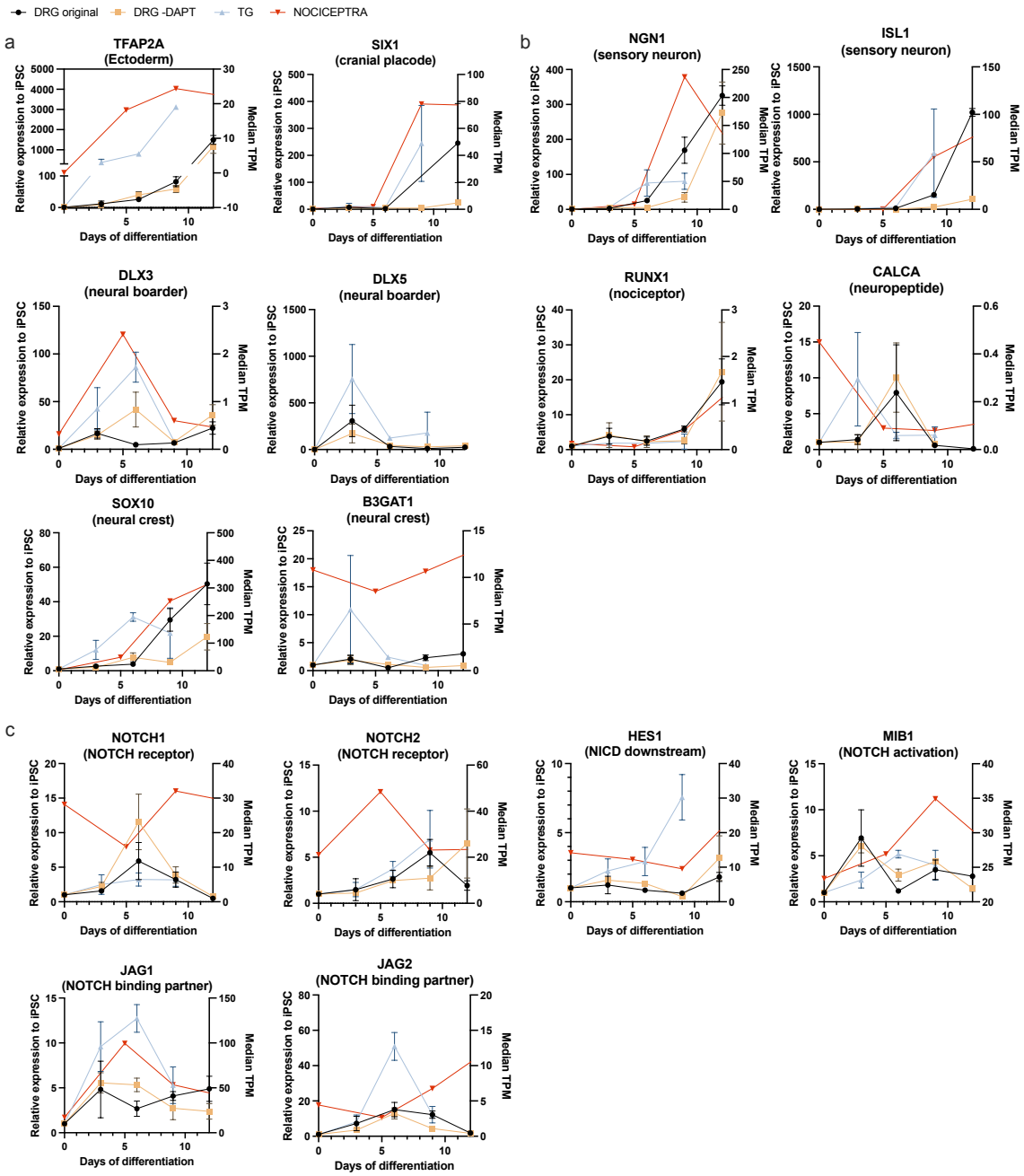


Figure S22: Temporal expression profiles of key markers in early SBAD02 DRG and TG iNociceptors from 2D culturing conditions. For each panel: Left y-axis denoting relative quantification (by RT-qPCR) results of markers for (a) ectodermal lineage, (b) sensory neuron progenitors, and (c) NOTCH pathway in early SBAD02 DRG and TG iNociceptors, no amplification of SIX1 in DRG d9 samples; The right y-axis demoting absolute quantification (by RNAseq) obtained from NOCICEPTRA[7], from which DLX5 returned no results. For RT-qPCR results, n=3 per time point per protocol. Error bars standard deviations.

S3.6 Supplementary information on determining the appropriate methodology for transcriptional circadian studies *in vitro*

S3.6.1 Pilot test of circadian RT-qPCR methodology with NHDFs

We first optimised the experimental design with NHDFs before attempts on iNociceptors (Section 3.2). There were no circadian trends in the abundance of any mRNA candidates. Time point-specific fluctuations across multiple genes (e.g. +41 and +45) were likely a technical artefact during sample collection (Figure S23).

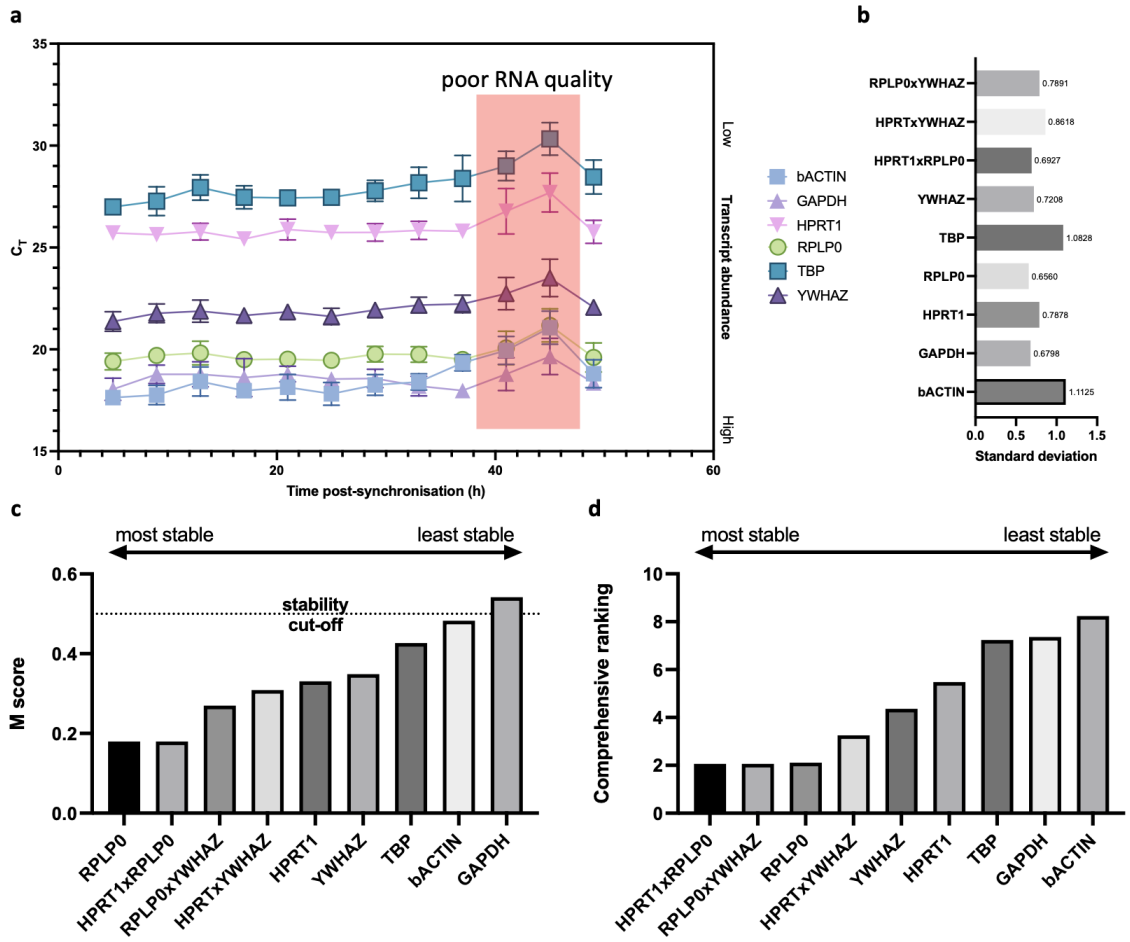


Figure S23: Evaluation of stable reference genes for mRNA relative quantification by RT-qPCR in NHDFs.
(a) C_T values and (b) total standard deviations of 6 different reference genes in NHDF, n=6 technical replicates (pooled regardless of synchronisation methods) of the same colony per time point, 3ng cDNA per reaction. (a) Error bars standard deviations per time point. (c-d) (c) GeNorm analysis and (d) comprehensive ranking of single and double reference gene stability in NHDF.

We computed the geometric means between each pair of the three candidates of smallest standard deviations in NHDFs. To demonstrate the impact of reference gene stability on visualising circadian trends, fold change of *PER2* and *BMAL1* transcripts were graphed relative to all single and double reference candidates in NHDFs (Figure S24). Relative quantification can be misleading when unstable reference, such as *TBP* at +33 and +37, was applied.

We chose the double reference system *HPRT1/RPLP0* in NHDFs based on the comprehensive stability ranking, tighter spread between technical replicates, and visually the shape of curve. *BMAL1* and *CRY1* exhibited a typical cycle of 25-26 hours under FK synchronisation. The acrophase of BMAL1 and CRY1 appeared relatively in sense with each other but distinct to that of PER2, which confirms recent reports[243]. *PER2* and *CRY2* were antisense to *BMAL1* for the first 25 hours, followed by a non-canonical sustained high expression, which was confirmed by alternative methods of protein abundance (see Section S3.7).

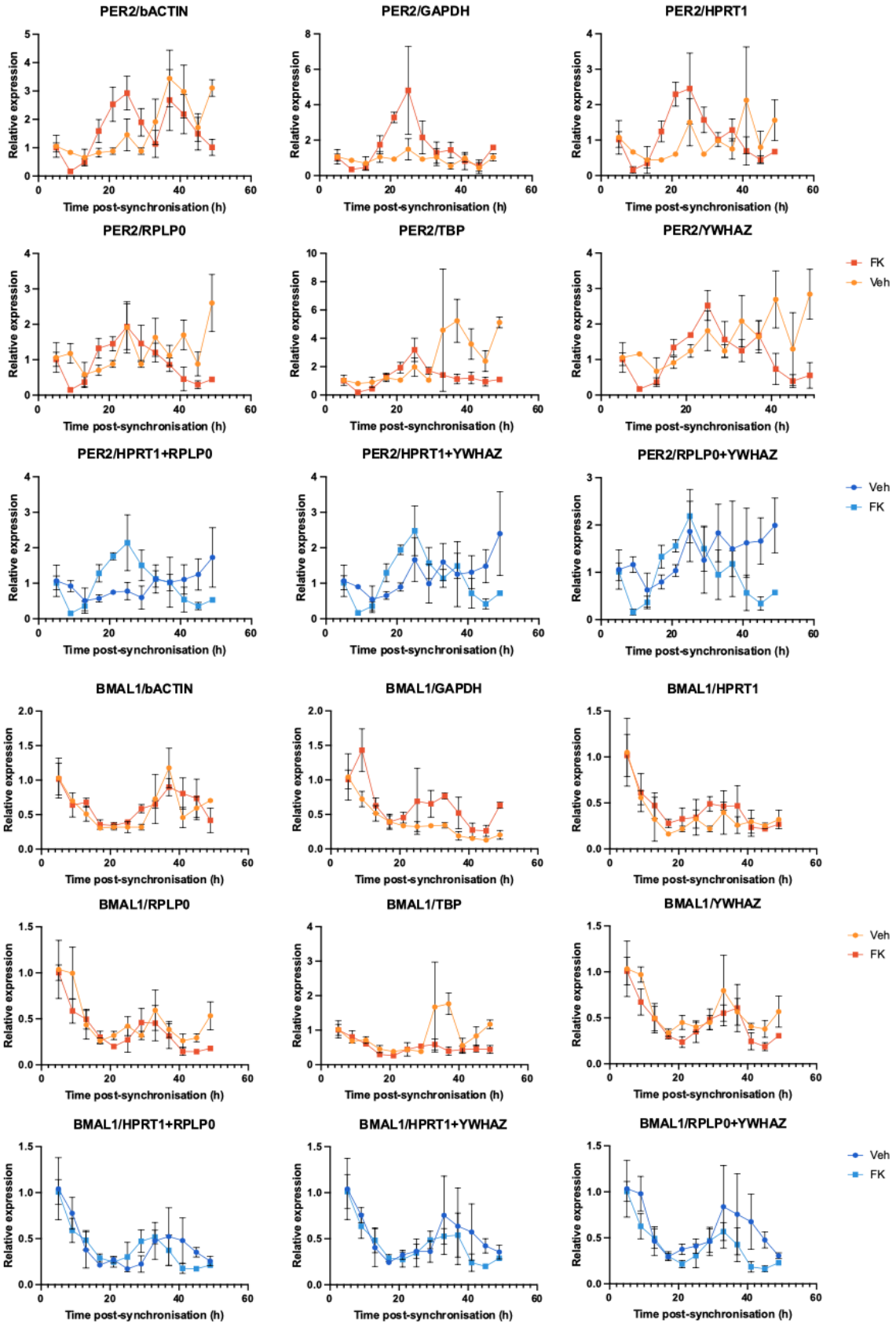
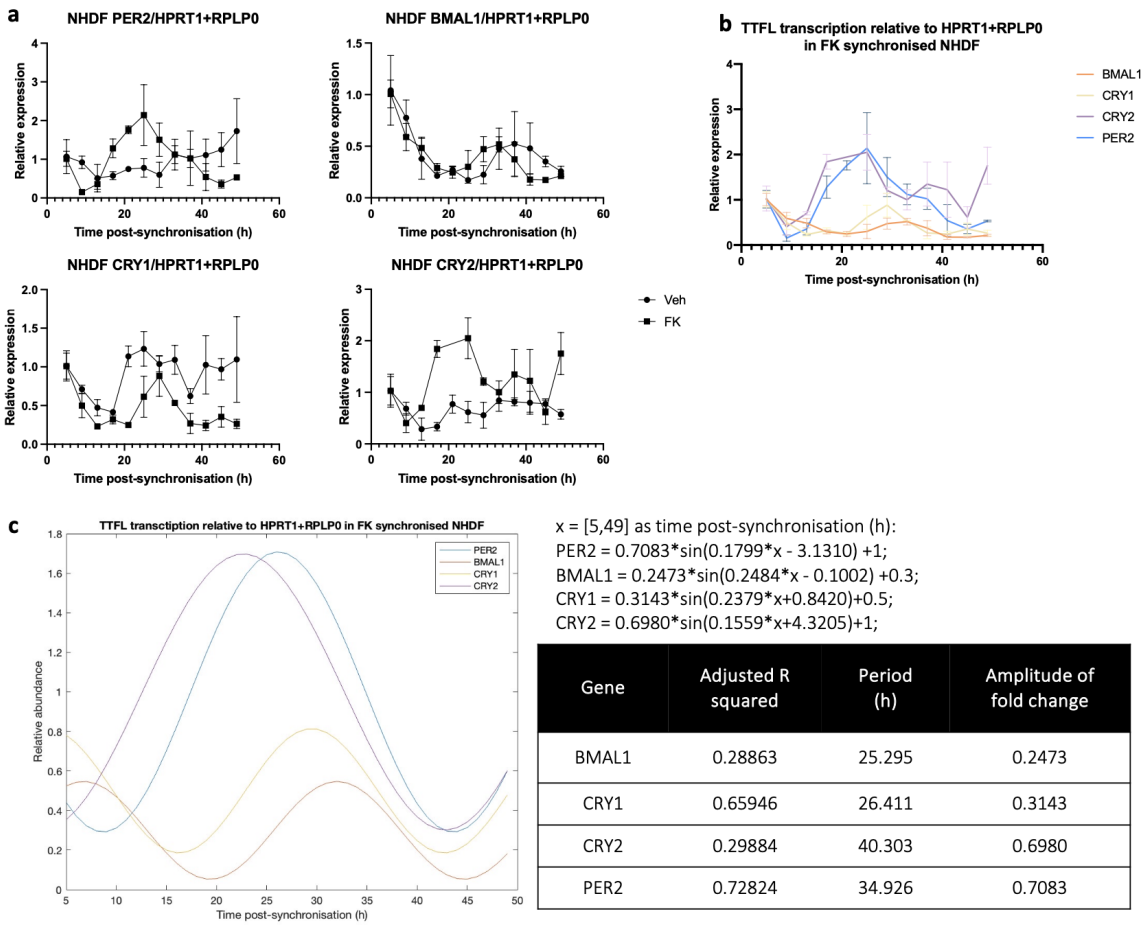


Figure S24: Relative expression of PER2 (top) and BMAL1 (bottom) in NHDFs normalised with different single or double reference genes. n=3 technical replicates per time point per synchronisation method. 3ng cDNA per reaction. Error bar standard deviations.



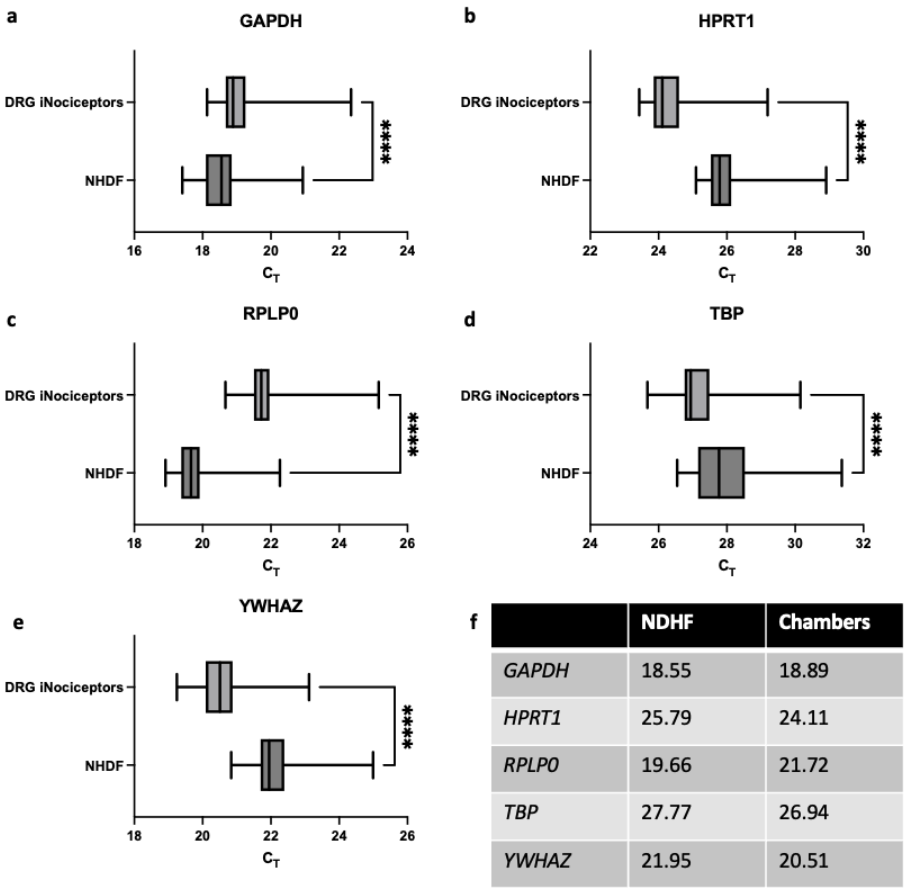
x = [5,49] as time post-synchronisation (h):
PER2 = 0.7083*sin(0.1799*x - 3.1310) +1;
BMAL1 = 0.2473*sin(0.2484*x - 0.1002) +0.3;
CRY1 = 0.3143*sin(0.2379*x+0.8420)+0.5;
CRY2 = 0.6980*sin(0.1559*x+4.3205)+1;

Gene	Adjusted R squared	Period (h)	Amplitude of fold change
BMAL1	0.28863	25.295	0.2473
CRY1	0.65946	26.411	0.3143
CRY2	0.29884	40.303	0.6980
PER2	0.72824	34.926	0.7083

Figure S25: Transcriptional abundance of canonical TTFL gene expression in chemically synchronised NHDFs.
(a) Time series of transcription of 4 canonical clock genes in FK synchronised NHDFs in comparison to vehicle control. n =3 technical replicates per time point per synchronisation method. 3ng cDNA per reaction. Error bar standard deviation. (b-c) (b) Phase and amplitude comparison and (c) mathematical curve fitting of 4 canonical clock genes in FK synchronised NHDFs.

S3.6.2 Comparison between the natural expression level of reference gene candidates in NHDF and DRG iNociceptors

Despite using human-specific primers, we suspected that iNociceptor RNA from individual samples would have been diluted, to various extents, by rat astrocytes. We reasoned that the impact of dilution in C_Ts of different genes should remain roughly the same within the same sample, thereby cancelling out the effect of variation for stability or $\Delta\Delta C_T$ calculations. C_T values of reference candidates were compared in Chambers DRG iNociceptor samples (Figure S26). C_T medians were in fact closer than expected. Statistical significance between cell types was partially a consequence of tissue-specific expression and likely due to high sample numbers.



f

	NDHF	Chambers
GAPDH	18.55	18.89
HPRT1	25.79	24.11
RPLP0	19.66	21.72
TBP	27.77	26.94
YWHAZ	21.95	20.51

Figure S26: Variation in C_T levels of reference gene candidates in NHDF and Chambers' DRG iNociceptors.
(a-e) Comparison of C_T of candidate reference genes between NHDF and iNociceptors. 3ng load/well (n=72 in NHDFs and n=104 in iNociceptors). Statistical significance by non-parametric one-way ANOVA. (f) Summary of medians of reference gene C_Ts.

S3.7 Optimisation of quantifying circadian protein via ImageStream in NHDFs as a pilot test and positive control

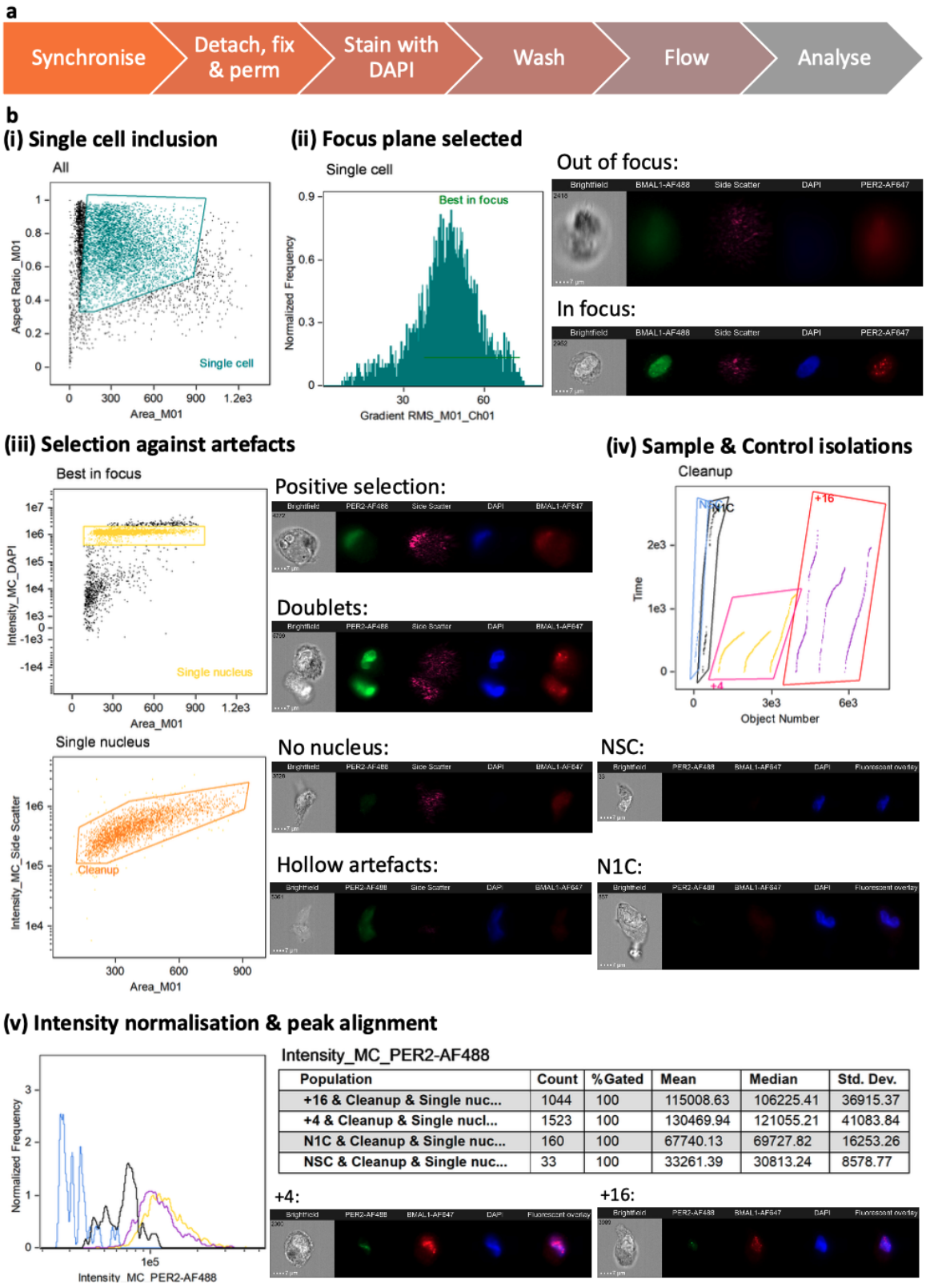
Optimisation of quantifying circadian protein via ImageStream in NHDFs as a pilot test and positive control

The typical analysis process of ImageStream began by pooling all replicates and all samples of interest to avoid bias during analysis (Figure S27). From all readouts, single cell populations (i) within the plane of focus (ii) were identified. We then excluded artefacts, doublets, and debris (iii) by gating against cells with out-of-range DAPI and low side scatter. At this point, most NSC cells should already be excluded as low DAPI samples. The remaining data entries were visually verified for abnormal backgrounds (usually in the DAPI channel).

Technical replicates (iv) of the same treatment or sample were grouped by the time of flow sequence. A minimal of 1000 cells were secured for all synchronised samples. Variations in the final cell counts were mostly due to cell loss during staining and handling. We then confirmed the intensity peak shift against negative controls for each fluorophore (v). Fluorescence pixel intensity was gated against N1C as background to display the image panels.

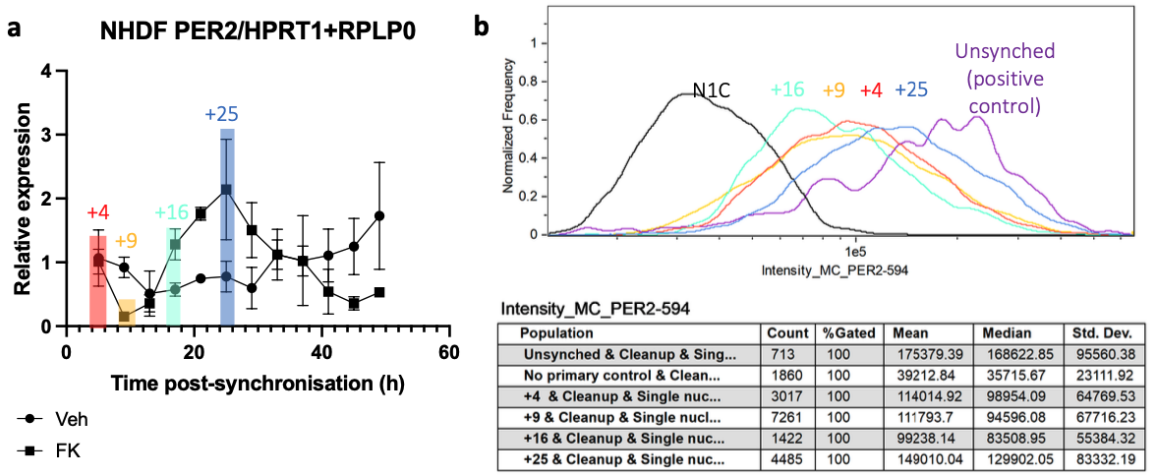
Using NHDF as a positive control, we pilot-tested the concordance of transcriptional and translational activities of BMAL1, PER2, and CRY1. The time points of choice included the theoretical peak and trough for PER2 and the experimental ones obtained in Section S3.6. We did not sample regularly and with enough temporal resolution for proper nuclear translocation analysis in NHDFs.

Figure S27: Typical quality control and data clean-up process for ImageStream on quantifying TTFL protein expression and translocation in NHDFs as a positive control (figure see next page). (a) Schematics of workflow. (b) Representative sample analysis process in unsynchronised NHDFs, using NSC and N1C as negative controls.



(Caption see previous page)

We first examined whether the unconventional oscillation of *PER2* expression by RT-qPCR was reflected at protein level (Figure S28). PER2 immunoreactivity mostly matched up with transcript abundance except for the trough of signal intensity at +16. It is likely, due to the delay of rhythm in translation, that the true trough of net protein was somewhere between +9 and +16 that the trial sampling did not capture.



Intensity_MC_PER2-594

Population	Count	%Gated	Mean	Median	Std. Dev.
Unsynched & Cleanup & Sing...	713	100	175379.39	168622.85	95560.38
No primary control & Clean...	1860	100	39212.84	35715.67	23111.92
+4 & Cleanup & Single nuc...	3017	100	114014.92	98954.09	64769.53
+9 & Cleanup & Single nucl...	7261	100	111793.7	94596.08	67716.23
+16 & Cleanup & Single nuc...	1422	100	99238.14	83508.95	55384.32
+25 & Cleanup & Single nuc...	4485	100	149010.04	129902.05	83332.19

Figure S28: Complete ImageStream results of PER2 expression in chemically synchronised NHDFs. (a) PER2 transcription abundance by RT-qPCR relative to HPRT1 x RPLP0, extract from Figure S25. n = 3 technical replicates per time point per synchronising treatment. Error bars standard deviations. (b) ImageStream peak shift of PER2 expression in FK-synchronised NHDF.

The mouse Bmal1 homolog to the human isoform BMAL1b remains highly nuclear regardless of circadian time[243]. However, the human-specific cytoplasmic isoform and antigen specificity complicated our result.

We cross-referenced two different antibodies for BMAL1 (Figure S29) to avoid species overlap in different staining combinations. Proteintech rabbit polyclonal anti-BMAL1 (14268-1-AP) was raised against a recombinant BMAL1 fusion protein containing animo acids 1-303, containing both the NLS and product translated from exon 8 where the BMAL1 primer pair anneals. In contrast, Santa Cruz mouse monoclonal anti-BMAL1 (sc-365645) was raised against amino acids 441-610 near the flexible C-terminus of human BMAL1 which identifies both isoforms (Figure S29d).

Fluctuations in signal intensities of 14268-1-AP matched with transcription analysis while signal from Santa Cruz mouse monoclonal anti-BMAL1 (sc-365645) demonstrated a biphasic presence (+9/+25) or absence (+4/+16) shift.

Signals from sc-365645 appeared to be more limited inside the nuclei (Figure S31 right, co-stained with CRY1). It was beyond the scale of the project to detect the extent of DAPI bleed-through, thus the possibility of channel cross-talk remained. In contrast, signals from 14268-1-AP were partially retained in the cytoplasm at all time points investigated (Figure S31 left, co-stained with PER2). The cytoplasmic signal of 14268-1-AP formed time-sensitive puncta.

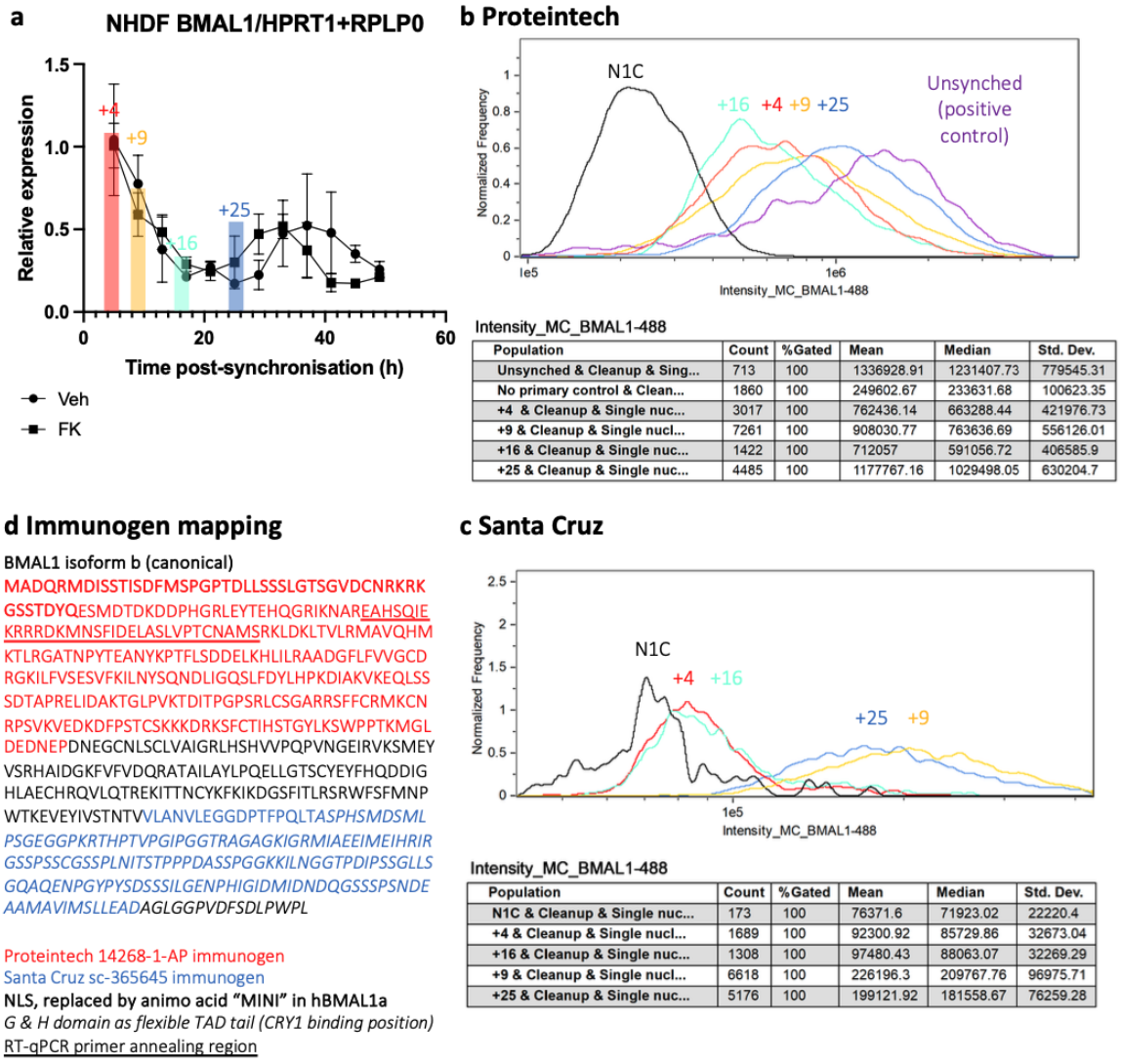
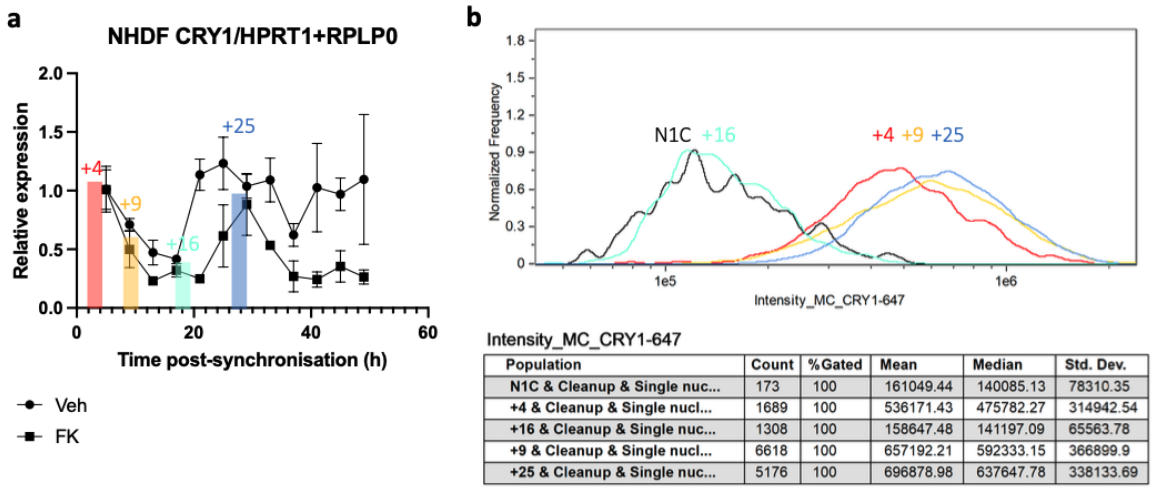


Figure S29: Complete ImageStream results of BMAL1 expression in chemically synchronised NHDFs.
(a) BMAL1 transcription abundance by RT-qPCR relative to HPRT1 x RPLP0, extract from Figure S25. n = 3 technical replicates per time point per synchronising treatment. Error bars standard deviations. (b-c) ImageStream peak shift of BMAL1 expression in FK-synchronised NHDF using two different antibodies. (d) Immunogen primer alignment in hBMAL1b amino acid sequence.

Similarly, CRY1 immunoreactivity mostly matched up with transcript abundance except for lower presence of +4 (Figure S30). CRY1 also demonstrated time-sensitive presence of puncta (Figure S31b), which were not previously documented in the literature.



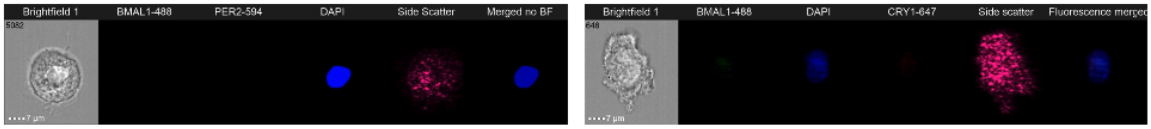
Intensity_MC_CRY1-647

Population	Count	%Gated	Mean	Median	Std. Dev.
N1C & Cleanup & Single nuc...	173	100	161049.44	140085.13	78310.35
+4 & Cleanup & Single nucl...	1689	100	536171.43	475782.27	314942.54
+16 & Cleanup & Single nuc...	1308	100	158647.48	141197.09	65563.78
+9 & Cleanup & Single nucl...	6618	100	657192.21	592333.15	366899.9
+25 & Cleanup & Single nuc...	5176	100	696878.98	637647.78	338133.69

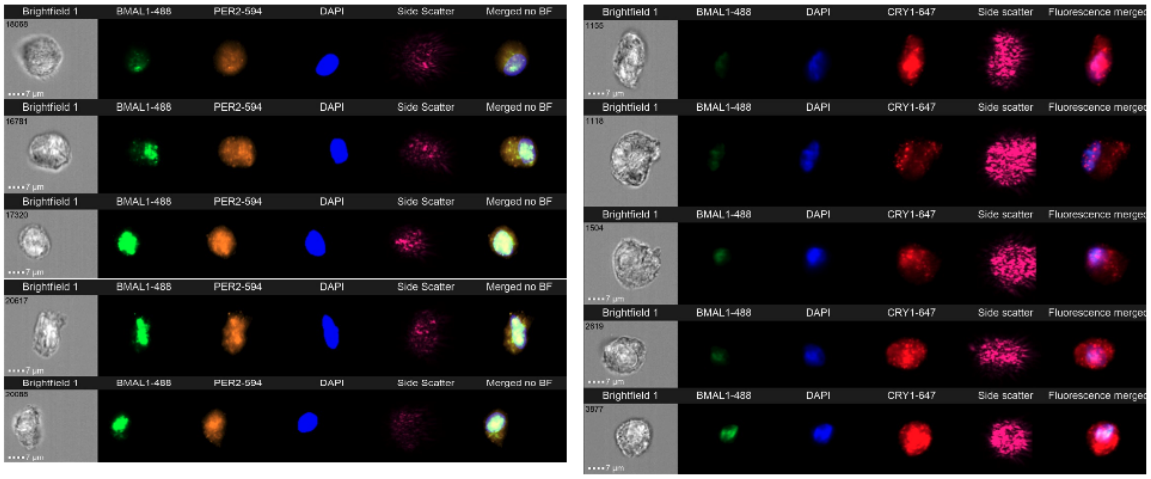
Figure S30: Complete ImageStream results of CRY1 expression in chemically synchronised NHDFs. (a) CRY1 transcription abundance by RT-qPCR relative to HPRT1 x RPLP0, extract from Figure S25. n = 3 technical replicates per time point per synchronising treatment. Error bars standard deviations. (b) ImageStream peak shift of CRY1 expression in FK-synchronised NHDF.

Overall, we were satisfied with using ImageStream for circadian investigation in more robust oscillator lines such as NDHFs. However, cconsistent and gentle detachment of neurons were significantly more difficult in neuron-glia co-cultures. Therefore, we had to resolve back to tranditional western blotting within the scope of the current project.

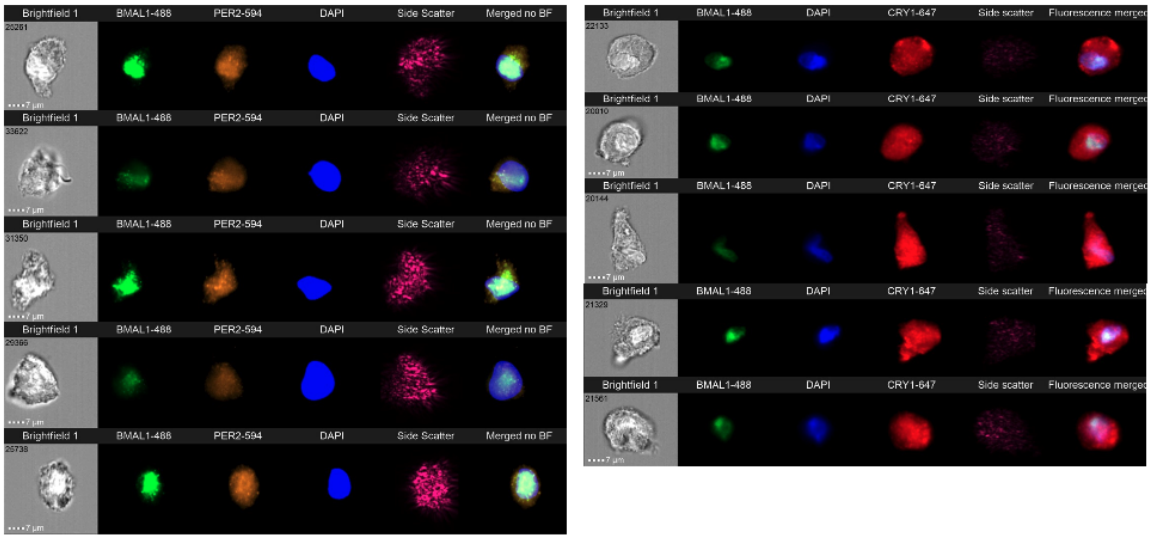
a. N1C



b. +4



c. +9



(Figure continuing on next page)

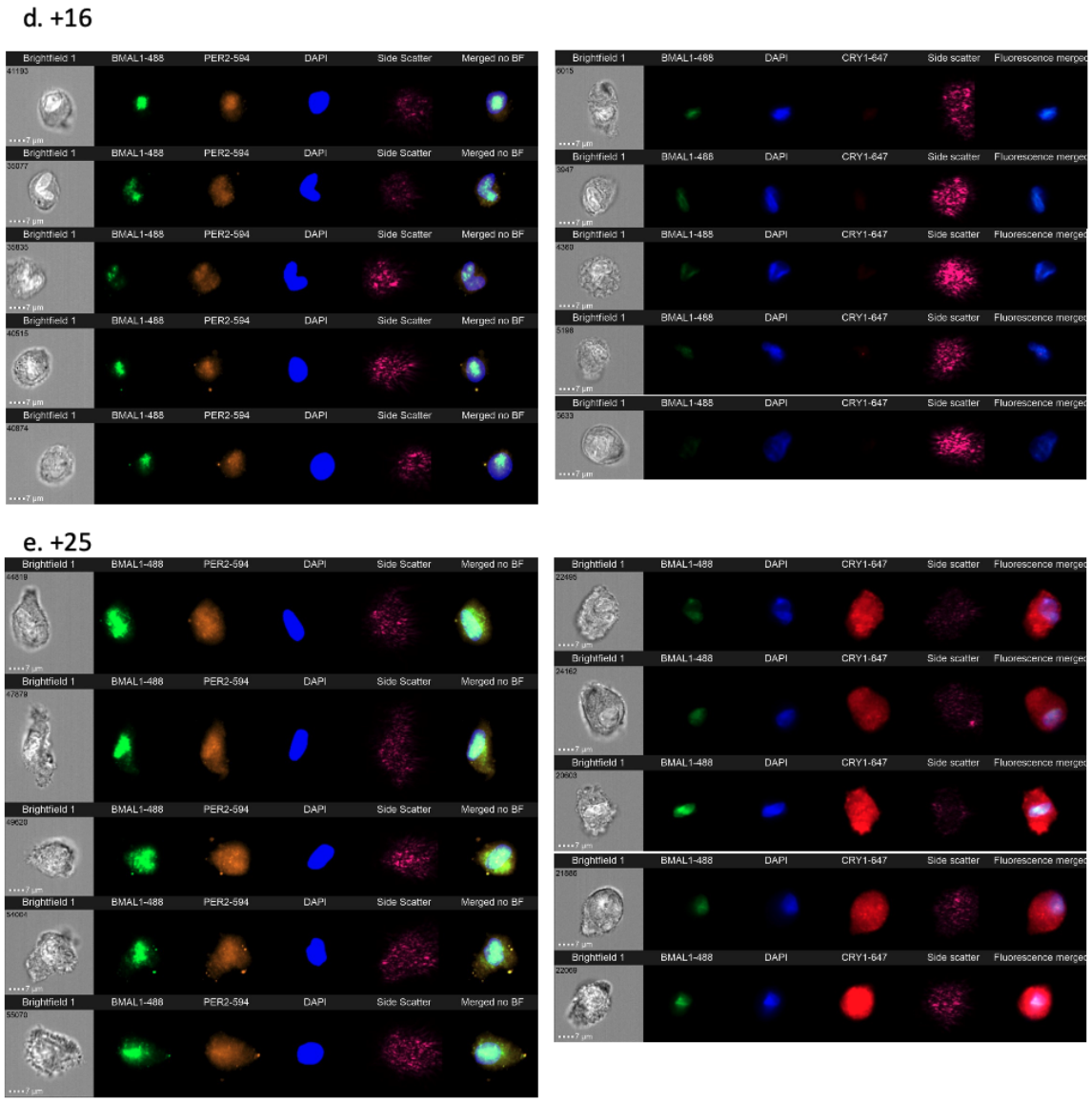
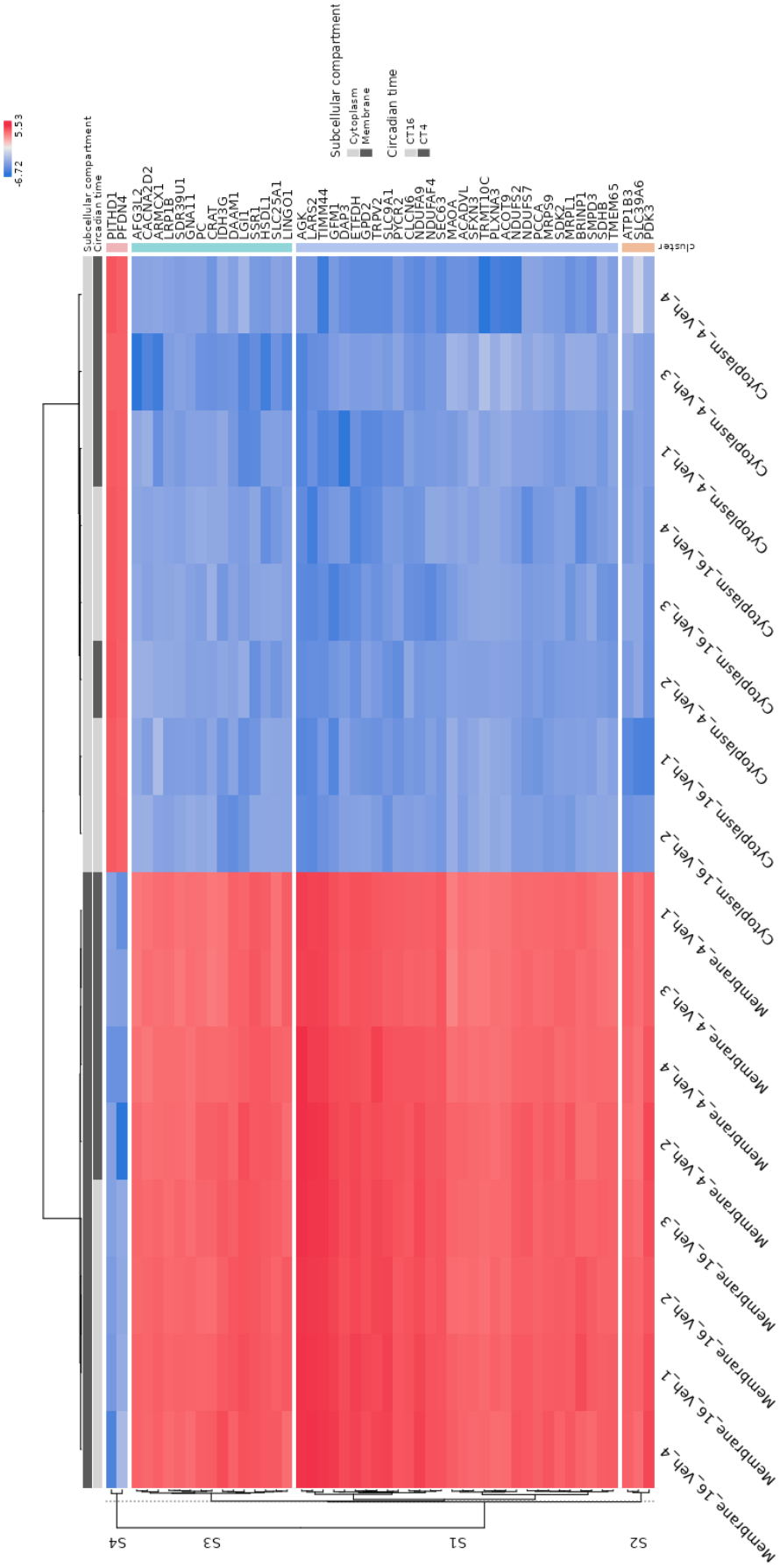


Figure S31: Representative images of BMAL1, PER2, and CRY1 in NHDFs from ImageStream analysis.
(a) N1C as fluorescence background for either staining combo. (b-e) Representative images of clock gene immunoreactivity in NHDFs at (b) 4-, (c) 9-, (d) 16-, and (e) 25-hour post-synchronisation by FK. Bin selected at highest relative frequency from Intensity histograms for each time point.

S3.8 Supplementary information on subcellular proteomics of FK synchronised Chambers' iNociceptors.

S3.8.1 HCA across all samples

Figure S32: Sample clustering based on non-biased HCA for subcellular fraction proteomics in chemically synchronised Chmaber's iNociceptors (figure see next page).


5.53
-6.72
Subcellular compartment
Cytoplasm
Membrane
Circadian time
CT16
CT4
Subcellular compartment
Circadian time
cluster
PITHD1
PFDN4
AFG3L2
ACAA2D2
AMACR1
ARPIB
SDR39U1
GNA11
PC
CRAT
IDH3G
DAAM1
GAT1
SSR1
HSDL1
SLC25A1
LINGO1
AGK
LARS2
TIMM44
GFM1
DAP3
EPDR1
TRPV2
SLC9A1
PYCR2
CLCN6
NDUFA9
NDUFAF4
MACO3
ACADVL
SFXN3
TRMT10C
PLXNA3
ACOT9
NDUFS2
NDUFS7
MRPS9
SDK2
MRPL1
BRINP1
SMPD3
SDHB
TMEM65
ATP1B3
SLC39A6
PDK3
Cytoplasm_4_Veh_4
Cytoplasm_4_Veh_3
Cytoplasm_4_Veh_1
Cytoplasm_16_Veh_4
Cytoplasm_16_Veh_3
Cytoplasm_4_Veh_2
Cytoplasm_16_Veh_1
Cytoplasm_16_Veh_2
Membrane_4_Veh_1
Membrane_4_Veh_3
Membrane_4_Veh_4
Membrane_4_Veh_2
Membrane_16_Veh_3
Membrane_16_Veh_2
Membrane_16_Veh_1
Membrane_16_Veh_4
S4
S3
S1
S2

S3.8.2 Original western blots

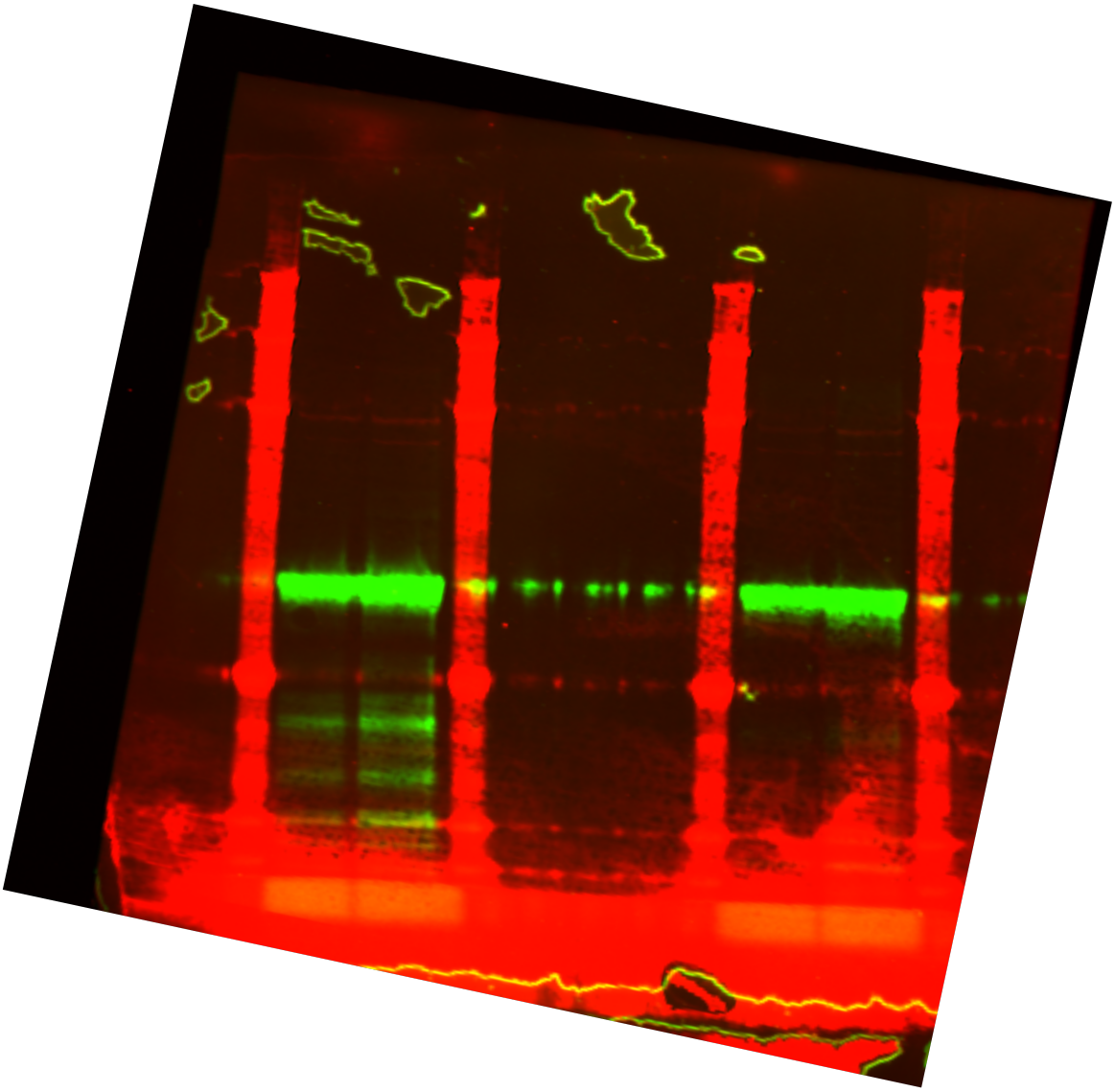


Figure S33: Confirmation of BMAL1 protein expression in chemically synchronised Chambers' iNociceptors by western blotting.
n=2 per time point.

Bibliography

[1] Liting Wei et al. “The molecular drivers of pain rhythmicity as novel therapeutic opportunities”. In: *Nat. Commun. (In press)* (2026). DOI: 10.1101/2022.07.15.499708.

[2] Galbha Duggal et al. “A highly efficient method to differentiate CGRP-expressing peptidergic nociceptors from human induced pluripotent stem cells”. In: *Stem Cell Rep. (In press)* (2026).

[3] Xinyu Li et al. “Methodology & Molecular basis of the circadian rhythmicity of pain in preclinical research: A narrative review (in prep).” In: (2026).

[4] Diana Tavares-Ferreira et al. “Spatial transcriptomics of dorsal root ganglia identifies molecular signatures of human nociceptors”. In: *Sci. Transl. Med* 14.632 (2022), pp. 1–18. ISSN: 19466242. DOI: 10.1126/scitranslmed.abj8186.

[5] Lite Yang et al. “Human and mouse trigeminal ganglia cell atlas implicates multiple cell types in migraine”. In: *Neuron* 110.11 (2022), pp. 1806–1821. ISSN: 08966273. DOI: 10.1016/j.neuron.2022.03.003.

[6] Pradipta Ray et al. “Comparative transcriptome profiling of the human and mouse dorsal root ganglia: an RNA-seq-based resource for pain and sensory neuroscience research.” In: *Pain* 159.7 (July 2018), pp. 1325–1345. ISSN: 1872-6623 (Electronic). DOI: 10.1097/j.pain.0000000000001217.

[7] Maximilian Zeidler et al. “NOCICEPTRA: Gene and microRNA Signatures and Their Trajectories Characterizing Human iPSC-Derived Nociceptor Maturation”. In: *Adv. Sci* 8.21 (2021), pp. 1–21. ISSN: 21983844. DOI: 10.1002/advs.202102354.

[8] International Association for the Study of Pain. *IASP Terminology*. URL: https://www.iasp-pain.org/resources/terminology/.

[9] Allan I Basbaum et al. “Cellular and molecular mechanisms of pain.” In: *Cell* 139.2 (Oct. 2009), pp. 267–284. ISSN: 1097-4172 (Electronic). DOI: 10.1016/j.cell.2009.09.028.

[10] Simon Vermeiren, Eric J. Bellefroid, and Simon Desiderio. “Vertebrate Sensory Ganglia: Common and Divergent Features of the Transcriptional Programs Generating Their Functional Specialization”. In: *Front. Cell Dev. Biol* 8 (Oct. 2020). ISSN: 2296634X. DOI: 10.3389/fcell.2020.587699.

[11] Yang Liu and Qiufu Ma. “Generation of somatic sensory neuron diversity and implications on sensory coding”. In: *Curr. Opin. Neurobiol.* 21.1 (Feb. 2011), pp. 52–60. ISSN: 09594388. DOI: 10.1016/j.conb.2010.09.003.

[12] Santosh K. Mishra et al. “TRPV1-lineage neurons are required for thermal sensation”. In: *EMBO* 30.3 (Feb. 2011), pp. 582–593. ISSN: 02614189. DOI: 10.1038/emboj.2010.325.

[13] Michael J Caterina et al. “The capsaicin receptor: a heat-activated ion channel in the pain pathway”. In: *Nature* 389 (1997), pp. 819–824.

[14] Jozsef Lazar et al. “Kinetics of penetration influence the apparent potency of vanilloids on TRPV1”. In: *Mol. Pharmacol.* 69.4 (Apr. 2006), pp. 1166–1173. ISSN: 0026895X. DOI: 10.1124/mol.105.019158.

[15] Erhu Cao et al. “TRPV1 structures in distinct conformations reveal activation mechanisms”. In: *Nature* 504.7478 (2013), pp. 113–118. ISSN: 00280836. DOI: 10.1038/nature12823.

[16] Zhiwei Feng et al. “Structural insight into tetrameric hTRPV1 from homology modeling, molecular docking, molecular dynamics simulation, virtual screening, and bioassay validations”. In: *JCIM* 55.3 (Mar. 2015), pp. 572–588. ISSN: 1549960X. DOI: 10.1021/ci5007189.

[17] Tibor Rohacs. “Phosphoinositide regulation of TRPV1 revisited”. In: *Pflug. Arch. Eur. J. Physiol* 467.9 (Sept. 2015), pp. 1851–1869. ISSN: 14322013. DOI: 10.1007/s00424-015-1695-3.

[18] Kaihua Zhang, David Julius, and Yifan Cheng. “Structural snapshots of TRPV1 reveal mechanism of polymodal functionality”. In: *Cell* 184.20 (Sept. 2021), pp. 5138–5150. ISSN: 10974172. DOI: 10.1016/j.cell.2021.08.012.

[19] David L Bennett et al. “The role of voltage-gated sodium channels in pain signaling”. In: *Physiol Rew* 99 (2019), pp. 1079–1151. DOI: 10.1152/physrev.00052.2017.-Acute. URL: www.prv.org.

[20] Stephanie Shiers, Rebecca M. Klein, and Theodore J. Price. “Quantitative differences in neuronal subpopulations between mouse and human dorsal root ganglia demonstrated with RNAscope in situ hybridization”. In: *Pain* 161.10 (2020), pp. 2410–2424. ISSN: 18726623. DOI: 10.1097/j.pain.0000000000001973.

[21] David D. McKemy. “TRPM8: The Cold and Menthol Receptor”. In: *TRP Ion Channel Function in Sensory Transduction and Cellular Signaling Cascades*. Ed. by WB Liedtke and S Heller. Boca Raton (FL): CRC Press/Taylor & Francis, 2007. Chap. 13. URL: https://www.ncbi.nlm.nih.gov/books/NBK5238/#.

[22] Tatiana F. Almeida, Suely Roizenblatt, and Sergio Tufik. “Afferent pain pathways: A neuroanatomical review”. In: *Brain Res.* 1000.1-2 (2004), pp. 40–56. ISSN: 00068993. DOI: 10.1016/j.brainres.2003.10.073.

[23] Steven J. Middleton et al. “Studying human nociceptors: From fundamentals to clinic”. In: *Brain* 144.5 (May 2021), pp. 1312–1335. ISSN: 14602156. DOI: 10.1093/brain/awab048.

[24] Andrew J. Todd. “Identifying functional populations among the interneurons in laminae I-III of the spinal dorsal horn”. In: *Mol. Pain* 13 (2017), pp. 1–19. ISSN: 17448069. DOI: 10.1177/1744806917693003.

[25] Alice Arcourt et al. “Touch Receptor-Derived Sensory Information Alleviates Acute Pain Signaling and Fine-Tunes Nociceptive Reflex Coordination”. In: *Neuron* 93.1 (Jan. 2017), pp. 179–193. ISSN: 10974199. DOI: 10.1016/j.neuron.2016.11.027.

[26] Saad S Nagi et al. “An ultrafast system for signaling mechanical pain in human skin”. In: *Sci. Adv* 5 (2019). URL: https://www.science.org.

[27] Min Jung et al. “Cross-species transcriptomic atlas of dorsal root ganglia reveals species-specific programs for sensory function”. In: *Nat. Commun.* 14.1 (Dec. 2023). ISSN: 20411723. DOI: 10.1038/s41467-023-36014-0.

[28] Minh Q. Nguyen et al. “Single-nucleus transcriptomic analysis of human dorsal root ganglion neurons”. In: *eLife* 10 (2021), pp. 1–21. ISSN: 2050084X. DOI: 10.7554/eLife.71752.

[29] Stephanie I Shiers et al. “Convergence of peptidergic and non-peptidergic protein markers in the human dorsal root ganglion and spinal dorsal horn.” In: *Comp. Neurol* 529.10 (July 2021), pp. 2771–2788. ISSN: 1096-9861 (Electronic). DOI: 10.1002/cne.25122.

[30] Charlotte Rostock et al. “Human vs. Mouse Nociceptors-Similarities and Differences”. In: *Neuroscience* 387 (Sept. 2018), pp. 13–27. ISSN: 18737544. DOI: 10.1016/j.neuroscience.2017.11.047.

[31] Silke Miller et al. “Immunohistochemical localization of the calcitonin gene-related peptide binding site in the primate trigeminovascular system using functional antagonist antibodies”. In: *Neuroscience* 328 (July 2016), pp. 165–183. ISSN: 18737544. DOI: 10.1016/j.neuroscience.2016.04.046.

[32] Nima Ghitani et al. “A distributed coding logic for thermosensation and inflammatory pain”. In: *Nature* 642.8069 (June 2025), pp. 1016–1023. ISSN: 14764687. DOI: 10.1038/s41586-025-08875-6.

[33] David A. Yarmolinsky et al. “Differential modification of ascending spinal outputs in acute and chronic pain states”. In: *Neuron* 113.8 (Apr. 2025), pp. 1223–1239. ISSN: 08966273. DOI: 10.1016/j.neuron.2025.01.031.

[34] Jun Wang, Shao Wu Ou, and Yun Jie Wang. “Distribution and function of voltage-gated sodium channels in the nervous system”. In: *Channels* 11.6 (Nov. 2017), pp. 534–554. ISSN: 19336969. DOI: 10.1080/19336950.2017.1380758.

[35] Josephine Lai et al. “Voltage-Gated Sodium Channels and Hyperalgesia”. In: *Ann. Rev. Pharmacol. Toxicol* 44 (2004), pp. 371–397. ISSN: 03621642. DOI: 10.1146/annurev.pharmtox.44.101802.121627.

[36] Wonseok Chang et al. “Expression and Role of Voltage-Gated Sodium Channels in Human Dorsal Root Ganglion Neurons with Special Focus on Nav1.7, Species

Differences, and Regulation by Paclitaxel". In: *Neurosci. Bull* 34.1 (Feb. 2018), pp. 4–12. ISSN: 19958218. DOI: 10.1007/s12264-017-0132-3.

[37] Juan J Toledo-Aral et al. "Identification of PN1, a predominant voltage-dependent sodium channel expressed principally in peripheral neurons". In: *PNAS* 94 (1997), pp. 1527–1532.

[38] Mohamed Chahine and Michael E O'Leary. "Regulation/Modulation of Sensory Neuron Sodium Channels". In: *Voltage Gated Sodium Channels*. Ed. by Peter C Ruben. Berlin, Heidelberg: Springer Berlin Heidelberg, 2014, pp. 111–135. ISBN: 978-3-642-41588-3. DOI: 10.1007/978-3-642-41588-3{_}6.

[39] Theodore R Cummins, James R Howe, and Stephen G Waxman. "Slow Closed-State Inactivation: A Novel Mechanism Underlying Ramp Currents in Cells Expressing the hNE/PN1 Sodium Channel". In: *J. Neurosci* 18.23 (1998), pp. 9607–9619.

[40] Lunbin Deng et al. "Nav1.7 is essential for nociceptor action potentials in the mouse in a manner independent of endogenous opioids". In: *Neuron* (June 2023). ISSN: 08966273. DOI: 10.1016/j.neuron.2023.05.024.

[41] Lucy A. McDermott et al. "Defining the Functional Role of Na V 1.7 in Human Nociception". In: *Neuron* 101.5 (Mar. 2019), pp. 905–919. ISSN: 10974199. DOI: 10.1016/j.neuron.2019.01.047.

[42] Aristos J. Alexandrou et al. "Subtype-selective small molecule inhibitors reveal a fundamental role for Nav1.7 in nociceptor electrogenesis, axonal conduction and presynaptic release". In: *PLoS ONE* 11.4 (Apr. 2016). ISSN: 19326203. DOI: 10.1371/journal.pone.0152405.

[43] Wen He et al. "Functional confirmation that the R1488* variant in SCN9A results in complete loss-of-function of NaV 1.7". In: *BMC Med. Genet* 19.1 (July 2018). ISSN: 14712350. DOI: 10.1186/s12881-018-0643-4.

[44] Nathaniel T Blair and Bruce P Bean. "Roles of Tetrodotoxin (TTX)-Sensitive Na Current, TTX-Resistant Na Current, and Ca 2 Current in the Action Potentials of Nociceptive Sensory Neurons". In: *J. Neurosci* 22.23 (2002), pp. 10277–10290.

[45] Sulayman D. Dib-Hajj, Joel A. Black, and Stephen G. Waxman. “Na v 1.9: A sodium channel linked to human pain”. In: *Nat. Rev. Neurosci* 16.9 (Aug. 2015), pp. 511–519. ISSN: 14710048. DOI: 10.1038/nrn3977.

[46] Sulayman D. Dib-Hajj et al. “Two tetrodotoxin-resistant sodium channels in human dorsal root ganglion neurons”. In: *FEBS Letters* 462.1-2 (Nov. 1999), pp. 117–120. ISSN: 00145793. DOI: 10.1016/S0014-5793(99)01519-7.

[47] Pin Ye et al. “Scorpion toxin BmK I directly activates Nav1.8 in primary sensory neurons to induce neuronal hyperexcitability in rats”. In: *Protein and Cell* 6.6 (June 2015), pp. 443–452. ISSN: 16748018. DOI: 10.1007/s13238-015-0154-4.

[48] Joel A. Black et al. “Changes in the expression of tetrodotoxin-sensitive sodium channels within dorsal root ganglia neurons in inflammatory pain”. In: *Pain* 108.3 (Apr. 2004), pp. 237–247. ISSN: 03043959. DOI: 10.1016/j.pain.2003.12.035.

[49] Michael F Jarvis et al. “A-803467, a potent and selective Na v 1.8 sodium channel blocker, attenuates neuropathic and inflammatory pain in the rat”. In: *PNAS* 104.20 (May 2007), pp. 8520–8525. DOI: 10.1073/pnas.0611364104.

[50] S. K. Joshi et al. “Involvement of the TTX-resistant sodium channel Nav 1.8 in inflammatory and neuropathic, but not post-operative, pain states”. In: *Pain* 123.1-2 (July 2006), pp. 75–82. ISSN: 03043959. DOI: 10.1016/j.pain.2006.02.011.

[51] Bradley J Kerr et al. “A role for the TTX-resistant sodium channel Nav 1.8 in NGF-induced hyperalgesia, but not neuropathic pain”. In: *NeuroReports* 12 (2001). URL: http://journals.lww.com/neuroreport.

[52] Michael S Gold et al. “Redistribution of Na V 1.8 in Uninjured Axons Enables Neuropathic Pain”. In: *J. Neurosci* 23.1 (2003), pp. 158–166.

[53] Josephine Lai et al. “Inhibition of neuropathic pain by decreased expression of the tetrodotoxin-resistant sodium channel, NaV1.8”. In: *Pain* 95 (2002), pp. 143–152.

[54] Niklas Schuelert and Jason J. McDougall. “Involvement of Nav 1.8 sodium ion channels in the transduction of mechanical pain in a rodent model of osteoarthritis”. In: *Arthritis Res. Ther* 14.1 (Jan. 2012). ISSN: 14786354. DOI: 10.1186/ar3553.

[55] Joost P.H. Drenth and Stephen G. Waxman. "Mutations in sodium-channel gene SCN9A cause a spectrum of human genetic pain disorders". In: *J. Clin. Invest* 117.12 (Dec. 2007), pp. 3603–3609. ISSN: 00219738. DOI: 10.1172/JCI33297.

[56] Catharina G. Faber et al. "Gain of function Na V1.7 mutations in idiopathic small fiber neuropathy". In: *Ann. Neurol* 71.1 (Jan. 2012), pp. 26–39. ISSN: 03645134. DOI: 10.1002/ana.22485.

[57] Brian S. Tanaka et al. "Gain-of-function mutation of a voltage-gated sodium channel NaV1.7 associated with peripheral pain and impaired limb development". In: *J. Biol. Chem* 292.22 (June 2017), pp. 9262–9272. ISSN: 1083351X. DOI: 10.1074/jbc.M117.778779.

[58] Catharina G. Faber et al. "Gain-of-function Nav1.8 mutations in painful neuropathy". In: *PNAS* 109.47 (Nov. 2012), pp. 19444–19449. ISSN: 00278424. DOI: 10.1073/pnas.1216080109.

[59] Jianying Huang et al. "Gain-of-function mutations in sodium channel NaV1.9 in painful neuropathy". In: *Brain* 137.6 (2014), pp. 1627–1642. ISSN: 14602156. DOI: 10.1093/brain/awu079.

[60] Enrico Leipold et al. "A de novo gain-of-function mutation in SCN11A causes loss of pain perception". In: *Nat. Genet* 45.11 (Nov. 2013), pp. 1399–1407. ISSN: 10614036. DOI: 10.1038/ng.2767.

[61] Christopher Geoffrey Woods et al. "The phenotype of congenital insensitivity to pain due to the NaV 1.9 variant p.L811P". In: *Eur. J. Hum. Genet* 23.5 (May 2015), pp. 561–563. ISSN: 14765438. DOI: 10.1038/ejhg.2014.166.

[62] Yingsha Zhang et al. "Rapid single-step induction of functional neurons from human pluripotent stem cells". In: *Neuron* 78.5 (2013), pp. 785–798. ISSN: 08966273. DOI: 10.1016/j.neuron.2013.05.029.

[63] Elizabeth J Akin et al. "Building sensory axons: Delivery and distribution of Na V 1.7 channels and effects of inflammatory mediators". In: *Sci. Adv* 5 (2019), pp. 4755–4778.

[64] Liting Sun et al. “Nav1.7 and Nav1.8 form supramolecular active clusters with TRKB in mouse and human DRG neurons during development of neuropathic pain”. In: *MedRxiv* (Nov. 2022). DOI: 10.1101/2022.11.05.22281929.

[65] Grant P. Higerd-Rusli et al. “The fates of internalized NaV1.7 channels in sensory neurons: Retrograde cotransport with other ion channels, axon-specific recycling, and degradation”. In: *J. Biol. Chem* 299.1 (Jan. 2023). ISSN: 1083351X. DOI: 10.1016/j.jbc.2022.102816.

[66] William D Snider and Inmaculada Silos-Santiago. “Dorsal root ganglion neurons require functional neurotrophin receptors for survival during development”. In: *Phil. Trans. R. Soc. Lond.* 351 (1996), pp. 395–403.

[67] Yunfu Sun et al. “A central role for Islet1 in sensory neuron development linking sensory and spinal gene regulatory programs”. In: *Nat. Neurosci* 11.11 (Nov. 2008), pp. 1283–1293. ISSN: 10976256. DOI: 10.1038/nn.2209.

[68] Subham Seal and Anne H. Monsoro-Burq. “Insights Into the Early Gene Regulatory Network Controlling Neural Crest and Placode Fate Choices at the Neural Border”. In: *Front. Physiol* 11 (Nov. 2020). ISSN: 1664042X. DOI: 10.3389/fphys.2020.608812.

[69] Ramiro D. Almeida and Carlos B. Duarte. “p75NTR processing and signaling: Functional role”. In: *Handbook of Neurotoxicity*. Vol. 3. Springer New York, Jan. 2014, pp. 1899–1923. ISBN: 9781461458364. DOI: 10.1007/978-1-4614-5836-4{_}25.

[70] Parinaz Bina et al. “Neurogenin 2 and Neuronal Differentiation 1 Control Proper Development of the Chick Trigeminal Ganglion and Its Nerve Branches”. In: *J. Dev. Biol* 11.1 (Mar. 2023). ISSN: 22213759. DOI: 10.3390/jdb11010008.

[71] Qiufu Ma et al. “NEUROGENIN1 and NEUROGENIN2 control two distinct waves of neurogenesis in developing dorsal root ganglia”. In: *Genes Dev* 13 (1999), pp. 1717–1728. URL: www.genesdev.org.

[72] Mariela Zirlinger et al. “Transient expression of the bHLH factor neurogenin-2 marks a subpopulation of neural crest cells biased for a sensory but not a neuronal fate”. In: *PNAS* 99.12 (2002), pp. 8084–8089.

[73] Tian Lu et al. “Decoding transcriptional identity in developing human sensory neurons and organoid modeling”. In: *Cell* 187 (Nov. 2024), pp. 1–20. ISSN: 00928674. DOI: 10.1016/j.cell.2024.10.023.

[74] Iain M Dykes et al. “Brn3a regulates neuronal subtype specification in the trigeminal ganglion by promoting Runx expression during sensory differentiation”. In: *Neural Dev* 5.3 (2010).

[75] Iain M Dykes et al. “Brn3a and Islet1 Act Epistatically to Regulate the Gene Expression Program of Sensory Differentiation”. In: *J. Neurosci* 31.27 (July 2011), p. 9789. DOI: 10.1523/JNEUROSCI.0901-11.2011.

[76] Ken Ichi Inoue, Takashi Shiga, and Yoshiaki Ito. “Runx transcription factors in neuronal development”. In: *Neural Dev* 3.1 (2008). ISSN: 17498104. DOI: 10.1186/1749-8104-3-20.

[77] Ditsa Levaneon et al. “The Runx3 transcription factor regulates development and survival of TrkC dorsal root ganglia neurons”. In: *EMBO* 21.13 (2002), pp. 3454–3463.

[78] Min Zou et al. “Brn3a/Pou4f1 regulates dorsal root ganglion sensory neuron specification and axonal projection into the spinal cord”. In: *Dev. Biol* 364.2 (Apr. 2012), pp. 114–127. ISSN: 1095564X. DOI: 10.1016/j.ydbio.2012.01.021.

[79] Ina Kramer et al. “A role for Runx transcription factor signaling in dorsal root ganglion sensory neuron diversification”. In: *Neuron* 49.3 (Feb. 2006), pp. 379–393. ISSN: 08966273. DOI: 10.1016/j.neuron.2006.01.008.

[80] Jessica M. Rosin, Deborah M. Kurrasch, and John Cobb. “Shox2 is required for the proper development of the facial motor nucleus and the establishment of the facial nerves”. In: *BMC Neurosci* 16.1 (July 2015). ISSN: 14712202. DOI: 10.1186/s12868-015-0176-0.

[81] Alexandra Scott et al. “Transcription factor short stature homeobox 2 is required for proper development of tropomyosin-related kinase B-expressing mechanosensory neurons”. In: *J. Neurosci* 31.18 (May 2011), pp. 6741–6749. ISSN: 02706474. DOI: 10.1523/JNEUROSCI.5883-10.2011.

[82] Nikolai E. Lazarov. *Neurobiology of orofacial proprioception*. Dec. 2007. DOI: 10.1016/j.brainresrev.2007.08.009.

[83] Clare V.H. Baker, Michael R. Stark, and Marianne Bronner-Fraser. “Pax3-expressing trigeminal placode cells can localize to trunk neural crest sites but are committed to a cutaneous sensory neuron fate”. In: *Dev. Biol* 249.2 (2002), pp. 219–236. ISSN: 00121606. DOI: 10.1006/dbio.2002.0767.

[84] Luca Bartesaghi et al. “PRDM12 Is Required for Initiation of the Nociceptive Neuron Lineage during Neurogenesis”. In: *Cell Rep* 26.13 (Mar. 2019), pp. 3484–3492. ISSN: 22111247. DOI: 10.1016/j.celrep.2019.02.098.

[85] Simon Desiderio et al. “Prdm12 Directs Nociceptive Sensory Neuron Development by Regulating the Expression of the NGF Receptor TrkA”. In: *Cell Rep* 26.13 (Mar. 2019), pp. 3522–3536. ISSN: 22111247. DOI: 10.1016/j.celrep.2019.02.097.

[86] Teresa Valdés-Sánchez et al. “BDNF is essentially required for the early postnatal survival of nociceptors”. In: *Dev. Biol* 339.2 (Mar. 2010), pp. 465–476. ISSN: 1095564X. DOI: 10.1016/j.ydbio.2010.01.001.

[87] Chih Li Chen et al. “Runx1 determines nociceptive sensory neuron phenotype and is required for thermal and neuropathic pain”. In: *Neuron* 49.3 (Feb. 2006), pp. 365–377. ISSN: 08966273. DOI: 10.1016/j.neuron.2005.10.036.

[88] Qiufu Ma. “A functional subdivision within the somatosensory system and its implications for pain research”. In: *Neuron* 110.5 (2022), pp. 749–769. ISSN: 10974199. DOI: 10.1016/j.neuron.2021.12.015.

[89] Azusa Kobayashi et al. “Runx1 promotes neuronal differentiation in dorsal root ganglion”. In: *Mol. Cell. Neurosci* 49.1 (2012), pp. 23–31. ISSN: 10447431. DOI: 10.1016/j.mcn.2011.08.009.

[90] Eduardo Gascon et al. “Hepatocyte growth factor-met signaling is required for Runx1 extinction and peptidergic differentiation in primary nociceptive neurons”. In: *J. Neurosci* 30.37 (Sept. 2010), pp. 12414–12423. ISSN: 02706474. DOI: 10.1523/JNEUROSCI.3135-10.2010.

[91] Lilian N. Nwosu et al. “Blocking the tropomyosin receptor kinase A (TrkA) receptor inhibits pain behaviour in two rat models of osteoarthritis”. In: *Ann Rheum Dis* 75.6 (2016), pp. 554–561. ISSN: 14682060. DOI: 10.1136/annrheumdis-2014-207203.

[92] Nancy E. Lane et al. “Tanezumab for the Treatment of Pain from Osteoarthritis of the Knee”. In: *NEJM* 363.16 (Oct. 2010), pp. 1521–1531. ISSN: 0028-4793. DOI: 10.1056/nejmoa0901510.

[93] Panna Sanga et al. “Efficacy, safety, and tolerability of fulranumab, an anti-nerve growth factor antibody, in the treatment of patients with moderate to severe osteoarthritis pain”. In: *Pain* 154.10 (2013). ISSN: 0304-3959.

[94] Paul J Tiseo et al. “Fasinumab (REGN475), an antibody against nerve growth factor for the treatment of pain: Results from a double-blind, placebo-controlled exploratory study in osteoarthritis of the knee”. In: *Pain* 155.7 (2014). ISSN: 0304-3959.

[95] Eva M. Sánchez-Robles et al. “Monoclonal antibodies for chronic pain treatment: Present and future”. In: *Int. J. Mol. Sci* 22.19 (Oct. 2021). ISSN: 14220067. DOI: 10.3390/ijms221910325.

[96] X. Q. Shu, A Llinas, and L M Mendell. “Effects of trkB and trkC neurotrophin receptor agonists on thermal nociception: a behavioral and electrophysiological study”. In: *Pain* 80 (1999), pp. 463–470.

[97] Jing Zhao et al. “Nociceptor-derived brain-derived neurotrophic factor regulates acute and inflammatory but not neuropathic pain”. In: *Mol. Cell. Neurosci* 31.3 (Mar. 2006), pp. 539–548. ISSN: 10447431. DOI: 10.1016/j.mcn.2005.11.008.

[98] Xian Bin Wang et al. “A novel primary culture method for high-purity satellite glial cells derived from rat dorsal root ganglion”. In: *Neural Regen. Res* 14.2 (2019), pp. 339–345. ISSN: 18767958. DOI: 10.4103/1673-5374.244797.

[99] Rachel Wilson et al. “Human peptidergic nociceptive sensory neurons generated from human epidermal neural crest stem cells (hEPI-NCSC)”. In: *PLoS ONE* 13.6 (2018), pp. 1–18. ISSN: 19326203. DOI: 10.1371/journal.pone.0199996.

[100] Susan M. Carlton. “Nociceptive primary afferents: They have a mind of their own”. In: *J. Physio.* 592.16 (2014), pp. 3403–3411. ISSN: 14697793. DOI: 10.1113/jphysiol.2013.269654.

[101] Andrew F. Russo. “Overview of Neuropeptides: Awakening the Senses?” In: *Headache* 57 (May 2017), pp. 37–46. ISSN: 15264610. DOI: 10.1111/head.13084.

[102] Ji Song Guan et al. “Interaction with vesicle luminal protachykinin regulates surface expression of δ-opioid receptors and opioid analgesia”. In: *Cell* 122.4 (Aug. 2005), pp. 619–631. ISSN: 00928674. DOI: 10.1016/j.cell.2005.06.010.

[103] Chiara Salio et al. “Neuropeptides as synaptic transmitters”. In: *Cell Tissue Res* 326.2 (Nov. 2006), pp. 583–598. ISSN: 0302766X. DOI: 10.1007/s00441-006-0268-3.

[104] Michael P. Nusbaum, Dawn M. Blitz, and Eve Marder. “Functional consequences of neuropeptide and small-molecule co-transmission”. In: *Nat. Rev. Neurosci* 18.7 (July 2017), pp. 389–403. ISSN: 14710048. DOI: 10.1038/nrn.2017.56.

[105] Adalberto Merighi. “Costorage of high molecular weight neurotransmitters in large dense core vesicles of mammalian neurons”. In: *Front. Cell. Neurosci* 12 (Aug. 2018). ISSN: 16625102. DOI: 10.3389/fncel.2018.00272.

[106] Jacqueline A Sobota et al. “Dynamics of peptidergic secretory granule transport are regulated by neuronal stimulation”. In: *BMC Neurosci* 11.32 (2010). URL: http://www.biomedcentral.com/1471-2202/11/32.

[107] Isabel Devesa et al. “αCGRP is essential for algesic exocytotic mobilization of TRPV1 channels in peptidergic nociceptors”. In: *PNAS* 111.51 (Dec. 2014), pp. 18345–18350. ISSN: 10916490. DOI: 10.1073/pnas.1420252111.

[108] Bo Zhao et al. “Transport of receptors, receptor signaling complexes and ion channels via neuropeptide-secretory vesicles”. In: *Cell Res* 21.5 (May 2011), pp. 741–753. ISSN: 10010602. DOI: 10.1038/cr.2011.29.

[109] Felipe A. Pinho-Ribeiro, Waldiceu A. Verri, and Isaac M. Chiu. “Nociceptor Sensory NeuronâImmune Interactions in Pain and Inflammation”. In: *Trends Immunol* 38.1 (Jan. 2017), pp. 5–19. ISSN: 14714981. DOI: 10.1016/j.it.2016.10.001.

[110] Ali H. Shaib et al. “Paralogs of the calcium-dependent activator protein for secretion differentially regulate synaptic transmission and peptide secretion in sensory neurons”. In: *Front. Cell. Neurosci* 12 (Sept. 2018). ISSN: 16625102. DOI: 10.3389/fncel.2018.00304.

[111] F A Russell et al. “Calcitonin Gene-Related Peptide: Physiology and Pathophysiology”. In: *Physiol Rev* 94 (2014), pp. 1099–1142. DOI: 10.1152/physrev.00034.2013.-Calcitonin.

[112] H Kashiba, Y Ueda, and E Senbat. “Coexpression of preprorachykinin-A, ð¼-calcitonin gene-related peptide, somatostatin, and neurotrophin receptor family messenger RNAs in rat dorsal root ganglion neurons”. In: *Neuroscience* 70.1 (1996), pp. 179–189.

[113] I. L Gibbins et al. “Co-localization of calcitonin gene-related peptide-like immunoreactivity with Substance P in cutaneous, vascular and visceral sensory neurons of guinea pigs”. In: *Neurosci. Lett* 57 (1985), pp. 125–130.

[114] Y Lee et al. “Coexistence of calcitonin gene-related peptide and substance P-like peptide in single cells of the trigeminal ganglion of the rat: immunohistochemical analysis”. In: *Brain Res* 330 (1985), pp. 194–196.

[115] Gerhard Skofitsch and David M Jacobowitz. “Calcitonin Gene-Related Peptide Coexists With Substance P in Capsaicin Sensitive Neurons and Sensory Ganglia of the Rat”. In: *Peptides* 6 (1985), pp. 747–754.

[116] Marina Del Fiacco and Marina Quartu. “Somatostatin, galanin and peptide histidine isoleucine in the newborn and adult human trigeminal ganglion and spinal nucleus:

immunohistochemistry, neuronal morphometry and colocalization with substance P". In: *J. Chem. Neuroanat* 7 (1994), pp. 171–184.

[117] Sofia Lyng Wæver and Kristian Agmund Haanes. "Differentially localizing isoforms of the migraine component calcitonin gene-related peptide (CGRP), in the mouse trigeminal ganglion: βCGRP is translated but, unlike αCGRP, not sorted into axons". In: *J. Headache Pain* 26.1 (Dec. 2025), p. 11. ISSN: 11292377. DOI: 10.1186/s10194-024-01945-6.

[118] L Holford, P Case, and S Lawson. "Substance P (SP), neurofilament (NF), peripherin (PER) and SSEA4 immunocytochemistry of human dorsal root ganglion (DRG) neurones obtained from post-mortem tissue: A quantitative analysis". In: *J. Physiol* 473 (1993), p. 128. ISSN: 0022-3751.

[119] Maria Prośba-Mackiewicz, Albina Ółtowska, and Jerzy Dziewiątkowski. "Substance-P of neural cells in human trigeminal ganglion". In: *Folia Morphol* 59.4 (2000), pp. 327–331. ISSN: 0015-5659. URL: www.fm.viamedica.pl.

[120] Caroline Perner et al. "Substance P Release by Sensory Neurons Triggers Dendritic Cell Migration and Initiates the Type-2 Immune Response to Allergens". In: *Immunity* 53.5 (Nov. 2020), pp. 1063–1077. ISSN: 10974180. DOI: 10.1016/j.immuni.2020.10.001.

[121] Alireza Mashaghi et al. "Neuropeptide substance P and the immune response". In: *Cell Mol. Life Sci* 73.22 (June 2016), pp. 4249–4264. ISSN: 14209071. DOI: 10.1007/s00018-016-2293-z.

[122] W. Zieglgänsberger. "Substance P and pain chronicity". In: *Cell Tissue Res* 375.1 (Jan. 2019), pp. 227–241. ISSN: 14320878. DOI: 10.1007/s00441-018-2922-y.

[123] Late N Jancsó, Aurelia Jancsó-Gábor, and J Szolcsányi. "Direct evidence for neurogenic inflammation and its prevention by denervation and by pretreatment with capsaicin". In: *Br. J. Pharmac. Chemother* 31 (1967), pp. 138–151.

[124] Smriti Iyengar, Michael H. Ossipov, and Kirk W. Johnson. "The role of calcitonin gene-related peptide in peripheral and central pain mechanisms including migraine".

In: *Pain* 158.4 (Apr. 2017), pp. 543–559. ISSN: 18726623. DOI: 10.1097/j.pain.0000000000000831.

[125] Dustin P. Green et al. "A Mast-Cell-Specific Receptor Mediates Neurogenic Inflammation and Pain". In: *Neuron* 101.3 (Feb. 2019), pp. 412–420. ISSN: 10974199. DOI: 10.1016/j.neuron.2019.01.012.

[126] D. B. Carr and A. W. Lipkowski. "Neuropeptides and pain". In: *Agressologie* 31.4 (1990), pp. 173–177. ISSN: 00021148. DOI: 10.1186/1744-859x-9-s1-s3.

[127] Peter J. Goadsby et al. "A Controlled Trial of Erenumab for Episodic Migraine". In: *NEJM* 377.22 (Nov. 2017), pp. 2123–2132. ISSN: 0028-4793. DOI: 10.1056/nejmoa1705848.

[128] Renato Oliveira, Raquel Gil-Gouveia, and Francesca Puledda. "CGRP-targeted medication in chronic migraine - systematic review". In: *J. Headache Pain* 25.1 (Apr. 2024), p. 51. ISSN: 1129-2377. DOI: 10.1186/s10194-024-01753-y.

[129] Stephen D. Silberstein et al. "Fremanezumab for the Preventive Treatment of Chronic Migraine". In: *NEJM* 377.22 (Nov. 2017), pp. 2113–2122. ISSN: 0028-4793. DOI: 10.1056/nejmoa1709038.

[130] Ray Hill. "NK1 (substance P) receptor antagonists â why are they not analgesic in humans?" In: *TiPs* 21.7 (2000), pp. 244–246. DOI: 10.1016/s0165-6147(00)01502-9.

[131] Arthur E Frankel et al. "Preliminary results from a phase I study of substance P-saporin in terminal cancer patients with intractable pain". eng. In: *Journal of clinical oncology* 32.31_suppl (2014), p. 191. ISSN: 0732-183X.

[132] Donald Iain MacDonald et al. "Pain persists in mice lacking both Substance P and CGRPα signaling". In: *eLife* 13 (Mar. 2025). DOI: 10.7554/elife.93754.

[133] Monika Liguz-Lecznar, Joanna Urban-Ciecko, and Malgorzata Kossut. "Somatostatin and somatostatin-containing neurons in shaping neuronal activity and plasticity". In: *Front. Neural Circuits* 10 (June 2016). ISSN: 16625110. DOI: 10.3389/fncir.2016.00048.

[134] Jeffrey B Malick and Jeffrey M Goldstein. *ANALGESIC ACTIVITY OF SUBSTANCE P FOLLOp1ING INTRACEREBRAL ADMINISTRATION IN RAT 1 S*. Tech. rep. 1978, pp. 835–844.

[135] Janice L K Hylden and George L Wilcox. *Intrathecal substance P elicits a caudally-directed biting and scratching behavior in mice*. Tech. rep. 1981, pp. 212–215.

[136] Gabor Petho et al. "Evidence for a novel, neurohumoral antinociceptive mechanism mediated by peripheral capsaicin-sensitive nociceptors in conscious rats". In: *Neuropeptides* 62 (Apr. 2017), pp. 1–10. ISSN: 15322785. DOI: 10.1016/j.npep.2017.02.079.

[137] Janos Szolcsányi et al. "Release of somatostatin and its role in the mediation of the anti-inflammatory effect induced by antidromic stimulation of sensory fibres of rat sciatic nerve". In: *Br. J. Pharmacol* 123 (1998), pp. 936–942.

[138] Janos Szolcsányi et al. "Systemic anti-inflammatory effect induced by counter-irritation through a local release of somatostatin from nociceptors". In: *Br. J. Pharmacol* 125.4 (1998), pp. 916–922. ISSN: 00071188. DOI: 10.1038/sj.bjp.0702144.

[139] Tie-Jun Sten Shi et al. "Somatostatin and its 2A receptor in dorsal root ganglia and dorsal horn of mouse and human: expression, trafficking and possible role in pain". In: *Mol. Pain* 10.12 (2014). ISSN: 17448069. DOI: 10.1186/1744-8069-8-9.

[140] Zsuzsanna Helyes et al. "Impaired defense mechanism against inflammation, hyperalgesia, and airway hyperreactivity in somatostatin 4 receptor gene-deleted mice". In: *PNAS* 106.31 (2009).

[141] BoglÃ¡rka Kántás et al. "Novel drug-like somatostatin receptor 4 agonists are potential analgesics for neuropathic pain". In: *Int. J. Mol. Sci* 20.24 (Dec. 2019). ISSN: 14220067. DOI: 10.3390/ijms20246245.

[142] Ãva Szőke et al. "Small molecule somatostatin receptor subtype 4 (sst4) agonists are novel anti-inflammatory and analgesic drug candidates". In: *Neuropharmacology* 178 (Nov. 2020). ISSN: 18737064. DOI: 10.1016/j.neuropharm.2020.108198.

[143] Zhiyun Zhang et al. “Understanding of Spinal Wide Dynamic Range Neurons and Their Modulation on Pathological Pain”. In: *J. Pain Res* 17 (2024), pp. 441–457. ISSN: 11787090. DOI: 10.2147/JPR.S446803.

[144] Ronald Melzack and Patrick D Wall. “Pain Mechanisms: A New Theory A gate control system modulates sensory input from the skin before it evokes pain perception and response”. In: *Novenlber* 150 (1965), p. 3699. URL: https://www.science.org.

[145] Massieh Moayedi and Karen D. Davis. “Theories of pain: From specificity to gate control”. In: *J. Neurophysiol* 109.1 (2013), pp. 5–12. ISSN: 00223077. DOI: 10.1152/jn.00457.2012.

[146] Hanns Ulrich Zeilhofer, Hendrik Wildner, and Gonzalo E. Yévenes. “Fast synaptic inhibition in spinal sensory processing and pain control”. In: *Physiol. Rev* 92.1 (Jan. 2012), pp. 193–235. ISSN: 00319333. DOI: 10.1152/physrev.00043.2010.

[147] Christopher J Garrison, Patrick M Dougherty, and Susan M Carlton. “GFAP Expression in Lumbar Spinal Cord of Naive and Neuropathic Rats Treated with MK-801”. In: *Exp. Neurol* 129 (1994), pp. 237–243.

[148] P Honore et al. “Murine Models of Inflammatory, Neuropathic and Cancer Pain Each Generates A Unique Set of Neurochemical Changes in the Spinal Cord and Sensory Neurons”. In: *Neuroscience* 98.3 (2000), pp. 585–598. URL: www.elsevier.com/locate/neuroscience.

[149] Ru Rong Ji, Temugin Berta, and Maiken Nedergaard. “Glia and pain: Is chronic pain a gliopathy?” In: *Pain*. Vol. 154. SUPPL. 1. Elsevier B.V., 2013. DOI: 10.1016/j.pain.2013.06.022.

[150] E C Urch, T Donovan-Rodriguez, and H A Dickenson. “Alterations in dorsal horn neurones in a rat model of cancer-induced bone pain”. In: *Pain* 106.3 (2003). ISSN: 0304-3959.

[151] Laila J. Zai and Jean R. Wrathall. “Cell proliferation and replacement following contusive spinal cord injury”. In: *GLIA* 50.3 (May 2005), pp. 247–257. ISSN: 08941491. DOI: 10.1002/glia.20176.

[152] Hiroshi Baba et al. “Removal of GABAergic inhibition facilitates polysynaptic A fiber-mediated excitatory transmission to the superficial spinal dorsal horn”. In: *Mol. Cell. Neurosci* 24.3 (2003), pp. 818–830. ISSN: 10447431. DOI: 10.1016/S1044-7431(03)00236-7.

[153] Jing Cao et al. “GABAergic disinhibition induced pain hypersensitivity by upregulating NMDA receptor functions in spinal dorsal horn”. In: *Neuropharmacology* 60.6 (May 2011), pp. 921–929. ISSN: 00283908. DOI: 10.1016/j.neuropharm.2011.01.034.

[154] Qiaochu Fu et al. “MHC-I promotes apoptosis of GABAergic interneurons in the spinal dorsal horn and contributes to cancer induced bone pain”. In: *Exp. Neurol* 286 (Dec. 2016), pp. 12–20. ISSN: 10902430. DOI: 10.1016/j.expneurol.2016.09.002.

[155] Luke A. Henderson et al. “Chronic pain: Lost inhibition?” In: *J. Neurosci* 33.17 (Apr. 2013), pp. 1754–1782. ISSN: 02706474. DOI: 10.1523/JNEUROSCI.0174-13.2013.

[156] Thang M Khuong et al. “Nerve injury drives a heightened state of vigilance and neuropathic sensitization in Drosophila”. In: *Sci. Adv* 5 (2019), pp. 4099–4109.

[157] Alban Latremoliere and Clifford J. Woolf. “Central Sensitization: A Generator of Pain Hypersensitivity by Central Neural Plasticity”. In: *J. Pain* 10.9 (Sept. 2009), pp. 895–926. ISSN: 15265900. DOI: 10.1016/j.jpain.2009.06.012.

[158] Jason G Meisner, Adam D Marsh, and Daniel R Marsh. “Loss of GABAergic Interneurons in Laminae I-III of the Spinal Cord Dorsal Horn Contributes to Reduced GABAergic Tone and Neuropathic Pain after Spinal Cord Injury”. In: *J. Neurotrauma* 27.4 (2010), pp. 729–737. DOI: 10.1089/neu.2009.1166.

[159] Kimberly A Moore et al. “Partial Peripheral Nerve Injury Promotes a Selective Loss of GABAergic Inhibition in the Superficial Dorsal Horn of the Spinal Cord”. In: *J. Neurosci* 22.15 (2002).

[160] Steven A. Prescott. “Synaptic inhibition and disinhibition in the spinal dorsal horn”. In: *Prog. Mol. Biol. Transl. Sci* 131 (2015), pp. 359–383. ISSN: 18780814. DOI: 10.1016/bs.pmbts.2014.11.008.

[161] Zhi Zhang et al. “Epigenetic suppression of GAD65 expression mediates persistent pain”. In: *Nat. Med* 17.11 (Nov. 2011), pp. 1448–1455. ISSN: 10788956. DOI: 10.1038/nm.2442.

[162] Tyler J. Browne et al. “Projection Neuron Axon Collaterals in the Dorsal Horn: Placing a New Player in Spinal Cord Pain Processing”. In: *Front. Physiol* 11 (Dec. 2020). ISSN: 1664042X. DOI: 10.3389/fphys.2020.560802.

[163] Wafa A.A. Alsulaiman et al. “Characterisation of lamina I anterolateral system neurons that express Cre in a Phox2a-Cre mouse line”. In: *Sci. Rep* 11.1 (2021), pp. 1–18. ISSN: 20452322. DOI: 10.1038/s41598-021-97105-w. URL: https://doi.org/10.1038/s41598-021-97105-w.

[164] Marie Rose Hirsch et al. “Forced expression of Phox2 homeodomain transcription factors induces a branchio-visceromotor axonal phenotype”. In: *Dev. Biol* 303.2 (2007), pp. 687–702. ISSN: 00121606. DOI: 10.1016/j.ydbio.2006.12.006.

[165] R. Brian Roome et al. “Phox2a Defines a Developmental Origin of the Anterolateral System in Mice and Humans”. In: *Cell Rep* 33.8 (2020). ISSN: 22111247. DOI: 10.1016/j.celrep.2020.108425.

[166] Racheli Wercberger et al. “Pain and itch processing by subpopulations of molecularly diverse spinal and trigeminal projection neurons”. In: *PNAS* 118.28 (2021), pp. 1–12. ISSN: 10916490. DOI: 10.1073/pnas.2105732118.

[167] Pere Boadas-Vaello et al. “Neuroplasticity of Supraspinal Structures Associated with Pathological Pain”. In: *Anat. Rec* 300.8 (Aug. 2017), pp. 1481–1501. ISSN: 19328494. DOI: 10.1002/ar.23587.

[168] Che Badariah Ab Aziz and Asma Hayati Ahmad. “The role of the thalamus in modulating pain”. In: *Malays. J. Med. Sci* 13.2 (2006).

[169] Daria Andreeva et al. “Satellite Glial Cells: Morphology, functional heterogeneity, and role in pain”. In: *Front. Cell. Neurosci* 16 (2022). ISSN: 16625102. DOI: 10.3389/fncel.2022.1019449.

[170] Pauline Meriau, Rejji Kuruvilla, and Valeria Cavalli. “Satellite glial cells: Shaping peripheral input into the brain-body axis?” In: *Neuron* 113 (2025). ISSN: 10974199. DOI: 10.1016/j.neuron.2025.05.031.

[171] Menachem Hanani and David C. Spray. “Emerging importance of satellite glia in nervous system function and dysfunction”. In: *Nat. Rev. Neurosci* 21.9 (2020), pp. 485–498. ISSN: 14710048. DOI: 10.1038/s41583-020-0333-z. URL: http://dx.doi.org/10.1038/s41583-020-0333-z.

[172] Artem Sinegubov et al. “Heterogeneity and Potency of Peripheral Glial Cells in Embryonic Development and Adults”. In: *Front. Mol. Neurosci* 15.March (2022). ISSN: 16625099. DOI: 10.3389/fnmol.2022.737949.

[173] Aurelia A. Mapps et al. “Diversity of satellite glia in sympathetic and sensory ganglia”. In: *Cell Rep* 38.5 (Feb. 2022). ISSN: 22111247. DOI: 10.1016/j.celrep.2022.110328.

[174] Ole A. Ahlgreen et al. “Mapping satellite glial cell heterogeneity reveals distinct spatial organization and signifies functional diversity in the dorsal root ganglion”. In: *BioRxiv* (May 2025). DOI: 10.1101/2025.05.19.654813.

[175] Parisa Gazerani. “Satellite Glial Cells in Pain Research: A Targeted Viewpoint of Potential and Future Directions”. In: *Front. Pain Res* 2 (2021). ISSN: 2673561X. DOI: 10.3389/fpain.2021.646068.

[176] Breanne L. Harty and Kelly R. Monk. “Unwrapping the unappreciated: recent progress in Remak Schwann cell biology”. In: *Curr. Opin. Neurobiol* 47 (Dec. 2017), pp. 131–137. ISSN: 18736882. DOI: 10.1016/j.conb.2017.10.003.

[177] Carla Taveggia and M Laura Feltri. “Beyond Wrapping: Canonical and Noncanonical Functions of Schwann Cells”. In: *Annu. Rev. Neurosci* 45 (2022), pp. 561–580. DOI: 10.1146/annurev-neuro-110920.

[178] Wendy Marie Campana. “Schwann cells: activated peripheral glia and their role in neuropathic pain”. In: *Brain Behav. Immun* 21.5 (July 2007), pp. 522–527.

[179] Ruth M. Stassart, Jose A. Gomez-Sanchez, and Alison C. Lloyd. “Schwann Cells as Orchestrators of Nerve Repair: Implications for Tissue Regeneration and Pathologies”. In: *Cold Spring Harb. Perspect. Biol* 16.6 (June 2024). ISSN: 19430264. DOI: 10.1101/cshperspect.a041363.

[180] Joseph S. Takahashi. “Transcriptional architecture of the mammalian circadian clock”. In: *Nat. Rev. Genet* 18.3 (2017), pp. 164–179. ISSN: 14710064. DOI: 10.1038/nrg.2016.150.

[181] Yoichi Minami, Koji L Ode, and Hiroki R Ueda. “Mammalian Circadian Clock: The Roles of Transcriptional Repression and Delay”. In: *Circadian Clocks*. Ed. by Achim Kramer and Martha Merrow. Berlin, Heidelberg: Springer Berlin Heidelberg, 2013, pp. 359–377. ISBN: 978-3-642-25950-0. DOI: 10.1007/978-3-642-25950-0{_}15.

[182] Yanrong Zhuang et al. “Circadian clocks are modulated by compartmentalized oscillating translation”. In: *Cell* (June 2023). ISSN: 00928674. DOI: 10.1016/j.cell.2023.05.045.

[183] Monica Gallego and David M. Virshup. “Post-translational modifications regulate the ticking of the circadian clock”. In: *Nat. Rev. Mol. Cell Biol* 8.2 (Feb. 2007), pp. 139–148. ISSN: 14710072. DOI: 10.1038/nrm2106.

[184] Arisa Hirano, Ying Hui Fu, and Louis J. Ptáek. “The intricate dance of post-translational modifications in the rhythm of life”. In: *Nat. Struct. Mol. Biol* 23.12 (Dec. 2016), pp. 1053–1060. ISSN: 15459985. DOI: 10.1038/nsmb.3326.

[185] Jason P. DeBruyne, David R. Weaver, and Steven M. Reppert. “CLOCK and NPAS2 have overlapping roles in the suprachiasmatic circadian clock”. In: *Nat. Neurosci.* 10.5 (May 2007), pp. 543–545. ISSN: 10976256. DOI: 10.1038/nn1884.

[186] Genevieve Konopka et al. “Human-Specific Transcriptional Networks in the Brain”. In: *Neuron* 75.4 (Aug. 2012), pp. 601–617. ISSN: 08966273. DOI: 10.1016/j.neuron.2012.05.034.

[187] Miles R. Fontenot et al. “Novel transcriptional networks regulated by clock in human neurons”. In: *Genes Dev* 31.21 (Nov. 2017), pp. 2121–2135. ISSN: 15495477. DOI: 10.1101/gad.305813.117.

[188] Hiroki R. Ueda et al. “A transcription factor response element for gene expression during circadian night”. In: *Nature* 418.6897 (Aug. 2002), pp. 534–539. ISSN: 0028-0836. DOI: 10.1038/nature00906.

[189] Yasuko O. Abe et al. “Rhythmic transcription of Bmal1 stabilizes the circadian timekeeping system in mammals”. In: *Nat. Commun* 13.1 (2022). ISSN: 20411723. DOI: 10.1038/s41467-022-32326-9.

[190] Takao Miki, Zhaoyang Zhao, and Cheng Chi Lee. “Interactive Organization of the Circadian Core Regulators PER2, BMAL1, CLOCK and PML”. In: *Sci. Rep* 6 (July 2016). ISSN: 20452322. DOI: 10.1038/srep29174.

[191] Jiwon Lee et al. “A splice variant of human Bmal1 acts as a negative regulator of the molecular circadian clock”. In: *Exp. Mol. Med* 50.12 (2018). ISSN: 20926413. DOI: 10.1038/s12276-018-0187-x.

[192] Maureen K Bunger et al. “Mop3 Is an Essential Component of the Master Circadian Pacemaker in Mammals”. In: *Cell* 103.7 (2000), pp. 1009–1017.

[193] Samreen N Haque, Sathwik R Booreddy, and David K Welsh. “Effects of BMAL1 Manipulation on the Brain’s Master Circadian Clock and Behavior”. In: *Yale J. Biol. Med* 92 (2019), pp. 251–258.

[194] Guangrui Yang et al. “Timing of expression of the core clock gene Bmal1 influences its effects on aging and survival”. In: *Sci. Transl. Med.* 8.324 (2016).

[195] Xiao Yu et al. “Circadian factor BMAL1 in histaminergic neurons regulates sleep architecture”. In: *Curr. Biol* 24.23 (Dec. 2014), pp. 2838–2844. ISSN: 18790445. DOI: 10.1016/j.cub.2014.10.019.

[196] Erin L. McDearmon et al. “Dissecting the functions of the mammalian clock protein BMAL1 by tissue-specific rescue in mice”. In: *Science* 314.5803 (Nov. 2006), pp. 1304–1308. ISSN: 00368075. DOI: 10.1126/science.1132430.

[197] Zhiwei Zhang et al. “PER2 binding to HSP90 enhances immune response against oral squamous cell carcinoma by inhibiting IKK/NF-κB pathway and PD-L1 expression”. In: *J. Immuno. Ther. Cancer* 11.11 (Nov. 2023). ISSN: 20511426. DOI: 10.1136/jitc-2023-007627.

[198] Afaf Akladious et al. “Bmal1 knockdown suppresses wake and increases immobility without altering orexin A, corticotrophin-releasing hormone, or glutamate decarboxylase”. In: *CNS Neurosci. Ther* 24.6 (June 2018), pp. 549–563. ISSN: 17555949. DOI: 10.1111/cns.12815.

[199] Erik S. Musiek et al. “Circadian clock proteins regulate neuronal redox homeostasis and neurodegeneration”. In: *J. Clin. Investig* 123.12 (Dec. 2013), pp. 5389–5400. ISSN: 00219738. DOI: 10.1172/JCI70317.

[200] Kaiden H. Price et al. “Modulation of learning and memory by the targeted deletion of the circadian clock gene Bmal1 in forebrain circuits”. In: *Behav. Brain Res* 308 (July 2016), pp. 222–235. ISSN: 18727549. DOI: 10.1016/j.bbr.2016.04.027.

[201] James O. Early et al. “Circadian clock protein BMAL1 regulates IL-1β in macrophages via NRF2”. In: *PNAS* 115.36 (Sept. 2018), E8460–E8468. ISSN: 10916490. DOI: 10.1073/pnas.1800431115.

[202] Laura E. Hand et al. “The circadian regulator Bmal1 in joint mesenchymal cells regulates both joint development and inflammatory arthritis”. In: *Arthritis Res. Ther* 21.1 (Jan. 2019). ISSN: 14786362. DOI: 10.1186/s13075-018-1770-1.

[203] Tongyu Li et al. “H. pylori infection induced BMAL1 expression and rhythm disorder aggravate gastric inflammation”. In: *EBioMedicine* 39 (Jan. 2019), pp. 301–314. ISSN: 23523964. DOI: 10.1016/j.ebiom.2018.11.043.

[204] Khoa D Nguyen et al. “Circadian Gene Bmal1 Regulates Diurnal Oscillations of Ly6C hi Inflammatory Monocytes”. In: *Science* 341 (2013), pp. 1483–1488.

[205] Yumiko Oishi et al. “Bmal1 regulates inflammatory responses in macrophages by modulating enhancer RNA transcription”. In: *Sci. Rep* 7.1 (Dec. 2017). ISSN: 20452322. DOI: 10.1038/s41598-017-07100-3.

[206] Kenneth A. Dyar et al. “Muscle insulin sensitivity and glucose metabolism are controlled by the intrinsic muscle clock”. In: *Mol. Metab* 3.1 (Feb. 2014), pp. 29–41. ISSN: 22128778. DOI: 10.1016/j.molmet.2013.10.005.

[207] Brendan M Gabriel et al. “Disrupted circadian oscillations in type 2 diabetes are linked to altered rhythmic mitochondrial metabolism in skeletal muscle”. In: *Sci. Adv* 7 (2021).

[208] Biliana Marcheva et al. “Disruption of the clock components CLOCK and BMAL1 leads to hypoinsulinaemia and diabetes”. In: *Nature* 466.7306 (July 2010), pp. 627–631. ISSN: 14764687. DOI: 10.1038/nature09253.

[209] R. Daniel Rudic et al. “BMAL1 and CLOCK, two essential components of the circadian clock, are involved in glucose homeostasis”. In: *PLoS Biol* 2.11 (Nov. 2004). ISSN: 15449173. DOI: 10.1371/journal.pbio.0020377.

[210] Rohini V Khapre et al. “BMAL1âdependent regulation of the mTOR signaling pathway delays aging”. In: *Aging* 6.1 (2014).

[211] Roman V. Kondratov et al. “Early aging and age-related pathologies in mice deficient in BMAL1, the core component of the circadian clock”. In: *Genes Dev* 20.14 (July 2006), pp. 1868–1873. ISSN: 08909369. DOI: 10.1101/gad.1432206.

[212] Daniela Rojo et al. “BMAL1 loss in oligodendroglia contributes to abnormal myelination and sleep”. In: *Neuron* 111.22 (Nov. 2023), pp. 3604–3618. ISSN: 10974199. DOI: 10.1016/j.neuron.2023.08.002.

[213] Dalia Halawani et al. “Circadian clock regulator Bmal1 gates axon regeneration via Tet3 epigenetics in mouse sensory neurons.” In: *Nat. Commun* 14.1 (Aug. 2023), p. 5165. ISSN: 2041-1723. DOI: 10.1038/s41467-023-40816-7.

[214] Ilaria Barone et al. “Synaptic BMAL1 phosphorylation controls circadian hippocampal plasticity”. In: *Sci. Adv* 9 (2023).

[215] Jonathan O. Lipton et al. “The circadian protein BMAL1 regulates translation in response to S6K1-mediated phosphorylation”. In: *Cell* 161.5 (May 2015), pp. 1138–1151. ISSN: 10974172. DOI: 10.1016/j.cell.2015.04.002.

[216] Dominic Landgraf et al. “Genetic Disruption of Circadian Rhythms in the Suprachiasmatic Nucleus Causes Helplessness, Behavioral Despair, and Anxiety-like Behavior in Mice”. In: *Biol. Psychiatry* 80.11 (Dec. 2016), pp. 827–835. ISSN: 18732402. DOI: 10.1016/j.biopsych.2016.03.1050.

[217] Peiyuan Qiu et al. “BMAL1 knockout macaque monkeys display reduced sleep and psychiatric disorders”. In: *Natl. Sci. Rev* 6 (2019), pp. 87–100. ISSN: 2053714X. DOI: 10.1093/nsr/nwz002.

[218] Douglas M. Ruderfer et al. “Genomic Dissection of Bipolar Disorder and Schizophrenia, Including 28 Subphenotypes”. In: *Cell* 173.7 (June 2018), pp. 1705–1715. ISSN: 10974172. DOI: 10.1016/j.cell.2018.05.046.

[219] S. Yang et al. “Assessment of circadian function in fibroblasts of patients with bipolar disorder”. In: *Mol. Psychiatry* 14.2 (Feb. 2009), pp. 143–155. ISSN: 13594184. DOI: 10.1038/mp.2008.10.

[220] Tomas Petrasek et al. “The McGill Transgenic Rat Model of Alzheimer’s Disease Displays Cognitive and Motor Impairments, Changes in Anxiety and Social Behavior, and Altered Circadian Activity”. In: *Front. Aging Neurosci* 10 (Aug. 2018). ISSN: 16634365. DOI: 10.3389/fnagi.2018.00250.

[221] Y. Cai et al. “Expression of clock genes Per1 and Bmal1 in total leukocytes in health and Parkinson’s disease”. In: *Eur. J. Neurol* 17.4 (Apr. 2010), pp. 550–554. ISSN: 13515101. DOI: 10.1111/j.1468-1331.2009.02848.x.

[222] Ying Hui Wu et al. “Pineal clock gene oscillation is disturbed in Alzheimer’s disease, due to functional disconnection from the âmaster clockâ”. In: *FASEB* 20.11 (Sept. 2006), pp. 1874–1876. ISSN: 0892-6638. DOI: 10.1096/fj.05-4446fje.

[223] Yin Jiang et al. “Critical Roles of the Circadian Transcription Factor BMAL1 in Reproductive Endocrinology and Fertility”. In: *Front. Endocrinol* 13 (Mar. 2022). ISSN: 16642392. DOI: 10.3389/fendo.2022.818272.

[224] Christine K. Ratajczak, Katie L. Boehle, and Louis J. Muglia. “Impaired steroidogenesis and implantation failure in Bmal1 -/-mice”. In: *Endocrinology* 150.4 (Apr. 2009), pp. 1879–1885. ISSN: 00137227. DOI: 10.1210/en.2008-1021.

[225] Erica L. Schoeller et al. “Bmal1 is required for normal reproductive behaviors in male mice”. In: *Endocrinology* 157.12 (Dec. 2016), pp. 4914–4929. ISSN: 19457170. DOI: 10.1210/en.2016-1620.

[226] Yasufumi Shigeyoshi et al. “Restoration of circadian behavioural rhythms in a period null Drosophila mutant (per01) by mammalian period homologues mPer1 and mPer2”. In: *Genes to Cells* 7.2 (2002), pp. 163–171. ISSN: 13569597. DOI: 10.1046/j.1356-9597.2001.00503.x.

[227] Julie S. Pendergast, Rio C. Friday, and Shin Yamazaki. “Photic entrainment of period mutant mice is predicted from their phase response curves”. In: *J. Neurosci* 30.36 (Sept. 2010), pp. 12179–12184. ISSN: 02706474. DOI: 10.1523/JNEUROSCI.2607-10.2010.

[228] Lauren P Shearman et al. “Targeted Disruption of the mPer3 Gene: Subtle Effects on Circadian Clock Function”. In: *Mol. Cell. Biol* 20.17 (2000), pp. 6269–6275.

[229] Sarah Luck and P O. Westermark. “Circadian mRNA expression: Insights from modeling and transcriptomics”. In: *Cell. Mol. Life Sci.* 73.3 (Feb. 2016), pp. 497–521. ISSN: 14209071. DOI: 10.1007/s00018-015-2072-2.

[230] J. A. Ripperger and Urs Albrecht. “The circadian clock component PERIOD2: From molecular to cerebral functions”. In: *Progress in Brain Research*. Ed. by A Kalsbeek et al. Vol. 199. Elsevier B.V., 2012. Chap. 14, pp. 233–245. DOI: 10.1016/B978-0-444-59427-3.00014-9.

[231] A. Erzberger et al. “Genetic redundancy strengthens the circadian clock leading to a narrow entrainment range”. In: *J. R. Soc. Interface* 10.84 (July 2013). ISSN: 17425662. DOI: 10.1098/rsif.2013.0221.

[232] Nicola J. Smyllie et al. “Visualizing and Quantifying Intracellular Behavior and Abundance of the Core Circadian Clock Protein PERIOD2”. In: *Curr. Biol* 26.14 (July 2016), pp. 1880–1886. ISSN: 09609822. DOI: 10.1016/j.cub.2016.05.018.

[233] Martha Hotz Vitaterna et al. “Differential regulation of mammalian Period genes and circadian rhythmicity by cryptochromes 1 and 2”. In: *PNAS* 96.21 (Oct. 1999), pp. 12114–12119. URL: www.pnas.org.

[234] Binhai Zheng et al. “Nonredundant Roles of the mPer1 and mPer2 Genes in the Mammalian Circadian Clock”. In: *Cell* 105 (2001), pp. 683–694.

[235] Anthony H. Tsang et al. “Tissue-specific interaction of Per1/2 and Dec2 in the regulation of fibroblast circadian rhythms”. In: *J. Biol. Rhythms* 27.6 (Dec. 2012), pp. 478–489. ISSN: 07487304. DOI: 10.1177/0748730412462838.

[236] Hiroyuki Tamiya et al. “Rigid Cooperation of Per1 and Per2 proteins”. In: *Sci. Rep* 6 (Sept. 2016). ISSN: 20452322. DOI: 10.1038/srep32769.

[237] Henrik Oster et al. “Disruption of mCry2 restores circadian rhythmicity in mPer2 mutant mice”. In: *Genes Dev* 16.20 (Oct. 2002), pp. 2633–2638. ISSN: 08909369. DOI: 10.1101/gad.233702.

[238] Henrik Oster et al. “Loss of circadian rhythmicity in aging mPer1-/- mCry2-/- mutant mice”. In: *Genes Dev* 17.11 (June 2003), pp. 1366–1379. ISSN: 08909369. DOI: 10.1101/gad.256103.

[239] Henrik Oster, Gijsbertus T.J. Van der Horst, and Urs Albrecht. “Daily variation of clock output gene activation in behaviorally arrhythmic mPer/mCry triple mutant mice”. In: *Chronobiol. Int* 20.4 (2003), pp. 683–695. ISSN: 07420528. DOI: 10.1081/CBI-120022408.

[240] Jennifer L. Fribourgh et al. “Dynamics at the serine loop underlie differential affinity of cryptochromes for CLOCK:BMAL1 to control circadian timing”. In: *eLife* 9 (Feb. 2020). ISSN: 2050084X. DOI: 10.7554/eLife.55275.

[241] Rui Ye et al. “Biochemical analysis of the canonical model for the mammalian circadian clock”. In: *J. Biol. Chem* 286.29 (July 2011), pp. 25891–25902. ISSN: 00219258. DOI: 10.1074/jbc.M111.254680.

[242] Nicola J Smyllie et al. “Cryptochrome proteins regulate the circadian intracellular behavior and localization of PER2 in mouse suprachiasmatic nucleus neurons”. In: *PNAS* 119.4 (2022). DOI: 10.1073/pnas.2113845119/-/DCSupplemental.

[243] Nicola J. Smyllie et al. “Quantitative measures of clock protein dynamics in the mouse suprachiasmatic nucleus extends the circadian time-keeping model”. In: *EMBO* (2025). ISSN: 14602075. DOI: 10.1038/s44318-025-00426-z.

[244] Christian H. Gabriel et al. “Live-cell imaging of circadian clock protein dynamics in CRISPR-generated knock-in cells”. In: *Nat. Commun* 12.1 (Dec. 2021). ISSN: 20411723. DOI: 10.1038/s41467-021-24086-9.

[245] Rajindra P. Aryal et al. “Macromolecular Assemblies of the Mammalian Circadian Clock”. In: *Mol. Cell* 67.5 (Sept. 2017), pp. 770–782. ISSN: 10974164. DOI: 10.1016/j.molcel.2017.07.017.

[246] Xuemei Cao et al. “Molecular mechanism of the repressive phase of the mammalian circadian clock”. In: *PNAS* 118.2 (2021). DOI: 10.1073/pnas.2021174118/-/DCSupplemental.

[247] Jiameng Sun et al. “Hepatocyte Period 1 dictates oxidative substrate selection independent of the core circadian clock”. In: *Cell Rep* 43.10 (Oct. 2024). ISSN: 22111247. DOI: 10.1016/j.celrep.2024.114865.

[248] Isabelle Schmutz et al. “The mammalian clock component PERIOD2 coordinates circadian output by interaction with nuclear receptors”. In: *Genes Dev* 24.4 (Feb. 2010), pp. 345–357. ISSN: 08909369. DOI: 10.1101/gad.564110.

[249] Katja A Lamia et al. “AMPK Regulates the Circadian Clock by Cryptochrome Phosphorylation and Degradation”. In: *Science* 326 (Oct. 2009).

[250] Shogo Sato et al. “The circadian clock CRY1 regulates pluripotent stem cell identity and somatic cell reprogramming”. In: *Cell Rep* 42.6 (June 2023). ISSN: 22111247. DOI: 10.1016/j.celrep.2023.112590.

[251] Mali Chen et al. “PER1 Is a Prognostic Biomarker and Correlated With Immune Infiltrates in Ovarian Cancer”. In: *Front. Genet.* 12 (June 2021). ISSN: 16648021. DOI: 10.3389/fgene.2021.697471.

[252] Jiao Wang et al. “Disrupting Circadian Rhythm via the PER1-HK2 Axis Reverses Trastuzumab Resistance in Gastric Cancer”. In: *Cancer Res* 82.8 (Apr. 2022), pp. 1503–1517. ISSN: 15387445. DOI: 10.1158/0008-5472.CAN-21-1820.

[253] Guojun Yang et al. “Loss of the clock gene Per1 promotes oral squamous cell carcinoma progression via the AKT/mTOR pathway”. In: *Cancer Sci* 111.5 (May 2020), pp. 1542–1554. ISSN: 13497006. DOI: 10.1111/cas.14362.

[254] Hasan Dagmura et al. “Possible Association of PER2/PER3 Variable Number Tandem Repeat Polymorphism Variants with Susceptibility and Clinical Characteristics in Pancreatic Cancer”. In: *Genet. Test. Mol. Biomark* 25.2 (Dec. 2020), pp. 124–130. ISSN: 1945-0265. DOI: 10.1089/gtmb.2020.0179.

[255] Lianxia Guo et al. “PER2 integrates circadian disruption and pituitary tumorigenesis”. In: *Theranostics* 13.8 (2023), pp. 2657–2672. ISSN: 18387640. DOI: 10.7150/thno.82995.

[256] Juan Alfonso Redondo et al. “Per2 circadian oscillation sensitizes esophageal cancer cells to chemotherapy”. In: *Biology* 10.4 (Apr. 2021). ISSN: 20797737. DOI: 10.3390/biology10040266.

[257] Jiyoung Park et al. “Endogenous circadian reporters reveal functional differences of PERIOD paralogs and the significance of PERIOD:CK1 stable interaction”. In: *PNAS* 120.6 (Feb. 2023). ISSN: 10916490. DOI: 10.1073/pnas.2212255120.

[258] Ashley L. Russell et al. “Knockout of the circadian gene, Per2, disrupts corticosterone secretion and results in depressiveâlike behaviors and deficits in startle responses”. In: *BMC Neurosci* 22.1 (Dec. 2021). ISSN: 14712202. DOI: 10.1186/s12868-020-00607-y.

[259] Leandro Val Sayson et al. “The differential vulnerabilities of Per2 knockout mice to the addictive properties of methamphetamine and cocaine”. In: *Progress in Neuro-Psychopharmacology and Biological Psychiatry* 126 (Aug. 2023). ISSN: 18784216. DOI: 10.1016/j.pnpbp.2023.110782.

[260] Birgit Schittek and Tobias Sinnberg. “Biological functions of casein kinase 1 isoforms and putative roles in tumorigenesis”. In: *Mol. Cancer* 13.1 (Oct. 2014). ISSN: 14764598. DOI: 10.1186/1476-4598-13-231.

[261] Sabrina Klemz et al. “Protein phosphatase 4 controls circadian clock dynamics by modulating CLOCK/BMAL1 activity”. In: *Genes Dev* 35.15-16 (Aug. 2021), pp. 1161–1174. ISSN: 15495477. DOI: 10.1101/gad.348622.121.

[262] Stephen Beesley et al. “Wake-sleep cycles are severely disrupted by diseases affecting cytoplasmic homeostasis”. In: *PNAS* 117.45 (2020), pp. 28402–28411. DOI: 10.1073/pnas.2003524117/-/DCSupplemental.

[263] Yang An et al. “Decoupling PER phosphorylation, stability and rhythmic expression from circadian clock function by abolishing PER-CK1 interaction”. In: *Nat. Commun* 13.1 (Dec. 2022). ISSN: 20411723. DOI: 10.1038/s41467-022-31715-4.

[264] Chisato Iitaka et al. “A role for glycogen synthase kinase-3β in the mammalian circadian clock”. In: *J. Biol. Chem* 280.33 (Aug. 2005), pp. 29397–29402. ISSN: 00219258. DOI: 10.1074/jbc.M503526200.

[265] Mary L. Spengler et al. “A serine cluster mediates BMAL1-dependent CLOCK phosphorylation and degradation”. In: *Cell Cycle* 8.24 (Dec. 2009), pp. 4138–4146. ISSN: 15514005. DOI: 10.4161/cc.8.24.10273.

[266] Saurabh Sahar et al. “Regulation of BMAL1 protein stability and circadian function by GSK3β-mediated phosphorylation”. In: *PLoS ONE* 5.1 (Jan. 2010). ISSN: 19326203. DOI: 10.1371/journal.pone.0008561.

[267] John Vandermeer and Ivette Perfecto. “A keystone mutualism drives pattern in a power function”. In: *Science* 311.5763 (Feb. 2006), pp. 1000–1002. ISSN: 00368075. DOI: 10.1126/science.1121432.

[268] Rachel C. Besing et al. “Circadian rhythmicity of active GSK3 isoforms modulates molecular clock gene rhythms in the suprachiasmatic nucleus”. In: *J. Biol. Rhythms* 30.2 (Apr. 2015), pp. 155–160. ISSN: 15524531. DOI: 10.1177/0748730415573167.

[269] Erik J Eide et al. “The Circadian Regulatory Proteins BMAL1 and Cryptochromes Are Substrates of Casein Kinase Iϵ *”. In: *J. Biol. Chem* 277.19 (May 2002), pp. 17248–17254.

[270] Kamon Sanada, Toshiyuki Okano, and Yoshitaka Fukada. “Mitogen-activated protein kinase phosphorylates and negatively regulates basic helix-loop-helix-PAS transcription factor BMAL1”. In: *J. Biol. Chem* 277.1 (Jan. 2002), pp. 267–271. ISSN: 00219258. DOI: 10.1074/jbc.M107850200.

[271] Apirada Padlom et al. “Level of constitutively expressed BMAL1 affects the robustness of circadian oscillations”. In: *Sci. Rep* 12.1 (2022), pp. 1–13. ISSN: 20452322. DOI: 10.1038/s41598-022-24188-4.

[272] Min Zhou et al. “A Period2 Phosphoswitch Regulates and Temperature Compensates Circadian Period”. In: *Mol. Cell* 60.1 (2015), pp. 77–88. ISSN: 10974164. DOI: 10.1016/j.molcel.2015.08.022.

[273] Jonathan M. Philpott et al. “Biochemical mechanisms of period control within the mammalian circadian clock”. In: *Semin. Cell Dev. Biol* 126 (June 2022), pp. 71–78. ISSN: 10963634. DOI: 10.1016/j.semcdb.2021.04.012.

[274] Hyeong Min Lee et al. “The period of the circadian oscillator is primarily determined by the balance between casein kinase 1 and protein phosphatase 1”. In: *PNAS* 108.39 (Sept. 2011), pp. 16451–16456. ISSN: 00278424. DOI: 10.1073/pnas.1107178108.

[275] Peng Gao et al. “Phosphorylation of the cryptochrome 1 C-terminal tail regulates circadian period length”. In: *J. Biol. Chem* 288.49 (Dec. 2013), pp. 35277–35286. ISSN: 00219258. DOI: 10.1074/jbc.M113.509604.

[276] Na Liu and Eric Erquan Zhang. “Phosphorylation regulating the ratio of intracellular CRY1 protein determines the circadian period”. In: *Front. Neurol* 7.SEP (Sept. 2016). ISSN: 16642295. DOI: 10.3389/fneur.2016.00159.

[277] Phillip L Lowrey et al. “Positional Syntenic Cloning and Functional Characterization of the Mammalian Circadian Mutation tau”. In: *Science* 288 (2000).

[278] Ying Xu et al. “Functional consequences of a CKId mutation causing familial advanced sleep phase syndrome”. In: *Nature* 434 (2005). URL: www.nature.com/nature.

[279] Y. Xu et al. “Modeling of a Human Circadian Mutation Yields Insights into Clock Regulation by PER2”. In: *Cell* 128.1 (Jan. 2007), pp. 59–70. ISSN: 00928674. DOI: 10.1016/j.cell.2006.11.043.

[280] Haiyan Xu et al. “Cryptochrome 1 regulates the circadian clock through dynamic interactions with the BMAL1 C terminus”. In: *Nat. Struct. Mol. Biol* 22.6 (2015), pp. 476–484. ISSN: 15459985. DOI: 10.1038/nsmb.3018.

[281] Ray Zhang et al. “A circadian gene expression atlas in mammals: Implications for biology and medicine”. In: *PNAS* 111.45 (Nov. 2014), pp. 16219–16224. ISSN: 10916490. DOI: 10.1073/pnas.1408886111.

[282] Ludovic S. Mure et al. “Diurnal transcriptome atlas of a primate across major neural and peripheral tissues”. In: *Science* 359.6381 (Mar. 2018). ISSN: 10959203. DOI: 10.1126/science.aao0318.

[283] Michael Menaker, Zachary C. Murphy, and Michael T. Sellix. “Central control of peripheral circadian oscillators”. In: *Curr. Opin. Neurobiol* 23.5 (Oct. 2013), pp. 741–746. ISSN: 09594388. DOI: 10.1016/j.conb.2013.03.003.

[284] Biliana Marcheva et al. “A role for alternative splicing in circadian control of exocytosis and glucose homeostasis”. In: *Genes Dev* 34.15-16 (2020), pp. 1089–1105. ISSN: 15495477. DOI: 10.1101/GAD.338178.120.

[285] Yalcin Erzurumlu, Deniz Catakli, and Hatice Kubra Dogan. “Circadian Oscillation Pattern of Endoplasmic Reticulum Quality Control (ERQC) Components in Human Embryonic Kidney HEK293 Cells”. In: *J. Circadian Rhythms* 21.1 (2023), pp. 1–15. ISSN: 17403391. DOI: 10.5334/jcr.219.

[286] Yeliz Serin and Nilufer Acar Tek. “Effect of Circadian Rhythm on Metabolic Processes and the Regulation of Energy Balance”. In: *Ann. Nutr. Metab* 74.4 (May 2019), pp. 322–330. ISSN: 14219697. DOI: 10.1159/000500071.

[287] Kevin Thurley et al. “Principles for circadian orchestration of metabolic pathways”. In: *PNAS* 114.7 (Feb. 2017), pp. 1572–1577. ISSN: 10916490. DOI: 10.1073/pnas.1613103114.

[288] Jonathan Bieler et al. “Robust synchronization of coupled circadian and cell cycle oscillators in single mammalian cells”. In: *Mol. Sys. Biol* 10.7 (July 2014). ISSN: 1744-4292. DOI: 10.15252/msb.20145218.

[289] Celine Feillet et al. “Phase locking and multiple oscillating attractors for the coupled mammalian clock and cell cycle”. In: *PNAS* 111.27 (July 2014), pp. 9828–9833. ISSN: 10916490. DOI: 10.1073/pnas.1320474111.

[290] Akhilesh B. Reddy et al. “Circadian clocks: Neural and peripheral pacemakers that impact upon the cell division cycle”. In: *Mutat. Res.* 574.1-2 SPEC. ISS. (2005), pp. 76–91. ISSN: 00275107. DOI: 10.1016/j.mrfmmm.2005.01.024.

[291] Marta Budkowska et al. “The Influence of Circadian Rhythm on the Activity of Oxidative Stress Enzymes”. In: *Int. J. Mol. Sci* 23.22 (Nov. 2022). ISSN: 14220067. DOI: 10.3390/ijms232214275.

[292] Anna Marie Finger et al. “Intercellular coupling between peripheral circadian oscillators by TGF-β signaling”. In: *Sci. Adv* 7.30 (2021), pp. 1–20. ISSN: 23752548. DOI: 10.1126/sciadv.abg5174.

[293] Erik D. Herzog, Joseph S. Takahashi, and Gene D. Block. “Clock controls circadian period in isolated suprachiasmatic nucleus neurons”. In: *Nat. Neurosci.* 1.8 (1998), pp. 708–713. ISSN: 10976256. DOI: 10.1038/3708.

[294] Chak Foon Tso et al. “Astrocytes Regulate Daily Rhythms in the Suprachiasmatic Nucleus and Behavior”. In: *Curr. Biol* 27.7 (2017), pp. 1055–1061. ISSN: 09609822. DOI: 10.1016/j.cub.2017.02.037.

[295] Isabel Heyde and Henrik Oster. “Induction of internal circadian desynchrony by misaligning zeitgebers”. In: *Sci. Rep* 12.1 (Dec. 2022). ISSN: 20452322. DOI: 10.1038/s41598-022-05624-x.

[296] Michael L. H. J Hermes et al. “GABA and glutamate mediate rapid neurotransmission from suprachiasmatic nucleus to hypothalamic paraventricular nucleus in rat”. In: *J. Physiol* (1996), pp. 749–757.

[297] Thomas Dickmeis. “Glucocorticoids and the circadian clock”. In: *J. Endocrinol* 200.1 (2009), pp. 3–22. ISSN: 00220795. DOI: 10.1677/JOE-08-0415.

[298] Keisuke Ikegami et al. “Interconnection between circadian clocks and thyroid function”. In: *Nat. Rev. Endocrinol* 15.10 (Oct. 2019), pp. 590–600. ISSN: 17595037. DOI: 10.1038/s41574-019-0237-z.

[299] P. Pevet et al. “Melatonin in the multi-oscillatory mammalian circadian world”. In: *Chronobiol. Int* 23.1-2 (2006), pp. 39–51. ISSN: 07420528. DOI: 10.1080/07420520500482074.

[300] Christopher S. Colwell. “Linking neural activity and molecular oscillations in the SCN”. In: *Nat. Rev. Neurosci* 12.10 (2011), pp. 553–569. ISSN: 1471003X. DOI: 10.1038/nrn3086.

[301] David K. Welsh et al. “Individual neurons dissociated from rat suprachiasmatic nucleus express independently phased circadian firing rhythms”. In: *Neuron* 14.4 (1995), pp. 697–706. ISSN: 08966273. DOI: 10.1016/0896-6273(95)90214-7.

[302] Tetsuo Shirakawa et al. “Synchronization of circadian firing rhythms in cultured rat suprachiasmatic neurons”. In: *Eur. J. Neurosci* 12.8 (2000), pp. 2833–2838. ISSN: 0953816X. DOI: 10.1046/j.1460-9568.2000.00170.x.

[303] Pinar Pez\"{u}k et al. “Glucocorticoids as entraining signals for peripheral circadian oscillators”. In: *Endocrinology* 153.10 (Oct. 2012), pp. 4775–4783. ISSN: 00137227. DOI: 10.1210/en.2012-1486.

[304] Lauren E. Chun et al. “Variations in phase and amplitude of rhythmic clock gene expression across prefrontal cortex, hippocampus, amygdala, and hypothalamic paraventricular and suprachiasmatic nuclei of male and female rats”. In: *J. Biol. Rhythms* 30.5 (Oct. 2015), pp. 417–436. ISSN: 15524531. DOI: 10.1177/0748730415598608.

[305] Seung Hee Yoo et al. “PERIOD2::LUCIFERASE real-time reporting of circadian dynamics reveals persistent circadian oscillations in mouse peripheral tissues”. In: *PNAS* 101.15 (2004), pp. 5339–5346. ISSN: 00278424. DOI: 10.1073/pnas.0308709101.

[306] Nityanand Bolshette et al. “Circadian regulation of liver function: from molecular mechanisms to disease pathophysiology”. In: *Gastroenterol. Hepatol* 20.11 (Nov. 2023), pp. 695–707. ISSN: 17595053. DOI: 10.1038/s41575-023-00792-1.

[307] Kai-Florian Storch et al. “Extensive and divergent circadian gene expression in liver and heart”. In: *Nature* 417 (2002).

[308] J. Wuarin and Ueli Schibler. “Expression of the Liver-Enriched Transcriptional Activator Protein DBP Follows a Stringent Circadian Rhythm”. In: *Cell* 63 (1990), pp. 1257–1266.

[309] Mariko Izumo et al. “Differential effects of light and feeding on circadian organization of peripheral clocks in a forebrain Bmal1 mutant”. In: *eLife* 3 (2014). ISSN: 2050084X. DOI: 10.7554/eLife.04617.

[310] Steven A. Brown et al. “The period length of fibroblast circadian gene expression varies widely among human individuals”. In: *PLoS Biol* 3.10 (Oct. 2005). ISSN: 15449173. DOI: 10.1371/journal.pbio.0030338.

[311] Michihiro Mieda and Takeshi Sakurai. “Bmal1 in the nervous system is essential for normal adaptation of circadian locomotor activity and food intake to periodic feeding”. In: *J. Neurosci* 31.43 (Oct. 2011), pp. 15391–15396. ISSN: 02706474. DOI: 10.1523/JNEUROSCI.2801-11.2011.

[312] Camille Saini et al. “Real-time recording of circadian liver gene expression in freely moving mice reveals the phase-setting behavior of hepatocyte clocks”. In: *Genes Dev* 27.13 (July 2013), pp. 1526–1536. ISSN: 08909369. DOI: 10.1101/gad.221374.113.

[313] Flore Sinturel et al. “Circadian hepatocyte clocks keep synchrony in the absence of a master pacemaker in the suprachiasmatic nucleus or other extrahepatic clocks”. In: *Genes Dev* 35.5-6 (2021), pp. 329–334. ISSN: 15495477. DOI: 10.1101/GAD.346460.120.

[314] Nebojsa Nick Knezevic et al. “Circadian pain patterns in human pain conditions â A systematic review”. In: *Pain Practice* 23.1 (Jan. 2023), pp. 94–109. ISSN: 15332500. DOI: 10.1111/papr.13149.

[315] Arjen J.G. Meewisse et al. “Effect of time of day on outcomes in elective surgery aÂ systematic review”. In: *Anaesthesia* (2024). ISSN: 13652044. DOI: 10.1111/anae.16395.

[316] Mary R. Janevic et al. “Making Pain Research More Inclusive: Why and How”. In: *J. Pain* 23.5 (May 2022), pp. 707–728. ISSN: 15288447. DOI: 10.1016/j.jpain.2021.10.004.

[317] Jennifer Crodelle et al. “Modeling the daily rhythm of human pain processing in the dorsal horn”. In: *PLoS Comput. Biol* 15.7 (July 2019). ISSN: 15537358. DOI: 10.1371/journal.pcbi.1007106.

[318] I. Daguet et al. “Circadian rhythmicity of pain sensitivity in humans”. In: *Brain* 145.9 (2022), pp. 3225–3235. ISSN: 14602156. DOI: 10.1093/brain/awac147.

[319] Chung Jung Mun et al. “Exploring Endogenous Circadian Rhythm of Mechanical Pain Sensitivity in Healthy Adults”. In: *The Journal of Pain* (Feb. 2025), p. 105592. ISSN: 15265900. DOI: 10.1016/j.jpain.2025.105592.

[320] Yashar Yousefzadehfard, Bennett Wechsler, and Christine DeLorenzo. “Human circadian rhythm studies: Practical guidelines for inclusion/exclusion criteria and protocol”. In: *Neurobiol. Sleep Circadian Rhythms* 13 (Nov. 2022). ISSN: 24519944. DOI: 10.1016/j.nbscr.2022.100080.

[321] Cynthia Abboud et al. “Animal models of pain: Diversity and benefits”. In: *J. Neurosci Methods* 348 (Jan. 2021). ISSN: 1872678X. DOI: 10.1016/j.jneumeth.2020.108997.

[322] Deanna Marie Arble et al. “Circadian disruption and metabolic disease: Findings from animal models”. In: *Best Pract. Res. Clin. Endocrinol. Metab* 24.5 (Oct. 2010), pp. 785–800. ISSN: 1521690X. DOI: 10.1016/j.beem.2010.08.003.

[323] Blanca Martin-Burgos et al. “Methods for Detecting PER2:LUCIFERASE Bioluminescence Rhythms in Freely Moving Mice”. In: *J. Biol. Rhythms* 37.1 (Feb. 2022), pp. 78–93. ISSN: 15524531. DOI: 10.1177/07487304211062829.

[324] Frank Faltraco et al. “Synchronization of Fibroblasts Ex Vivo in Psychopharmacology”. In: *Pharmacopsychiatry* 56.3 (Dec. 2018), pp. 101–107. ISSN: 14390795. DOI: 10.1055/a-1151-4947.

[325] Jennifer R. Deuis, Lucie S. Dvorakova, and Irina Vetter. “Methods used to evaluate pain behaviors in rodents”. In: *Front. Mol. Neurosci* 10 (Sept. 2017). ISSN: 16625099. DOI: 10.3389/fnmol.2017.00284.

[326] Nicholas S. Gregory et al. “An overview of animal models of pain: Disease models and outcome measures”. In: *J. Pain* 14.11 (2013), pp. 1255–1269. ISSN: 15288447. DOI: 10.1016/j.jpain.2013.06.008.

[327] David J. Kennaway. “Melatonin research in mice: a review”. In: *Chronobiol. Int* 36.9 (Sept. 2019), pp. 1167–1183. ISSN: 15256073. DOI: 10.1080/07420528.2019.1624373.

[328] Zoe M. Tapp et al. “Mechanistic insights into chemotherapy-induced circadian disruption using rodent models”. In: *Trends Neurosci* 48.4 (Apr. 2025), pp. 283–296. ISSN: 1878108X. DOI: 10.1016/j.tins.2024.12.011.

[329] Laura Perissin et al. “Diurnal changes of tonic nociceptive responses in mice: Evidence for a proalgesic role of melatonin”. In: *Pain* 110.1-2 (July 2004), pp. 250–258. ISSN: 03043959. DOI: 10.1016/j.pain.2004.03.039.

[330] Rasneer S. Bains et al. “Assessing mouse behaviour throughout the light/dark cycle using automated in-cage analysis tools”. In: *J. Neurosci Methods* 300 (Apr. 2018), pp. 37–47. ISSN: 1872678X. DOI: 10.1016/j.jneumeth.2017.04.014.

[331] Hee Kee Kim et al. “Circadian regulation of chemotherapy-induced peripheral neuropathic pain and the underlying transcriptomic landscape”. In: *Sci. Rep* 10.1 (2020), pp. 1–13. ISSN: 20452322. DOI: 10.1038/s41598-020-70757-w.

[332] Suzanne M. Green-Fulgham et al. “Suppression of active phase voluntary wheel running in male rats by unilateral chronic constriction injury: Enduring therapeutic effects of a brief treatment of morphine combined with TLR4 or P2X7 antagonists”. In: *J. Neurosci. Res* 100.1 (Jan. 2022), pp. 265–277. ISSN: 10974547. DOI: 10.1002/jnr.24645.

[333] Magali Millecamps et al. “Circadian pattern of spontaneous behavior in monarthritic rats: A novel global approach to evaluation of chronic pain and treatment

effectiveness". In: *Arthritis and Rheumatism* 52.11 (Nov. 2005), pp. 3470–3478. ISSN: 00043591. DOI: 10.1002/art.21403.

[334] Konrad S. Jankowski. "Morning types are less sensitive to pain than evening types all day long". In: *EPJ* 17.7 (Aug. 2013), pp. 1068–1073. ISSN: 10903801. DOI: 10.1002/j.1532-2149.2012.00274.x.

[335] C. G. Bachmann et al. "Diurnal time course of heat pain perception in healthy humans". In: *Neurosci. Lett* 489.2 (Feb. 2011), pp. 122–125. ISSN: 03043940. DOI: 10.1016/j.neulet.2010.11.080.

[336] Joshua Aviram, Tamar Shochat, and Dorit Pud. "Pain Perception in Healthy Young Men Is Modified by Time-Of-Day and Is Modality Dependent". In: *Pain Medicine* 16 (2015), pp. 1137–1144. ISSN: 15264637. DOI: 10.1111/pme.12266.

[337] Ying Zhu et al. "The Diurnal Profile of Human Basal Pain Sensitivity and Skin Sympathetic Nerve Activity: A Healthy Volunteer Study". In: *Front. Neurosci* 16 (Mar. 2022). ISSN: 1662453X. DOI: 10.3389/fnins.2022.810166.

[338] Jacob R. Bumgarner, William H. Walker, and Randy J. Nelson. "Circadian rhythms and pain". In: *Neurosci. Behav. Rev* 129.August (2021), pp. 296–306. ISSN: 18737528. DOI: 10.1016/j.neubiorev.2021.08.004.

[339] Jacob R. Bumgarner, Evan W. McCray, and Randy J. Nelson. "The disruptive relationship among circadian rhythms, pain, and opioids". In: *Front. Neurosci* 17 (2023). ISSN: 1662453X. DOI: 10.3389/fnins.2023.1109480.

[340] Horst J. Koch and C. Raschka. "Diurnal Variation of Pain Perception in Young Volunteers Using the Tourniquet Pain Model". In: *Chronobiol. Int* 21.1 (2004), pp. 171–173. ISSN: 07420528. DOI: 10.1081/CBI-120027989.

[341] Jennifer Crodelle, Carolyn Vanty, and Victoria Booth. "Modeling homeostatic and circadian modulation of human pain sensitivity". In: *Front. Neurosci* 17 (2023). ISSN: 1662453X. DOI: 10.3389/fnins.2023.1166203.

[342] Megan Hastings Hagenauer et al. "The Modulation of Pain by Circadian and Sleep-Dependent Processes: A Review of the Experimental Evidence". In: *Women in Mathematical Biology*. Ed. by A. T. Layton and Miller. L. A. 2017.

[343] Mark J. Burish, Zheng Chen, and Seung Hee Yoo. "Emerging relevance of circadian rhythms in headaches and neuropathic pain". In: *Acta Physiologica* 225.1 (Jan. 2019). ISSN: 17481716. DOI: 10.1111/apha.13161.

[344] Sally Hu et al. "A Scoping Review of the Diurnal Variation in the Intensity of Neuropathic Pain". In: *Pain Medicine (United States)* 23.5 (May 2022), pp. 991–1005. ISSN: 15264637. DOI: 10.1093/pm/pnab336.

[345] Julia P. Segal et al. "Circadian control of pain and neuroinflammation". In: *J. Neurosci. Res* 96.6 (2018), pp. 1002–1020. ISSN: 10974547. DOI: 10.1002/jnr.24150.

[346] Nicholas Bellamy, Robert B Sothern, and Jane Campbell. "Aspects of diurnal rhythmicity in pain, stiffness, and fatigue in patients with fibromyalgia." In: *The Journal of Rheumatology* 31.2 (Feb. 2004), p. 379. URL: http://www.jrheum.org/content/31/2/379.abstract.

[347] Alicia Gonzalez-Martinez et al. *Time and headache: Insights into timing processes in primary headache disorders for diagnosis, underlying pathophysiology and treatment implications*. Nov. 2024. DOI: 10.1177/03331024241297652.

[348] N Bellamy, R B Sothern, and J Campbell. "Rhythmic variations in pain, stiffness, and manual dexterity in hand osteoarthritis". In: *Ann Rheum Dis* 61 (2002), pp. 1075–1080. URL: www.annrheumdis.com.

[349] Rainer H. Straub and Maurizio Cutolo. "Circadian rhythms in rheumatoid arthritis: Implications for pathophysiology and therapeutic management". In: *Arthritis and Rheumatism* 56.2 (Feb. 2007), pp. 399–408. ISSN: 00043591. DOI: 10.1002/art.22368.

[350] Ian Gilron, Joan M Bailey, and Elizabeth G Vandenkerkhof. "Chronobiological Characteristics of Neuropathic Pain Clinical Predictors of Diurnal Pain Rhythmicity". In: *Clin. J. Pain* 29.9 (2013), pp. 755–759. URL: http://journals.lww.com/clinicalpain.

[351] Mark Odrcich et al. "Chronobiological characteristics of painful diabetic neuropathy and postherpetic neuralgia: Diurnal pain variation and effects of analgesic therapy".

In: *Pain* 120.1-2 (Jan. 2006), pp. 207–212. ISSN: 03043959. DOI: 10.1016/j.pain.2005.10.007.

[352] Ian Gilron. *Impact of chronobiology on neuropathic pain treatment*. 2016. DOI: 10.2217/pmt-2015-0007.

[353] Ayako Niiro et al. "Diurnal Variation in Trigeminal Pain Sensitivity in Mice". In: *Front. Neurosci* 15 (Aug. 2021). ISSN: 1662453X. DOI: 10.3389/fnins.2021.703440.

[354] Jing Zhang et al. "Regulation of peripheral clock to oscillation of substance p contributes to circadian inflammatory pain". In: *Anesthesiology* 117.1 (2012), pp. 149–160. ISSN: 00033022. DOI: 10.1097/ALN.0b013e31825b4fc1.

[355] Yoon Mee Choi et al. "Extremely Low Frequency Magnetic Field Exposure Modulates the Diurnal Rhythm of the Pain Threshold in Mice". In: *Bioelectromagnetics* 24.3 (2003), pp. 206–210. ISSN: 01978462. DOI: 10.1002/bem.10094.

[356] Sedat Altug et al. "Biological time-dependent difference in effect of peroxynitrite demonstrated by the mouse hot plate pain model". In: *Chronobiol. Int* 23.3 (2006), pp. 583–591. ISSN: 07420528. DOI: 10.1080/07420520600650703.

[357] Lynn C Matsumiya et al. "Using the Mouse Grimace Scale to Reevaluate the Efficacy of Postoperative Analgesics in Laboratory Mice". In: *JAALAS* 51.1 (2012), pp. 42–49. ISSN: 1559-6109.

[358] Tianjiao Xia et al. "Regulation of the NR2B-CREB-CRTC1 signaling pathway contributes to circadian pain in murine model of chronic constriction injury". In: *Anesthesia and Analgesia* 122.2 (Feb. 2016), pp. 542–552. ISSN: 15267598. DOI: 10.1213/ANE.0000000000000991.

[359] Sai Yasukochi et al. "Sulfasalazine alleviates neuropathic pain hypersensitivity in mice through inhibition of SGK-1 in the spinal cord". In: *Biochem. Pharmacol.* 185 (Mar. 2021). ISSN: 18732968. DOI: 10.1016/j.bcp.2021.114411.

[360] Bin Shu et al. "Opioid infusions at different times of the day produce varying degrees of opioid-induced hyperalgesia". In: *Br. J. Anaesth* 131.6 (Dec. 2023), pp. 1072–1081. ISSN: 14716771. DOI: 10.1016/j.bja.2023.08.039.

[361] Chorong Han et al. “Regulation of headache response and transcriptomic network by the trigeminal ganglion clock”. In: *Headache* 64.2 (Feb. 2024), pp. 195–210. ISSN: 15264610. DOI: 10.1111/head.14670.

[362] Takahiro Akamine et al. “Accumulation of sorbitol in the sciatic nerve modulates circadian properties of diabetes-induced neuropathic pain hypersensitivity in a diabetic mouse model”. In: *BBRC* 503.1 (Sept. 2018), pp. 181–187. ISSN: 10902104. DOI: 10.1016/j.bbrc.2018.05.209.

[363] Naoki Kusunose et al. “Molecular basis for the dosing time-dependency of anti-allodynic effects of gabapentin in a mouse model of neuropathic pain”. In: *Mol. Pain* 6 (Nov. 2010). ISSN: 17448069. DOI: 10.1186/1744-8069-6-83.

[364] Wakaba Yamakawa et al. “Suppression of neuropathic pain in the circadian clock-deficient Per2m/m mice involves up-regulation of endocannabinoid system”. In: *PNAS Nexus* 3.1 (Jan. 2024). ISSN: 27526542. DOI: 10.1093/pnasnexus/pgad482.

[365] Tomohiko Takada et al. “Changes in the circadian rhythm of mRNA expression for μ-opioid receptors in the periaqueductal gray under a neuropathic pain-like state”. In: *Synapse* 67.5 (May 2013), pp. 216–223. ISSN: 08874476. DOI: 10.1002/syn.21633.

[366] Laura Perissin, Patrizia Facchin, and Carlo Adolfo Porro. “Diurnal variations in tonic pain reactions in mice”. In: *Life Sci* 67 (2000), pp. 1477–1488.

[367] Celia Piña-Leyva et al. “Hypothalamic A11 Nuclei Regulate the Circadian Rhythm of Spinal Mechanonociception through Dopamine Receptors and Clock Gene Expression”. In: *Life* 12.9 (Sept. 2022). ISSN: 20751729. DOI: 10.3390/life12091411.

[368] Satoru Koyanagi et al. “Glucocorticoid regulation of ATP release from spinal astrocytes underlies diurnal exacerbation of neuropathic mechanical allodynia”. In: *Nat. Commun* 7 (Oct. 2016). ISSN: 20411723. DOI: 10.1038/ncomms13102.

[369] Fabiana Carvalho et al. “PER3 variable number tandem repeat (VNTR) polymorphism modulates the circadian variation of the descending pain modulatory system in healthy subjects”. In: *Sci. Rep* 9.1 (Dec. 2019). ISSN: 20452322. DOI: 10.1038/s41598-019-45527-y.

[370] Charli E Harlow et al. “GWAS of Extended Prescription Analgesic Use Identifies Novel Genetic Loci in Chronic Pain”. In: *medRxiv* (Dec. 2024). DOI: 10.1101/2024.12.02.24318312. URL: http://medrxiv.org/lookup/doi/10.1101/2024.12.02.24318312.

[371] K C Brennan et al. “Casein Kinase Id Mutations in Familial Migraine and Advanced Sleep Phase”. In: *Sci. Transl. Med* 5.183 (2013).

[372] Yukie Shirakawa et al. “Circadian rhythm of PERIOD2::LUCIFERASE expression in the trigeminal ganglion of mice”. In: *Front. Neurosci* 17.March (2023). ISSN: 1662453X. DOI: 10.3389/fnins.2023.1142785.

[373] Yanhao Chu et al. “Single-nucleus transcriptome analysis reveals transcriptional profiles of circadian clock and pain related genes in human and mouse trigeminal ganglion”. In: *Front. Neurosci* 17 (2023). ISSN: 1662453X. DOI: 10.3389/fnins.2023.1176654.

[374] Pradipta R. Ray et al. “Transcriptome analysis of the human tibial nerve identifies sexually dimorphic expression of genes involved in pain, inflammation, and neuroimmunity”. In: *Front. Mol. Neurosci* 12 (Feb. 2019). ISSN: 16625099. DOI: 10.3389/fnmol.2019.00037.

[375] Vaskar Das et al. “Pharmacological targeting of the mammalian clock reveals a novel analgesic for osteoarthritis-induced pain”. In: *Gene* 655 (May 2018), pp. 1–12. ISSN: 18790038. DOI: 10.1016/j.gene.2018.02.048.

[376] Andrew Bellemer. “Thermotaxis, circadian rhythms, and TRP channels in Drosophila”. In: *Temperature* 2.2 (June 2015), pp. 227–243. ISSN: 23328959. DOI: 10.1080/23328940.2015.1004972.

[377] Hana Sehadova et al. “Temperature Entrainment of Drosophila’s Circadian Clock Involves the Gene nocte and Signaling from Peripheral Sensory Tissues to the Brain”. In: *Neuron* 64.2 (Oct. 2009), pp. 251–266. ISSN: 08966273. DOI: 10.1016/j.neuron.2009.08.026.

[378] Bruce. Stillman, David J.. Stewart, and Terri. Grodzicker. “Clocks and rhythms”. In: *Cold Spring Harb. Symp. Quant. Biol* 72 (2007), pp. 233–242.

[379] Shu Chuan Yang et al. “Changes in Gene Expression Patterns of Circadian-Clock, Transient Receptor Potential Vanilloid-1 and Nerve Growth Factor in Inflamed Human Esophagus”. In: *Sci. Rep* 5 (Sept. 2015). ISSN: 20452322. DOI: 10.1038/srep13602.

[380] Hiroyasu Onishi et al. “Rev-erbα gene expression in the mouse brain with special emphasis on its circadian profiles in the suprachiasmatic nucleus”. In: *J. Neurosci. Res* 68.5 (2002), pp. 551–557. DOI: https://doi.org/10.1002/jnr.10226.

[381] Shuzo Yamamoto et al. “Expression of the Per1 gene in the hamster: Brain atlas and circadian characteristics in the suprachiasmatic nucleus”. In: *J. Comp. Neurol* 430.4 (2001), pp. 518–532.

[382] Norimitsu Morioka et al. “Spinal astrocytes contribute to the circadian oscillation of glutamine synthase, cyclooxygenase-1 and clock genes in the lumbar spinal cord of mice”. In: *Neurochem. Int* 60.8 (2012), pp. 817–826. ISSN: 01970186. DOI: 10.1016/j.neuint.2012.03.005.

[383] Tatsuhiko Sugimoto et al. “Clock gene Per1 regulates the production of CCL2 and interleukin-6 through p38, JNK1 and NF-κB activation in spinal astrocytes”. In: *Mol. Cell. Neurosci* 59 (Mar. 2014), pp. 37–46. ISSN: 10447431. DOI: 10.1016/j.mcn.2014.01.003.

[384] Laura K Fonken et al. “Microglia inflammatory responses are controlled by an intrinsic circadian clock”. In: *Brain Behav. Immun* 45 (Sept. 2015), pp. 171–179. ISSN: 08891591. DOI: 10.1016/j.bbi.2014.11.009.

[385] A. Eblen-Zajjur et al. “Diurnal changes in ouabain-sensitive Na+,K+-ATPase activity in the rat spinal dorsal horn”. In: *Neurochemical J* 9.4 (2015), pp. 266–270. ISSN: 18197132. DOI: 10.1134/S181971241504008X.

[386] Norimitsu Morioka et al. “Downregulation of the spinal dorsal horn clock gene Per1 expression leads to mechanical hypersensitivity via c-jun N-terminal kinase and CCL2 production in mice”. In: *Mol. Cell. Neurosci* 72 (Apr. 2016), pp. 72–83. ISSN: 10959327. DOI: 10.1016/j.mcn.2016.01.007.

[387] M. A. Miguel Asai et al. “Rat brain opioid peptides-circadian rhythm is under control of melatonin”. In: *Neuropeptides* 41.6 (Dec. 2007), pp. 389–397. ISSN: 01434179. DOI: 10.1016/j.npep.2007.09.001.

[388] Diego A Golombek et al. “Time-dependent melatonin analgesia in mice: inhibition by opiate or benzodiazepine antagonism”. In: *Eur. J. Pharmacol* 194 (1991), pp. 25–30.

[389] Norimitsu Morioka et al. “Stimulation of nuclear receptor REV-ERBs suppresses production of pronociceptive molecules in cultured spinal astrocytes and ameliorates mechanical hypersensitivity of inflammatory and neuropathic pain of mice”. In: *Brain Behav. Immun.* 78 (May 2019), pp. 116–130. ISSN: 10902139. DOI: 10.1016/j.bbi.2019.01.014.

[390] Rachel Van Drunen and Kristin Eckel-Mahan. “Circadian Rhythms of the Hypothalamus: From Function to Physiology”. In: *Clocks and Sleep* 3.1 (Mar. 2021), pp. 189–226. ISSN: 26245175. DOI: 10.3390/clockssleep3010012.

[391] Daisuke Matsui, Seiichi Takekida, and Hitoshi Okamura. “Molecular Oscillation of Per1 and Per2 Genes in the Rodent Brain: An In Situ Hybridization and Molecular Biological Study”. In: *Kobe J. Med. Sci* 51.6 (2005), pp. 85–93.

[392] Masahiko Odo et al. “Changes in circadian rhythm for mRNA expression of melatonin 1A and 1B receptors in the hypothalamus under a neuropathic pain-like state”. In: *Synapse* 68.4 (Apr. 2014), pp. 153–158. ISSN: 08874476. DOI: 10.1002/syn.21728.

[393] Chengkang Zhang, Kimberly K. Truong, and Qun Yong Zhou. “Efferent projections of prokineticin 2 expressing neurons in the mouse suprachiasmatic nucleus”. In: *PLoS ONE* 4.9 (Sept. 2009). ISSN: 19326203. DOI: 10.1371/journal.pone.0007151.

[394] Dominic Landgraf, Jaimie E. Long, and David K. Welsh. “Depression-like behaviour in mice is associated with disrupted circadian rhythms in nucleus accumbens and periaqueductal grey”. In: *Eur. J. Neurosci* 43.10 (May 2016), pp. 1309–1320. ISSN: 14609568. DOI: 10.1111/ejn.13085.

[395] Emilie Sapin et al. “Localization of the brainstem GABAergic neurons controlling Paradoxical (REM) sleep”. In: *PLoS ONE* 4.1 (Jan. 2009). ISSN: 19326203. DOI: 10.1371/journal.pone.0004272.

[396] Jun Z. Li et al. “Circadian patterns of gene expression in the human brain and disruption in major depressive disorder”. In: *PNAS* 110.24 (June 2013), pp. 9950–9955. ISSN: 10916490. DOI: 10.1073/pnas.1305814110.

[397] Jiyao Sheng et al. “The Link between Depression and Chronic Pain: Neural Mechanisms in the Brain”. In: *Neural Plast* 2017 (June 2017). ISSN: 16875443. DOI: 10.1155/2017/9724371.

[398] Michikazu Abe et al. “Circadian Rhythms in Isolated Brain Regions”. In: *J. Neurosci* 1 (Jan. 2002), pp. 350–356.

[399] Malgorzata Jasinska et al. “Circadian rhythmicity of synapses in mouse somatosensory cortex”. In: *Eur. J. Neurosci* 42.8 (Oct. 2015), pp. 2585–2594. ISSN: 14609568. DOI: 10.1111/ejn.13045.

[400] Malgorzata Jasinska et al. “Circadian clock regulates the shape and content of dendritic spines in mouse barrel cortex”. In: *PLoS ONE* 14.11 (Nov. 2019). ISSN: 19326203. DOI: 10.1371/journal.pone.0225394.

[401] Malgorzata Jasinska et al. “Light-Modulated Circadian Synaptic Plasticity in the Somatosensory Cortex: Link to Locomotor Activity”. In: *Int. J. Mol. Sci* 25.23 (Dec. 2024). ISSN: 14220067. DOI: 10.3390/ijms252312870.

[402] Moon Jong Kim et al. “The Circadian Rhythm Variation of Pain in the Orofacial Region”. In: *JOMP* 40.3 (Sept. 2015), pp. 89–95. ISSN: 2288-9272. DOI: 10.14476/jomp.2015.40.3.89.

[403] Sven Benson et al. “Cortisol affects pain sensitivity and pain-related emotional learning in experimental visceral but not somatic pain: A randomized controlled study in healthy men and women”. In: *Pain* 160.8 (Aug. 2019), pp. 1719–1728. ISSN: 18726623. DOI: 10.1097/j.pain.0000000000001579.

[404] Matthew Alsaloum and Stephen G. Waxman. “iPSCs and DRGs: stepping stones to new pain therapies”. In: *Trends Mol. Med* 28.2 (Feb. 2022), pp. 110–122. ISSN: 1471499X. DOI: 10.1016/j.molmed.2021.11.005.

[405] Angelika Lampert et al. “Human sensory neurons derived from pluripotent stem cells for disease modelling and personalized medicine”. In: *Neurobio. Pain* 8 (2020), p. 100055. ISSN: 2452073X. DOI: 10.1016/j.ynpai.2020.100055. URL: https://doi.org/10.1016/j.ynpai.2020.100055.

[406] Yasuhiro Umemura et al. “Human Circadian Molecular Oscillation Development Using Induced Pluripotent Stem Cells”. In: *J. Biol. Rhythms* 34.5 (2019), pp. 525–532. ISSN: 15524531. DOI: 10.1177/0748730419865436.

[407] Stuart M. Chambers et al. “Highly efficient neural conversion of human ES and iPS cells by dual inhibition of SMAD signaling”. In: *Nat. Biotechnol* 27.3 (2009), pp. 275–280. ISSN: 10870156. DOI: 10.1038/nbt.1529.

[408] Stuart M. Chambers et al. “Combined small-molecule inhibition accelerates developmental timing and converts human pluripotent stem cells into nociceptors”. In: *Nat. Biotechnol* 30.7 (2012), pp. 715–720. ISSN: 10870156. DOI: 10.1038/nbt.2249.

[409] Julie I.R. Labau et al. “Recent advances for using human induced-pluripotent stem cells as pain-in-a-dish models of neuropathic pain”. In: *Exp. Neurol* 358.September (2022), p. 114223. ISSN: 10902430. DOI: 10.1016/j.expneurol.2022.114223.

[410] Serena Viventi and Mirella Dottori. “Modelling the dorsal root ganglia using human pluripotent stem cells: A platform to study peripheral neuropathies”. In: *Int. J. Biochem. Cell Biol* 100.June (2018), pp. 61–68. ISSN: 18785875. DOI: 10.1016/j.biocel.2018.05.005.

[411] Gareth T. Young et al. “Characterizing human stem cell-derived sensory neurons at the single-cell level reveals their ion channel expression and utility in pain research”. In: *Mol. Ther* 22.8 (2014), pp. 1530–1543. ISSN: 15250024. DOI: 10.1038/mt.2014.86.

[412] Maximilian Zeidler, Kai K. Kummer, and Michaela Kress. "Towards bridging the translational gap by improved modeling of human nociception in health and disease". In: *Pflug. Arch. Eur. J. Physiol* 474.9 (2022), pp. 965–978. ISSN: 14322013. DOI: 10.1007/s00424-022-02707-6.

[413] Kenyi Saito-Diaz et al. "Isolation of human pluripotent stem cell-derived sensory neuron subtypes by immunopanning". In: *Front. Cell Dev. Biol* 11 (2023). ISSN: 2296634X. DOI: 10.3389/fcell.2023.1101423.

[414] Tao Deng et al. "Scalable generation of sensory neurons from human pluripotent stem cells". In: *Stem Cell Rep* 18.4 (2023), pp. 1030–1047. ISSN: 22136711. DOI: 10.1016/j.stemcr.2023.03.006.

[415] Nesia A. Zurek et al. "Electrophysiological analyses of human dorsal root ganglia and human induced pluripotent stem cell-derived sensory neurons from male and female donors". In: *J. Pain* (Dec. 2023). ISSN: 15265900. DOI: 10.1016/j.jpain.2023.12.008.

[416] Pascal Roderer et al. "Emergence of nociceptive functionality and opioid signaling in human induced pluripotent stem cell-derived sensory neurons". In: *Pain* 164.8 (Aug. 2023), pp. 1718–1733. ISSN: 18726623. DOI: 10.1097/j.pain.0000000000002860.

[417] Clemens L. Schoepf et al. "Selected ionotropic receptors and voltage-gated ion channels: More functional competence for human induced pluripotent stem cell (ipsc)-derived nociceptors". In: *Brain Sci* 10.6 (2020). ISSN: 20763425. DOI: 10.3390/brainsci10060344.

[418] Anna Katharina Holzer et al. "Generation of Human Nociceptor-Enriched Sensory Neurons for the Study of Pain-Related Dysfunctions". In: *Stem Cells Transl. Med* 11.7 (July 2022), pp. 727–741. ISSN: 21576580. DOI: 10.1093/stcltm/szac031.

[419] Siddharth Nimbalkar et al. "Development of a functional human induced pluripotent stem cell-derived nociceptor MEA system as a pain model for analgesic drug testing". In: *Front. Cell Dev. Biol* 11.March (2023), pp. 1–11. ISSN: 2296634X. DOI: 10.3389/fcell.2023.1011145.

[420] Jannis E. Meents et al. “The role of Nav1.7 in human nociceptors: Insights from human induced pluripotent stem cell-derived sensory neurons of erythromelalgia patients”. In: *Pain* 160.6 (June 2019), pp. 1327–1341. ISSN: 18726623. DOI: 10.1097/j.pain.0000000000001511.

[421] Therese C. Alich et al. “Bringing to light the physiological and pathological firing patterns of human induced pluripotent stem cell-derived neurons using optical recordings”. In: *Front. Cell. Neurosci* 16 (Jan. 2023). ISSN: 16625102. DOI: 10.3389/fncel.2022.1039957.

[422] Marília Z.P. Guimaraes et al. “Generation of iPSC-Derived Human Peripheral Sensory Neurons Releasing Substance P Elicited by TRPV1 Agonists”. In: *Front. Mol. Neurosci* 11 (Aug. 2018). ISSN: 16625099. DOI: 10.3389/fnmol.2018.00277.

[423] Joel W. Blanchard et al. “Selective conversion of fibroblasts into peripheral sensory neurons”. In: *Nat. Neurosci.* 18.1 (2015), pp. 25–35. ISSN: 15461726. DOI: 10.1038/nn.3887.

[424] Brian J. Wainger et al. “Modeling pain in vitro using nociceptor neurons reprogrammed from fibroblasts”. In: *Nat. Neurosci.* 18.1 (2015), pp. 17–24. ISSN: 15461726. DOI: 10.1038/nn.3886.

[425] Katrin Schrenk-Siemens et al. “Human Stem Cell-Derived TRPV1-Positive Sensory Neurons: A New Tool to Study Mechanisms of Sensitization”. In: *Cells* 11.18 (Sept. 2022). ISSN: 20734409. DOI: 10.3390/cells11182905.

[426] Amy J. Hulme et al. “Molecular and Functional Characterization of Neurogenin-2 Induced Human Sensory Neurons”. In: *Front. Cell. Neurosci* 14.December (2020), pp. 1–18. ISSN: 16625102. DOI: 10.3389/fncel.2020.600895.

[427] Jong Hee Lee et al. “Single Transcription Factor Conversion of Human Blood Fate to NPCs with CNS and PNS Developmental Capacity”. In: *Cell Rep* 11.9 (2015), pp. 1367–1376. ISSN: 22111247. DOI: 10.1016/j.celrep.2015.04.056.

[428] Kinga Vojnits et al. “Chemotherapy-Induced Neuropathy and Drug Discovery Platform Using Human Sensory Neurons Converted Directly from Adult Peripheral

Blood". In: *Stem Cells Transl. Med* 8.11 (2019), pp. 1180–1191. ISSN: 21576580. DOI: 10.1002/sctm.19-0054.

[429] Ji-Il Kim et al. "Human assembloid model of the ascending neural sensory pathway". In: *Nature* 642 (2025), pp. 143–153. DOI: 10.1038/s41586-025-08808-3.

[430] Carolynn M Dude et al. "Activation of Pax3 target genes is necessary but not sufficient for neurogenesis in the ophthalmic trigeminal placode". In: *Dev. Biol* 326.2 (2009), pp. 314–326. DOI: 10.1016/j.ydbio.2008.11..

[431] Sunita Singh and Andrw K. Groves. "The Molecular Basis of Craniofacial Placode Development". In: *Wiley Interdiscip Rev Dev Biol* 5.3 (2016), pp. 363–376. DOI: 10.1002/wdev.226..

[432] Salim Megat et al. "Differences between dorsal root and trigeminal ganglion nociceptors in mice revealed by translational profiling". In: *J. Neurosci* 39.35 (Aug. 2019), pp. 6829–6847. ISSN: 15292401. DOI: 10.1523/JNEUROSCI.2663-18.2019.

[433] Zehra Dincer et al. "Specification of functional cranial placode derivatives from human pluripotent stem cells". In: *Cell Rep* 5.5 (2013), pp. 1387–1402. ISSN: 22111247. DOI: 10.1016/j.celrep.2013.10.048.

[434] Quentin Muller et al. "Development of an innervated tissue-engineered skin with human sensory neurons and Schwann cells differentiated from iPS cells". In: *Acta Biomaterialia* 82 (2018), pp. 93–101. ISSN: 18787568. DOI: 10.1016/j.actbio.2018.10.011.

[435] Jason Tchieu et al. "A Modular Platform for Differentiation of Human PSCs into All Major Ectodermal Lineages". In: *Cell Stem Cell* 21.3 (2017), pp. 399–410. ISSN: 18759777. DOI: 10.1016/j.stem.2017.08.015.

[436] Bastian Zimmer et al. "Human iPSC-derived trigeminal neurons lack constitutive TLR3-dependent immunity that protects cortical neurons from HSV-1 infection". In: *PNAS* 115.37 (2018), E8775–E8782. ISSN: 10916490. DOI: 10.1073/pnas.1809853115.

[437] Anil Kumar Kalia et al. “How to differentiate induced pluripotent stem cells into sensory neurons for disease modelling: a functional assessment”. In: *Stem Cell Res. Ther* 15.1 (Apr. 2024), p. 99. ISSN: 1757-6512. DOI: 10.1186/s13287-024-03696-2.

[438] Philippa Pettingill et al. “A causal role for TRESK loss of function in migraine mechanisms”. In: *Brain* 142.12 (2019), pp. 3852–3867. ISSN: 14602156. DOI: 10.1093/brain/awz342.

[439] Swetha E Murthy et al. “The mechanosensitive ion channel Piezo2 mediates sensitivity to mechanical pain in mice”. In: *Sci. Transl. Med* 10 (2018).

[440] Nicholas W. Villarino et al. “Labeling PIEZO2 activity in the peripheral nervous system”. In: *Neuron* 111.16 (Aug. 2023), pp. 2488–2501. ISSN: 10974199. DOI: 10.1016/j.neuron.2023.05.015.

[441] Chelsey J LeBlang et al. “Satellite glial contact enhances differentiation and maturation of human iPSC-derived sensory neurons”. In: *bioRxiv* (2024). DOI: 10.1101/2024.07.24.604966. URL: https://doi.org/10.1101/2024.07.24.604966.

[442] Yi Liu et al. “The pain target NaV1.7 is expressed late during human iPS cell differentiation into sensory neurons as determined in high-resolution imaging”. In: *Pflug. Arch. Eur. J. Physiol* 476.6 (June 2024), pp. 975–992. ISSN: 14322013. DOI: 10.1007/s00424-024-02945-w.

[443] Cedric Bardy et al. “Neuronal medium that supports basic synaptic functions and activity of human neurons in vitro”. In: *PNAS* 112.20 (May 2015), E2725–E2734. ISSN: 10916490. DOI: 10.1073/pnas.1504393112.

[444] Qin Li and Brian D Burrell. “CNQX and AMPA inhibit electrical synaptic transmission: a potential interaction between electrical and glutamatergic synapses”. In: *Brain Res* 1228 (2008), pp. 43–57. DOI: 10.1016/j.brainres.2008.06.035..

[445] Bryan James Black et al. “Phenotypic Screening of Prospective Analgesics Among FDA-Approved Compounds using an iPSC-Based Model of Acute and Chronic

Inflammatory Nociception". In: *Adv. Sci* 11.11 (Mar. 2024). ISSN: 21983844. DOI: 10.1002/advs.202303724.

[446] William Plumbly et al. "Derivation of nociceptive sensory neurons from hiPSCs with early patterning and temporally controlled NEUROG2 overexpression". In: *Cell Rep. Methods* 2.11 (2022), p. 100341. ISSN: 26672375. DOI: 10.1016/j.crmeth.2022.100341.

[447] Matthijs J. Warrens and Hanneke van der Hoef. "Understanding the Adjusted Rand Index and Other Partition Comparison Indices Based on Counting Object Pairs". In: *J. Classif* 39.3 (Nov. 2022), pp. 487–509. ISSN: 14321343. DOI: 10.1007/s00357-022-09413-z.

[448] Danielle Sambo et al. "Transient treatment of human pluripotent stem cells with dmso to promote differentiation". In: *JoVE* 2019.149 (July 2019). ISSN: 1940087X. DOI: 10.3791/59833.

[449] Johanna F. Dekkers et al. "High-resolution 3D imaging of fixed and cleared organoids". In: *Nature Prot* 14.6 (June 2019), pp. 1756–1771. ISSN: 17502799. DOI: 10.1038/s41596-019-0160-8.

[450] Dawidson A. Gomes et al. "c-Met must translocate to the nucleus to initiate calcium signals". In: *J. Biol. Chem* 283.7 (Feb. 2008), pp. 4344–4351. ISSN: 00219258. DOI: 10.1074/jbc.M706550200.

[451] Mei Kuang Chen et al. "H2O2 induces nuclear transport of the receptor tyrosine kinase c-MET in breast cancer cells via a membrane-bound retrograde trafficking mechanism". In: *J. Biol. Chem* 294.21 (May 2019), pp. 8516–8528. ISSN: 1083351X. DOI: 10.1074/jbc.RA118.005953.

[452] Tayla A. Rees et al. "CGRP and the Calcitonin Receptor are Co-Expressed in Mouse, Rat and Human Trigeminal Ganglia Neurons". In: *Front. Physiol* 13 (May 2022). ISSN: 1664042X. DOI: 10.3389/fphys.2022.860037.

[453] La Tasha K. Crawford and Michael J. Caterina. "Functional Anatomy of the Sensory Nervous System: Updates From the Neuroscience Bench". In: *Toxicol. Pathol* 48.1 (Jan. 2020), pp. 174–189. ISSN: 15331601. DOI: 10.1177/0192623319869011.

[454] S. Eftekhari et al. “Differential distribution of calcitonin gene-related peptide and its receptor components in the human trigeminal ganglion”. In: *Neuroscience* 169.2 (2010), pp. 683–696. ISSN: 03064522. DOI: 10.1016/j.neuroscience.2010.05.016.

[455] Perla Lazar et al. “The action of calcitonin gene-related peptide on astrocyte morphology and cyclic AMP accumulation in astrocyte cultures from neonatal rat brain”. In: *Neurosci. Lett* 130 (1991), pp. 99–102.

[456] Ambrish Kumar et al. “Alpha-Calcitonin Gene Related Peptide: New Therapeutic Strategies for the Treatment and Prevention of Cardiovascular Disease and Migraine”. In: *Front. Phyiol* 13 (Feb. 2022). ISSN: 1664042X. DOI: 10.3389/fphys.2022.826122.

[457] Jennifer Lawson et al. “Electrically-evoked oscillating calcium transients in mono- and co-cultures of iPSC glia and sensory neurons”. In: *Front. Cell. Neurosci* 17.March (2023), pp. 1–13. DOI: 10.3389/fncel.2023.1094070.

[458] Larry V. Pearce et al. “Combination of a rapidly penetrating agonist and a slowly penetrating antagonist affords agonist action of limited duration at the cellular level”. In: *Biomol. Ther* 27.5 (Sept. 2019), pp. 435–441. ISSN: 20054483. DOI: 10.4062/biomolther.2019.013.

[459] Narender R. Gavva et al. “AMG 9810 [(E)-3-(4-t-butylphenyl)-N-(2,3-dihydrobenzo[b][1,4] dioxin-6-yl)acrylamide], a novel vanilloid receptor 1 (TRPV1) antagonist with antihyperalgesic properties”. In: *J. Pharmacol. Exp. Ther* 313.1 (Apr. 2005), pp. 474–484. ISSN: 00223565. DOI: 10.1124/jpet.104.079855.

[460] Alicia Alpuente et al. “Dynamic fluctuations of salivary CGRP levels during migraine attacks: association with clinical variables and phenotypic characterization”. In: *J. Headache Pain* 25.1 (Apr. 2024), p. 58. ISSN: 1129-2377. DOI: 10.1186/s10194-024-01772-9.

[461] Jakob MÃ¸ller Hansen et al. “Calcitonin gene-related peptide triggers migraine-like attacks in patients with migraine with aura”. In: *Cephalalgia* 30.10 (Oct. 2010), pp. 1179–1186. ISSN: 03331024. DOI: 10.1177/0333102410368444.

[462] Heidi Hautakangas et al. “Genome-wide analysis of 102,084 migraine cases identifies 123 risk loci and subtype-specific risk alleles”. In: *Nat. Genet* 54.2 (Feb. 2022), pp. 152–160. ISSN: 15461718. DOI: 10.1038/s41588-021-00990-0.

[463] Johra Khan et al. *Genetics, pathophysiology, diagnosis, treatment, management, and prevention of migraine*. July 2021. DOI: 10.1016/j.biopha.2021.111557.

[464] Heidi G Sutherland, Bronwyn Jenkins, and Lyn R Griffiths. “Genetics of migraine: complexity, implications, and potential clinical applications”. In: *Lancet Neurol* 23 (2024), pp. 429–475. URL: www.thelancet.com/neurology.

[465] Francis Sahngun Nahm. “Nonparametric statistical tests for the continuous data: The basic concept and the practical use”. In: *Korean J. Anesthesiol* 69.1 (Feb. 2016), pp. 8–14. ISSN: 20057563. DOI: 10.4097/kjae.2016.69.1.8.

[466] Kane Meissel and Esther S Yao. “Using Cliff’s Delta as a Non-Parametric Effect Size Measure: An Accessible Web App and R Tutorial”. In: *Pract. Assess. Res. Eval* 29.2 (2024). ISSN: 1531-7714. URL: https://cliffdelta.shinyapps.io/calculator;.

[467] Xiaoli Song et al. “Trigeminal nerve-driven neurogenic inflammation linking migraine to glioblastoma invasion: a literature review”. In: *Front. Immunol* 16 (2025). ISSN: 16643224. DOI: 10.3389/fimmu.2025.1632154.

[468] Anja Holm et al. “RAMP1-dependent hormonal regulation of CGRP and its receptor in the trigeminal ganglion”. In: *J. Headache Pain* 26.1 (Dec. 2025). ISSN: 11292377. DOI: 10.1186/s10194-025-02071-7.

[469] Marc Vila Cuenca et al. “Vascularization of organoid microenvironments: Perfusable networks for organoid growth and maturation”. In: *Curr. Opin. Biomed. Eng* 34 (June 2025). ISSN: 24684511. DOI: 10.1016/j.cobme.2025.100586.

[470] Juan M. Jimenez-Andrade et al. “Vascularization of the dorsal root ganglia and peripheral nerve of the mouse: Implications for chemical-induced peripheral sensory neuropathies”. In: *Mol. Pain* 4 (Mar. 2008). ISSN: 17448069. DOI: 10.1186/1744-8069-4-10.

[471] Rui Zhou et al. “Vascularised organoids: Recent advances and applications in cancer research”. In: *Clin. Transl. Med* 15.3 (Mar. 2025). ISSN: 2001-1326. DOI: 10.1002/ctm2.70258.

[472] Anna K. Eigenbrodt et al. “Diagnosis and management of migraine in ten steps”. In: *Nat. Rev. Neurol* 17.8 (Aug. 2021), pp. 501–514. ISSN: 17594766. DOI: 10.1038/s41582-021-00509-5.

[473] Jan Hoffmann, Serapio M. Baca, and Simon Akerman. “Neurovascular mechanisms of migraine and cluster headache”. JCBFM. In: 39.4 (Apr. 2019), pp. 573–594. ISSN: 15597016. DOI: 10.1177/0271678X17733655.

[474] Lan Dao et al. “Modeling blood-brain barrier formation and cerebral cavernous malformations in human PSC-derived organoids”. In: *Cell Stem Cell* 31.6 (June 2024), pp. 818–833. ISSN: 18759777. DOI: 10.1016/j.stem.2024.04.019.

[475] Doris Krauter et al. “Spatial organization, chromatin accessibility and gene-regulatory programs defining mouse sensory neurons”. In: *Commun. Biol* 8.1 (Dec. 2025). ISSN: 23993642. DOI: 10.1038/s42003-025-08315-1.

[476] Menachem Hanani. “Satellite Glial Cells in Human Disease”. In: *Cells* 13.7 (Apr. 2024). ISSN: 20734409. DOI: 10.3390/cells13070566.

[477] Kota Miura, Kota. Miura, and Natasa. Sladoje. *Bioimage Data Analysis Workflows - Advanced Components and Methods*. 1st ed. Learning Materials in Biosciences. Cham: Springer Nature, 2022. ISBN: 3-030-76394-3.

[478] Meghan W. Sedovy et al. “Connexin 43 across the Vasculature: Gap Junctions and Beyond”. In: *J. Vasc. Res* 60.2 (Sept. 2023), pp. 101–113. ISSN: 14230135. DOI: 10.1159/000527469.

[479] Anna F. Rockel et al. “Neuro-mesodermal assembloids recapitulate aspects of peripheral nervous system development in vitro”. In: *Stem Cell Rep* 18.5 (May 2023), pp. 1155–1165. ISSN: 22136711. DOI: 10.1016/j.stemcr.2023.03.012.

[480] Hojae Bae et al. “Building vascular networks”. In: *Sci. Transl. Med* 4.160 (Nov. 2012). ISSN: 19466234. DOI: 10.1126/scitranslmed.3003688.

[481] Jianghui Meng et al. "TNFα induces co-trafficking of TRPV1/TRPA1 in VAMP1-containing vesicles to the plasmalemma via Munc18-1/syntaxin1/SNAP-25 mediated fusion". In: *Sci. Rep* 6 (Feb. 2016). ISSN: 20452322. DOI: 10.1038/srep21226.

[482] Menachem Hanani and Alexei Verkhratsky. "Satellite Glial Cells and Astrocytes, a Comparative Review". In: *Neurochem. Res* 46.10 (2021), pp. 2525–2537. ISSN: 15736903. DOI: 10.1007/s11064-021-03255-8. URL: https://doi.org/10.1007/s11064-021-03255-8.

[483] Seung Hyun Yoo. "pH- and Ca2+-dependent aggregation property of secretory vesicle matrix proteins and the potential role of chromogranins A and B in secretory vesicle biogenesis". In: *J. Biol. Chem* 271.3 (Jan. 1996), pp. 1558–1565. ISSN: 00219258. DOI: 10.1016/s0021-9258(17)44964-7.

[484] Minnie M. Wu et al. "Mechanisms of pH Regulation in the Regulated Secretory Pathway". In: *J. Biol. Chem* 276.35 (Aug. 2001), pp. 33027–33035. ISSN: 00219258. DOI: 10.1074/jbc.M103917200.

[485] Timothy J. Mead and Katherine E. Yutzey. "Notch pathway regulation of neural crest cell development in vivo". In: *Dev. Dyn* 241.2 (Feb. 2012), pp. 376–389. ISSN: 10588388. DOI: 10.1002/dvdy.23717.

[486] Chengxiang Qiu et al. "Systematic reconstruction of cellular trajectories across mouse embryogenesis". In: *Nat. Genet* 54.3 (Mar. 2022), pp. 328–341. ISSN: 15461718. DOI: 10.1038/s41588-022-01018-x.

[487] Sophie Wiszniak and Quenten Schwarz. "Notch signalling defines dorsal root ganglia neuroglial fate choice during early neural crest cell migration". In: *BMC Neurosci* 20.1 (Apr. 2019). ISSN: 14712202. DOI: 10.1186/s12868-019-0501-0.

[488] Mariko Kato Hayashi, Kaoru Sato, and Yuko Sekino. "Neurons Induce Tiled Astrocytes with Branches That Avoid Each Other". In: *Int. J. Mol. Sci* 23.8 (Apr. 2022). ISSN: 14220067. DOI: 10.3390/ijms23084161.

[489] Austin B. Keeler et al. "A developmental atlas of somatosensory diversification and maturation in the dorsal root ganglia by single-cell mass cytometry". In: *Nat.*

Neurosci. 25.11 (Nov. 2022), pp. 1543–1558. ISSN: 15461726. DOI: 10.1038/s41593-022-01181-8.

[490] Tamara Rosenbaum and Sidney A. Simon. "TRPV1 Receptors and Signal Transduction". In: *TRP Ion Channel Function in Sensory Transduction and Cellular Signaling Cascades*. Ed. by Wolfgang B Liedtke and Stefan Heller. Boca Raton (FL): CRC Press/Taylor & Francis, 2007. ISBN: 0849340489.

[491] M. J. Caterina et al. "Impaired Nociception and Pain Sensation in Mice Lacking the Capsaicin Receptor". In: *Science* 288.5464 (Apr. 2000), pp. 306–313. ISSN: 0036-8075. DOI: 10.1126/science.288.5464.306.

[492] Yaroslav M. Shuba. "Beyond Neuronal Heat Sensing: Diversity of TRPV1 Heat-Capsaicin Receptor-Channel Functions". In: *Front. Cell. Neurosci* 14 (Feb. 2021). ISSN: 16625102. DOI: 10.3389/fncel.2020.612480.

[493] Do Hoon Kwon et al. "Heat-dependent opening of TRPV1 in the presence of capsaicin". In: *Nat. Struct. Mol. Biol* 28.7 (July 2021), pp. 554–563. ISSN: 15459985. DOI: 10.1038/s41594-021-00616-3.

[494] JÃ¶rg Grandl et al. "Temperature-induced opening of TRPV1 ion channel is stabilized by the pore domain". In: *Nat. Neurosci* 13.6 (June 2010), pp. 708–714. ISSN: 10976256. DOI: 10.1038/nn.2552.

[495] Kun Yang et al. "Action of capsaicin on dorsal root-evoked synaptic transmission to substantia gelatinosa neurons in adult rat spinal cord slices". In: *Brain Res* 830 (1999), pp. 268–273.

[496] Valentina Comunanza et al. "Calcium-dependent inhibition of T-type calcium channels by TRPV1 activation in rat sensory neurons". In: *Pflug. Arch. Eur. J. Physiol* 462.5 (Nov. 2011), pp. 709–722. ISSN: 00316768. DOI: 10.1007/s00424-011-1023-5.

[497] Wenjun Zheng and Han Wen. "Heat activation mechanism of TRPV1: New insights from molecular dynamics simulation". In: *Temperature* 6.2 (Apr. 2019), pp. 120–131. ISSN: 23328959. DOI: 10.1080/23328940.2019.1578634.

[498] Thomas Voets et al. “The principle of temperature-dependent gating in cold-and heat-sensitive TRP channels”. In: *Nature* 430 (2004), pp. 748–754.

[499] Ardem Patapoutian et al. “Thermotrp channels and beyond: Mechanisms of temperature sensation”. In: *Nat. Rev. Neurosci* 4.7 (2003), pp. 529–539. ISSN: 14710048. DOI: 10.1038/nrn1141.

[500] Katharina GersâBarlag et al. “Transduction Mechanisms for Cold Temperature in Mouse Trigeminal and Vagal Ganglion Neurons Innervating Different Peripheral Organs”. In: *Acta Physiologica* 241.11 (Nov. 2025). ISSN: 1748-1708. DOI: 10.1111/apha.70111. URL: https://onlinelibrary.wiley.com/doi/10.1111/apha.70111.

[501] Kunitoshi Uchida. “TRPM3, TRPM4, and TRPM5 as thermo-sensitive channels”. In: *J. Physiol. Sci* 74.1 (Jan. 2024). ISSN: 18806546. DOI: 10.1186/s12576-024-00937-0.

[502] Makiko Kashio and Makoto Tominaga. *The TRPM2 channel: A thermo-sensitive metabolic sensor*. Sept. 2017. DOI: 10.1080/19336950.2017.1344801.

[503] Dan Wu et al. “Zcchc12-Containing Nociceptors Are Required for Noxious Heat Sensation”. In: *J. Neurosci* 42.13 (Mar. 2022), pp. 2690–2700. ISSN: 15292401. DOI: 10.1523/JNEUROSCI.1427-21.2022.

[504] Liu Yang et al. “FGF13 Selectively Regulates Heat Nociception by Interacting with Nav1.7”. In: *Neuron* 93.4 (Feb. 2017), pp. 806–821. ISSN: 10974199. DOI: 10.1016/j.neuron.2017.01.009.

[505] Sibah Hasan et al. “Assessment of circadian rhythms in humans: comparison of real-time fibroblast reporter imaging with plasma melatonin”. In: *FASEB* 26.6 (June 2012), pp. 2414–2423. ISSN: 0892-6638. DOI: 10.1096/fj.11-201699.

[506] Hitomi Kaneko, Taku Kaitsuka, and Kazuhito Tomizawa. “Response to Stimulations Inducing Circadian Rhythm in Human Induced Pluripotent Stem Cells”. In: *Cells* 9.3 (2020). ISSN: 20734409. DOI: 10.3390/cells9030620.

[507] Gianluigi Mazzoccoli et al. “Circadian transcriptome analysis in human fibroblasts from Hunter syndrome and impact of iduronate-2-sulfatase treatment”. In: *BMC Med. Genet* 6.1 (2013). ISSN: 17558794. DOI: 10.1186/1755-8794-6-37.

[508] Silke Kiessling et al. “Enhancing circadian clock function in cancer cells inhibits tumor growth”. In: *BMC Biol* 15.1 (Feb. 2017). ISSN: 17417007. DOI: 10.1186/s12915-017-0349-7.

[509] Uma Kizhuveetil et al. “Entrainment of superoxide rhythm by menadione in HCT116 colon cancer cells”. In: *Sci. Rep* 9.1 (Dec. 2019). ISSN: 20452322. DOI: 10.1038/s41598-019-40017-7.

[510] Kevin A. Feeney et al. “In-depth Characterization of Firefly Luciferase as a Reporter of Circadian Gene Expression in Mammalian Cells”. In: *J. Biol. Rhythms* 31.6 (Dec. 2016), pp. 540–550. ISSN: 15524531. DOI: 10.1177/0748730416668898.

[511] Tsuyoshi Hirota and Steve A. Kay. “High-Throughput Screening and Chemical Biology: New Approaches for Understanding Circadian Clock Mechanisms”. In: *Chem. Biol* 16.9 (Sept. 2009), pp. 921–927. ISSN: 10745521. DOI: 10.1016/j.chembiol.2009.09.002.

[512] Yang Shen et al. “NF-κB modifies the mammalian circadian clock through interaction with the core clock protein BMAL1”. In: *PLoS Genet* 17.11 (Nov. 2021). ISSN: 15537404. DOI: 10.1371/journal.pgen.1009933.

[513] Rafailia A.A. Beta et al. “Core clock regulators in dexamethasone-treated HEK 293T cells at 4Â h intervals”. In: *BMC Res. Notes* 15.1 (Dec. 2022). ISSN: 17560500. DOI: 10.1186/s13104-021-05871-7.

[514] Ann Atwood et al. “Cell-autonomous circadian clock of hepatocytes drives rhythms in transcription and polyamine synthesis”. In: *PNAS* 108.45 (Nov. 2011), pp. 18560–18565. ISSN: 00278424. DOI: 10.1073/pnas.1115753108.

[515] Sung Kook Chun and Selma Masri. “Circadian Control of Transcriptional and Metabolic Rhythms in Primary Hepatocytes”. In: *Methods in Molecular Biology,* vol. 2482. Humana Press Inc., 2022, pp. 169–179. DOI: 10.1007/978-1-0716-2249-0{_}11.

[516] Daisuke Yamajuku et al. “Real-time monitoring in three-dimensional hepatocytes reveals that insulin acts as a synchronizer for liver clock”. In: *Sci. Rep* 2 (2012). ISSN: 20452322. DOI: 10.1038/srep00439.

[517] K. Yagita et al. “Molecular mechanisms of the biological clock in cultured fibroblasts”. In: *Science* 292.5515 (2001), pp. 278–281. ISSN: 00368075. DOI: 10.1126/science.1059542.

[518] Francesca Agriesti, Olga Cela, and Nazzareno Capitanio. “"Time Is out of Joint" in Pluripotent Stem Cells: How and Why”. In: *Int. J. Mol. Sci* 25.4 (Feb. 2024). ISSN: 14220067. DOI: 10.3390/ijms25042063.

[519] Kenan Courtney, Sevilla Detera-Wadleigh, and Francis McMahon. “Cyclic Expression of Circadian Genes in Neural Progenitor Cells Derived from Human Induced Pluripotent Stem Cells”. In: *Biol. Psychiatry* 81.10, Supplement (2017), S205–S206. ISSN: 0006-3223. DOI: https://doi.org/10.1016/j.biopsych.2017.02.1114.

[520] Himanshu K. Mishra et al. “Circadian rhythms in bipolar disorder patient-derived neurons predict lithium response: preliminary studies”. In: *Mol. Psychiatry* 26.7 (2021), pp. 3383–3394. ISSN: 14765578. DOI: 10.1038/s41380-021-01048-7.

[521] Aurelio Balsalobre, Francesca Damiola, and Ueli Schibler. “A Serum Shock Induces Circadian Gene Expression in Mammalian Tissue Culture Cells”. In: *Cell* 93 (1998), pp. 929–937.

[522] Onelia Gagliano et al. “Synchronization between peripheral circadian clock and feeding-fasting cycles in microfluidic device sustains oscillatory pattern of transcriptome”. In: *Nat. Commun* 12.1 (2021), pp. 1–12. ISSN: 20411723. DOI: 10.1038/s41467-021-26294-9.

[523] Steven A. Brown et al. “Rhythms of Mammalian Body Temperature Can Sustain Peripheral Circadian Clocks”. In: *Curr. Biol* 12 (Sept. 2002), pp. 1574–1583.

[524] Weston T. Powell et al. “Temperature synchronisation of circadian rhythms in primary human airway epithelial cells from children”. In: *BMJ Open Respiratory Research* 9.1 (Oct. 2022). ISSN: 20524439. DOI: 10.1136/bmjresp-2022-001319.

[525] Kazuhiro Yagita and Hitoshi Okamura. "Forskolin induces circadian gene expression of rPer1, rPer2 and dbp in mammalian rat-1 fibroblasts". In: *FEBS Letters* 465.1 (2000), pp. 79–82. ISSN: 0014-5793. DOI: https://doi.org/10.1016/S0014-5793(99)01724-X.

[526] A. Balsalobre et al. "Resetting of circadian time in peripheral tissues by glucocorticoid signaling". In: *Science* 289.5488 (2000), pp. 2344–2347. ISSN: 00368075. DOI: 10.1126/science.289.5488.2344.

[527] Elan Ness-Cohn et al. "TimeTrial: An Interactive Application for Optimizing the Design and Analysis of Transcriptomic Time-Series Data in Circadian Biology Research". In: *J. Biol. Rhythms* 35.5 (Oct. 2020), pp. 439–451. ISSN: 15524531. DOI: 10.1177/0748730420934672.

[528] Aurelio Balsalobre, Lysiane Marcacci, and Ueli Schibler. "Multiple signaling pathways elicit circadian gene expression in cultured Rat-1 fibroblasts". In: *Curr. Biol* 10.20 (2000), pp. 1291–1294.

[529] Daniel Mauvoisin et al. "Circadian clock-dependent and -independent rhythmic proteomes implement distinct diurnal functions in mouse liver". In: *PNAS* 111.1 (2014), pp. 167–172. ISSN: 00278424. DOI: 10.1073/pnas.1314066111.

[530] Allan Giri and Isaac Kirubakaran Sundar. "Evaluation of stable reference genes for qPCR normalization in circadian studies related to lung inflammation and injury in mouse model". In: *Sci. Rep* 12.1 (2022), pp. 1–14. ISSN: 20452322. DOI: 10.1038/s41598-022-05836-1.

[531] Rok Kosir et al. "Determination of reference genes for circadian studies in different tissues and mouse strains". In: *BMC Mol. Biol* 11.60 (2010). URL: http://www.biomedcentral.com/1471-2199/11/60.

[532] Reiko Nakao et al. "Determination of reference genes that are independent of feeding rhythms for circadian studies of mouse metabolic tissues". In: *Mol. Genet. Metab* 121.2 (June 2017), pp. 190–197. ISSN: 10967206. DOI: 10.1016/j.ymgme.2017.04.001.

[533] Valeria Valente et al. “Selection of suitable housekeeping genes for expression analysis in glioblastoma using quantitative RT-PCR”. In: *Ann. Neurosci* 21.2 (2014), pp. 62–63. ISSN: 09763260. DOI: 10.5214/ans.0972.7531.210207.

[534] Ritsuko Matsumura et al. “Compensation for intracellular environment in expression levels of mammalian circadian clock genes”. In: *Sci. Rep* 4 (2014), pp. 1–6. ISSN: 20452322. DOI: 10.1038/srep04032.

[535] Jeremy M. White et al. “Reference Gene Optimization for Circadian Gene Expression Analysis in Human Adipose Tissue”. In: *J. Biol. Rhythms* 35.1 (Feb. 2020), pp. 84–97. ISSN: 15524531. DOI: 10.1177/0748730419883043.

[536] Jo Vandesompele et al. “Accurate normalization of real-time quantitative RT-PCR data by geometric averaging of multiple internal control genes”. In: *Genome Biol* 3.7 (2002), pp. 1–0034. URL: http://genomebiology.com/2002/3/7/research/0034.1Correspondence:.rankSpeleman..

[537] Fuliang Xie, Jianyu Wang, and Baohong Zhang. “RefFinder: a web-based tool for comprehensively analyzing and identifying reference genes”. In: *Funct. Integr. Genom* 23.2 (June 2023). ISSN: 14387948. DOI: 10.1007/s10142-023-01055-7.

[538] Nikolaus Fortelny et al. “Can we predict protein from mRNA levels?” In: *Nature* 547.7664 (2017), E19–E20. ISSN: 1476-4687. DOI: 10.1038/nature22293. URL: https://doi.org/10.1038/nature22293.

[539] Mathias Wilhelm et al. “Mass-spectrometry-based draft of the human proteome”. In: *Nature* 509.7502 (2014), pp. 582–587. ISSN: 14764687. DOI: 10.1038/nature13319.

[540] Murodzhon Akhmedov et al. “Omics Playground: a comprehensive self-service platform for visualization, analytics and exploration of Big Omics Data”. In: *NAR Genom. Bioinform* 2.1 (Mar. 2020), lqz019. ISSN: 2631-9268. DOI: 10.1093/nargab/lqz019. URL: https://doi.org/10.1093/nargab/lqz019.

[541] Weijia Kong et al. “Dealing with missing values in proteomics data”. In: *Proteomics* 22.23-24 (Dec. 2022). ISSN: 16159861. DOI: 10.1002/pmic.202200092.

[542] Kathryn A. McGurk et al. “The use of missing values in proteomic data-independent acquisition mass spectrometry to enable disease activity discrimination”. In: *Bioinformatics* 36.7 (Apr. 2020), pp. 2217–2223. ISSN: 14602059. DOI: 10.1093/bioinformatics/btz898.

[543] M. Walid Qoronfleh et al. “Selective Enrichment of Membrane Proteins by Partition Phase Separation for Proteomic Studies”. In: *J. Biomed. Biotechnol* 2003.4 (Oct. 2003), pp. 249–255. ISSN: 11107243. DOI: 10.1155/S1110724303209244.

[544] Gisel Barés et al. “Mammalian TatD DNase domain containing 1 (TATDN1) is a proteostasis-responsive gene with roles in ventricular structure and neuromuscular function”. In: *FEBS* (2025). ISSN: 17424658. DOI: 10.1111/febs.70077.

[545] Adham Farah et al. “A role for leucine-rich, glioma inactivated 1 in regulating pain sensitivity”. In: *Brain* 148.3 (Mar. 2025), pp. 1001–1014. ISSN: 14602156. DOI: 10.1093/brain/awae302.

[546] Bobbie Jo M. Webb-Robertson et al. “Review, evaluation, and discussion of the challenges of missing value imputation for mass spectrometry-based label-free global proteomics”. In: *J. Proteome Res* 14.5 (May 2015), pp. 1993–2001. ISSN: 15353907. DOI: 10.1021/pr501138h.

[547] John Healy and Leland McInnes. “Uniform manifold approximation and projection”. In: *Nat. Rev. Methods Primers* 4.1 (Dec. 2024). ISSN: 26628449. DOI: 10.1038/s43586-024-00363-x.

[548] Michael I. Love, Wolfgang Huber, and Simon Anders. “Moderated estimation of fold change and dispersion for RNA-seq data with DESeq2”. In: *Genome Biology* 15.12 (Dec. 2014). ISSN: 1474760X. DOI: 10.1186/s13059-014-0550-8.

[549] Mark D. Robinson, Davis J. McCarthy, and Gordon K. Smyth. “edgeR: A Bioconductor package for differential expression analysis of digital gene expression data”. In: *Bioinformatics* 26.1 (Nov. 2009), pp. 139–140. ISSN: 14602059. DOI: 10.1093/bioinformatics/btp616.

[550] Matthew E. Ritchie et al. “Limma powers differential expression analyses for RNA-sequencing and microarray studies”. In: *Nucleic Acids Res* 43.7 (Jan. 2015), e47. ISSN: 13624962. DOI: 10.1093/nar/gkv007.

[551] Alexandra Pokhilko, Anthony Nash, and M. Zameel Cader. “Common transcriptional signatures of neuropathic pain”. In: *Pain* 161.7 (July 2020), pp. 1542–1554. ISSN: 18726623. DOI: 10.1097/j.pain.0000000000001847.

[552] Alexandros H Kanellopoulos et al. “ Mapping protein interactions of sodium channel Na V 1.7 using epitopeâtagged geneâtargeted mice ”. In: *EMBO* 37.3 (Feb. 2018), pp. 427–445. ISSN: 0261-4189. DOI: 10.15252/embj.201796692.

[553] S. Laínez et al. “ GABA A receptor associated protein (GABARAP) modulates TRPV1 expression and channel function and desensitization ”. In: *FASEB* 24.6 (June 2010), pp. 1958–1970. ISSN: 0892-6638. DOI: 10.1096/fj.09-151472.

[554] Mirjam J. Eberhardt et al. “Methylglyoxal activates nociceptors through transient receptor potential channel A1 (TRPA1): A possible mechanism of metabolic neuropathies”. In: *J. Biol. Chem* 287.34 (Aug. 2012), pp. 28291–28306. ISSN: 1083351X. DOI: 10.1074/jbc.M111.328674.

[555] Ryan B. Griggs et al. “Methylglyoxal requires AC1 and TRPA1 to produce pain and spinal neuron activation”. In: *Front. Neurosci* 11.DEC (Dec. 2017). ISSN: 1662453X. DOI: 10.3389/fnins.2017.00679.

[556] David A. Andersson et al. “Methylglyoxal Evokes Pain by Stimulating TRPA1”. In: *PLoS ONE* 8.10 (Oct. 2013). ISSN: 19326203. DOI: 10.1371/journal.pone.0077986.

[557] Angelika Bierhaus et al. “Methylglyoxal modification of Na v 1.8 facilitates nociceptive neuron firing and causes hyperalgesia in diabetic neuropathy”. In: *Nat. Med* 18.6 (June 2012), pp. 926–933. ISSN: 10788956. DOI: 10.1038/nm.2750.

[558] Qian Huang et al. “Methylglyoxal mediates streptozotocin-induced diabetic neuropathic pain via activation of the peripheral TRPA1 and Nav1.8 channels”. In: *Metab. Clin. Exp* 65.4 (Apr. 2016), pp. 463–474. ISSN: 15328600. DOI: 10.1016/j.metabol.2015.12.002.

[559] Jonathan D. Enders et al. “Ketogenic diet prevents methylglyoxal-evoked nociception by scavenging methylglyoxal”. In: *Pain* 163.12 (Dec. 2022), E1207–E1216. ISSN: 18726623. DOI: 10.1097/j.pain.0000000000002667.

[560] M. J. Benitez et al. “Hsp90 activity is necessary to acquire a proper neuronal polarization”. In: *Biochimica et Biophysica Acta - Molecular Cell Research* 1843.2 (Feb. 2014), pp. 245–252. ISSN: 01674889. DOI: 10.1016/j.bbamcr.2013.11.013.

[561] Nashaat Z. Gerges et al. “Independent functions of hsp90 in neurotransmitter release and in the continuous synaptic cycling of AMPA receptors”. In: *J. Neurosci* 24.20 (May 2004), pp. 4758–4766. ISSN: 02706474. DOI: 10.1523/JNEUROSCI.0594-04.2004.

[562] Nivedita Verma et al. “Heat shock proteins in chronic pain: From molecular chaperones to pain modulators”. In: *Neuropharmacology* 266 (Mar. 2025). ISSN: 18737064. DOI: 10.1016/j.neuropharm.2024.110263.

[563] Wei Lei et al. “Heat-shock protein 90 (Hsp90) promotes opioid-induced antinociception by an ERK mitogen-activated protein kinase (MAPK) mechanism in mouse brain”. In: *J. Biol. Chem* 292.25 (June 2017), pp. 10414–10428. ISSN: 1083351X. DOI: 10.1074/jbc.M116.769489.

[564] Paul Bejarano et al. “Identification of the Hsp90 Isoforms and Co-Chaperones that Repress Opioid Anti-Nociception in the Spinal Cord”. In: *FASEB* 34.S1 (Apr. 2020), p. 1. ISSN: 0892-6638. DOI: https://doi.org/10.1096/fasebj.2020.34.s1.05462. URL: https://doi.org/10.1096/fasebj.2020.34.s1.05462.

[565] Yaomin Wang et al. “Expression of ectopic heat shock protein 90 in male and female primary afferent nociceptors regulates inflammatory pain”. In: *Pain* 163.6 (June 2022), pp. 1091–1101. ISSN: 18726623. DOI: 10.1097/j.pain.0000000000002511.

[566] Alexandre Charlet et al. “Abnormal nociception and opiate sensitivity of STOP null mice exhibiting elevated levels of the endogenous alkaloid morphine”. In: *Mol. Pain* 6.96 (2010). URL: http://www.molecularpain.com/content/6/1/96.

[567] Simona Antonacci et al. “Conserved RNA-binding proteins required for dendrite morphogenesis in Caenorhabditis elegans sensory neurons”. In: *G3: Genes, Genomes, Genetics* 5.4 (2015), pp. 639–653. ISSN: 21601836. DOI: 10.1534/g3.115.017327.

[568] Jin Ye et al. “Structural basis of GABARAP-mediated GABAA receptor trafficking and functions on GABAergic synaptic transmission”. In: *Nat. Commun* 12.1 (Dec. 2021). ISSN: 20411723. DOI: 10.1038/s41467-020-20624-z.

[569] Arthur Macha et al. “Gephyrin filaments represent the molecular basis of inhibitory postsynaptic densities”. In: *Nat. Commun* 16.1 (Sept. 2025), p. 8293. ISSN: 2041-1723. DOI: 10.1038/s41467-025-63748-w. URL: https://www.nature.com/articles/s41467-025-63748-w.

[570] Louis Etienne Lorenzo et al. “Gephyrin clusters are absent from small diameter primary afferent terminals despite the presence of GABAA receptors”. In: *J. Neurosci* 34.24 (2014), pp. 8300–8317. ISSN: 15292401. DOI: 10.1523/JNEUROSCI.0159-14.2014.

[571] Ashleigh E. Schaffer et al. “Biallelic loss of human CTNNA2, encoding αN-catenin, leads to ARP2/3 complex overactivity and disordered cortical neuronal migration”. In: *Nat. Genet* 50.8 (Aug. 2018), pp. 1093–1101. ISSN: 15461718. DOI: 10.1038/s41588-018-0166-0.

[572] Sylvanus Toikumo et al. “Etiological basis for chronic pain genetic variation in brain and dorsal root ganglia cell types”. In: *medRxiv* (July 2025). DOI: 10.1101/2025.07.03.25330832.

[573] Keira J.A. Johnston et al. “Genome-wide association study of multisite chronic pain in UK biobank”. In: *PLoS Genet* 15.6 (June 2019). ISSN: 15537404. DOI: 10.1371/journal.pgen.1008164.

[574] Wenli Yu et al. “Raf1 interacts with OIP5 to participate in oxaliplatin-induced neuropathic pain”. In: *Life Sci* 281 (Sept. 2021). ISSN: 18790631. DOI: 10.1016/j.lfs.2021.119804.

[575] Pavel Hanč and Ulrich H. von Andrian. “No pain, no gainÂ âÂ how nociceptors orchestrate tissue repair”. In: *Cell Res* 34.10 (Oct. 2024), pp. 673–674. ISSN: 17487838. DOI: 10.1038/s41422-024-00979-4.

[576] Timea Aczél et al. “Transcriptional Alterations in the Trigeminal Ganglia, Nucleus and Peripheral Blood Mononuclear Cells in a Rat Orofacial Pain Model”. In: *Front. Mol. Neurosci* 11 (June 2018). ISSN: 16625099. DOI: 10.3389/fnmol.2018.00219.

[577] Guoxin Ni et al. “PPP6C negatively regulates sting-dependent innate immune responses”. In: *mBio* 11.4 (July 2020), pp. 1–13. ISSN: 21507511. DOI: 10.1128/mBio.01728-20.

[578] Jinghan Yang et al. “Mechanism and effects of STINGâIFN-I pathway on nociception: A narrative review”. In: *Front. Mol. Neurosci* 15 (Jan. 2023). ISSN: 16625099. DOI: 10.3389/fnmol.2022.1081288.

[579] Qi Chen et al. “Unveiling adcyap1 as a protective factor linking pain and nerve regeneration through single-cell RNA sequencing of rat dorsal root ganglion neurons”. In: *BMC Biol* 21.1 (Dec. 2023). ISSN: 17417007. DOI: 10.1186/s12915-023-01742-8.

[580] Georgios Baskozos et al. “Molecular and cellular correlates of human nerve regeneration: ADCYAP1/PACAP enhance nerve outgrowth”. In: *Brain* 143.7 (July 2020), pp. 2009–2026. ISSN: 14602156. DOI: 10.1093/brain/awaa163.

[581] Masahiro Ohsawa et al. “Modulation of nociceptive transmission by pituitary adenylate cyclase activating polypeptide in the spinal cord of the mouse”. In: *Pain* 100 (2002). URL: www.elsevier.com/locate/pain.

[582] Noboru Imai. “Molecular and Cellular Neurobiology of Circadian and Circannual Rhythms in Migraine: A Narrative Review”. In: *Int. J. Mol. Sci* 24.12 (June 2023). ISSN: 14220067. DOI: 10.3390/ijms241210092.

[583] Theodora Kalpachidou et al. *Rho GTPases in the physiology and pathophysiology of peripheral sensory neurons*. 2019. DOI: 10.3390/cells8060591.

[584] Ken Honjo et al. “Nociceptor-Enriched Genes Required for Normal Thermal Nociception”. In: *Cell Reports* 16.2 (July 2016), pp. 295–303. ISSN: 22111247. DOI: 10.1016/j.celrep.2016.06.003.

[585] Erich J. Baker et al. “GeneWeaver: A web-based system for integrative functional genomics”. In: *Nucleic Acids Research* 40.D1 (Jan. 2012). ISSN: 03051048. DOI: 10.1093/nar/gkr968.

[586] Janine M. Wotton et al. “Identifying genetic determinants of inflammatory pain in mice using a large-scale gene-targeted screen”. In: *Pain* 163.6 (June 2022), pp. 1139–1157. ISSN: 18726623. DOI: 10.1097/j.pain.0000000000002481.

[587] Jung Wook Park et al. “Differential trigeminovascular nociceptive responses in the thalamus in the familial hemiplegic migraine 1 knock-in mouse: A Fos protein study”. In: *Neurobiology of Disease* 64 (Apr. 2014), pp. 1–7. ISSN: 09699961. DOI: 10.1016/j.nbd.2013.12.004.

[588] Binbin Wang et al. “PKM2 is involved in neuropathic pain by regulating ERK and STAT3 activation in rat spinal cord”. In: *Journal of Headache and Pain* 19.1 (Dec. 2018). ISSN: 11292377. DOI: 10.1186/s10194-018-0836-4.

[589] Joel A Black et al. “Expression of Nav1.7 in DRG neurons extends from peripheral terminals in the skin to central preterminal branches and terminals in the dorsal horn”. In: *Mol. Pain* 8.82 (2012). ISSN: 17448069. DOI: 10.1186/1744-8069-8-9.

[590] Jose A. Gomez-Sanchez et al. “After nerve injury, lineage tracing shows that myelin and Remak Schwann cells elongate extensively and branch to form repair Schwann cells, which shorten radically on remyelination”. In: *J. Neurosci* 37.37 (2017), pp. 9086–9099. ISSN: 15292401. DOI: 10.1523/JNEUROSCI.1453-17.2017.

[591] Gaoxingyu Huang et al. “High-resolution structures of human Nav1.7 reveal gating modulation through α-π helical transition of S6IV”. In: *Cell Rep* 39.4 (Apr. 2022). ISSN: 22111247. DOI: 10.1016/j.celrep.2022.110735.

[592] Peter V. Hornbeck et al. “PhosphoSitePlus, 2014: Mutations, PTMs and recalibrations”. In: *Nucleic Acids Res* 43.D1 (Jan. 2015), pp. D512–D520. ISSN: 13624962. DOI: 10.1093/nar/gku1267.

[593] Sidharth Tyagi et al. “Compartment-specific regulation of NaV1.7 in sensory neurons after acute exposure to TNF-α”. In: *Cell Rep* 43.2 (Feb. 2024). ISSN: 22111247. DOI: 10.1016/j.celrep.2024.113685.

[594] P. A. Dotsenko et al. “Candidate SNP markers of changes in the expression levels of the human SCN9A gene as a hub gene for pain generation, perception, response and anesthesia”. In: *Vavilovskii Zh. Genet. Sel* 28.8 (2024), pp. 808–821. ISSN: 25003259. DOI: 10.18699/vjgb-24-89.

[595] Francesco Portaluppi et al. “Circadian rhythm of calcitonin gene-related peptide in uncomplicated essential hypertension”. In: *J. Hypertension* 10.10 (1992), pp. 1227–1234. ISSN: 14735598. DOI: 10.1097/00004872-199210000-00017.

[596] Giorgio Trasforini et al. “Circadian profile of plasma calcitonin gene-related peptide in healthy man”. In: *JCEM* 73.5 (1991), pp. 945–951. ISSN: 19457197. DOI: 10.1210/jcem-73-5-945.

[597] Sunil J Wirnalawansa. “Circadian Variation of Plasma Calcitonin Gene-Related Peptide in Man”. In: *J. Neuroendocrinol* 3.3 (1991), pp. 319–322.

[598] Clara M. Kerth et al. “Phosphorylation of a chronic pain mutation in the voltage-gated sodium channel Nav1.7 increases voltage sensitivity”. In: *J. Biol. Chem* 296 (Jan. 2021). ISSN: 1083351X. DOI: 10.1074/jbc.RA120.014288.

[599] Takako Noguchi, Lexie L. Wang, and David K. Welsh. “Fibroblast PER2 circadian rhythmicity depends on cell density”. In: *J. Biol. Rhythms* 28.3 (June 2013), pp. 183–192. ISSN: 07487304. DOI: 10.1177/0748730413487494.

[600] Myriam Heiman et al. “Cell type-specific mRNA purification by translating ribosome affinity purification (TRAP)”. In: *Nat. Prot* 9.6 (2014), pp. 1282–1291. ISSN: 17502799. DOI: 10.1038/nprot.2014.085.

[601] Ewa K Zuba-Surma et al. “The ImageStream System: a key step to a new era in imaging”. In: *FOLIA HISTOCHEMICA ET CYTOBIOLOGICA* (2007), pp. 279–290.

[602] Joan Chang et al. “Endocytic recycling is central to circadian collagen fibrillogenesis and disrupted in fibrosis”. In: *eLife* (Jan. 2025). DOI: 10.7554/eLife.95842.3.

[603] Romain A. Colas et al. “Impaired production and diurnal regulation of vascular RvD n-3 DPA increase systemic inflammation and cardiovascular disease”. In: *Circ. Res* 122.6 (Mar. 2018), pp. 855–863. ISSN: 15244571. DOI: 10.1161/CIRCRESAHA.117.312472.

[604] Elyse Neolani Greenberg et al. “Circadian control of interferon-sensitive gene expression in murine skin”. In: *PNAS* 117.11 (2020), pp. 5761–5771. DOI: 10.1073/pnas.1915773117/-/DCSupplemental.

[605] Mariko Izumo et al. “Quantitative analyses of circadian gene expression in mammalian cell cultures”. In: *PLoS Comput. Biol* 2.10 (2006), pp. 1248–1261. ISSN: 15537358. DOI: 10.1371/journal.pcbi.0020136.

[606] Yasuhiro Umemura and Kazuhiro Yagita. “Development of the Circadian Core Machinery in Mammals”. In: *J. Mol. Biol* 432.12 (2020), pp. 3611–3617. ISSN: 10898638. DOI: 10.1016/j.jmb.2019.11.026.

[607] Hamid Dolatshad, Andrew J. Cary, and Fred C. Davis. “Differential expression of the circadian clock in maternal and embryonic tissues of mice”. In: *PLoS ONE* 5.3 (2010). ISSN: 19326203. DOI: 10.1371/journal.pone.0009855.

[608] Elzbieta Kowalska et al. “The circadian clock starts ticking at a developmentally early stage”. In: *J. Biol. Rhythms* 25.6 (2010), pp. 442–449. ISSN: 07487304. DOI: 10.1177/0748730410385281.

[609] Maria Seron-Ferre, Gullermo J. Valenzuela, and Claudia Torres-Farfan. “Circadian clocks during embryonic and fetal development”. In: *Birth Defects Research Part C - Embryo Today: Reviews* 81.3 (2007), pp. 204–214. ISSN: 1542975X. DOI: 10.1002/bdrc.20101.

[610] Lars Behrend et al. “Interaction of casein kinase 1 delta (CK1d) with post-Golgi structures, microtubules and the spindle apparatus”. In: *EJCB* 79 (Apr. 2000).

[611] Jeff Kuret et al. “Casein kinase 1 is tightly associated with paired-helical filaments isolated from Alzheimer’s disease brain”. In: *J. Neurochem* 69.6 (1997), pp. 2506–2515. ISSN: 00223042. DOI: 10.1046/j.1471-4159.1997.69062506.x.

[612] Sandeep Rajkumar, Tobias M. Böckers, and Alberto Catanese. “Fast and efficient synaptosome isolation and post-synaptic density enrichment from hiPSC-motor neurons by biochemical sub-cellular fractionation”. In: *STAR Protocols* 4.1 (Mar. 2023). ISSN: 26661667. DOI: 10.1016/j.xpro.2023.102061.

[613] Jeremy Schwartzentruber et al. “Molecular and functional variation in iPSC-derived sensory neurons”. In: *Nat. Genet* 50.1 (Jan. 2018), pp. 54–61. ISSN: 15461718. DOI: 10.1038/s41588-017-0005-8.

[614] Siim Pauklin and Ludovic Vallier. “XThe cell-cycle state of stem cells determines cell fate propensity”. In: *Cell* 155.1 (Sept. 2013), p. 135. ISSN: 10974172. DOI: 10.1016/j.cell.2013.08.031.

[615] Anna Grazia Monteduro et al. “Organs-on-chips technologies â A guide from disease models to opportunities for drug development”. In: *Biosensors and Bioelectronics* 231 (July 2023). ISSN: 18734235. DOI: 10.1016/j.bios.2023.115271.

[616] Emiliano Hergenreder et al. “Combined small-molecule treatment accelerates maturation of human pluripotent stem cell-derived neurons”. In: *Nat. Biotechnol* (Jan. 2024). ISSN: 1087-0156. DOI: 10.1038/s41587-023-02031-z.

[617] Gabriele Ciceri et al. “An epigenetic barrier sets the timing of human neuronal maturation”. In: *Nature* 626.8000 (Feb. 2024), pp. 881–890. ISSN: 14764687. DOI: 10.1038/s41586-023-06984-8.

[618] Marta Cubero-Sarabia, Anna Maria Kapetanaki, and Massimo Vassalli. *Biophysical assays to test cellular mechanosensing: moving towards high throughput*. Dec. 2024. DOI: 10.1007/s12551-024-01263-w.

[619] Silvana Lobo et al. “A protocol for karyotyping and genetic editing of induced pluripotent stem cells with homology-directed repair mediated CRISPR/Cas9”. In: *Biology Methods and Protocols* 10.1 (2025). ISSN: 23968923. DOI: 10.1093/biomethods/bpaf018.

[620] Cagla Eroglu and Ben A. Barres. “Regulation of synaptic connectivity by glia”. In: *Nature* 468.7321 (Nov. 2010), pp. 223–231. ISSN: 00280836. DOI: 10.1038/nature09612.

[621] Lena Tveriakhina et al. “Temporal dynamics and stoichiometry in human Notch signaling from Notch synaptic complex formation to nuclear entry of the Notch intracellular domain”. In: *Dev. Cell* (Apr. 2024). ISSN: 15345807. DOI: 10.1016/j.devcel.2024.03.021.

[622] Parinya Noisa et al. “Notch signaling regulates the differentiation of neural crest from human pluripotent stem cells”. In: *J. Cell Sci* 127.9 (2014), pp. 2083–2094. ISSN: 14779137. DOI: 10.1242/jcs.145755.

[623] Asta Arendt-Tranholm et al. “Single-cell characterization of the human C2 dorsal root ganglion recovered from C1-2 arthrodesis surgery: implications for neck pain”. In: *bioRxiv* (Mar. 2025). DOI: 10.1101/2025.03.24.645122. URL: http://biorxiv.org/lookup/doi/10.1101/2025.03.24.645122.

[624] Ranjinidevi Ambalavanar, Masayuki Moritani, and Dean Dessem. “Trigeminal P2X3 receptor expression differs from dorsal root ganglion and is modulated by deep tissue inflammation”. In: *Pain* 117.3 (Oct. 2005), pp. 280–291. ISSN: 03043959. DOI: 10.1016/j.pain.2005.06.029.

[625] Fay Cooper and Anestis Tsakiridis. “Shaping axial identity during human pluripotent stem cell differentiation to neural crest cells”. In: *Biochem. Soc. Trans* 50.1 (Feb. 2022), pp. 499–511. ISSN: 14708752. DOI: 10.1042/BST20211152.

[626] Fay Cooper et al. “Rostrocaudal patterning and neural crest differentiation of human pre-neural spinal cord progenitors in vitro.” eng. In: *Stem Cell Rep* (Mar. 2022). ISSN: 2213-6711 (Electronic). DOI: 10.1016/j.stemcr.2022.02.018.

[627] Robert M. Caudle et al. “Sex differences in mouse Transient Receptor Potential Cation Channel, Subfamily M, Member 8 expressing trigeminal ganglion neurons”. In: *PLoS ONE* 12.5 (May 2017). ISSN: 19326203. DOI: 10.1371/journal.pone.0176753.

[628] Robert E. Sorge et al. “Different immune cells mediate mechanical pain hypersensitivity in male and female mice”. In: *Nat. Neurosci.* 18.8 (Aug. 2015), pp. 1081–1083. ISSN: 15461726. DOI: 10.1038/nn.4053.

[629] Diana Tavares-Ferreira et al. “Sex Differences in Nociceptor Translatomes Contribute to Divergent Prostaglandin Signaling in Male and Female Mice”. In: *Biol. Psychiatry* 91.1 (Jan. 2022), pp. 129–140. ISSN: 18732402. DOI: 10.1016/j.biopsych.2020.09.022.

[630] M. Fischera et al. “The incidence and prevalence of cluster headache: A meta-analysis of population-based studies”. In: *Cephalalgia* 28.6 (June 2008), pp. 614–618. ISSN: 03331024. DOI: 10.1111/j.1468-2982.2008.01592.x.

[631] Shagun Singh et al. “Female-selective mechanisms promoting migraine”. In: *J. Headache and Pain* 25.1 (Dec. 2024). ISSN: 11292377. DOI: 10.1186/s10194-024-01771-w.

[632] Antonio L. Aguilar-Shea and Javier Diaz-de-Teran. “Migraine review for general practice”. In: *Atencion Primaria* 54.2 (Feb. 2022). ISSN: 15781275. DOI: 10.1016/j.aprim.2021.102208.

[633] Songyi Park et al. “Differences in Neuropathology between Nitroglycerin-Induced Mouse Models of Episodic and Chronic Migraine”. In: *Int. J. Mol. Sci* 25.7 (Apr. 2024). ISSN: 14220067. DOI: 10.3390/ijms25073706.

[634] Andrew M. Blumenfeld et al. “Effectiveness and Safety of Chronic Migraine Preventive Treatments: A Systematic Literature Review”. In: *Pain and Therapy* 12.1 (Feb. 2023), pp. 251–274. ISSN: 2193651X. DOI: 10.1007/s40122-022-00452-3.

[635] Christian Lampl et al. “The comparative effectiveness of migraine preventive drugs: a systematic review and network meta-analysis”. In: *J. Headache Pain* 24.1 (Dec. 2023). ISSN: 11292377. DOI: 10.1186/s10194-023-01594-1.

[636] Yohannes W. Woldeamanuel et al. “RNA-seq reveals transcriptomic differences in circadian-related genes of the choroid plexus in a preclinical chronic migraine model”. In: *bioRxiv* (June 2025). DOI: 10.1101/2025.06.03.657705.

[637] Sacha A. Malin, Brian M. Davis, and Derek C. Molliver. “Production of dissociated sensory neuron cultures and considerations for their use in studying neuronal function and plasticity”. In: *Nat. Prot* 2.1 (Feb. 2007), pp. 152–160. ISSN: 17542189. DOI: 10.1038/nprot.2006.461.

[638] Minghan Hu. "Visualization of Trigeminal Ganglion Neuronal Activities in Mice". In: *Curr. Protoc. Cell Biol* 83.1 (June 2019). ISSN: 19342616. DOI: 10.1002/cpcb.84.

[639] Adam Frankish et al. "GENCODE reference annotation for the human and mouse genomes". In: *Nucleic Acids Res* 47.D1 (Jan. 2019), pp. D766–D773. ISSN: 0305-1048. DOI: 10.1093/nar/gky955.

[640] L L Nikitenko et al. "Differential and cell-specific expression of calcitonin receptor-like receptor and receptor activity modifying proteins in the human uterus". In: *Mol. Hum. Reprod* 7.7 (July 2001), pp. 655–664. ISSN: 1360-9947. DOI: 10.1093/molehr/7.7.655.

[641] Jian Ping Lai et al. "Quantification of substance P mRNA in human immune cells by real-time reverse transcriptase PCR assay". In: *CDLI* 9.1 (2002), pp. 138–143. ISSN: 1071412X. DOI: 10.1128/CDLI.9.1.138-143.2002.

[642] Trisia Breitkopf et al. "Somatostatin expression in human hair follicles and its potential role in immune privilege". In: *J. Invest. Dermatol* 133.7 (2013), pp. 1722–1730. ISSN: 15231747. DOI: 10.1038/jid.2013.53.

[643] Jian Ping Lai et al. "Detection of full-length and truncated neurokinin-1 receptor mRNA expression in human brain regions". In: *J. Neurosci.Met* 168.1 (Feb. 2008), pp. 127–133. ISSN: 01650270. DOI: 10.1016/j.jneumeth.2007.10.004.

[644] Laure Verrier et al. "Neural differentiation, selection and transcriptomic profiling of human neuromesodermal progenitor-like cells in vitro". In: *Development (Cambridge)* 145.16 Special Issue (2018). ISSN: 14779129. DOI: 10.1242/dev.166215.

[645] Sascha R.A. Alles and Peter A. Smith. "Peripheral Voltage-Gated Cation Channels in Neuropathic Pain and Their Potential as Therapeutic Targets". In: *Front. Pain Res* 2 (2021). ISSN: 2673561X. DOI: 10.3389/fpain.2021.750583.

[646] Matthias Arzt et al. "LABKIT: Labeling and Segmentation Toolkit for Big Image Data". In: *Front. Comput. Sci* 4 (Feb. 2022). ISSN: 26249898. DOI: 10.3389/fcomp.2022.777728.

[647] Jose Octavio Goncalves de Freitas et al. “Does dexamethasone act in neuropeptides SP and CGRP in neurogenic inflammation of the skin? An experimental study”. In: *Acta Cirurgica Brasileira* 30.8 (Aug. 2015), pp. 523–528. ISSN: 16782674. DOI: 10.1590/S0102-86502015008000002.

[648] Paul V. Beum et al. “Quantitative analysis of protein co-localization on B cells opsonized with rituximab and complement using the ImageStream multispectral imaging flow cytometer”. In: *J. Immunol. Methods* 317.1-2 (Dec. 2006), pp. 90–99. ISSN: 00221759. DOI: 10.1016/j.jim.2006.09.012.